

ADVANCED TURBINE STUDY

FINAL REPORT

Prepared Under Contract NAS8-33821
for
National Aeronautics and Space Administration
George C. Marshall Space Flight Center
Marshall Space Center, Alabama 35812

Prepared by
Pratt & Whitney
Government Products Division
P. O. Box 2691, West Palm Beach, Florida 33402

(NASA-CR-178707) ADVANCED TURBINE STUDY
Final Report, 1 Aug. 1982 - 15 Aug. 1985
(Pratt and Whitney Aircraft) 188 p
HC A09/MF A01

N86-20495

CSCL 21H

G3/20

Unclas
04272



**UNITED
TECHNOLOGIES
PRATT & WHITNEY**

ADVANCED TURBINE STUDY

FINAL REPORT

Prepared Under Contract NAS8-33821
for
National Aeronautics and Space Administration
George C. Marshall Space Flight Center
Marshall Space Center, Alabama 35812

Prepared by
Pratt & Whitney
Government Products Division
P. O. Box 2691, West Palm Beach, Florida 33402



FOREWORD

This final report presents the results of the work performed under Contract NAS8-33821, covering the period 1 August 1982 to 15 August 1985. This work was conducted for the National Aeronautics and Space Administration George C. Marshall Space Flight Center (NASA MSFC) by Pratt & Whitney/Government Products Division (P&W/GPD). Mr. J. H. Castro was the engineering manager for this effort and author of this report. The following personnel have contributed to the material presented in this report: D. E. Paulus, P. A. Allard, H. M. Gibson, J. R. Mullaly, and T. L. Woods.

CONTENTS

<i>Section</i>		<i>Page</i>
I	INTRODUCTION	I-1
II	SUMMARY	II-1
III	TECHNICAL ACTIVITY — ORIGINAL PROGRAM	III-1
	A. Task 1 — Case 2 and 3 Analysis	III-1
	B. Task 2 — Subtask 201, Specimen Design	III-8
	C. Task 2 — Subtask 202, Specimen Fabrication	III-17
	D. Task 2 — Subtask 203, Specimen Test	III-50
	E. Task 3 — Subtask 301, Airfoil Design and Analysis	III-51
	F. Task 4 — Airfoil Fabrication and Task 5 — Test Follow Up	III-70
IV	TECHNICAL ACTIVITY — REDIRECTED PROGRAM	IV-1
	A. Task 1 — Hardware Design	IV-1
	B. Task 2 — Hardware Fabrication	IV-7
	C. Task 3 — Turbine Blade Testing and Data Analysis	IV-13
V	CONCLUSIONS AND COMMENTS	V-1
	APPENDIX A. SUMMARY OF SPUTTER DEPOSITION WORK	A-1
	APPENDIX B. ADVANCED TURBINE STUDY ENGINEERING DRAWINGS	B-1
	APPENDIX C. VERIFICATION OF ATS BLADE GRAIN QUALI- TY AND ORIENTATION BY GRAIN ETCH AND LAUE X-RAY METHODS	C-1

SECTION II SUMMARY

The original objective of this phase of the Advanced Turbine Study (ATS) Program was to investigate the feasibility of an advanced convective cooling concept applied to rocket turbine airfoils operating in a high-pressure hydrogen and methane environment. The concept consisted of a central structural member in which grooves are machined or etched. The grooves are temporarily filled with a removable filler and the entire airfoil is covered with a layer of electroformed or sputtered nickel, or nickel base alloy. After the filler is removed, the low thermal resistance of the thin nickel closure allows the wall temperature to be significantly reduced by heat transfer to the coolant.

The program was divided into six tasks. The following describe the six original tasks as presented by the program plan submitted to NASA on 27 August 1982.

- Task 1 — Turbine Performance Appraisal

The thermal analyses of the Case 2 and Case 3 turbines, as defined in NASA Contract NAS8-33821 modification S/A-1, will be revised using the advanced convective cooling techniques.

The results will be compared to test data under Task 5 to gage the accuracy of the analytical techniques. In Case 2, hydrogen is used as the coolant medium with 80 pounds/second flow. In Case 3, the coolant used is methane with a 280 pounds/second flow.

- Task 2 — Coolant Geometry Evaluation

Cylindrical test specimens will be used to establish fabrication techniques and determine the optimum coolant geometry. Cast cylinders of a nickel alloy will be cored to achieve a wall thickness approximating the airfoil wall thickness. Analytically chosen coolant geometries will be intalled on the outer diameter (OD) surface of the cylinders. The cylinders will be subjected to fluidized bed tests which will thermally cycle each coolant geometry in the same manner. The data from these tests will be used to select the airfoil coolant geometries.

- Task 3 — Test Hardware Design and Analysis

Design and analysis of test hardware for verification of a hydrogen and methane advanced cooling concept will be accomplished under this task. A common turbine airfoil contour will be used for both hydrogen and methane testing. The airfoil contour will be a constant cross section from root to tip, without twist, and designed to fit in the Marshall Space Flight Center (MSFC) "Space Shuttle Main Engine (SSME) Turbine Airfoil Tester." The airfoil coolant groove designs will be based on the thermal shock test results accomplished under Task 2. The groove designs may be different for the hydrogen and methane test airfoils, if analysis indicates a change is required for improved durability. A typical airfoil cross section is shown in Figure II-1.

The coolant feed system to the test airfoil will also be designed under this task. It will be a mount plate similar to Item 5 on the MSFC test rig drawing,

SECTION I INTRODUCTION

In essentially all liquid-fueled rocket engines developed previously, turbine life and inlet temperature were not major design factors. Since these engines were generally used for expendable missions, life requirements were comparatively low. The engines were of medium chamber pressure (i.e., 500 to 1000 psia) and most used the gas generator cycle. Power could be maintained in the event of any efficiency reduction or excess pressure loss by increasing turbine flowrate, rather than turbine inlet temperature (TIT), with only a minor effect on overall engine performance. However, the advent of the reusable, high-pressure staged combustion engine has completely changed this situation. Since these systems are intended to be reused, the turbine has to be designed for an engine life of several hundred cycles. Any performance shortcomings in the engine, due to excessive parasitic flows, high-pressure losses, or low efficiency, can be overcome only by increasing the TIT. Therefore, turbine technology represents a critical design limit for the next generation of reusable main engines.

In the first phase of the Advanced Turbine Study (ATS), it was found that conventional turbine airfoil cooling schemes would not provide adequate cooling durability in a high temperature and pressure rocket turbine environment (Reference Final Report FR-15978). The reason for this is that conventionally cooled airfoils are mainly cooled convectively through a 0.04 to 0.06 inch thick wall. This type of cooling in a high-heat-flux, high-temperature rocket turbine environment creates huge thermal gradients with very little cooling (approximately 50°F) of the hot side wall. The hot side wall would then experience rapid fatigue cracking and melting in such an environment.

The current phase of the Advanced Turbine Study investigated an advanced convective cooling scheme for high-pressure, high-temperature rocket turbine vanes and blades. This advanced cooling concept consists of a turbine airfoil in which cooling channels (grooves) are machined into the exterior surface. The grooves are temporarily filled with a removable filler and the entire airfoil is covered with a thin layer of sputtered nickel alloy. The filler is then removed. When coolant flows through the channels, the low thermal resistance of the thin, high conductivity layer allows the hot side wall temperature to be significantly reduced by minimizing the gradient through the wall. The advantage of this scheme is that the cooling passages are located close to the hot side wall, thus minimizing the thermal gradient and providing better hot side wall cooling. The majority of the wall runs very cool and provides adequate strength to carry gas bending and centrifugal loads.

Due to difficulties encountered during fabrication of the hardware for this cooling scheme, it was determined that an extensive development program would be required to incorporate the advanced cooling concept into a turbine blade design. Since such a development program was out of the scope of the Advanced Turbine Study, the program was redirected by NASA to fabricate and test a "hot core" type of blade design which will provide improved turbine blade life over a conventional solid blade. This type of hollow blade, with hot gasses flowing through it, can be tested in the NASA facility to quantify its life improvement. In P&W's hot core configuration, the blades are fabricated from PWA 1480 single-crystal material. The enhanced material properties obtained from this alloy (compared with the directionally solidified alloy currently used in the SSME) plus the lower strain produced by the hot core configuration, result in a blade with improved life characteristics. This improved life characteristic can, if necessary, be traded for an increase in the operating turbine inlet temperature, to provide increased output horsepower for a given life requirement. The improved life can also be traded for a reduction in turbine replacement costs, at given inlet temperature and mission requirements.

Section A-A, and will contain coolant passages and instrumentation access. Coordination with MSFC to include detailed test rig drawings, and capabilities will be required to ensure compatible test articles. Figure II-2 shows the proposed fixture.

A test program and required instrumentation will be recommended to properly evaluate the cooling design and verify the analysis. This test will be performed by NASA at the MSFC's "SSME Turbine Blade Tester."

- Task 4 — Test Airfoil Fabrication

Two cooled airfoils will be fabricated: one for hydrogen operation and one for methane. In addition, two uncooled airfoils will be provided as slaves. The cooled airfoils will contain the necessary provisions for pressure and temperature measurements and will be delivered with the instrumentation installed.

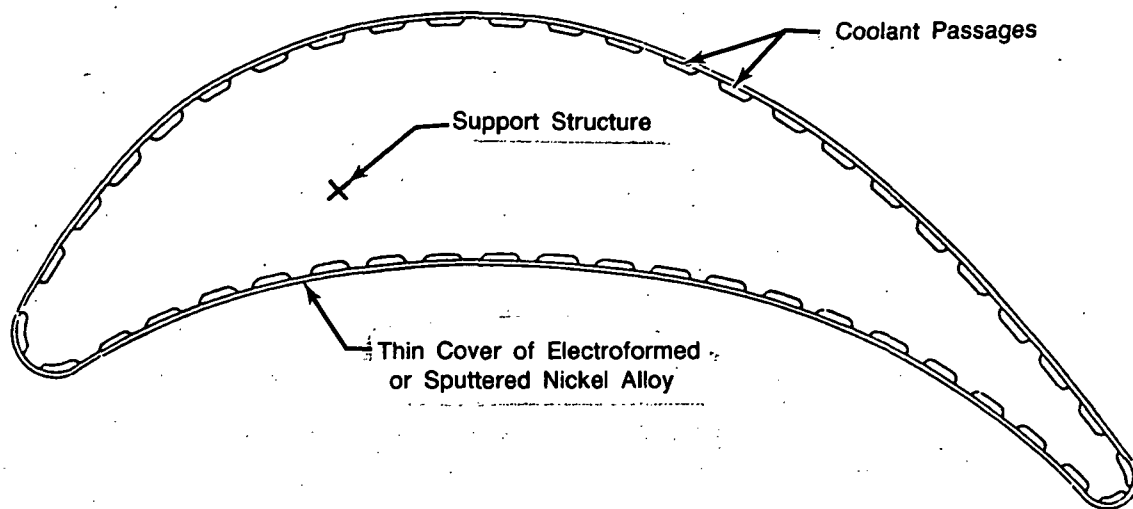
One mount plate will be fabricated to contain either test airfoil and two slaves. It will contain a coolant passage from the airfoil attachment to an AN fitting on the outside plate, and an instrumentation passage. This plate will attach to the SSME Turbine Blade Tester in the same fashion as the existing mount.

- Task 5 — Analysis of Test Results

The testing of the two articles will be done by NASA in their SSME Turbine Blade Tester. Instrumentation readings during the testing of the cooling scheme will ensure that the hot gas and coolant temperature and pressure match the conditions used in the analysis. Pratt & Whitney will analyze the metal temperature data, perform metallurgical evaluation of the airfoils, and adjust the cyclic life prediction to agree with the physical hardware condition. Similar adjustments to cyclic life predictions will be done for Cases 2 and 3.

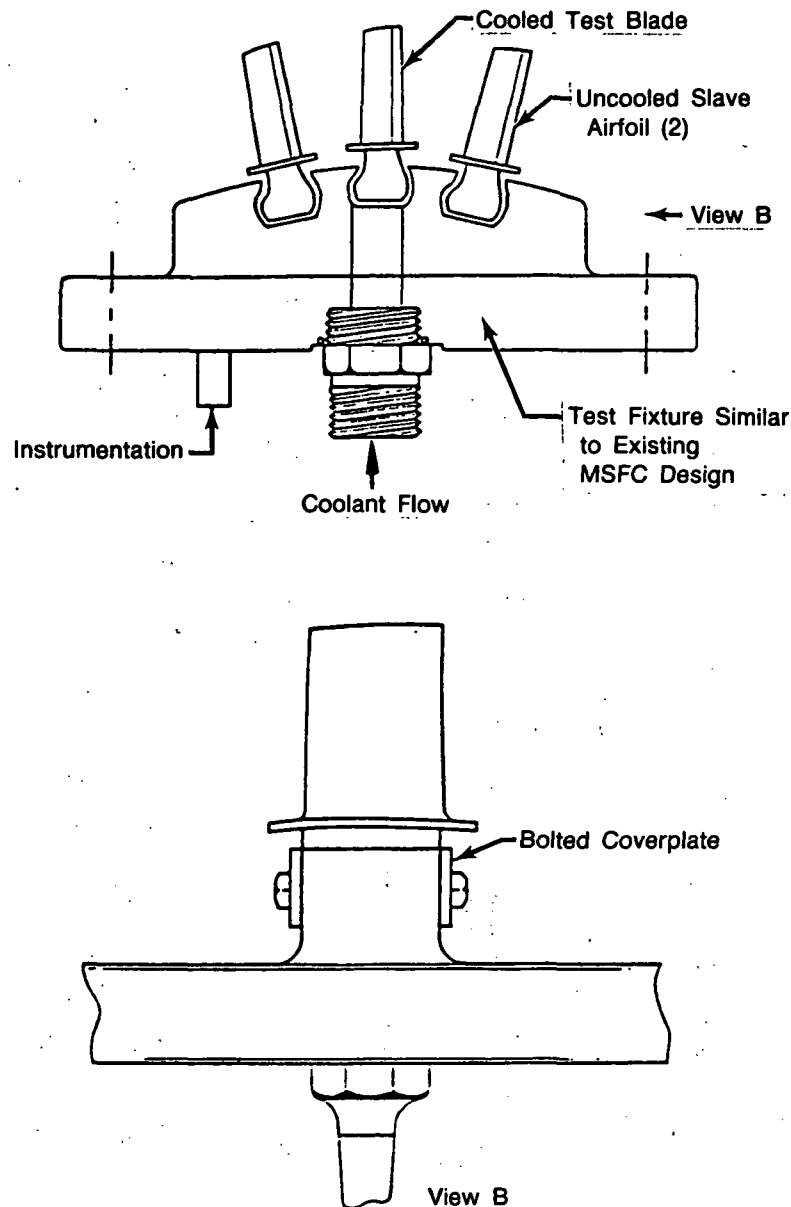
- Task 6 — Reports

Bimonthly progress reports will be submitted in the same manner as the previous Advanced Turbine Study effort. A final report will be issued at the end of the contract period.



FD 301916

Figure II-1. Advanced Convection Cooling Scheme



FD 301917

Figure II-2. Proposed Test Fixture

The program, initiated in August 1982, remained on schedule throughout the selection of the candidate materials, the design of the fluidized bed test specimens, the preliminary design of the test hardware, and the reevaluation of the thermal analysis of Case 2 and Case 3 from the previous phase of the program. During the fabrication of the fluidized bed test specimens, difficulties were encountered. These difficulties were caused by poor bond strength between the test cylinders and the sputtered closeout layer. Several experiments were undertaken to evaluate and resolve this problem. It was determined that an extensive sputtering developing program would be required to incorporate the advanced cooling concept into a turbine blade design. Such a program was out of the scope for the Advanced Turbine Study.

A different turbine blade concept, a hot core blade fabricated out of PWA 1480 single-crystal material, was then proposed to NASA by P&W. The hot core design consists of a hollow blade with an orifice on the pressure side of the blade. Mainstream flow is bled into the core through this orifice and exits the core at the blade tip. The hot mainstream flow bled into the core allows the inside of the blade to run hotter, minimizing the blades thermal gradient, and, therefore, reducing the thermal strain in the blade. The thermal gradients (thermal strains) in the blades are also reduced by the inherent reduction in wall thickness associated with the hot core blade. When the enhanced material properties from the PWA 1480 single-crystal material are used, this reduced thermal strain can be translated into a life improvement of 3.5 times that of a solid blade design.

The NASA accepted P&W's proposal and the program was redirected to design and fabricate the hot core blade concept hardware. The hardware was tested by NASA MSFC in their SSME blade tester rig. The redirected work was accomplished within the original funding bounds of the program. The redirected program was structured into the following four tasks:

- Task 1 — Hardware Design

Task 1 consists of the design of the hot core blade (Figure II-3) and the generation of engineering drawings which later were used to fabricate the blades and blade holding fixture.

- Task 2 — Hardware Fabrication

Task 2 consists of the procurement of raw materials and the fabrication and instrumentation of the hot core blade hardware.

- Task 3 — Turbine Blade Testing and Data Analysis

Task 3 consists of the performance of the turbine blade tests at NASA and the evaluation of the test results.

- Task 4 — Reports

Task 4 consists of the bimonthly progress reports and the final report.

The fabrication for the redirected ATS Program hardware was completed on schedule and within budget. Thirteen blades were delivered to NASA MSFC: nine hollow blades and four solid blades. A blade holding fixture and associated hardware were also delivered to NASA.

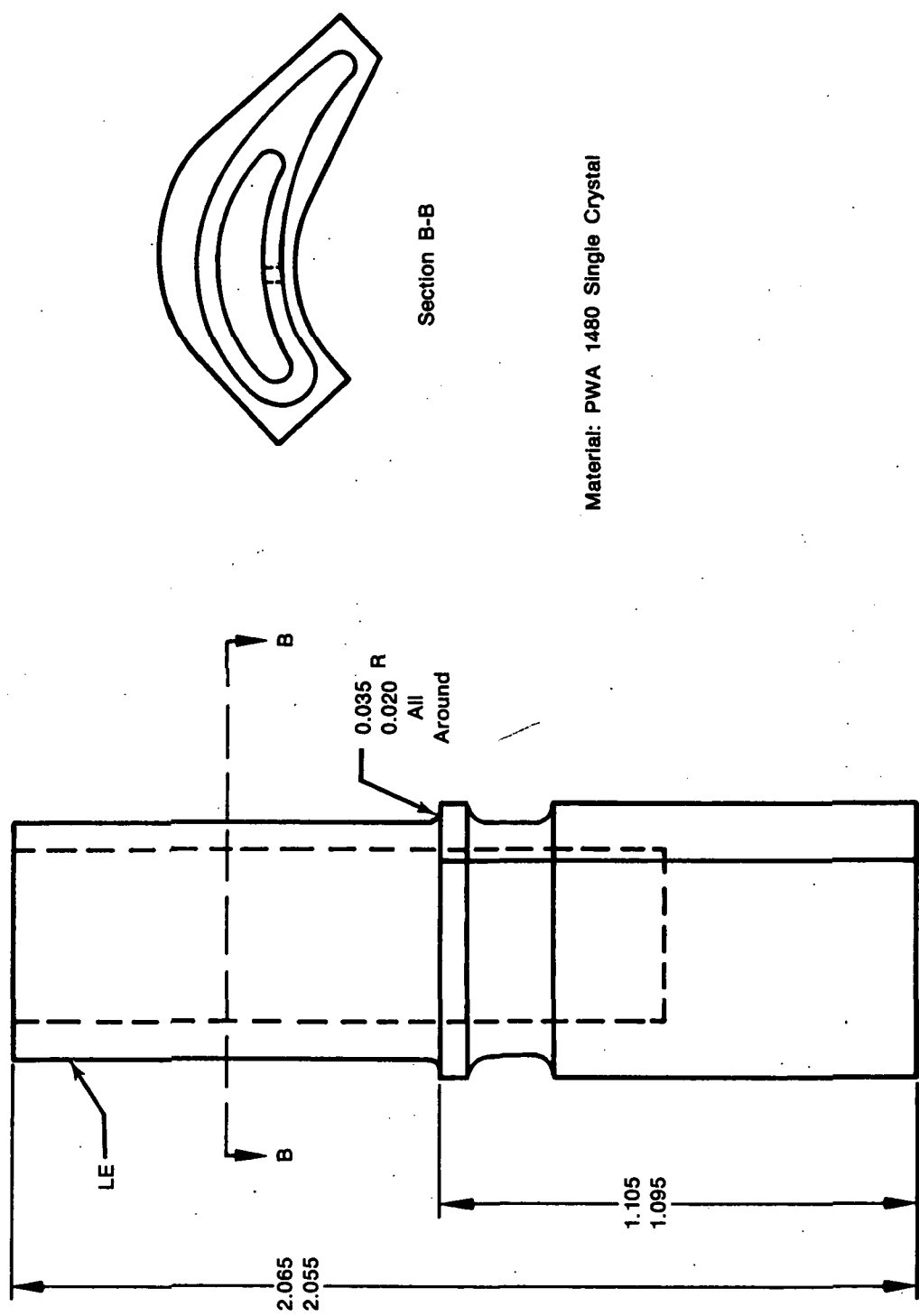
To date MSFC has completed two test series for 71 cycles and 73 cycles each. The general conclusions obtained from the testing are:

- The preferred P&W thin wall airfoil design with single-crystal material will meet low cycle fatigue (LCF) life goals
- Initial blade cracking generally occurred on the pressure side, in the platform fillet radius
- Cored parts are significantly more crack resistant than solid parts
- Thin wall and ventilated parts are the superior configurations for this rocket environment

- Based on current testing, it is expected that current high-pressure fuel turbopump (HPFTP) blade life will be approximately doubled with PWA 1480 single-crystal material, but will still fall short of reasonable life goals.

The ATS hardware testing was temporarily halted by MSFC in order to use their test facility for a different program. The ATS hardware testing will be resumed in early fall 1985.

Four additional blades (two hollow and two solid blades) were delivered to MSFC at NASA's request under Modification 12 of Contract NAS8-33821. The NASA-supplied material for these blades was Mar-M 246. This hardware will be tested along with the PWA 1480 single-crystal blades when NASA resumes testing during fall 1985.



Material: PWA 1480 Single Crystal

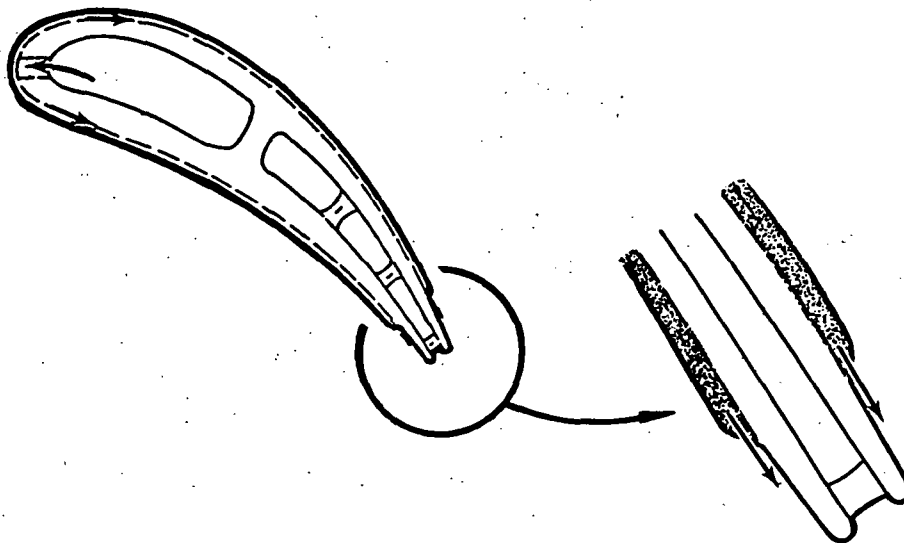
FD 267794

Figure II-3. Hot Core Blade

SECTION III TECHNICAL ACTIVITY — ORIGINAL PROGRAM

A. TASK 1 — CASE 2 AND 3 ANALYSIS

The cooling scheme used in the advanced convective design study for Cases 2 and 3 is shown in Figure III-1. In this scheme, coolant enters the hollow core and passes radially up into the blade or vane. From the core, the coolant enters the small chordwise passages through leading edge holes which connect the core to the passages. The coolant then proceeds chordwise in the grooves and exits near the trailing edge. For production quantities, the cored blade/vane and grooves would be integrally casted. The sputtered cover would then have to be applied to the casting.



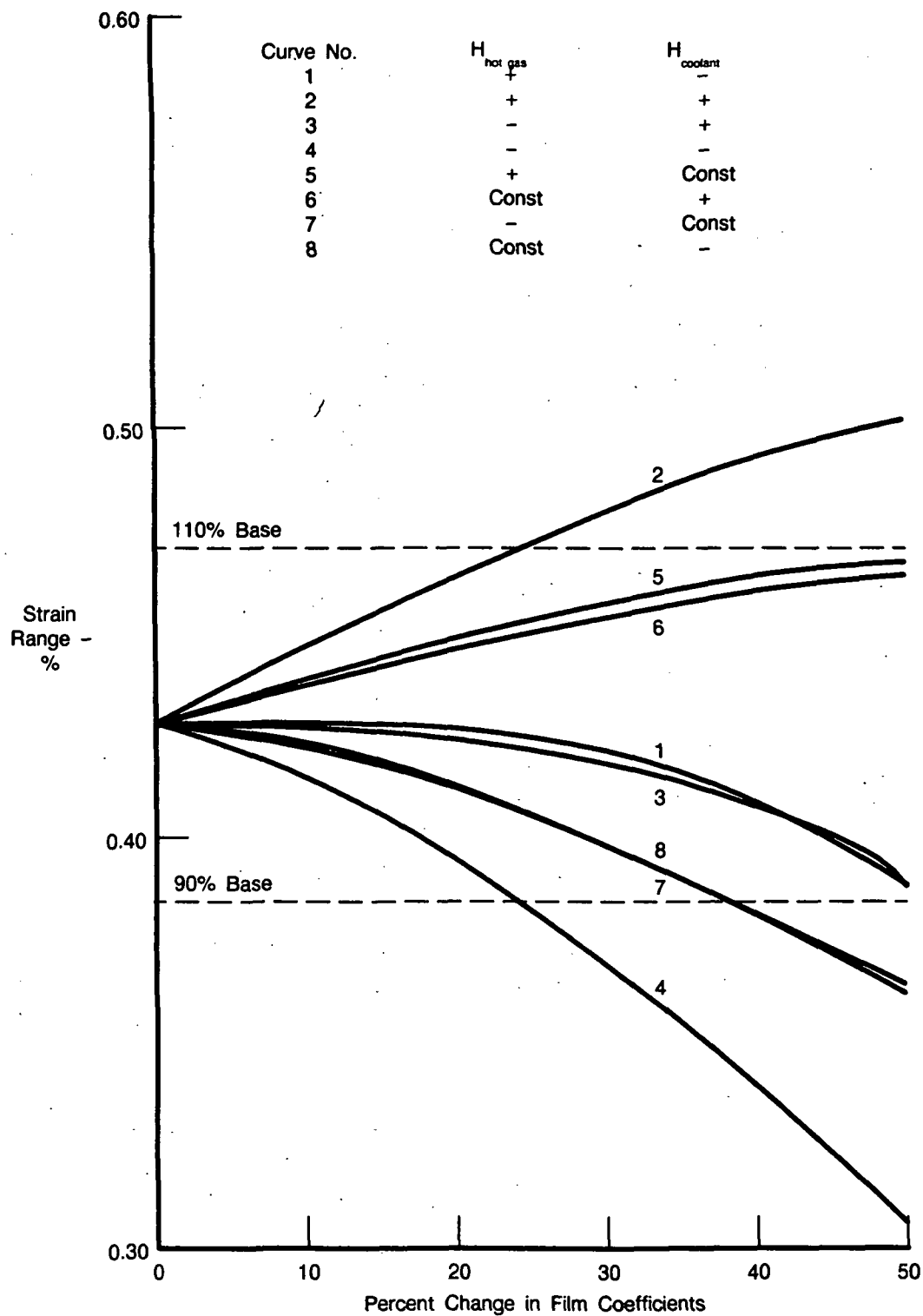
FD 267752

Figure III-1. Convectively Cooled Engine Configuration

The coolant grooves are 0.035 inch wide and have 0.045 inch lands between grooves. The grooves are 0.012 inch deep except for the H_2/O_2 1st-stage vanes which have 0.023 inch deep grooves. The 1st-stage vanes use 2% of turbine inlet flow for cooling and the 1st-stage blades also use 2% flow for cooling.

1. Task 1 — Subtask 101, Case 2 Analysis

For the case 2 analysis, the fuel used was hydrogen with an 80 pounds/second flow. The case 2 analysis began with a study to assess the impact of inaccuracies in calculating heat transfer film coefficients. In any heat transfer analysis the calculation of film coefficients using empirical correlations is only approximate. An inaccuracy of $\pm 25\%$ is possible. This parametric study varied coolant and hot gas heat transfer film coefficients on the 1st-stage turbine blades by as much as 50%, in order to see the impact on metal temperature and thermal strains. Figures III-2 through III-4 illustrate the results of this study. Figure III-2 shows that 25% inaccuracy in film coefficients would result in 10% (or less) inaccuracy in thermal strain range. Figures III-3 and III-4 show that maximum and average metal temperature variation will be less than, or equal to 75 and 60°F, respectively, for a 25% inaccuracy in film coefficients. These inaccuracies, though not desirable, are considered acceptable and by assessing their magnitude they can be accounted for in hardware design.



FDA 302517

Figure III-2. Case 2 1st-Stage Blade Strain Range versus Variations in Film Coefficients

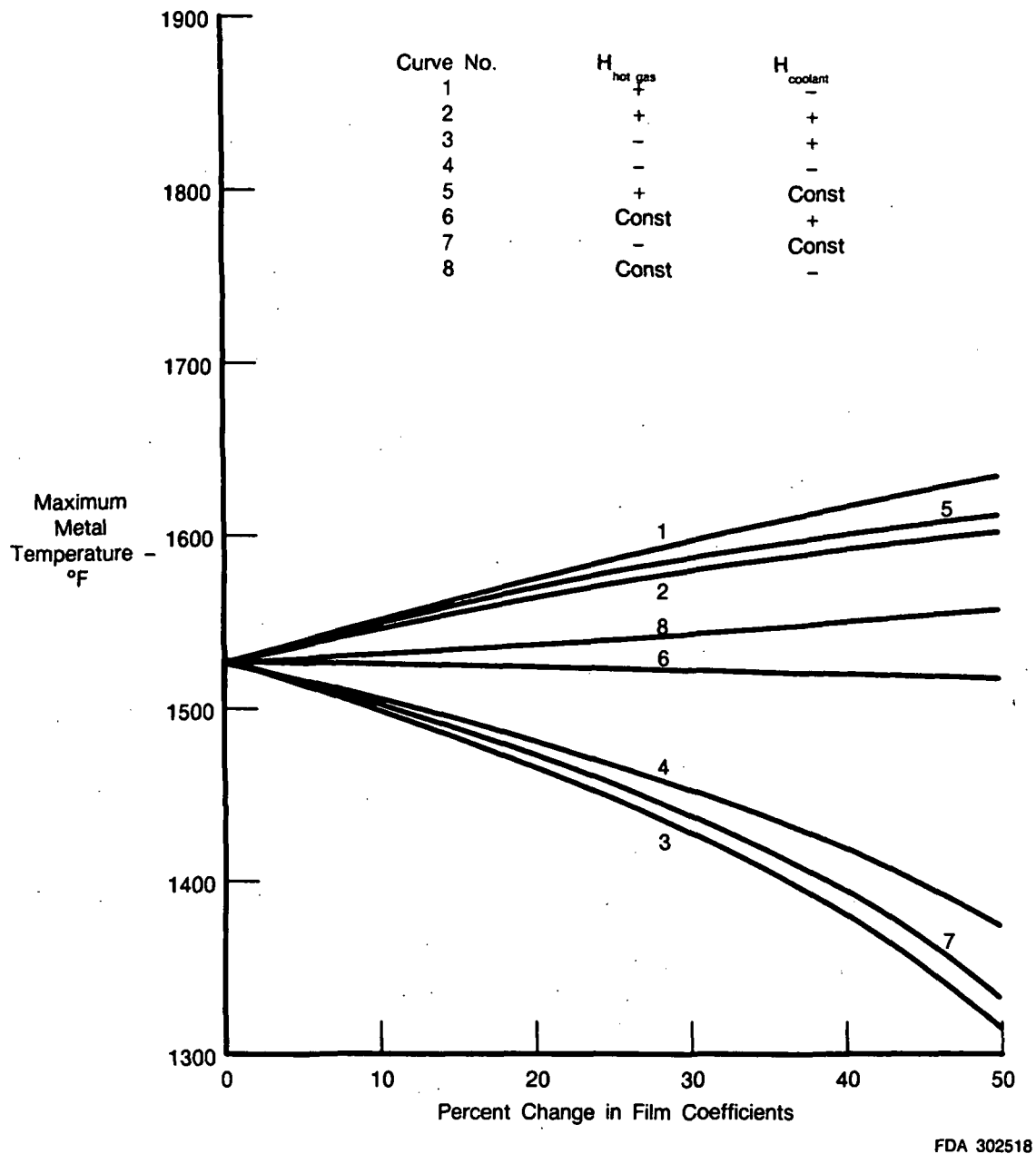
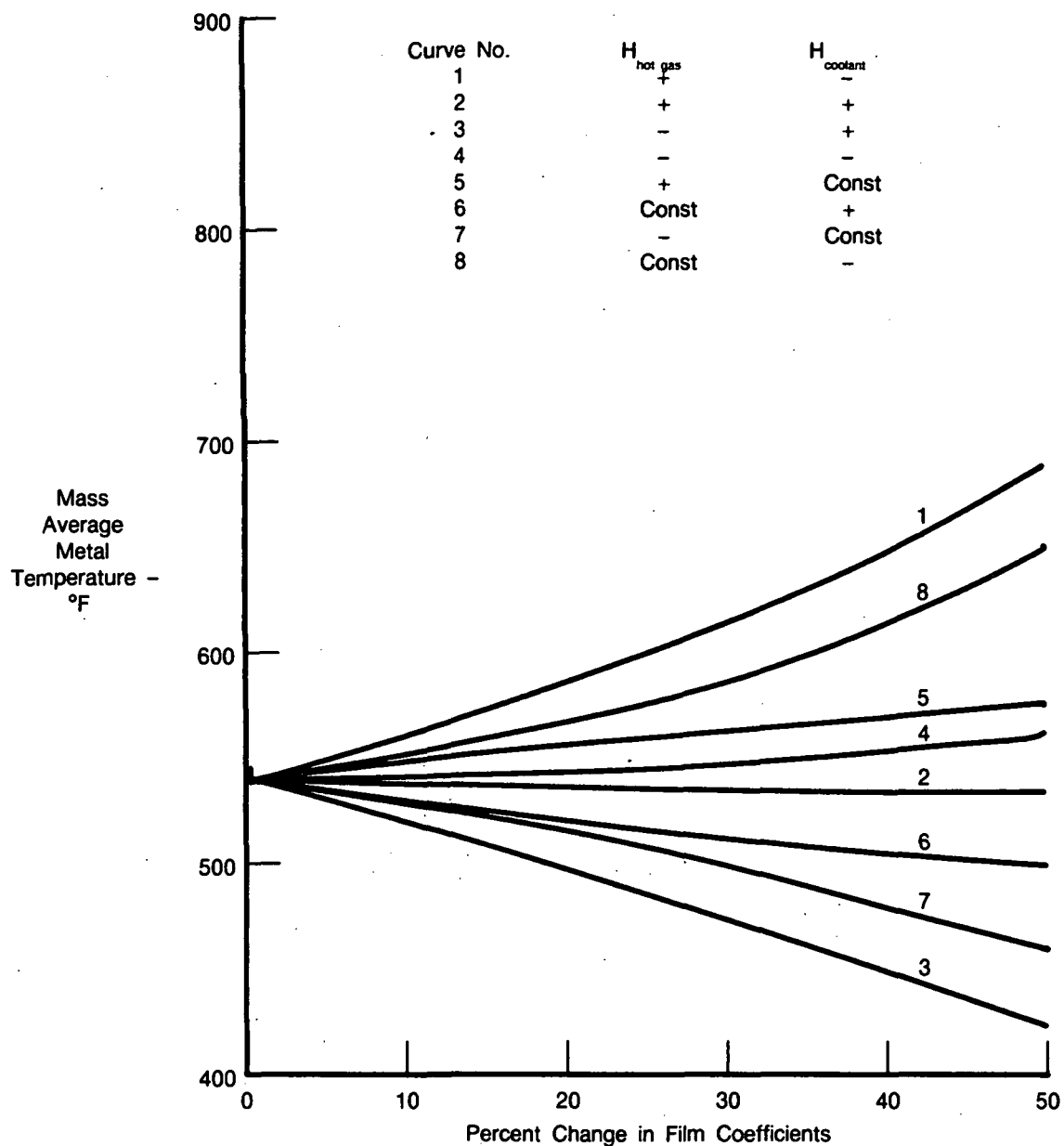


Figure III-3. Case 2 1st-Stage Blade Maximum Metal Temperature versus Variations in Film Coefficients

The turbine horsepower (hp) delivered versus turbine inlet temperature (TIT) curves for Case 2 (hydrogen) are shown in Figure III-5. The three labeled curves represent an uncooled turbine, an advanced convectively cooled turbine using 4% of inlet flow for airfoil cooling, and a film cooled turbine using 13% of inlet flow for airfoil cooling. The numbered solid lines are lines of constant cyclic life for the advanced convective cooled turbine, while the numbered dashed lines are lines of constant cyclic life for the film cooled turbine.



FDA 302519

Figure III-4. Case 2 1st-Stage Blade Average Metal Temperature versus Variations in Film Coefficients

If life considerations are ignored, the uncooled turbine would show the highest horsepower output versus TIT with the all convective cooled turbine having the next best horsepower output and the film cooled turbine showing the lowest horsepower payoff at a given TIT. Table III-1 lists the turbine parameters which influence the horsepower output of the turbine and explains the differences between the three turbine horsepower levels.

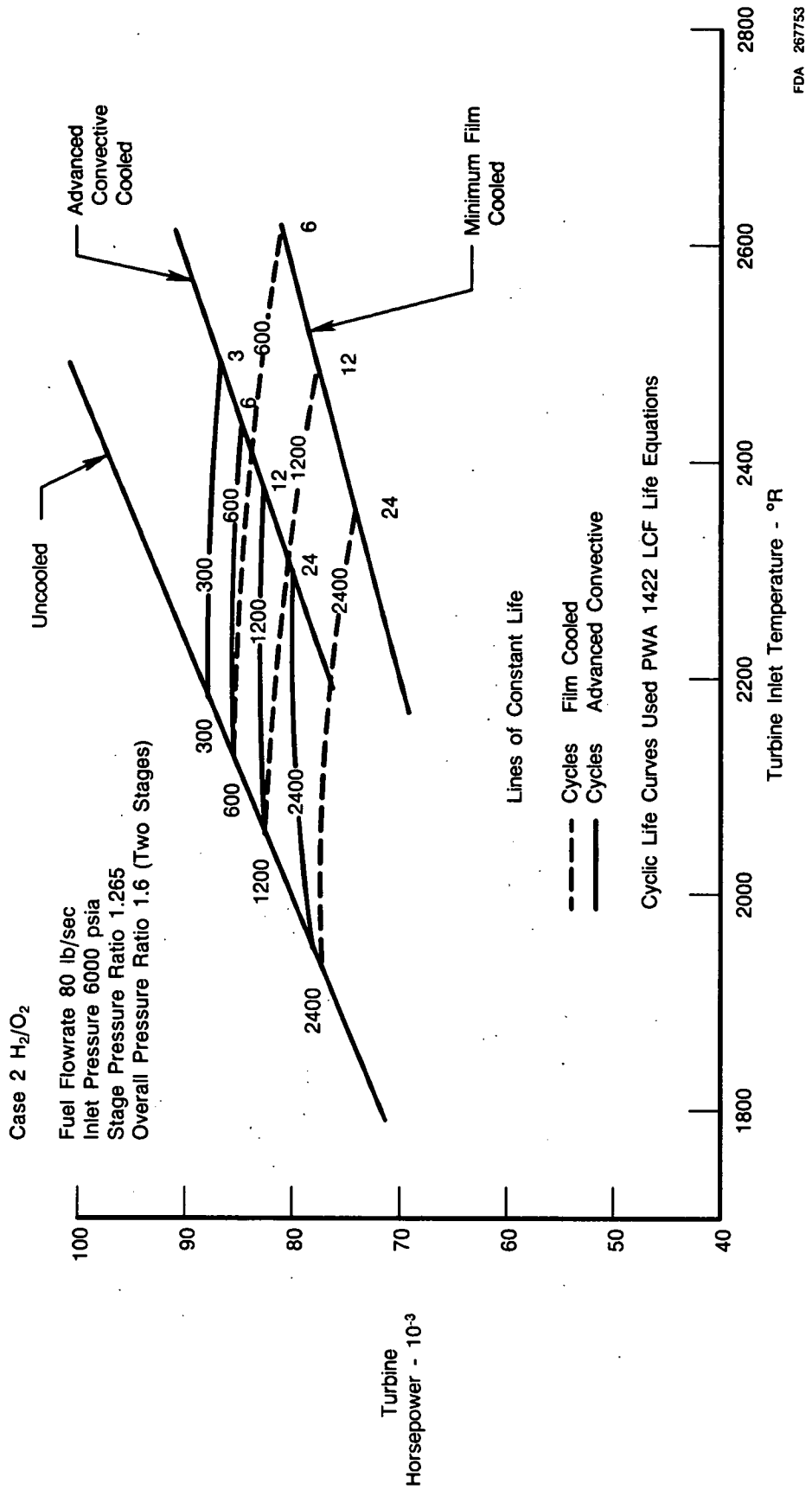


Figure III-5. ATS Case 2 H_2/O_2 Delivered Turbine Horsepower versus Turbine Inlet Temperature

Table III-1. Turbine Parameters for Case 2 at 2200°R Turbine Inlet Temperature

	<i>Uncooled</i>	<i>Convective Cooled</i>	<i>Film Cooled</i>
Horsepower	88,200	76,600	70,000
\dot{W} Blade (lb/sec)*	150	139	134
T Mixed (°R)*	2,200	2,155	2,140
Efficiency (%)	82.5	77.5	75.3

* Mainstream flow and temperature into 1st-stage blade that is available to do work.

4041C

Basically, the less coolant that is used in a turbine, the higher its efficiency and the more flow there is to do work; consequently, the more horsepower it can deliver.

The horsepower output of the turbine is only one consideration; the other consideration is turbine life. The comparison of the horsepower output of a cooled versus an uncooled turbine should be done at a constant life level. The following conclusions are drawn by using the lines of constant life when comparing overall turbine capability.

As shown in Figure III-5, the advanced convective cooled turbine offers an advantage over the film cooled turbine. For example, for a 2400 cycle life, the advanced convectively cooled turbine can obtain 80,000 horsepower at 2315°R TIT, which is a 4% gain over the uncooled turbine. For the same life, the film cooled turbine could obtain 74,000 horsepower at 2350°R TIT which is a 4% decrease over the uncooled turbine.

For the high TIT levels (2400°R) and for lower cyclic life, the advanced convectively cooled turbine shows no horsepower gain over the uncooled turbine. It should be noted that the uncooled turbine blades were optimized in this study to reduce transient thermal strains and thus should provide greater life than the current space shuttle hardware, and that an optimized advanced cooled turbine could give a greater than 4% performance gain over current space shuttle main engine (SSME) hardware.

The low cycle fatigue (LCF) life curves shown in Figure III-5 were calculated using an equation which is a function of strain range and metal temperature. The initial study (i.e., first phase of the program) used a curve of LCF life versus strain range which was not temperature dependent. This modification will make the LCF lives in Figure III-5 more accurate.

2. Task 1 — Subtask 102, Case 3 Analysis Methane

In Case 3, the fuel used was methane with a 280 pounds/second flow. The turbine horsepower delivered versus TIT curves for Case 3 (methane) are shown in Figure III-6. The three labeled curves are for an uncooled turbine, an advanced convectively cooled turbine using 4% of inlet flow for airfoil cooling, and a film cooled turbine using 12% of inlet flow for airfoil cooling.

If life considerations are ignored, the uncooled turbine would show the highest horsepower output versus TIT, with the all convective cooled turbine having the next best horsepower output and the film cooled turbine showing the lowest horsepower payoff at a given TIT. Table III-2 lists the turbine parameters which influence the horsepower output of the turbine and explains the differences between the three turbine horsepower levels.

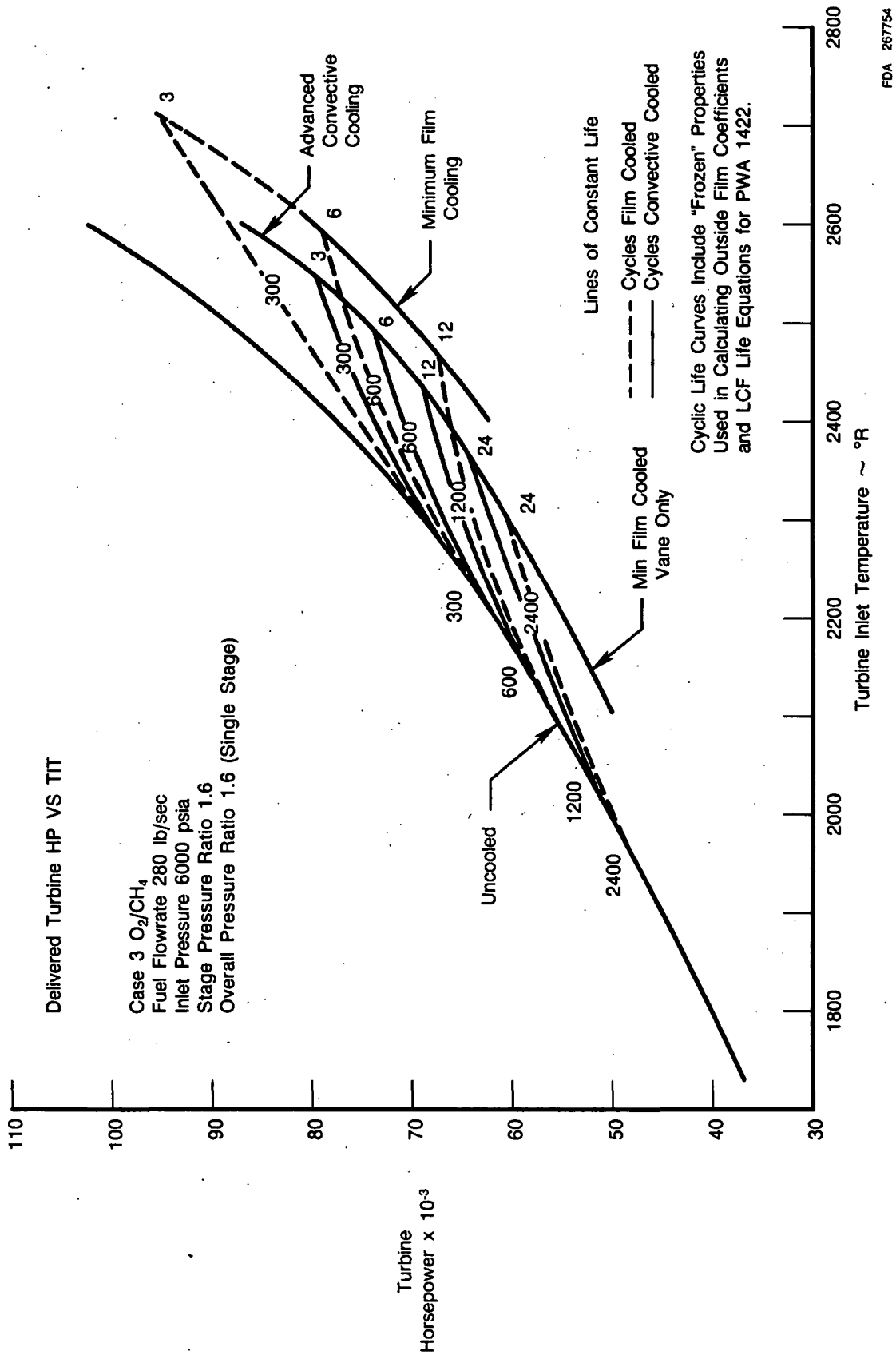


Figure III-6. ATS Case 3 O_2/CH_4 Delivered Turbine Horsepower versus Turbine Inlet Temperature

Table III-2. Turbine Parameters for Case 3 at 2600°R Turbine Inlet Temperature

	Uncooled	Convective Cooled	Film Cooled
Horsepower	102,100	86,740	80,130
\dot{W} Blade (lb/sec)*	505	466	453
T Mixed (°R)*	2,600	2,551	2,454
Efficiency (%)	85.5	80.5	79.0

* Mainstream flow and temperature into 1st-stage blade that is available to do work.

4041C

Basically, the less coolant that is used in a turbine the higher its efficiency and the more flow there is to do work; consequently, the more horsepower it can deliver.

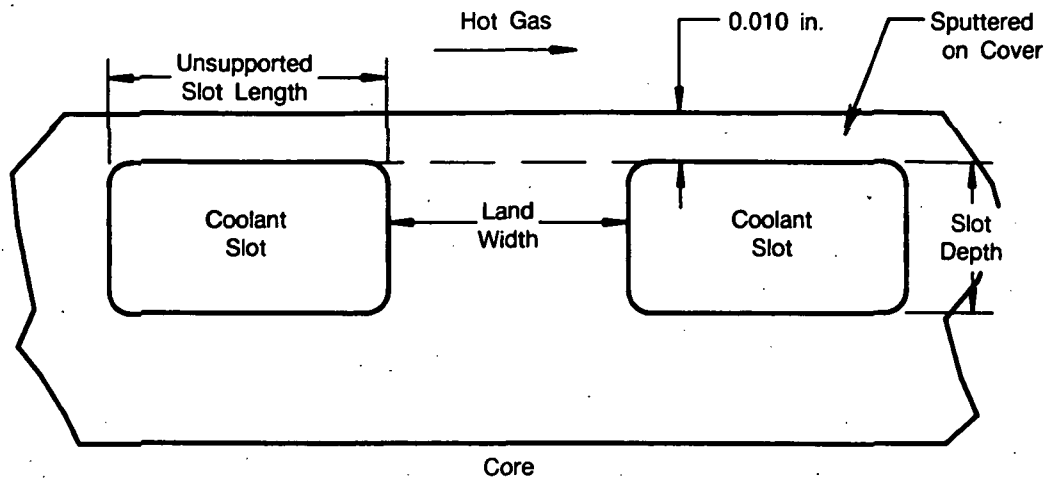
The horsepower output of the turbine is only one consideration; the other consideration is turbine life. The comparison of the horsepower output of a cooled versus an uncooled turbine should be done at a constant life level. The following conclusions are drawn by using the lines of constant life when comparing turbine capability.

The payoff for cooling is much greater with the methane cycle than for the hydrogen cycle. For example, for a 1200 cycle life, the advanced convectively cooled turbine can deliver 69,000 horsepower at 2440°R TIT, and the film cooled turbine delivers 52,500 horsepower. This is a 31% increase over an uncooled blade with convective cooling and a 28% increase over an uncooled blade with film cooling. At 2500°R TIT, the film cooled turbine offers more advantage than the convectively cooled turbine.

The outside film coefficients used in the life analysis of the methane turbine presented above, were modeled using frozen combustion products for methane. These should provide a more accurate assessment of the turbine environment. This change accounts for the differences in the shape of the lines of constant life on the horsepower versus TIT curve, when compared to the information presented in the final report of the first phase of the Advanced Turbine Study (FR-15978, dated 12 April 1982, Figure 2.5-3).

B. TASK 2 — SUBTASK 201, SPECIMEN DESIGN

The advanced convective cooling concept investigated in this program is specially suited for high-pressure, high-temperature rocket turbine vanes and blades. This concept consists of a turbine airfoil in which cooling channels (grooves) are machined into the exterior surface. The grooves are temporarily filled with a removable filler and the entire airfoil is covered with a thin layer of electroplated or sputtered nickel alloy. The filler is then removed. The low thermal resistance of the thin, high conductivity layer allows the hot side wall temperature to be significantly reduced by minimizing the gradient through the wall. A typical cross section of a cooled blade wall is shown in Figure III-7. The advantage of this scheme is that the cooling passages are located close to the hot side wall, thus minimizing the thermal gradient and providing better hot side wall cooling. This causes the majority of the wall to run very cool and provide adequate strength to carry gas bending and centrifugal loads.



FDA 301918

Figure III-7. Typical Section of Cooled Blade Wall

Early in the program, preference was given to electroplating over sputtering as a method of fabricating the thin conductive layer around the airfoil. The reasons for this were the simplicity and the lower cost of electroplating as compared to sputtering.

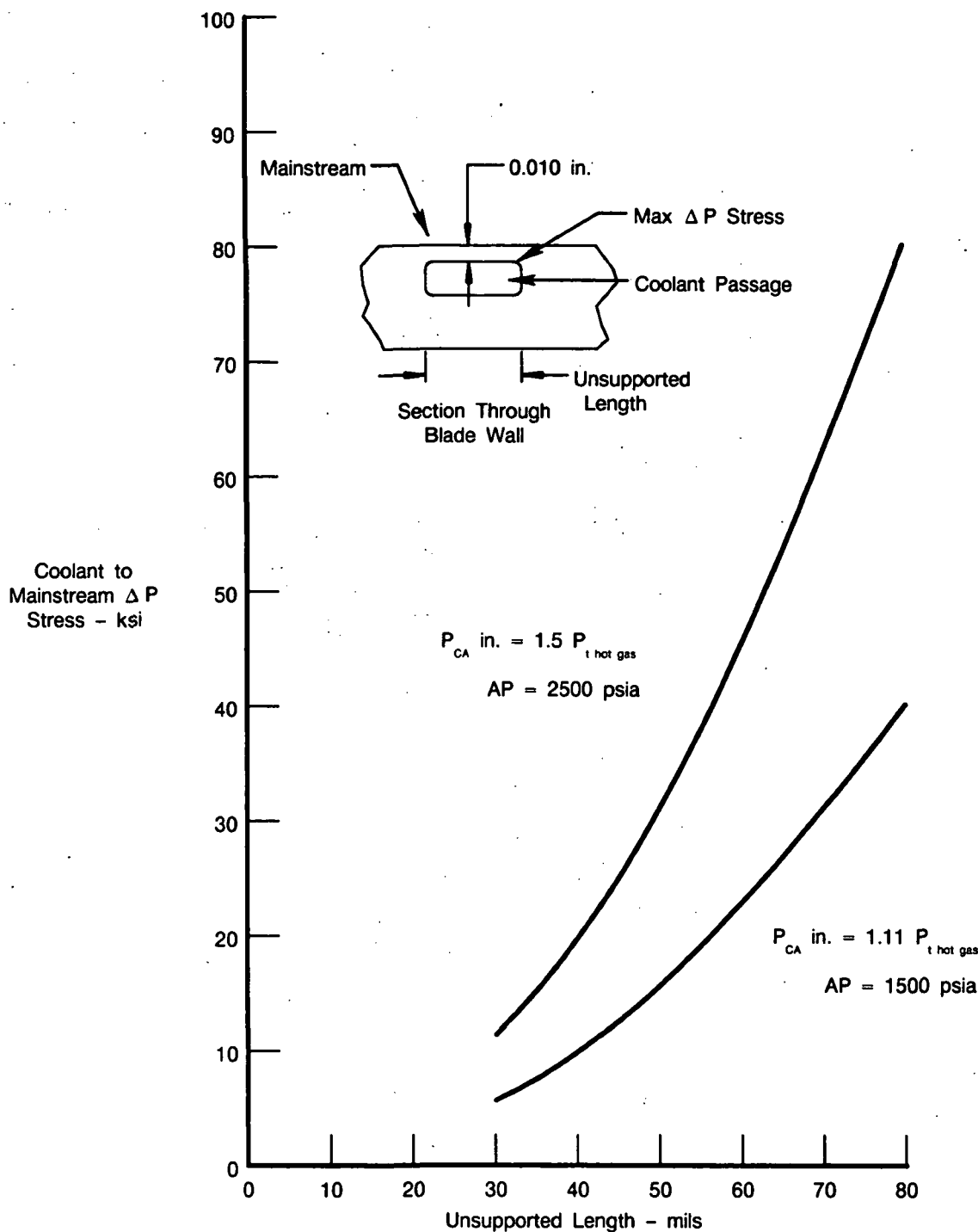
It was determined that an advanced turbine blade alloy would have to be used as a coolant-groove cover layer, since analysis showed that pure nickel (the original choice for the cover layer material) did not have the necessary strength at the required temperatures to withstand the operating loads (See the Material Selection, Section B.1 for details). This rendered electroplating unacceptable. The limitation of electroplating is that it can only be used to plate pure elements or elements that are very close in the galvanic series scale (like cobalt and nickel).

The chosen method of deposition of the cover layer is sputtering. The sputtering technique is a high energy deposition which provides a chemical bond with the bonding lands on the blade. This process has been used successfully to deposit different alloys on turbine airfoils.

Sputter deposition is accomplished with a system comprised of vacuum pumps and gages, power supplies, and specifically designed electrodes; all of these parts are collectively referred to as "deposition geometry." For this program, the deposition geometry shown in Figure III-8 was used. The parts were rotated in coaxial alignment with a cylindrical target in the water-cooled sleeve. Solenoid coils surround the deposition geometry and its vacuum housing to provide a magnetic field, which provides an additional control on ion-current density in the system.

A clean part is installed in the system and the system pumped to ultrahigh vacuum (less than 10^{-6} torr). A rare gas, krypton for this program, is bled into the system to bring system pressure to the 10^{-3} torr range. A gas flow at constant pressure is maintained with a leak valve and throttled vacuum pumps. Several modes of gaseous electrical discharge can be established to effect sputter cleaning, rapid deposition rate, etc., as required. For example, in the triode mode a plasma is established in the region between the filaments and anode. When a high negative voltage is applied to the target, ions are accelerated from the plasma. The accelerated ion has sufficient energy to eject or "sputter" atoms from the target surface. The ejected atoms travel at high speeds and impact the substrate surface where they accumulate to buildup a cover layer. The substrate receives a considerable amount of electron bombardment in the triode mode, which causes the part to heatup. This heatup can be minimized by operating in an inverted

elevated temperature oxygen and water vapor environment and lack of experience in manufacturing hollow airfoil shapes with this material. The search for an acceptable material was switched to the typical cast alloys used in turbine airfoils.



FDA 301919

Figure III-9. Stress in Cover Due to Coolant to Mainstream Pressure Differential in Rig

The final selection of the material was based on NASA Report TND-8071, October 1975, "Comparative Thermal Fatigue Resistance of Twenty-Six Nickel and Cobalt-Base Alloys." The alloys were thermally shocked in a fluidized bed. A summary of the results is provided in Figure III-10. Since the sputtering process of applying the cover gives an equiaxed grain structure, the material selection for the cover was limited to equiaxed materials. Since the strains in the remainder of the airfoil are lower than in the cover layer, as shown in Figure III-11, it is reasonable to also select an equiaxed material for the airfoil. Also, a better bond might result by using the same material and grain structure for both the cover layer and the airfoil.

The best equiaxed material was B1900 + Hf (Reference Figure III-10). However, P&W experience with cast, production airfoils made of B1900 + Hf is that shrinkage porosity is encountered in cluster areas. This causes material weaknesses which severely degrade the material properties. Thus, instead of B1900 + Hf, a similar alloy Mar-M 247 (PWA 1447) was selected for the ATS blade and cover layer materials. A comparison of the chemical compositions of the two nickel alloys is presented in Figure III-12. The castability of Mar-M 247 in solid and hollow parts is excellent and clustered porosity is not evident. The alloy Mar-M 247 has equal to, or superior, thermomechanical fatigue properties when compared to B1900 + Hf. Thus, P&W feels that Mar-M 247 will provide a distinct advantage over B1900 + Hf for the ATS program.

An attempt was made to procure and test two sets of fluidized bed test samples (i.e., the two top materials identified in the study). Quotes were requested from vendors, and the impact to the program was investigated. The investigation showed that it would have been too costly and out of the program scope. Also, because of the lead times involved for the material procurement and manufacturing of the blades for the SSME Blade Tester, a decision on the blade material had to be made before the fluidized bed test results became available. For these reasons, it was decided that it was not feasible to pursue the two top materials; the decision was made to continue the program within its original scope using Mar-M 247 (PWA 1447), the best material choice.

2. Coolant Geometry Determination

In order to select the optimum coolant groove-land geometry combination, analytically chosen coolant geometries would be machined on the outer diameter (OD) surfaces of cast test cylinders. The grooves would then be filled and the cylinders covered with the thin conductive nickel alloy layer. Upon removing the filler material, the cylinder would be subjected to thermal cycling in a fluidized bed test. These test results would then be used to select the optimum coolant groove-land geometry combination.

To help select the coolant groove-land geometry, an analytical study was conducted at elevated temperature engine conditions. The study varied the distances between coolant passages (land widths) and determined the maximum metal temperature. The results of the study are shown in Figure III-13. Land width must be minimized by selecting the smallest land that can provide a structurally adequate bond plane. A small land will minimize the maximum metal temperature encountered on the foil hot surface.

A separate study was also performed to evaluate the effects of coolant-to-mainstream pressure differential on coolant groove width. As shown in Figure III-9, large groove widths will result in very large stresses in the blade cover layer.

FDA 301920

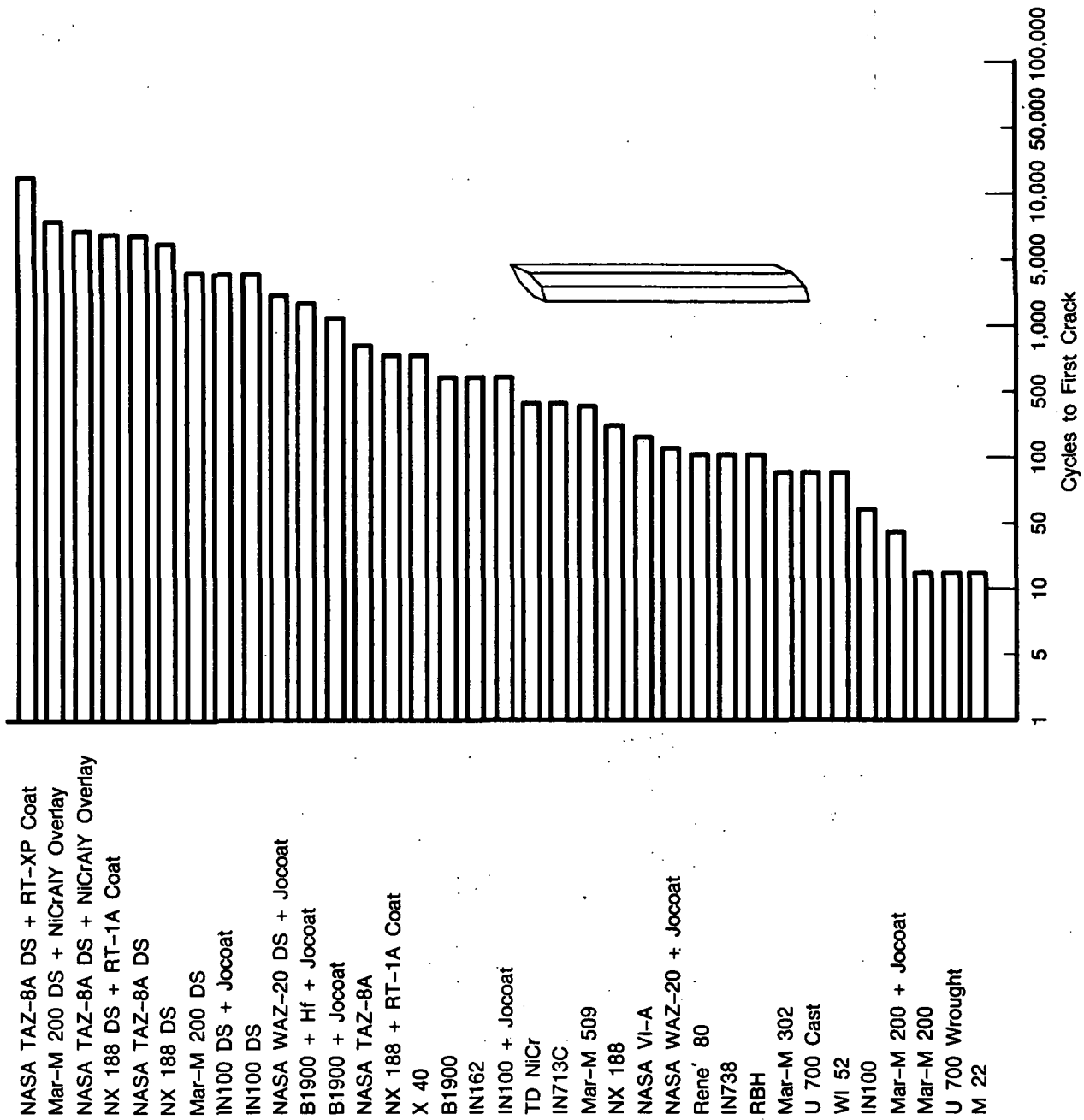
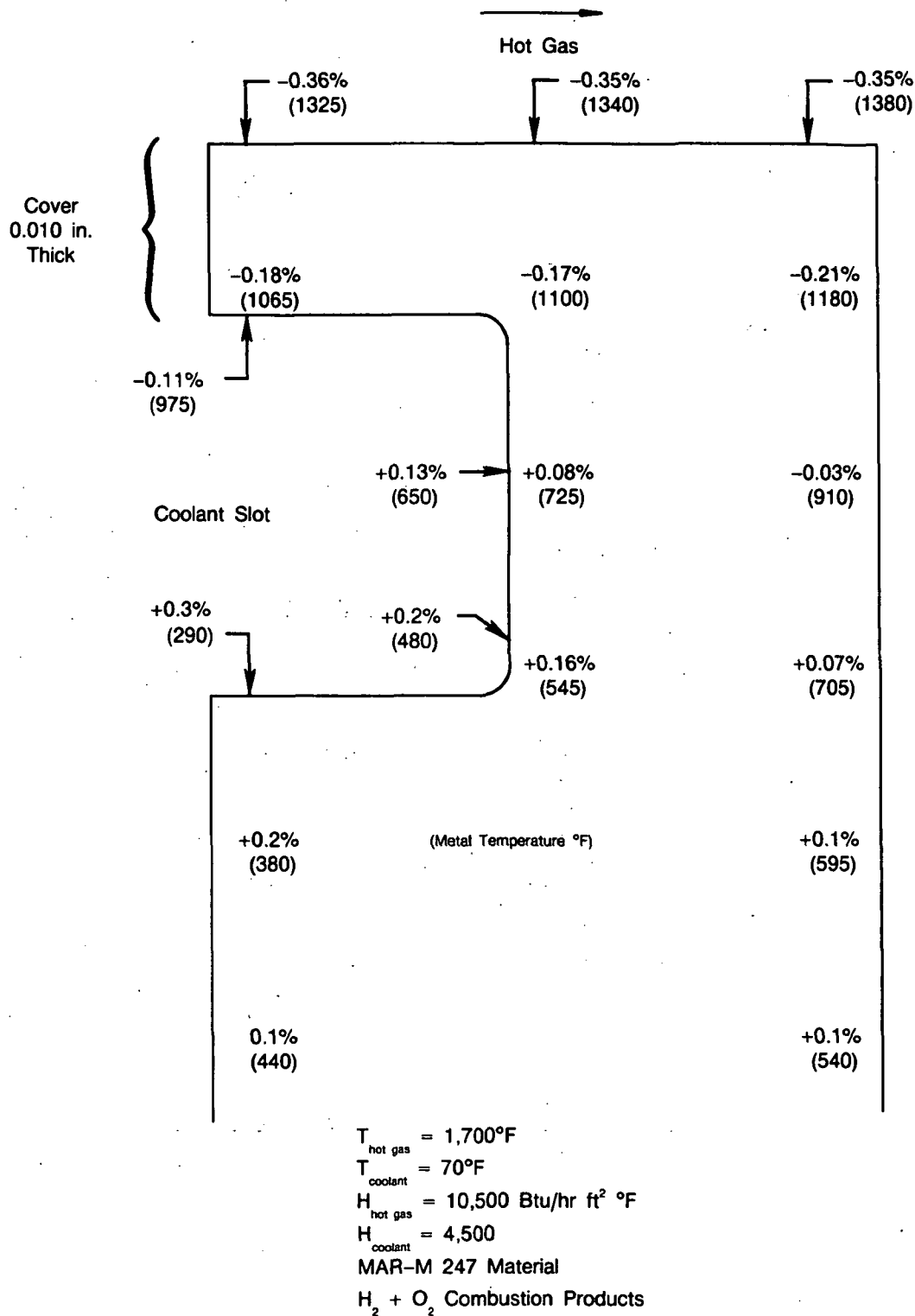


Figure III-10. Comparative Thermal Fatigue Resistance (Bed Temperatures, 1088 and 316°C (1990 and 600°F), With a Three-Minute Immersion in Each Bed)



FDA 301921

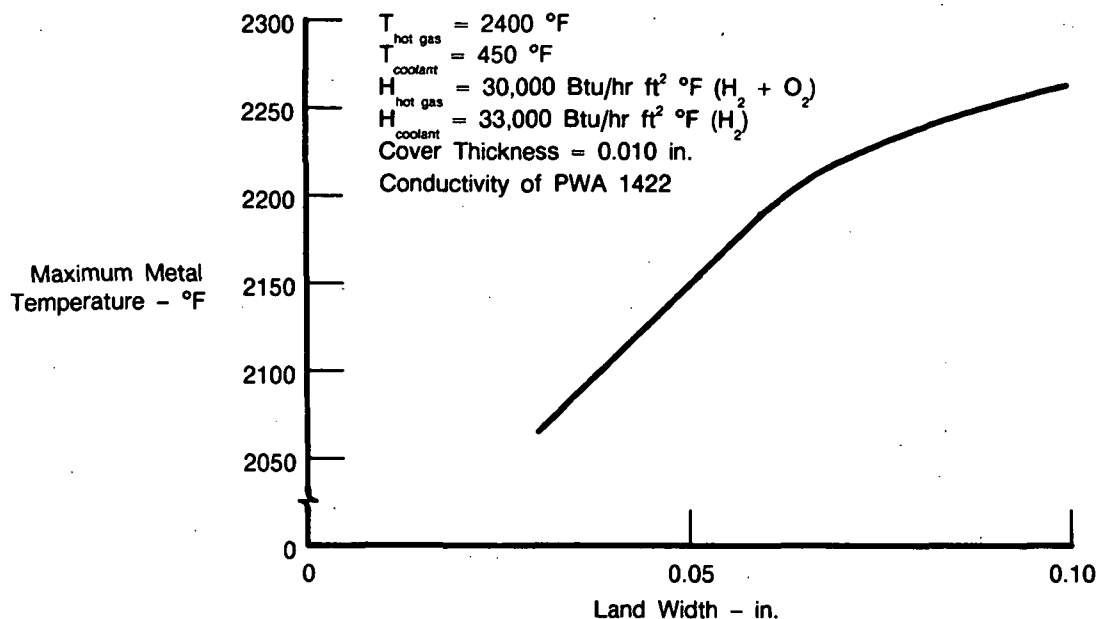
Figure III-11. Thermal Strains in Cooled Blade at Steady-State Rig Condition

	Ni	Cr	Co	Ti	Al	Mo	C	W	Ta	Hf
Mar-M 247	R	8.4	10.0	1.05	5.5	0.65	0.15	10.0	3.05	1.4
B1900 + Hf	R	8.0	10.0	1.0	6.0	6.0	0.11	0	4.25	1.15

R = Remainder

FDA 301922

Figure III-12. Chemical Composition Comparison

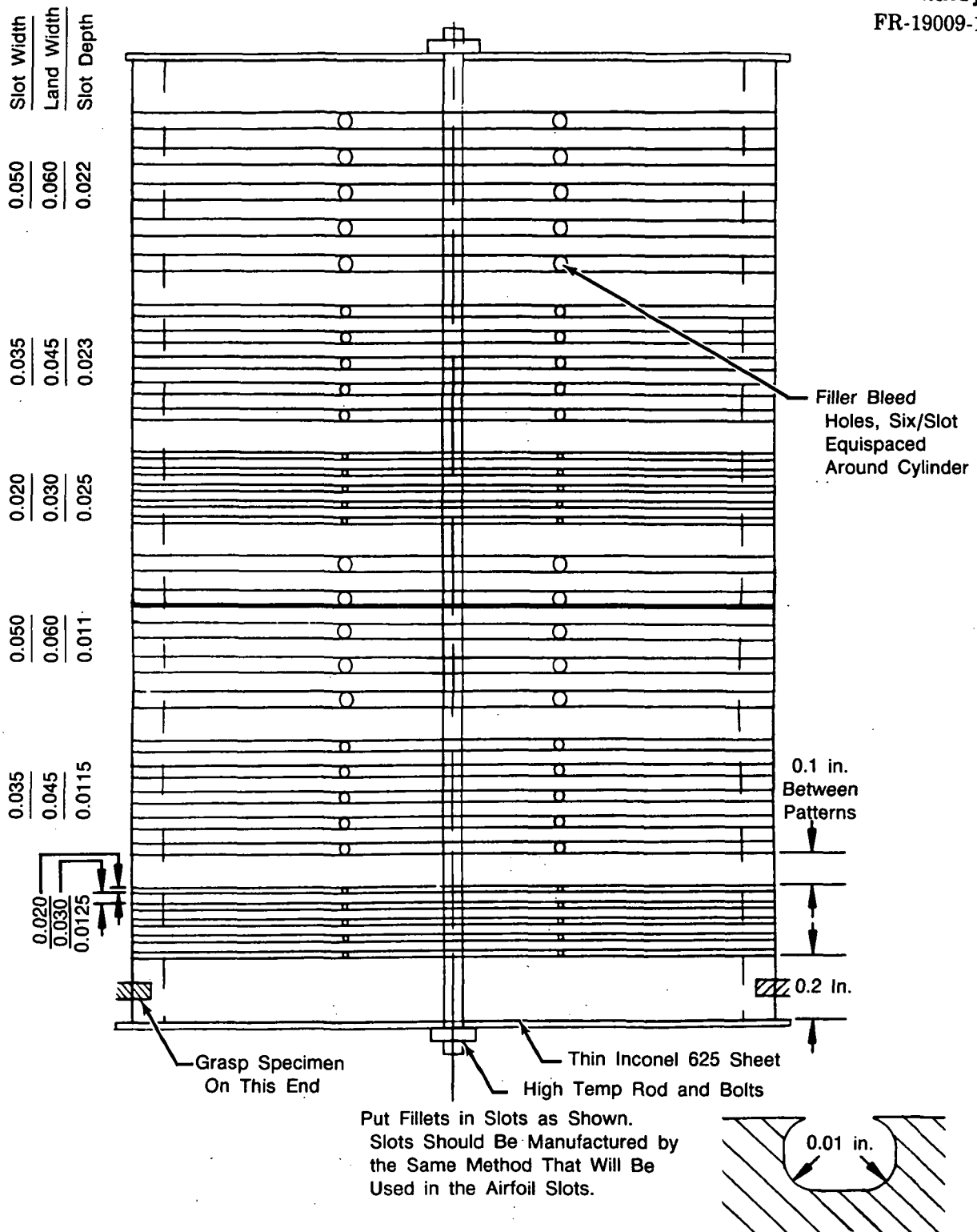


FDA 301924

Figure III-13. Maximum Metal Temperature versus Land Width for Advanced Engine Conditions, $\text{H}_2 + \text{O}_2$ Propellants

Based on these studies, six coolant groove-land geometry combinations were selected to be tested in the fluidized bed test. The groove patterns chosen covered the useful range of groove depth, groove width, and land width combinations. The maximum groove width was set at 0.05 inch. Larger groove widths would result in very high stresses due to the coolant-to-mainstream pressure differential. Two groove depths were selected, a shallow groove (0.011 to 0.012 inch) and a deeper one (0.022 to 0.025 inch). Very shallow grooves would be impractical, since manufacturing tolerances would cause wide variations in coolant flow area. Very deep grooves would be impractical because they would seriously reduce the load carrying cross sectional area of the airfoil. Land widths of 0.030, 0.045, and 0.060 inches were selected. Smaller land widths would provide too little space for a good bond with the sputtered cover. Larger land widths would reduce the cooling in the center of the land sections due to the longer conduction paths to the coolant passage.

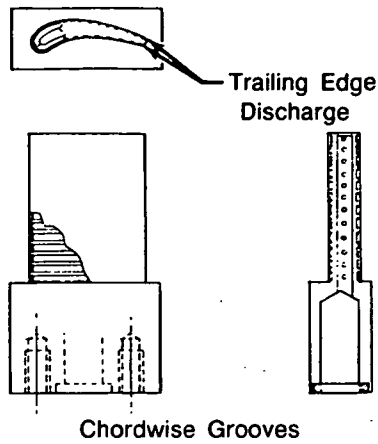
Figure III-14 shows the six selected coolant groove land geometry combinations and illustrates the fluidized bed test specimen assembly. The coolant grooves run perpendicular to the test cylinder centerline and around its circumference. Each groove has six equally spaced holes of the same diameter as the groove width. These holes will be used to leach the filler material after the closeout layer has been applied to the cylinder.



FD 253258

Figure III-14. Advanced Turbine Study Fluidized Bed Specimen

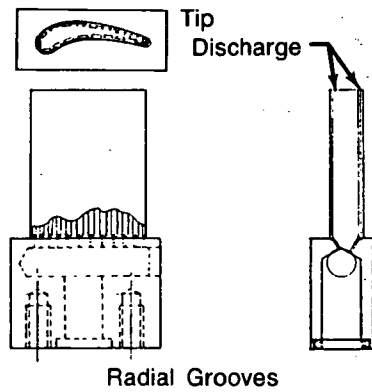
As shown in Figure III-14, the coolant grooves run circumferentially (chordwise in an airfoil) around the test cylinder rather than longitudinally (radially in an airfoil) as originally proposed. This was the result of a study conducted in which four coolant groove paths were evaluated. The different groove paths, their advantages and disadvantages are illustrated in Figure III-15.

**Advantages**

1. Rupture of Local Cover Does Not Affect All Coolant Passages.
2. Coolant Dump Pressure Known at Trailing Edge.
3. Coolant Feed Path Similar to Existing Successful Designs.

Disadvantages

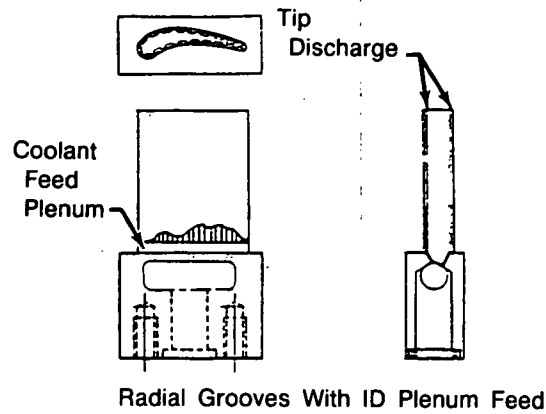
1. Grooves Are Perpendicular to Pull Stress. Deep Grooves Would Reduce Pull Load Carrying Area. Manufacturing Limitations Will Be Determined for Groove Depth.

**Advantages**

1. Grooves in Direction of Pull Stress.
2. Rupture of Any Cover Does Not Affect the Rest of Passages.

Disadvantages

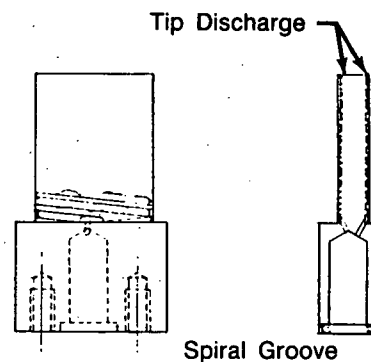
1. Multi-Feed Holes in High Stress ID Region
2. Coolant Dump Pressure Not Accurately Known.
3. Trailing Edge May Be Difficult To Cool.

**Advantages**

1. Grooves in Direction of Pull Stress.
2. Need Only a Few Coolant Feed Holes in High Stress ID Region.

Disadvantages

1. Coolant Dump Pressure Not Accurately Known
2. Rupture of Cover Over ID Plenum Would Rob All Radial Passages.
3. Large Plenum at ID Would Minimize Pull Load Carrying Area.

**Advantages**

1. High Velocity, High Coolant Film Coefficient Due to Small Coolant Flow Area.
2. Need for Only One Coolant Feed Hole in High Stress ID Region.

Disadvantages

1. Rupture of Cover Anywhere Robs All Coolant Downstream.
2. Coolant Groove Depth Has To Be Large in Order to Keep Coolant Pressure Drop Reasonable.
3. Coolant Dump Pressure Not Accurately Known.

Figure III-15. Groove Paths Considered

FD 301925

C. TASK 2 — SUBTASK 202, SPECIMEN FABRICATION

Six cast PWA 1447 fluidized bed test cylinders were procured from the Howmet Dover casting facilities. The cylinders were approximately 3 inches long by 2 inches in diameter and hollow with a wall thickness of approximately 0.200 inch. Upon being received at P&W, the cylinders were machined to 1.950 ± 0.001 inch outside diameter and a wall thickness of 0.200 ± 0.005 inch.

On a production basis the coolant grooves would be cast as part of the casting process of the turbine airfoil. Cast-in grooves should be of high quality and cost effective for larger quantities, but the cost of die making made it prohibitive for this project.

Because of these reasons, an investigation was undertaken to determine the optimum method of incorporating the grooves in the fluidized bed test cylinders and the blades. The investigation results indicated that machining was the optimum way of incorporating the grooves in the cylinders. Three different methods of incorporating the grooves were investigated: two chemical milling methods using different masks and a machining method. These methods are outlined below.

- *Chemically Milled Groove No. 1*

The groove was chemically milled using PS 249 nickel-base chemical milling solution at 130°F. The maskant used was Turcoform 522 (PMC 1779) chemical milling maskant. The maskant was applied by brushing three separate thin coats on the cylinder and drying between each application. The groove was made manually by carefully cutting the maskant away with a razor blade. Although the maskant was removed fairly uniformly, when the piece was placed in the chemical milling solution the maskant loosened in various areas and produced a jagged channel 0.024 inch deep in 150 minutes (Figures III-16 and III-17).

- *Chemically Milled Groove No. 2*

The groove was chemically milled, using PS 249 chemical milling solution and Tuffil epoxy as the maskant. The Tuffil, which is the consistency of putty, was very difficult to apply in a uniformly thin manner. The uniformly thin layer was desired in order to keep the eccentricity to a minimum after using an 0.020 inch wide cutter to machine the Tuffil from the base material. The piece then was chemically milled for 150 minutes, producing a groove 0.028 to 0.055 inch wide and 0.013 to 0.025 inch deep. Next, the excess Tuffil was machined away and the piece was immersed in a heavy duty 20% potassium hydroxide solution at 200°F to remove the remainder (Figures III-18 and III-19).

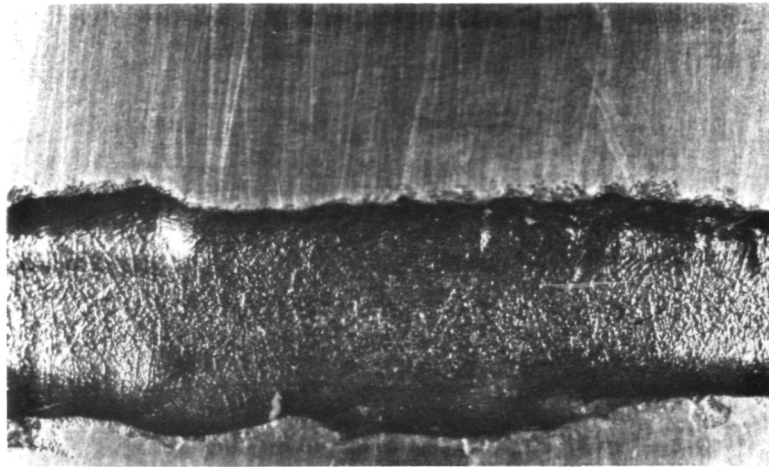
- *Machined Groove*

The first groove was machined using the Monarch NC Machining Center. The cutter was a solid carbide four-toothed side-cutting milling cutter 0.050 inch thick, intended to produce an 0.050 inch wide channel. The first pass, 0.011 inch deep, was machined at 1182 rpm and 1.5 inches per minute feed. This produced no appreciable wear on the cutter, so another 0.011 inch deep identical pass was made into the same groove. (This resulted in a total depth of channel of 0.022 inch). Another pass was then made into the same groove using a feed of 2 inches per minute. Again, no appreciable wear on the cutter was noted. The last pass was made using a feed of 3 inches per minute without appreciable cutter wear. The final channel was approximately 0.050 inch wide and 0.040 inch deep. The NC tape was prepared by the Computer Aided Machining (CAM) Group. No significant difficulties were encountered machining the alloy, provided that the cutter was solid carbide (Figures III-19 and III-20).

This machining method was chosen because it provided the best dimensional

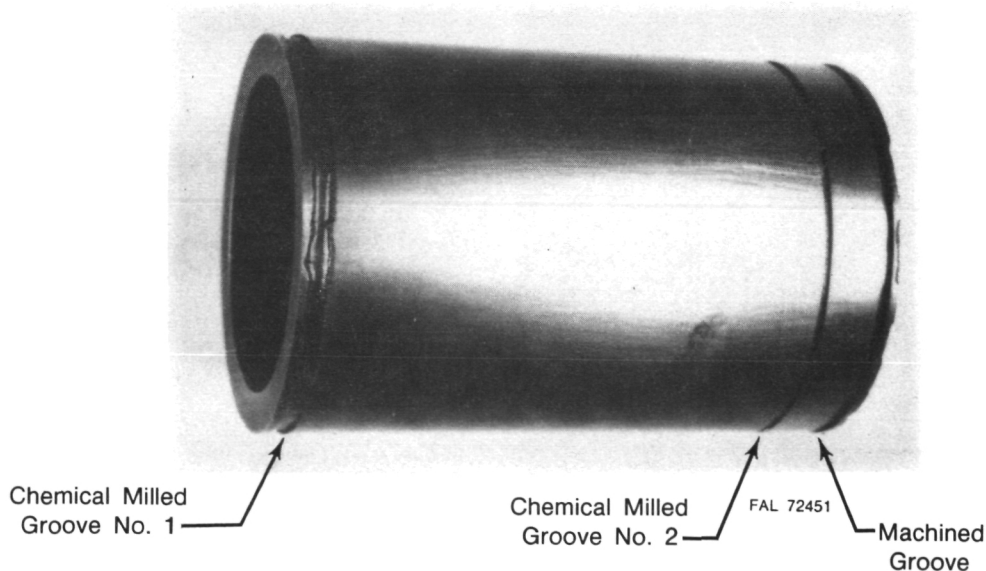
control for the grooves as well as the best groove surface finish, as shown in Table III-3. The comparison of the machined groove to the chemically milled Groove No. 2 is shown in Figure III-21.

After determining the optimum means of incorporating the grooves into the test cylinders, the remaining cylinders were sent to the shop to be machined, as shown in Figure III-14.



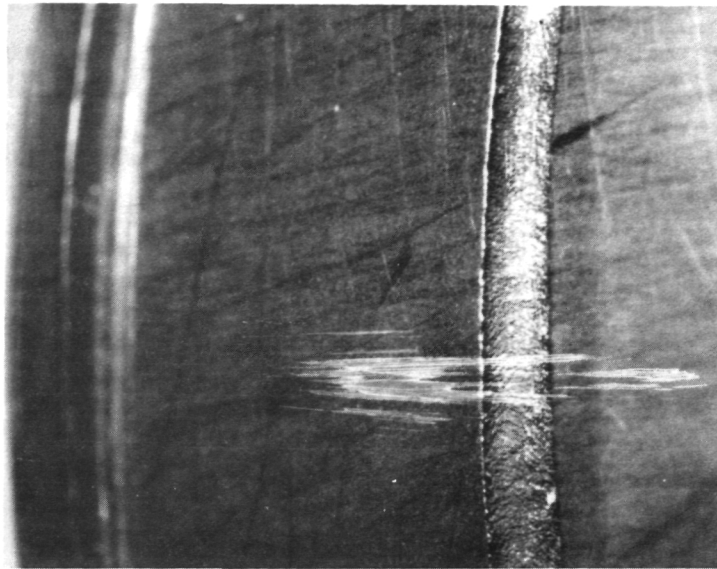
FAL 72575

Figure III-16. Chemically Milled Groove No. 1 Detail (10X)



FD 301932

Figure III-17. Fluidized Bed Test Cylinder — Chemically Milled Groove No. 1 Detail



FAL 72453

Figure III-18. Chemically Milled Groove No. 2 Detail (10X)

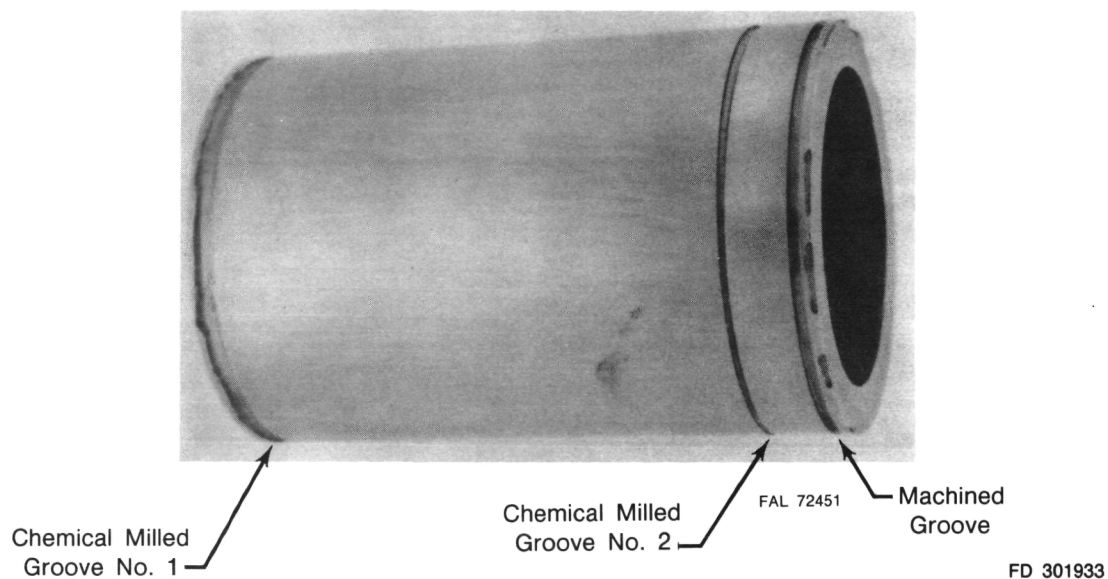
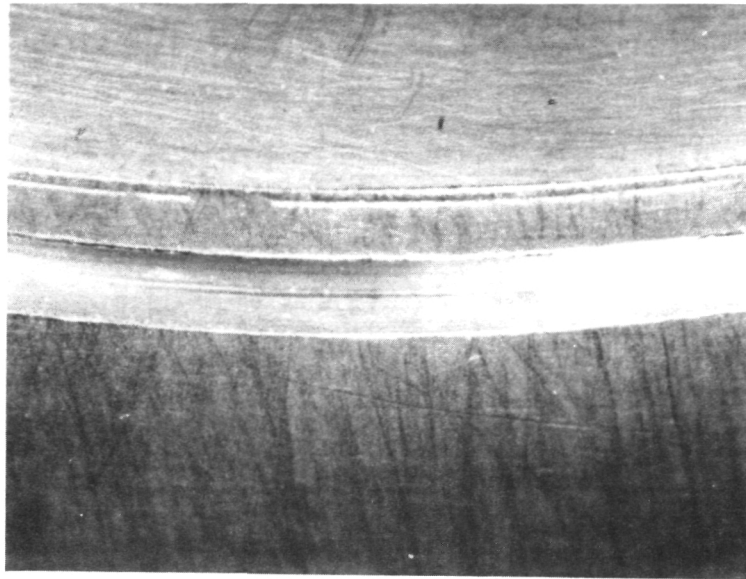


Figure III-19. Fluidized Bed Test Cylinder — Chemically Milled Groove No. 2 and Machined Groove Detail

The finished machined cylinder is shown in Figures III-22 and III-23. The machining of the cylinders was performed using a Monarch NC Machining Center, with an NC tape prepared by the Computer Aided Machining group. Blade cutters 0.020, 0.035, and 0.050 inch thick were tip-ground in-house to provide the necessary tools to cut the bottom of the grooves with the required 0.010 inch fillet radius (reference Figure III-14). The cutting of the grooves proved to be very difficult and time consuming, especially for the 0.020 inch wide grooves. The difficulty was caused by the small grooves dimensions and the tight tolerances required (± 0.0015 inch). Due to the complexity of the job, the machining of the cylinders took longer than estimated. Because of

budgetary reasons, it was decided to cut the number of cylinders to be manufactured from 6 to 4 and eliminate the two sets of 0.020 inch wide slots. The 0.020 inch wide slots were the most difficult to machine and the most time consuming. In addition, experiments performed in the laboratory showed that the 0.020 inch wide slots were also the most difficult to fill. Upon completion of the machining, the cylinders were delivered to the laboratory for the slot filling and sputtering operations.



FAL 72455

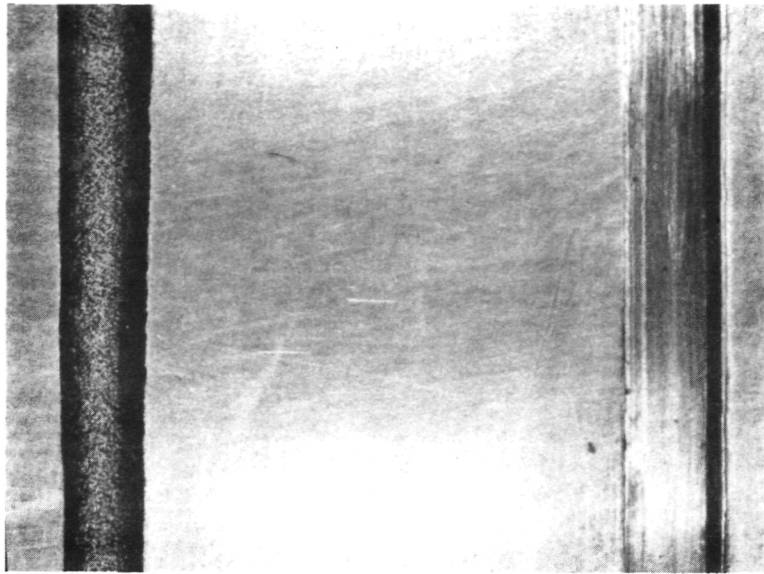
Figure III-20. Machined Groove Detail (10X)

Table III-3. Groove Dimensions Comparison in Fluidized Bed Test Cylinder for Machined Groove and Chemically Milled No. 2 Groove

Location (deg)	Groove Width		Groove Depth	
	Machined Groove (in.)	Chem Milled No. 2 Groove (in.)	Machined Groove (in.)	Chem Milled No. 2 Groove (in.)
0 (top)	0.052	0.047	0.040	0.025
45	0.052	0.055	0.040	0.025
90	0.052	0.042	0.041	0.021
135	0.052	0.039	0.040	0.018
180	0.052	0.034	0.040	0.015
225	0.052	0.032	0.040	0.015
270	0.053	0.028	0.041	0.013
315	0.052	0.034	0.039	0.015

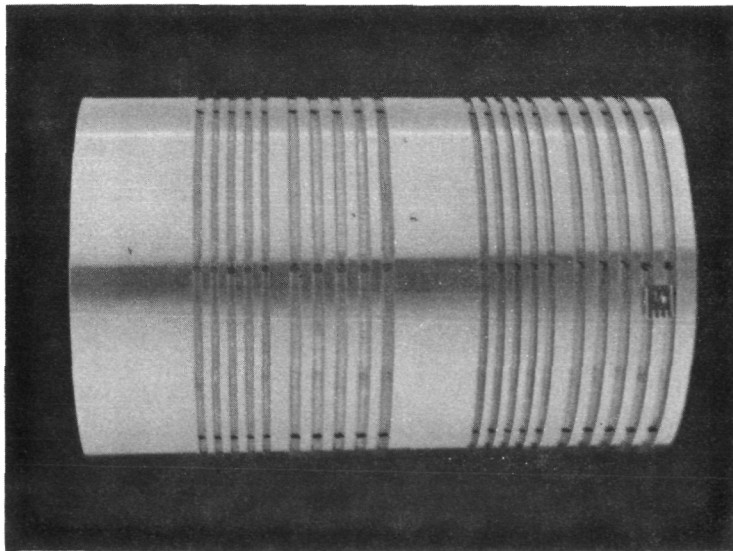
4041C

It is important to point out that the cylinders could have been machined using a lathe, in a much more simple and inexpensive manner. But this process would not have been applicable to machining the blades for the rig, since the blades can not be turned in a lathe. The intent of the cylinder fabrication was to duplicate the fabrication process to be used in the blades and to learn from this experience.



FAL 72452

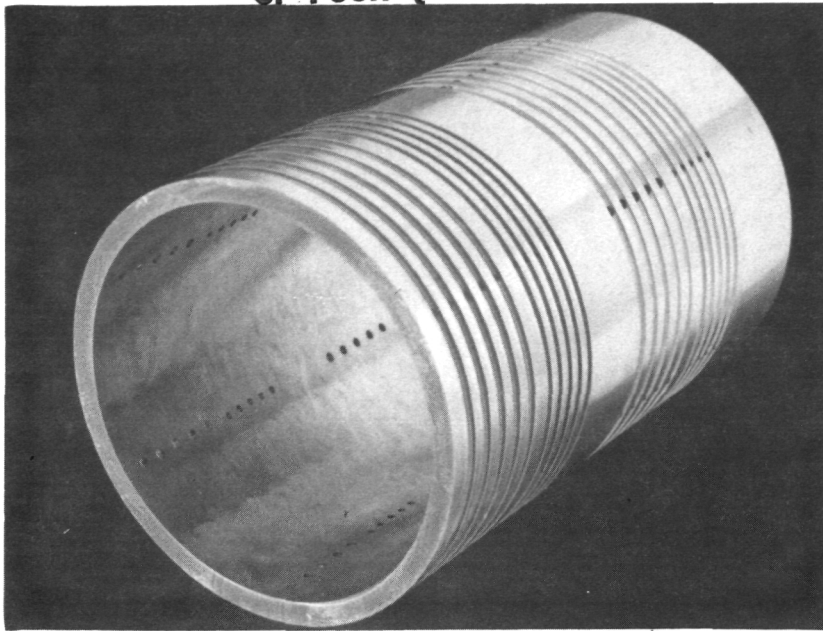
Figure III-21. Comparison of Chemically Milled Groove No. 2 and Machined Groove (10X)



FE 355156

Figure III-22. Finished Machined Cylinder

ORIGINAL PAGE IS
OF POOR QUALITY



FE 355157

Figure III-23. Finished Machined Cylinder

While the cylinders were being machined, laboratory experiments were underway to obtain the best material and method to be used in filling the grooves. Prior to sputtering, three methods of filling the grooves were investigated by using available (this accounts for the different material and diameter) bar stock in which grooves, which closely approximated the test cylinder groove dimensions, were machined by using a lathe. These methods were:

- Aluminum wire was pressed into the groove and made to conform to the groove geometry
- Aluminum was sputtered on the bar to fill the grooves
- A silica base slurry was used to fill the groove.

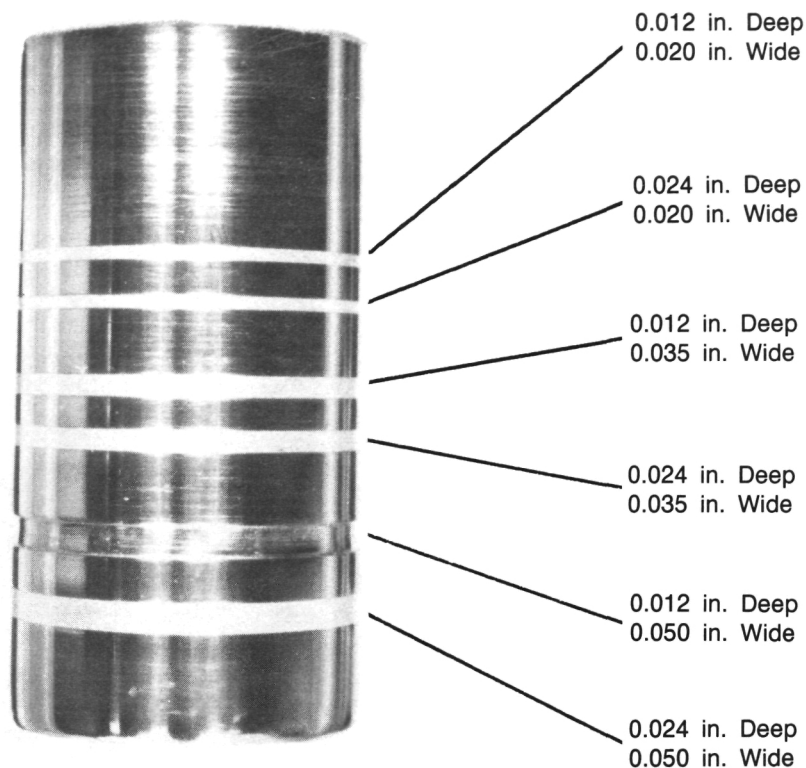
1. Groove Filling Experiments

a. Aluminum Wire

Grooves of the same approximate size as those in the test cylinders were machined (using a lathe) into a 0.625 inch diameter section of PWA 658 (IN100) round bar stock. Aluminum wire (of unknown purity) was used to fill the grooves. A 0.060 inch diameter wire was pounded (lightly beaten into place with a small hammer) into the 0.050 inch wide by 0.024 inch deep groove without difficulty. The wire would not stay in place within the 0.050 inch wide by 0.012 inch deep groove, probably due to lack of side wall area for effective mechanical holding. The 0.060 inch diameter aluminum wire was thinned down to 0.040 inch diameter for filling the 0.035 inch wide grooves and to 0.025 inch diameter for filling the 0.020 inch wide grooves; then, the wire was installed in the grooves by the method described above.

Immersion of the aluminum wire into a 7 molar solution of NaOH proved an effective method of thinning it to any required diameter.

After the grooves were filled with the aluminum wire, the excess aluminum was machined flush with the round bar surface. The whole specimen was then lightly cleaned using 600 grit silicon carbide abrasive paper. Figure III-24 shows the appearance of this specimen after groove filling.



Magnification 3×

FD 301926

*Figure III-24. Aluminum Wires Beat Into Grooves in PWA 658 Round Bar Stock
(Trimmed Back to the Original Surface OD by Lathe and Hand)*

b. Sputtered Aluminum

A second specimen, a PWA 1422 round bar of 0.5 inch diameter, was machined on a metal lathe to produce grooves with the same dimensions as those on the actual cylindrical test specimen. This grooved rod was then coated with sputtered aluminum in a hollow-cathode DC coater.

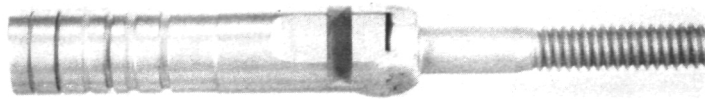
The substrate temperature was kept low, approximately 950°F to avoid melting the aluminum deposit. The coating cycle was allowed to run for 24 hours, which produced an average coating thickness of 31.8 mils. The deposit had a lustrous finish, defect-free to the unaided eye.

After removal from the coater, the substrate was fixtured on the 6 inch lathe and turned back to its original OD, final finishing to remove all aluminum from the OD surface was

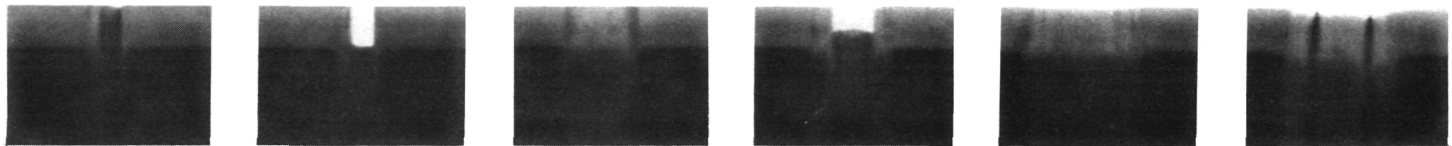
performed using No. 600 grit silicon carbide abrasive paper. The grooves were examined by using a photographic technique to obtain profiles of the sputtered deposits, which were used as models to illustrate the effects of groove dimensions on the filling process. It was observed that the ideal groove from a sputtered deposit viewpoint would be both wide and shallow. In this case, the grooves which filled best were 0.050 inch and 0.035 inch wide by 0.012 inch deep. Figure III-25 shows the PWA 1422 bar before and after groove filling by sputtering and the cross section of the filled-in groove.

PWA 1422
Grooved Rig Bar

Prior to Coating
With Aluminum



Aluminum Deposit Profiles



0.012 in. Deep
0.020 in. Wide

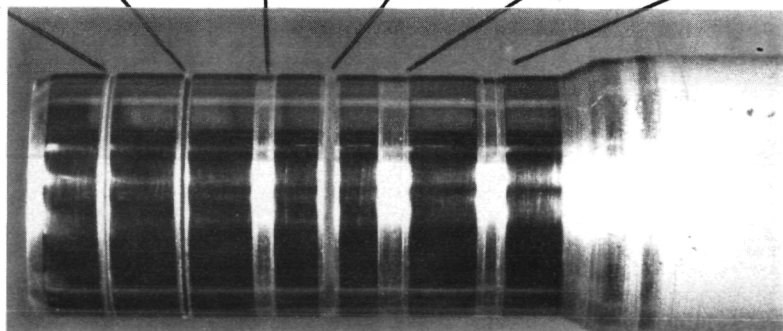
0.024 in. Deep
0.020 in. Wide

0.012 in. Deep
0.035 in. Wide

0.024 in. Deep
0.035 in. Wide

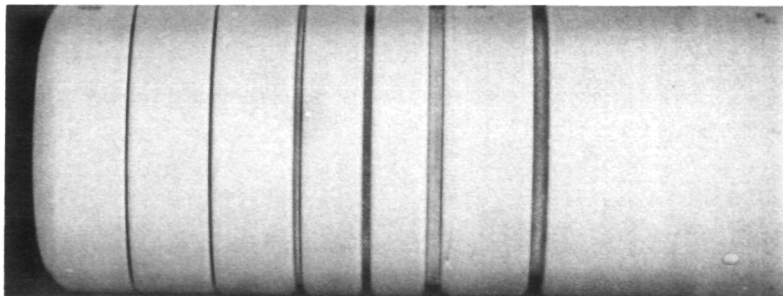
0.012 in. Deep
0.050 in. Wide

0.024 in. Deep
0.050 in. Wide



Aluminum Deposit
Machined Back
to Original Rig
Bar Surface

Mag 3×



Run 5-83-002

Sputtered Aluminum on
PWA 1422 Rig Bar

As Coated

Mag 3×

FD 301927

Figure III-25. Sputter-Filled Groove in PWA 1422 Bar

c. Silica Base Slurry

A third specimen was machined in the lathe out of 0.625 inch diameter PWA 658 round bar stock. A slurry of high porosity fused silicon with a colloidal silica (30% SiO₂) binder was forced into the grooves machined in the specimen. After air drying for one hour, the specimen was heated for 30 minutes to drive off excess moisture, then baked at 600°F for one hour.

Examination of the cured filler material in the grooves showed no separation between the filler and the groove side wall and no serious shrinkage related problems in the filler. Figure III-26 shows the PWA 658 grooved specimen in stages of filling. Figure III-27 illustrates one of the grooves filled with the silica and cured for one hour at 600°F.

2. NaOH Leaching of Aluminum (99.99%) and Silica Fillers

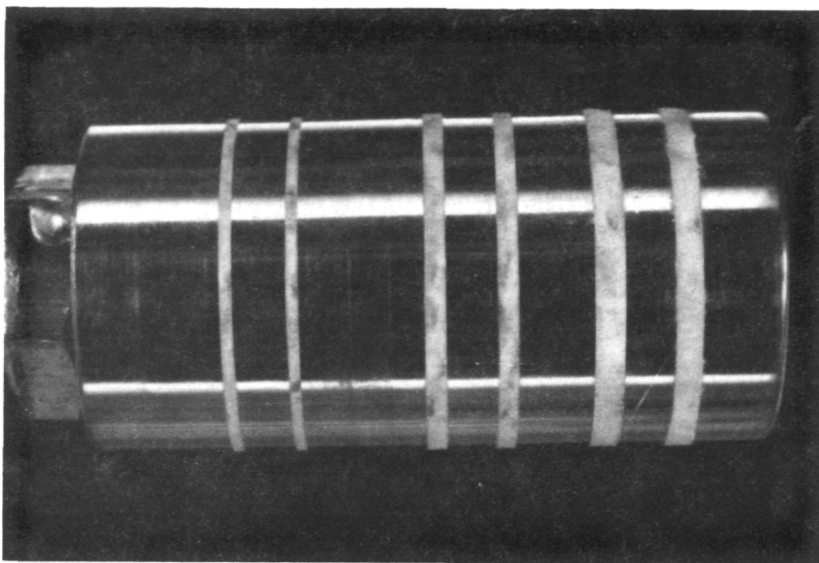
The criteria for a successful filler material indicates that it not only has to be applied to fill the grooves, but it also must be removed after the sputtering operation has taken place. With this in mind, it was decided to compare the leachability (ability to remove the material by chemical means) of the two materials in question — aluminum and silica base slurry. The results are contained in Table III-4.

The leaching rate of the silica material was determined using a 7 molar NaOH solution with and without ultrasonic cavitation and was compared to the leaching rate of pure aluminum under the same conditions. Figure III-28 is a graph illustrating the relative rates of material removal. It should be noted, however, that this data has been obtained from bulk material which is fully accessible to the NaOH solution. In actual practice, it is expected that the surface area of the filler material actually exposed to the leaching solution will be greatly restricted so that the actual time required to remove a like amount of material may be several orders of magnitude higher.

Based on the faster leaching rates and the more uniform filling coverage in the cylinder's grooves, it was decided to use the silica base slurry as the filling material for the grooves in the fluidized test cylinders and the blades. The one drawback associated with the slurry is that once it is dry, the cylinders must be handled with great care due to the fragility of the cured slurry.

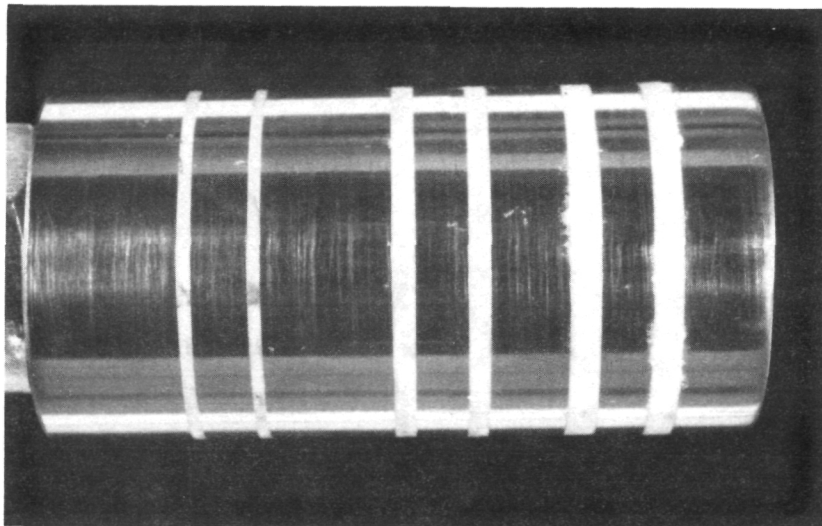
3. Sputtering the Cover

During subsequent handling of the silica-filled grooved specimen, shown in Figure III-26, much of the filler material was jarred loose and lost. With the purpose of obtaining early insight into the effects of sputtering a metallic overlay on the ceramic filler material, this specimen was used as a substrate during initial sputtering cycles required to clean up the new PWA 1447 hollow-cathode targets. The first overlay deposit put on this specimen was sputtered on using magnetic coils around the target OD (outside the chamber walls) which helped maintain a DC diode discharge near the target inner diameter (ID). This, in effect, kept the plasma from heating up the substrate. The coating produced by this scheme is shown in Figure III-29. The deposit had a coarse, cauliflower-like surface, which indicates an open, columnar structure. The grain size over the ceramic filler was several times larger than that over the metal. No bonding (deposit continuity) was shown between the cover on the ceramic and the metal. Any cracks or gaps originally present on the substrate surface were still evident.

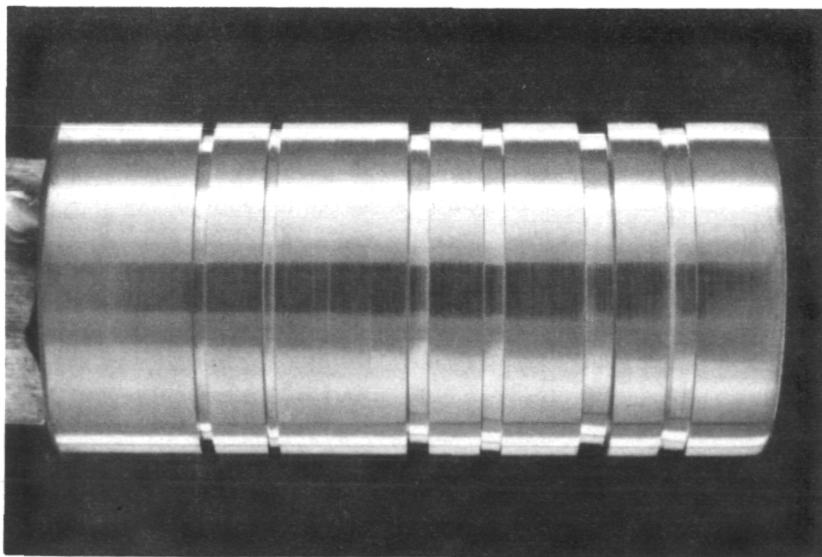


Specimen Air Dried
One hour, Heated to 170°F
for 30 min, Then
Baked at 600°F for One hour

FD 301928

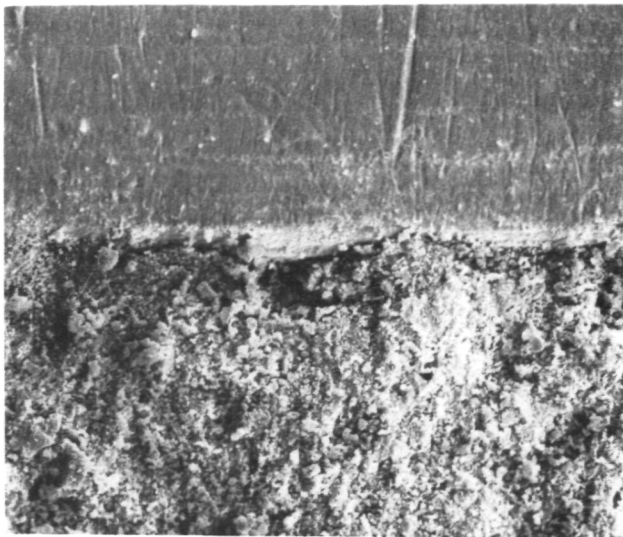


Silica Slurry Pressed
Into Grooves



PWA 658 Round Bar
Grooved Specimen

Figure III-26. Silica-Filled Groove Specimen



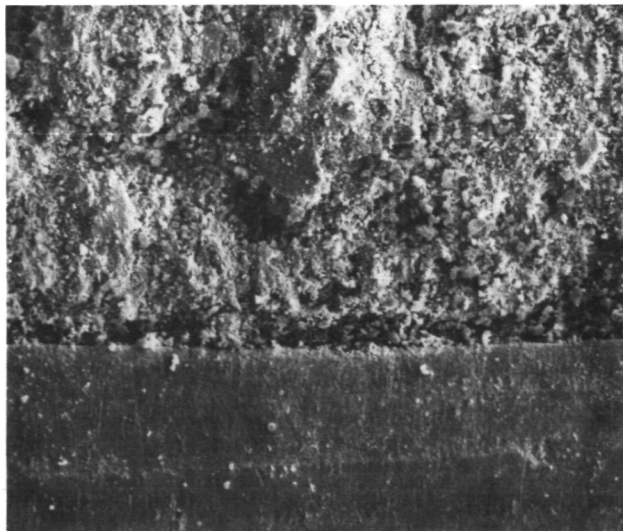
Groove
Land

Silica

FD 301929



Silica in Mid Groove



Silica

Groove
Land

Figure III-27. SEM Photomicrographs of 0.035 by 0.024 Inch Deep Groove (Filled With Silica Slurry and Oven Baked at 170°F for 30 Minutes Then at 600°F for 1 Hour. 500X Mag)

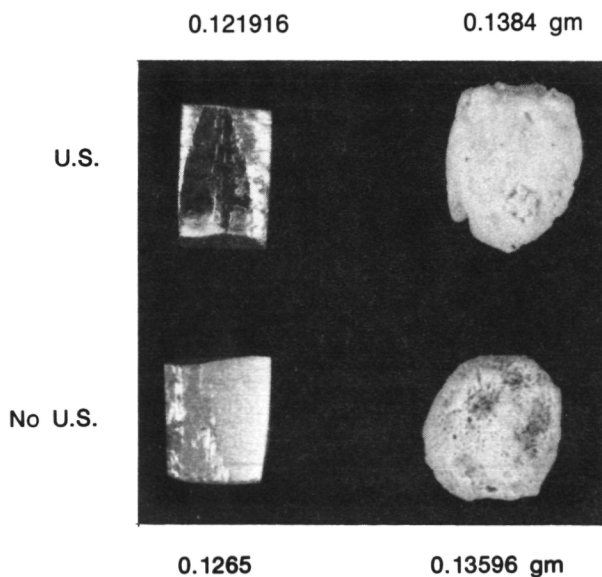
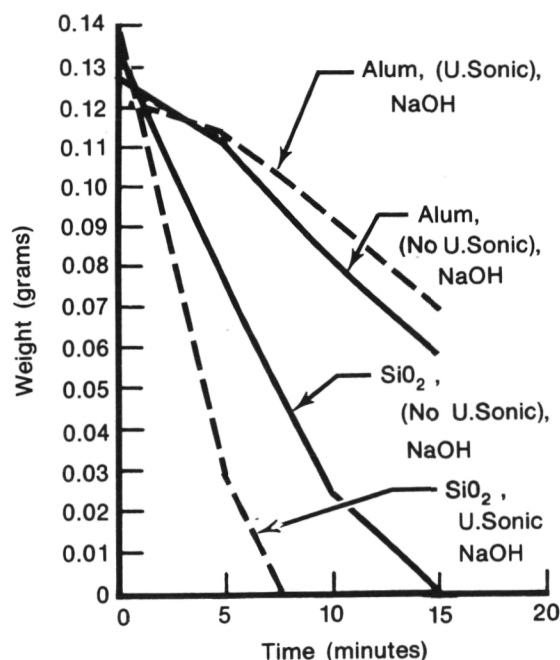
Table III-4. Leachability Test Results (Weights Shown Are in Grams)

NaOH Solution: 28 grams of pelletized NaOH in 100 ml H₂O

- 7 molar solution
- Heated to 140 to 160°F
- Static test done on hotplate
- Ultrasonic test done in heated ultrasonic tank

		Before Test	After 5 min	After 10 min	After 15 min
No Ultra Sonic	Wt of SiO ₂	0.13596	0.0758	0.0236	All material in solution at end of 15 min
	Wt of Al	0.1265	0.1106	0.0811	0.0578
With Ultra Sonic	Wt of SiO ₂	0.1384	0.0289	Fully Dis- solved after 2.5 min of this period	
	Wt of Al	0.12196	0.0909	0.090	0.0696

4041C



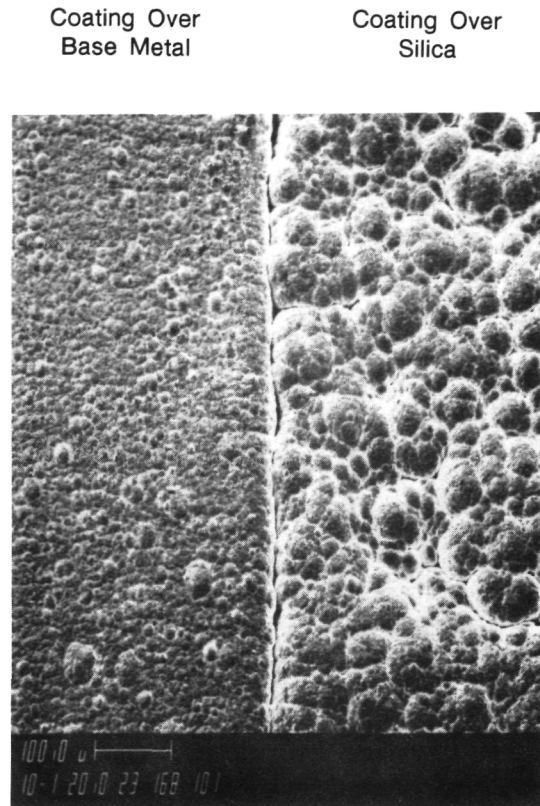
Test Specimens Prior to NaOH Leaching

FD 253290

Figure III-28. Relative Rates of Material Removal

This specimen was left in place without change to be used again as a substrate during a sputtering cycle which employed a DC triode discharge. In this mode, the plasma is not confined to the area near the surface of the target and can affect the substrate by ionic bombardment. The surface of the substrate itself can be sputtered off even as material sputtered from the target is being deposited. By manipulating the negative bias applied to the substrate, the factors of heat and back-sputtering can be employed to tailor the coating microstructure within certain limits. Figure III-30 shows the effect of using bias during a DC triode sputtering operation. Although the

original surface, as shown in Figure III-29, was severely cracked and coarse, this surface shows the coating over the boundary between the ceramic and metal to be almost fully continuous. Thus, this was the method employed to cover the fluidized bed cylinders and the blades.



FD 301930

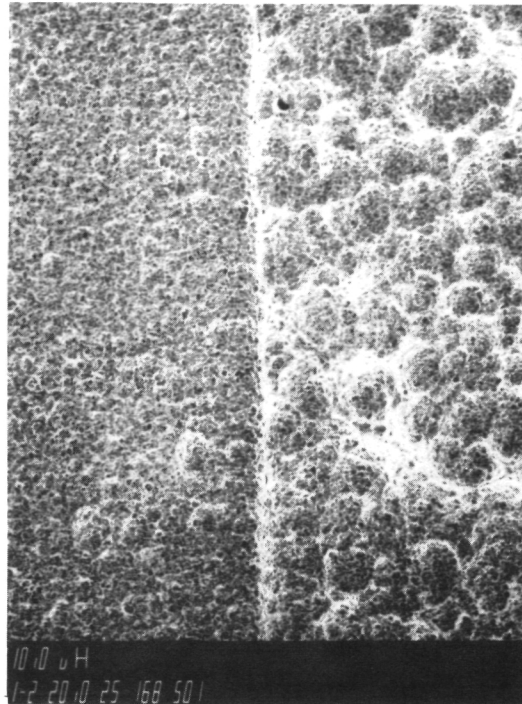
Figure III-29. Run 5-83-004 (100X) PWA 1447 Sputtered Onto PWA 658 Grooved Round Bar. Grooves Were Filled With a Fused Silica Slurry

4. Silica Groove Filling Experiments

One of the machined fluidized bed test specimens was used in an experiment to determine the effects of sputtering the cover material, PWA 1447, over the grooves filled with silica slurry. The high-purity fused silica was mixed with a colloidal silica binder to form a thick slurry, which was then forced into the grooves machined about the OD of the test cylinder. The excess slurry was removed by drawing a single-edge razor blade across the cylinder surface, then lightly rubbing over the grooves with clean white paper. This final rub tended to smooth off the silica deposit by transporting material from the high points to fill in any cracks or voids.

Coating Over
Base Metal

Coating Over
Silica

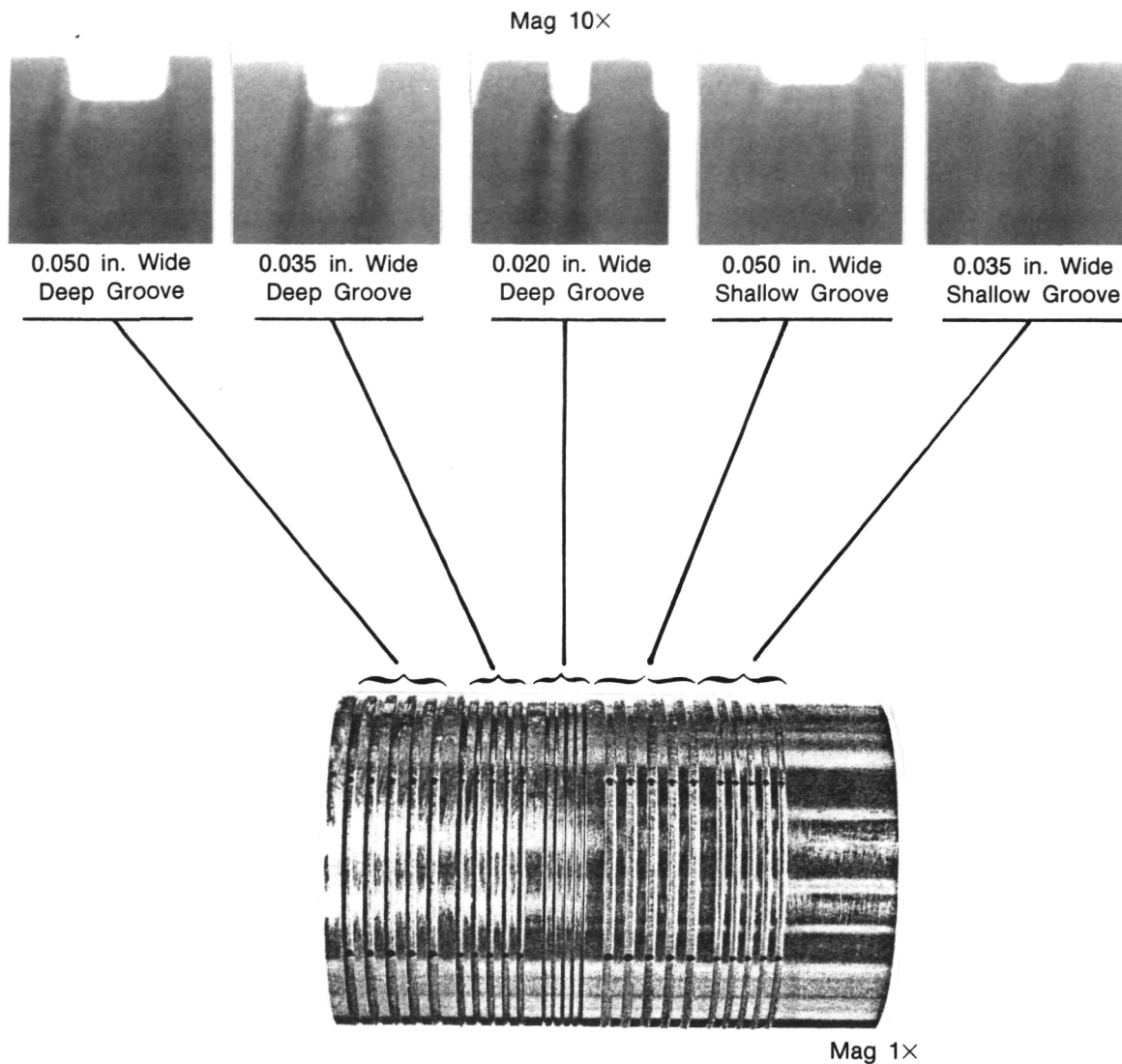


FD 301931

Figure III-30. Run 5-83-005 (100X) DC Triode — High Bias on Substrate. Substrate Is Same Specimen Coated in Run 5-83-004. Surface was Left as Is

The specimen was heated at 170°F for 30 minutes to drive off moisture, then baked at 600°F for one hour.

The deeper grooves proved relatively easy to fill by this method, but the shallow grooves presented a problem. There seems to be very little adhesion of the silica slurry to the metal cylinder and not much cohesion within the slurry itself. The primary mechanism which contains the slurry in the grooves is probably friction between the silica particles and friction between the particles and the side wall of the grooves. As shown in Figure III-31, there is very little side wall in the shallow grooves, hence it is difficult to contain the silica slurry in the shallow grooves. Figure III-32 illustrates the steps taken to fill the grooves with silica. The first attempt was unsuccessful due to the aforementioned problems with shallow grooves. Extreme care was used during the second attempt to avoid disturbing the fill material. After firing the cylinder, the fill material (though still delicate) could be handled using moderate care.

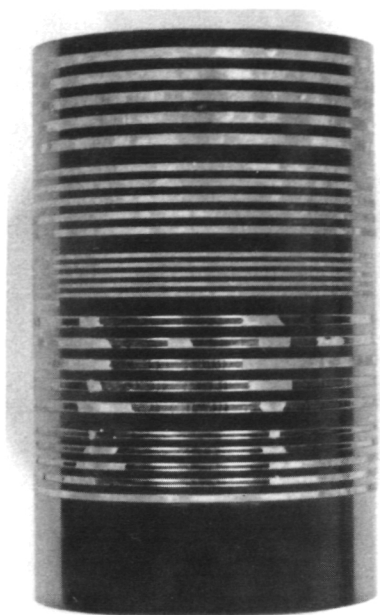


FD 302538

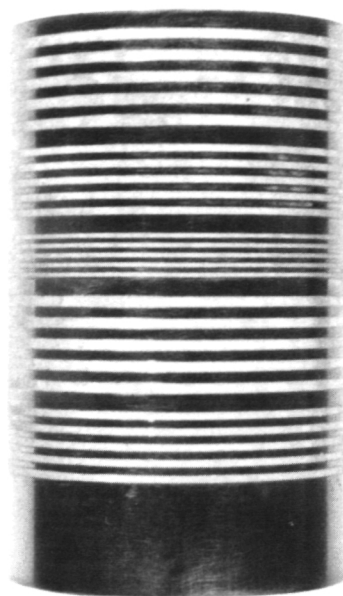
Figure III-31. Groove Geometry of Machined Fluidized Bed Test Cylinder

The above specimen was placed in the sputtering chamber and coated with approximately 10 mils of PWA 1447. The substrate was rotated at $\frac{1}{3}$ rpm during coating to obtain a more uniform deposit thickness about its circumference. This coating cycle was run using a triode discharge. The substrate was biased with a negative voltage, which was switched periodically from -10 vdc to -100 vdc in an attempt to deposit, as nearly as possible over the rough silica surface, a "deposit free" coating.

Figure III-33 shows the net result of this coating experiment. Apparently the stresses induced by the developing coating overcame the holding force that the groove had on the silica filler. Coating cracks and loss of filler cohesiveness were seen over every groove on the cylinder. The result of this experiment showed that the silica slurry is not a good groove filler material.



First Fill Attempt
Most of the Silica Was
Dislodged During Clean-
Up of Excess Slurry from
the Cylinder Surface



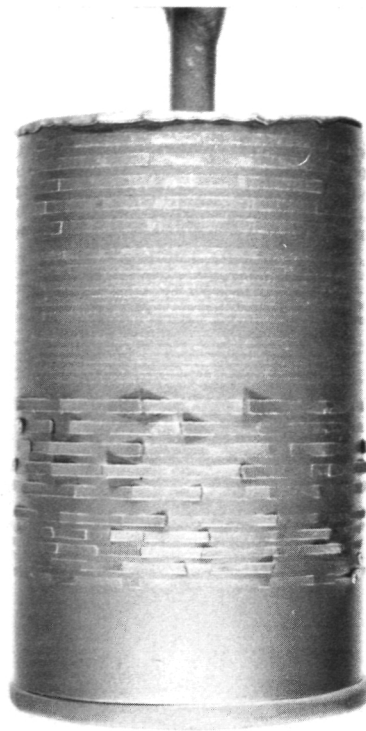
Second Fill Attempt
Extreme Care Was Taken
To Avoid Disturbing the
Slurry Deposit in Grooves



As Fired at 600° F/1 hr
After Firing the Cylinder May
Be Handled With Moderate Care

FD 302539

Figure III-32. Appearance of Fluidized Bed Test Cylinder During Stages of Groove Filling With a Silica Slurry



Run 5-83-005

Mag 1×

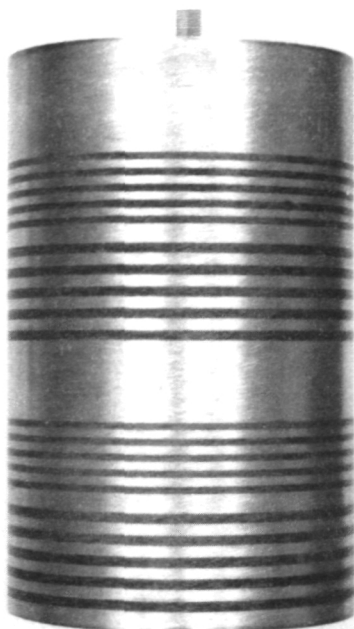
FD 302540

Figure III-33. Run 5-83-005 — Fluidized Bed Test Specimen as Sputtered With PWA 1447. The PWA 1447 Coating was Applied Over Grooves Filled With Silica

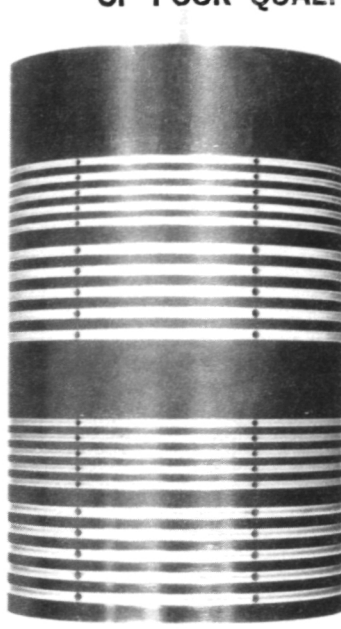
5. Aluminum Groove Filling Experiments

The rest of the coating experiments were performed using aluminum as the groove filler material. A method for filling the deep grooves in the cylinder with aluminum was developed and used successfully to process three test specimens. A thin aluminum coat (approximately 0.2 mils) was sputtered onto the grooved cylinder to form a well adhered, compliant layer on the grooved wall. The steps illustrated in Figure III-34 describe this process in detail.

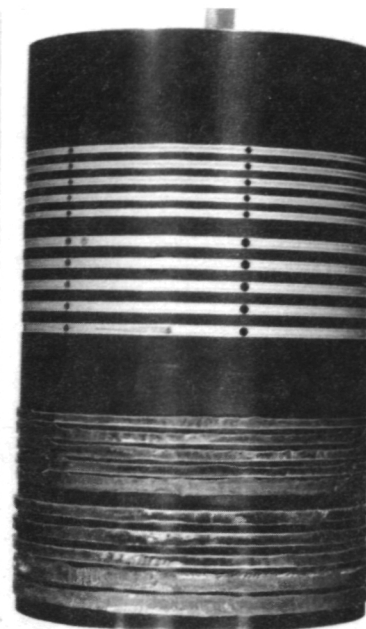
The earlier difficulties encountered with the shallow grooves, during experiments with silica, surfaced again with this method of groove filling. The lack of sufficient side-wall area on the shallow grooves prevented swaging of the aluminum wire, which is necessary to anchor it in place. None of the shallow grooves were successfully filled using aluminum wire. To fill these shallow grooves, and also to clean up any gaps or machining defects in the wire-filled grooves, the cylinders were sputtered with 6061 aluminum.



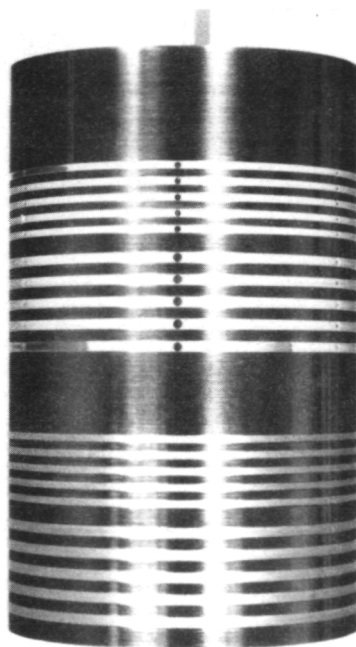
Step A



Step B



Step C



Step D

Step A A Test Cylinder Which Has a Thin Coat of Sputtered Aluminum Is Immersed in a Bath of Molten Wax. The Wax Is Then Removed Flush to the Cylinder Surface Using a Razor Blade and Fine Abrasive Paper

Step B The Cylinder Is Then Immersed In a Soln of NaOH Which Removes All Aluminum Not Covered by Wax. The Wax Is Then Removed by Immersion In Hot Degreasing Solvent

Step C Aluminum Weld Wire (AMS 4043) Is "Peened" Into the Grooves Using a Vibrating Electro Engraver With a Rounded Tip. The Wire Diameter Is Approximately 0.005 in. Larger Than the Groove Width for Proper Swaging Action

Step D Finally, the Excess Aluminum Wire Is Trimmed Back Flush to Cylinder Surface on a Lathe and Finished With Fine (No. 600) Abrasive Paper

FD 302541

Figure III-34. Technique Used to Fill Grooves in Test Cylinders With Aluminum Wire

The first cylinder to go through this process was done in sputtering run 5-83-009. This specimen was held by an uncooled, rotating fixture. The results are displayed in Figure III-35. Later temperature studies revealed that the substrate temperature reached approximately 1071°F, apparently hot enough to cause the aluminum deposit to alloy with the substrate material. A polished cross section of the coated cylinder wall revealed that some of the material from the PWA 1447 substrate diffused outward into the coating as deposition was taking place. This can be illustrated by the hardness data also shown in Figure III-35. Normally, sputtered

aluminum is very soft, below 70 HV (Hardness, Vickers), as was shown in later tests. The aluminum coating in this cross section was found to have a hardness of 543 HV, significantly higher (harder) than that of the PWA 1447 base material. The alloy formed was very brittle, as shown by violent chipping-off of the deposit encountered during later lathe machining of the cylinder.

The remaining two cylinders were processed using a water cooled holder to reduce the temperature of the substrate during deposition, thus reducing the possibility of alloying. Figure III-36 depicts these two cylinders as they appeared after machining back to the original OD and finishing with No. 600 SiC abrasive paper. Some striations can be seen in the aluminum, which are caused by lathe cutting operations, but generally the finish looks entirely suited for sputtering a "near-defect-free" overlay coating. Microscopic examination of the surface of both cylinders revealed no cracks, voids, or other defects in the filler material, nor separations between the filler and the groove walls.

An additional technique for filling the grooves was also investigated. Figure III-37 shows the product of a brief experiment to plasma-spray aluminum (AMS 4043) into the grooves of a fluidized bed test specimen. This is the same cylinder which was previously used to experiment with silica groove filling techniques and then coated with a cover of sputtered PWA 1447. The coating was machined away and the remaining silica removed from the grooves. Several grooves have spots which are filled with sputtered PWA 1447, in places where the silica filler fell out prior to the sputtering of the cover layer.

The cylinder was machined back to flush with the original OD and finished with No. 600 SiC paper. The aluminum finish looks somewhat, but not much, rougher than the sputtered aluminum filler. The leach-out holes in the grooves were not plugged prior to plasma spraying, thus the holes are (for the most part) still very visible through the aluminum filler. It should be noted that the actual spraying time required to fill the grooves was a matter of minutes, rather than the hours required to fill them by sputtering. However, the sprayed deposit may be "gassy" and perhaps may contain oxides or other contaminants.

An experiment was performed to determine the time required to leach out an aluminum deposit from a passage (tunnel) of the same geometry that was used for the cooling passages of the blade-tester blade. The size of these passages was expected to be 0.035 inch wide by 0.012 inch deep, with the length of the tunnel to be approximately one inch. A test fixture was fabricated to simulate the cooling passage and a leach test was conducted.

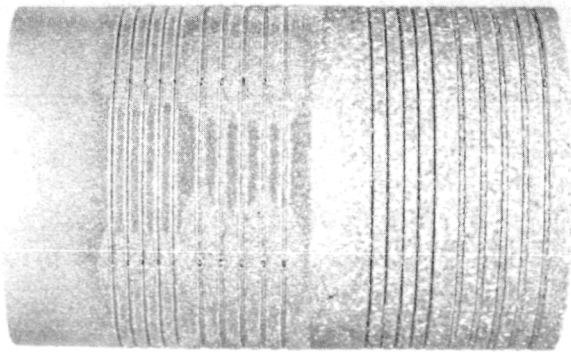
The step-by-step procedure used in this investigation is illustrated in Figure III-38. Verification of full removal of the encapsulated aluminum was accomplished by comparing the weight of the aluminum strip to that of the weight loss of the specimen after a period of time in a 7 molar NaOH solution. As a final check, when no further weight loss could be induced by leaching, the nickel plate covering the aluminum strip (now a tunnel) was peeled back to expose the area leached out (Figure III-38). The test revealed that a time span of two hours would be sufficient to remove all of the aluminum from passages with this geometry.

Prior to sputtering the PWA 1447 closeout layers on the two actual fluidized bed test cylinders, a sputtering run was made to clean up the chamber after prior aluminum sputtering cycles. The substrate selected to be coated with PWA 1447 in this run was a cast PWA 1447 rig bar. The coating cycle was run using the same parameters — triode mode, negatively biased substrate. The run was continued for two hours and fifteen minutes and produced a coating approximately 0.003 inch thick.

ORIGINAL PAGE IS
OF POOR QUALITY

Run 5-83-009
Sputtered Aluminum Over PWA 1447
Fluidized Bed Test Cylinder

During Coating, the Cylinder Was Held on an Uncooled Fixture.

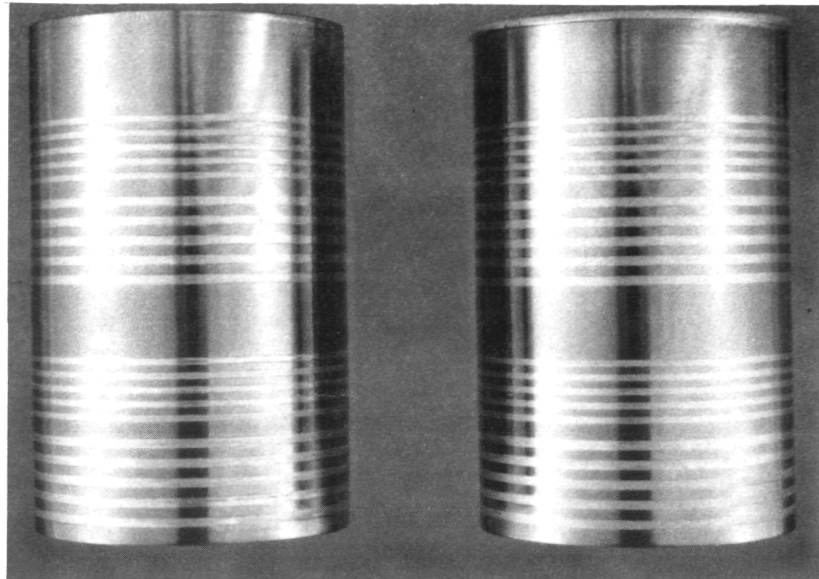


Material	Hardness
Aluminum Deposit Alloyed	543 HV
Interface	481 HV
PWA 1447 Base	366 HV

Note: Hardness Test Done
Using a Vicker's
Pyramid Indenter With
a 300gm Load

FD 302542

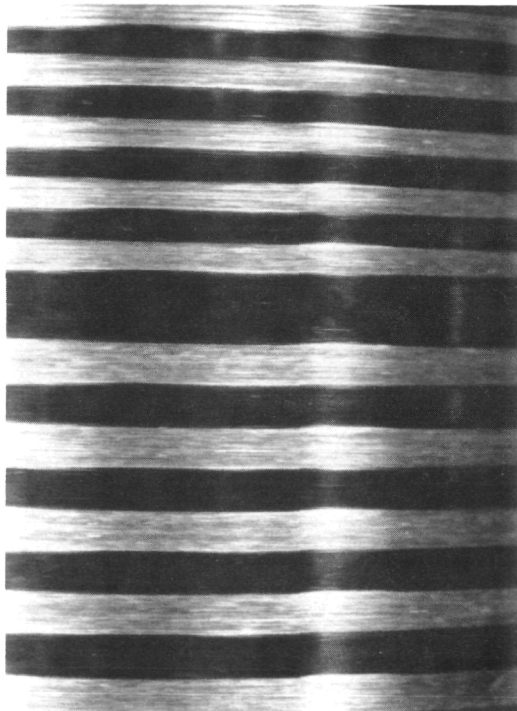
Figure III-35. Overall Appearance and Hardness Testing of Alloyed Aluminum on PWA 1447



Run 5-83-016

Run 5-83-017

Mag 1×



Typical Appearance of Aluminum Filled Grooves
After Lathe Machining Back to the Cylinder
Surface and Finishing With No. 600 Grit
Abrasive Paper

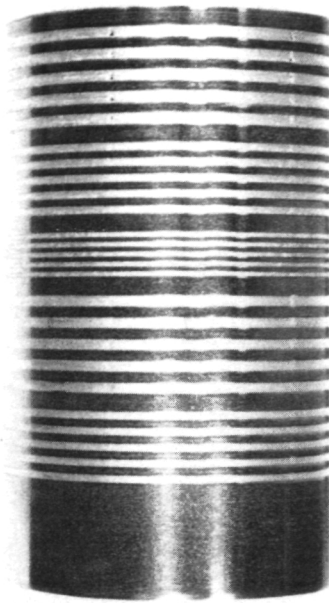
Note: These Two Cylinders Were Coated While
Held on a Water-Cooled Copper Fixture

Mag 4×

FD 302543

Figure III-36. Sputtered Aluminum in Fluidized Bed Test Cylinder Grooves

A cross section was cut from the middle of this bar and processed for metallurgical examination. Microprobe scans of these areas showed that the sputtered coating was similar in chemical composition (within the tolerance range of the microprobe) to the PWA specifications for this material, as depicted in Table III-5. Metallurgical evaluation also showed that, although this was a cleanup run for the chamber with a newly reinstalled target and some contamination was to be expected, the interface and the sputtered deposit looked clean and virtually defect-free. The few spots found along the interface were actually bits of embedded silicon carbide, remnants of processing the rig bar by grit blasting at some earlier date.



Mag 1×

The Cylinder Was Machined Back Flush to the Original
OD Surface.

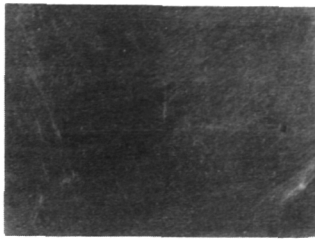
FD 302544

Figure III-37. Plasma Sprayed Aluminum (AMS 4043) in Grooves on PWA 1447 Test Cylinder

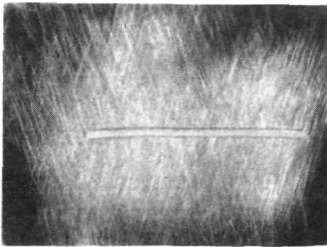
Table III-6 contains the hardness values for the same cross section. A Zwick microhardness tester was used to obtain hardness values of the coating, to further illustrate its similarity to (or difference from) material known to be PWA 1447. The data presented here indicates that the hardness of the sputtered deposit does not differ significantly from that of the cast PWA 1447.

6. Sputtering of PWA 1447 Cover Material

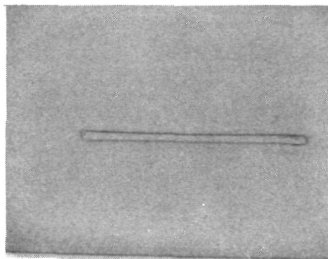
The fluidized bed test cylinder which had grooves filled with plasma sprayed aluminum was the first specimen selected for application of the PWA 1447 close-out (cover) layer. It was intended to use this specimen as a trial run to evaluate the behavior of the sputtering system (i.e., check out control parameter settings) before committing one of the new cylinders. A thermocouple was wired to the OD of this cylinder and the surface temperature was monitored during coating deposition. Various sputtering parameters were adjusted to formulate a cycle which would deposit a defect-free, well bonded coating in a reasonable amount of time, while minimizing the process temperature in order to limit interdiffusion of the PWA 1447 and the aluminum.



Two Holes, 1 in. Apart, Were Drilled Into a Stainless Steel Baseplate. One Hole Had a Diameter of 0.035 in., the Other 0.014 in.



A Strip of Aluminum, 0.035 in. Wide, 0.012 in. High, and 1.10 in. Long Was Epoxied Onto the Baseplate So as to Span the Distance Between the Two Holes



The Fixture Was Then Nickel Plated. A Piece of Tape Covered the Backside of the Baseplate To Keep the Leaching Holes Open



The Assembly Then Was Immersed in a NaOH Solution, 7 Molar Concentration, and the Time Required to Completely Leach Out the Aluminum Through the Holes Was Charted

****It Was Determined That All of the Aluminum Would Be Leached Out in 2 hr

FD 302545

Figure III-38. Aluminum Leach Rate Study

This cylinder was held in the same water-cooled cylindrical copper fixture used to deposit aluminum earlier in the program. A twisted double strand of 18 AWG (0.040 inch diameter) bare copper wire was wrapped around the body of the holder to provide intimate contact with the ID of the test cylinder for more efficient heat transfer.

Table III-5. Microprobe Results of Sputtering Experiment 5-83-018 — Evaluation of Coating and Substrate Chemistry

<i>Element</i>	<i>PWA Spec</i>	<i>Substrate</i>	<i>Coating</i>
Ni	Bal	Bal	Bal
Cr	8.4	10.3	12.1
Co	10	9.4	10
Mo	0.65	0.7	0.7
Al	5.5	6.0	4.7
Ta	3.0	2.3	2.8
W	10	9.2	8.6
Hf	1.4	0.9	0.8
Ti	1.0	1.0	1.0
B	0.15	—	—
Zr	0.05	—	—

4041C

Table III-6. Microhardness Testing of Sputtered PWA 1447 Run 5-83-018

*Hardness Readings, in Hv, as Determined by a Zwich Microhardness Tester Using a Vicker's Pyramid Indenter Under a 300 gm Load.

*Values Shown are the Averages of 10 Readings at Each Location.

Cast PWA 1447 Base 395 HV (average pyramid height of 0.037 mm)

Sputtered PWA 1447 429 HV (average pyramid height of 0.036 mm)

4041C

An average thickness of 4 mils (0.004 inch) was obtained during 4.5 hours of deposition. During the deposition cycle, inordinate pressure fluctuations were experienced, caused by the outgassing of heated surfaces within the coating chamber. Upon removing the cylinder from the sputtering system, it was discovered that much of the coating over the grooves contained nodular defects. It is believed, that these defects were caused by the release of gases trapped in the aluminum filler during the plasma spray application. Later coating runs using cylinders with grooves filled with sputtered aluminum and aluminum wire showed considerably fewer defects of this type. It should be noted that due to limitations imposed by the attachment of the thermocouple, the cylinder was not rotated. Also, the metal sheath of the thermocouple placed the cylinder at ground potential which precluded the use of biasing to improve the deposit uniformity. Figure III-39 shows the condition of this cylinder as coated.

It was decided to leach out the aluminum at this point so that the remainder of the 10 mil (0.010 inch) thick coating could be applied under less restrictive conditions. The cylinder was immersed in a 7 molar NaOH solution maintained at 140 to 160°F. Prior experiments had determined that cooling channels of geometry similar to those in this cylinder would require approximately two hours to leach free of aluminum using this solution. However, this cylinder had seen prior service as a substrate in a coating experiment where PWA 1447 was sputtered over silica-filled grooves. The silica had fallen out in many places prior to and during the sputter coating cycle. The voids left by the wayward silica were filled by the PWA 1447 material which ultimately blocked the channel in several places. This blockage limited the flow, hence the effectiveness, of the NaOH leaching solution. Thus, rather than the two hours leaching time indicated by past experiments, this specimen required almost 24 hours of soaking along with frequent ultrasonic cleaning cycles (this problem would not be encountered in a new cylinder). After this time period, some small bubbles of gas were still being generated by the chemical reaction; but for the purposes of this initial experiment, it was determined that enough of the aluminum had been removed to continue processing of the cylinder. The leached out cylinder is shown in Figure III-40.



As Coated 1X

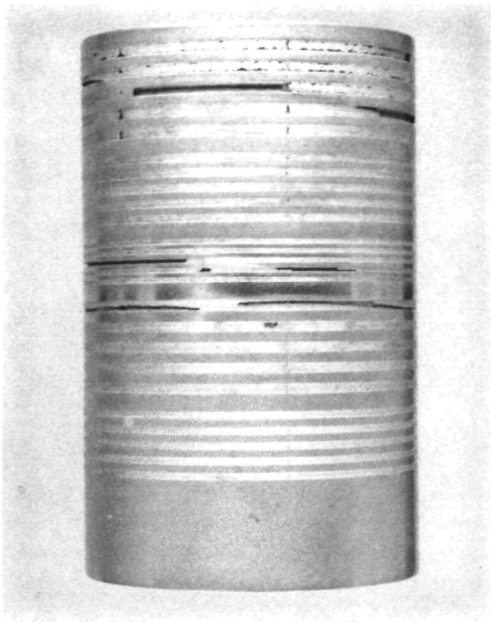
FD 267902

Figure III-39. Plasma Sprayed Aluminum Fluidized Bed Test Cylinder as Coated With PWA 1447 in Run 5-83-019

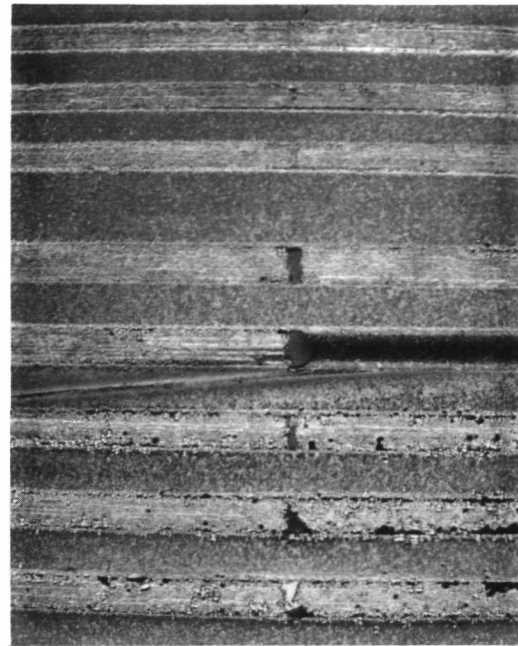
Coating of the cover layer on this cylinder was continued in sputter run 5-83-020. The specimen was fixtured on the same water-cooled holder as before, but this time no copper wire was added to fill the space between the OD of the holder body and the ID of the cylinder. The cylinder was inverted with respect to the vertical orientation observed during its first coating in order to obtain a more uniform coating thickness throughout its entire length. The thermocouple was removed which permitted a bias voltage of -25 vdc to be placed on the substrate. Also, for this second layer the target voltage was increased to 1.5 kvdc, which was 1.5 times the target voltage employed previously. The coating cycle was continued for five hours. The coating deposited during this experiment contained many nodular defects over the grooves where incomplete removal of the filler material probably resulted in the vaporization of the over-heated aluminum. Figure III-41 illustrates the appearance of the as-coated cylinder from run 5-83-020.

The next cylinder to be coated with a cover of PWA 1447 was one of the fluidized bed test cylinders which had the shallow grooves filled with sputtered aluminum and the deep grooves filled with aluminum wire. The parameters used for this coating run were adjusted to minimize the temperatures generated by the sputtering process to avoid alloying the aluminum. Despite precautions taken to reduce the heat, one side of the cylinder developed several nodular defects along the grooves. Also, during subsequent processing to leach the aluminum from the grooves, much of the PWA 1447 coating debonded from the cylinder, with the remaining coating easily removed by fingernailing. On this side of the cylinder even the "nodule free" deposit over the aluminum-filled grooves looked wavy, as if it had been deposited over a flowing surface. Figure III-42 illustrates the as-coated condition of this cylinder.

ORIGINAL PAGE IS
OF POOR QUALITY



As Leached 1X



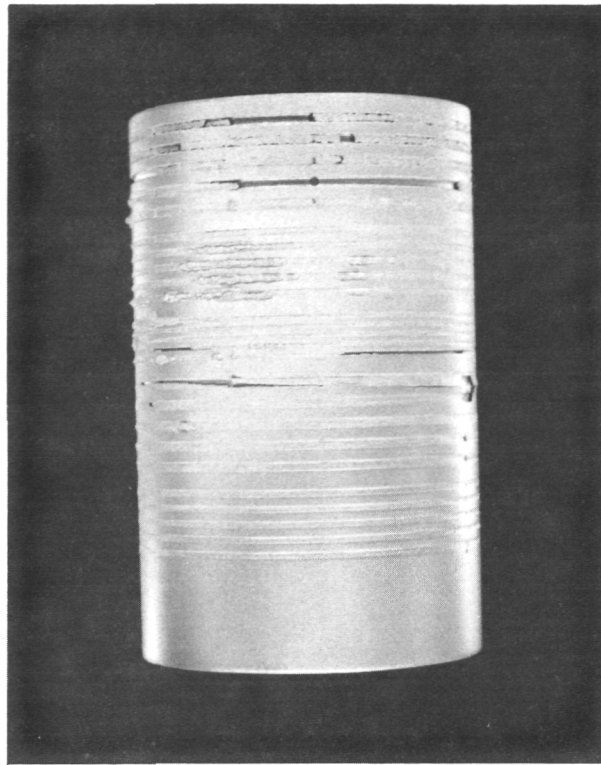
As Leached 4X

FD 267755

Figure III-40. Plasma Sprayed Aluminum Fluidized Bed Test Cylinder After Leaching Out Aluminum Filter from Grooves

To eliminate the localized heating which was believed to have caused the nodular defects, a modification was made to the sputtering chamber to permit the rotation of the cylinder about its axis during coating, while maintaining the option to water-cool the substrate fixture. This was accomplished by using a magnetically sealed rotatable vacuum feedthrough which sealed and rotated the 0.5 inch diameter stainless steel support tube connected to the substrate holder. The cooling water was fed to this tube using a fixed coupling fitted with a well greased O ring. This arrangement allowed the water feed and drain lines to remain stationary while supplying running water to the revolving substrate assembly.

The next cylinder selected for coating was the second fluidized bed test cylinder with sputtered and wire-formed aluminum within its grooves. This specimen was mounted on the modified water-cooled rotating holder. The double stranded copper wire was again used to provide intimate contact between the substrate and cooled holder surfaces. Again, every attempt was made to limit the temperature encountered by the substrate. In addition to temperature limiting procedures employed in prior experiments, this run omitted the typical predeposition sputter-clean (reverse sputtering) cycle used to outgas and ion scrub the substrate and target surfaces. To compensate for the omitted procedures, the chamber was pumped for three days under moderate heat ($<400^{\circ}\text{F}$) to remove as much gas as possible from the surfaces within.



5-83-020

Mag 1X

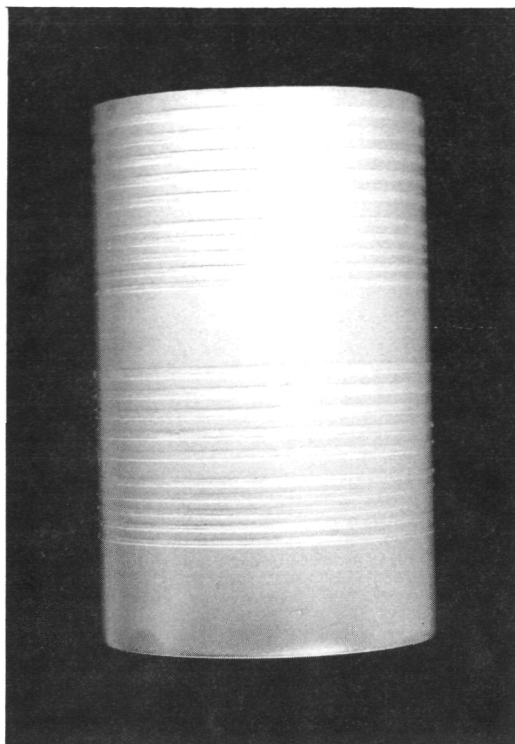
Second Coating of PWA 1447 Cover

FD 267756

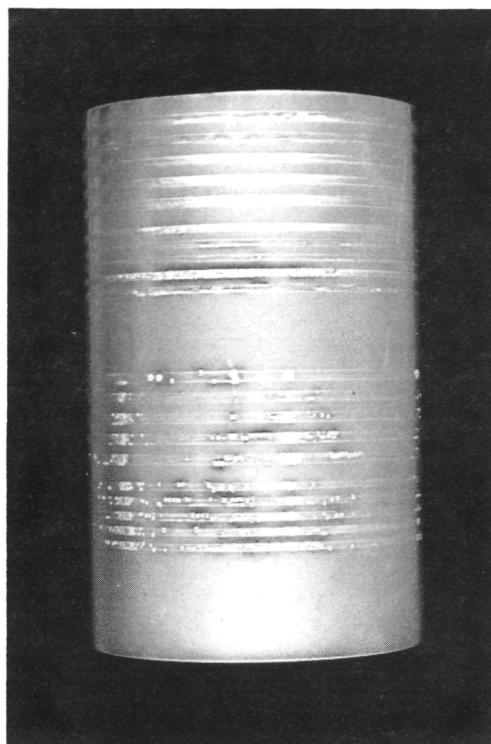
Figure III-41. Appearance of Fluidized Bed Test Cylinder After Second Coating of Sputtered PWA 1447

The coating from this run looked good except for a small area at the bottom end of the cylinder which contained a few nodular defects. During removal of the cylinder from the holder, it was noted that the copper wire used for heat transfer had not reached the cylinder bottom. One of the aluminum plugs used to fill the holes in the groove bottoms prior to sputtering of the aluminum filler protruded past the cylinder ID wall and blocked the path of the wire as it was wound in from the top of the fixture. This severely limited the heat flow away from the bottom third of the cylinder during coating. The appearance of this cylinder as-coated is shown in Figure III-43.

The second coating on this cylinder was applied with the aluminum groove filler still in place. Prior to fixturing, the cylinder was put on a lathe and No. 600 grit SiC paper was used to clean up the OD to provide a smooth surface for the final coat. Also, the ID was treated with No. 120 grit SiC paper to remove all protruding aluminum plugs. For this run, a single strand of copper wire was wound around the substrate holder and forced against the cylinder wall for maximum contact. The cylinder was inverted to provide more uniform coating thickness. During the coating cycle the water-cooled substrate holder was rotated at 1 rpm.



Best Side Mag 1X



Worst Side Mag 1X

Sputtering run 5-83-021 PWA 1447 sputtered over a PWA 1447 fluidized bed test cylinder having cooling grooves filled with aluminum wire and sputtered aluminum.

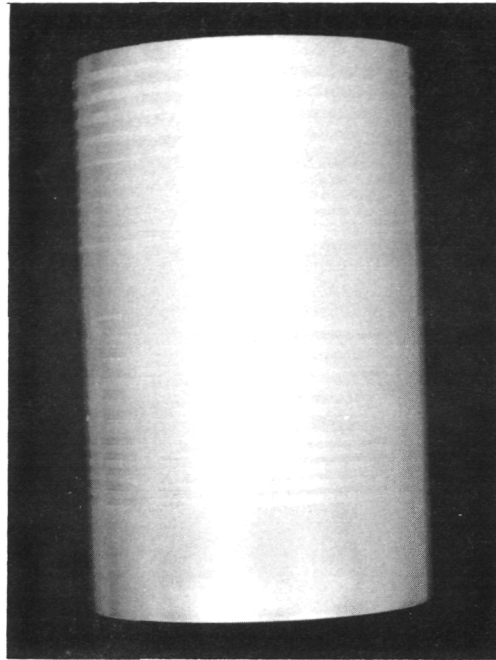
FD 267757

Figure III-42. Two Sides of the Fluidized Bed Test Cylinder Coated in Sputter Run 5-83-021

The resultant coating from this experiment looked good and was virtually defect-free. However, much of the coating flaked off later during the aluminum leaching process, indicating poor bonding. Figure III-44 shows the cylinder before and after the final coating in run 5-83-023. Figure III-45 illustrates the cylinder condition after leaching.

The underside of one of the debonded coating strips from the cylinder coated in run 5-83-023 was analyzed by X-Ray Energy Spectroscopy (XES) to determine the chemical makeup of the coating at the substrate interface. The results, as displayed in Figure III-46, did not show abnormal indications which might lead to coating debonding. Analyses of the surface of the cylinder itself in an area under a debonded strip showed no significant variation from specifications for PWA 1447. A deposit of unleached aluminum near one of the cooling holes in the cylinder was also charted by XES. This chart, displayed in Figure III-47, shows a significant amount of copper which could only have come from the copper wire used for heat transfer. Apparently, the aluminum plugs extending through the cylinder wall to the ID contacted the copper wire and alloying of the two occurred even at the relatively low temperatures seen close to the water-cooled substrate wall. The copper alloyed with the aluminum, along with traces of

other elements from the PWA 1447 base material, caused a drastic slowdown of the leaching process. An analysis of this alloyed aluminum is presented in Table III-7 along with a similar analysis of the aluminum wire used to plug the cooling holes.



Run 5-83-022 As-Coated

Mag 1X

FD 267903

*Figure III-43. PWA 1447 Sputtered Over PWA 1447 Test Cylinder, Run 5-83-022
(First Coat)*

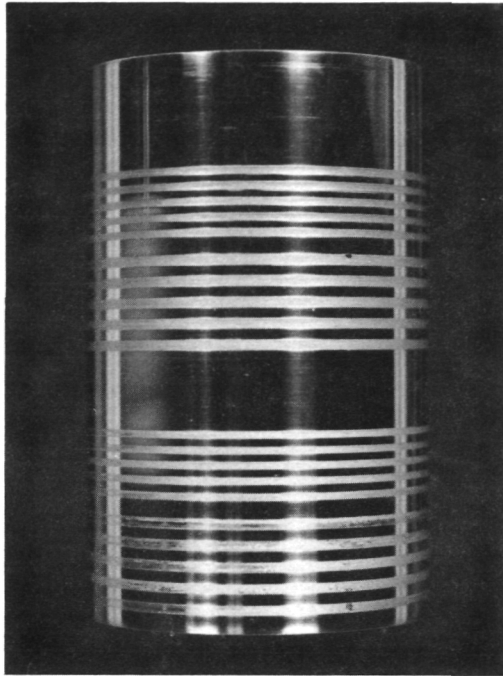
7. Bond Strength Investigation

To understand the lack of bonding strength between the PWA 1447 sputtered coating and substrate, an effort was initiated in the Materials Laboratory to evaluate this problem.

Acting on the suggestion from NASA that the thermal expansion difference between the aluminum and the PWA 1447 may have contributed to the coating debonding noted during leaching, an experiment was designed to duplicate these conditions in a controlled environment. A 0.062 inch hole was drilled approximately 0.25 inch deep into a PWA 1447 rig bar section, which measured approximately 0.5 inch diameter by 0.75 inch in length. Aluminum wire (4043), 0.060 inch diameter, was then forced into the hole by vibro-peening. The aluminum was ground down flush with the surface of the host bar section and the composite face was finished to No. 320 grit SiC paper to produce a smooth, flat surface. Next, a 0.01 inch thick layer of nickel was plated over the specimen. The plated specimen was immersed in boiling water for one hour to effect a "worst case" simulation of the heat derived from the aluminum leaching process. After this exercise, the sample was examined for any bulge (or depression) in the nickel plate over the aluminum wire, which might have been formed by thermal expansion mismatching between the PWA 1447 and the aluminum. No abnormalities were noted in the nickel plate. As a further check, the specimen was placed in an oven at 200°C. After 30 minutes the nickel plate still appeared flat and featureless. A cross section of the specimen was prepared and microscopically examined. Still no distinct bulge could be seen, but, an area approximately one-half the size of

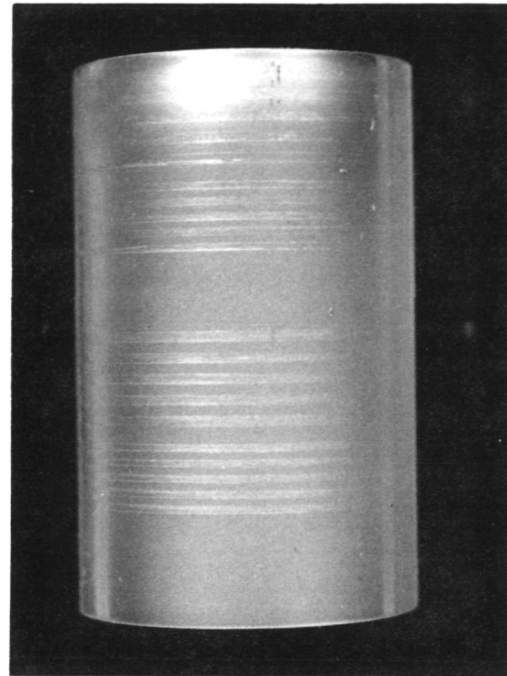
ORIGINAL PAGE IS
OF POOR QUALITY

the total flat surface area and centered over the aluminum wire had debonded and remained slightly lifted from the PWA 1447 surface. The progressive steps involved in this experiment are illustrated in Figure III-48.



Run 5-83-023 As Fixtured

1X



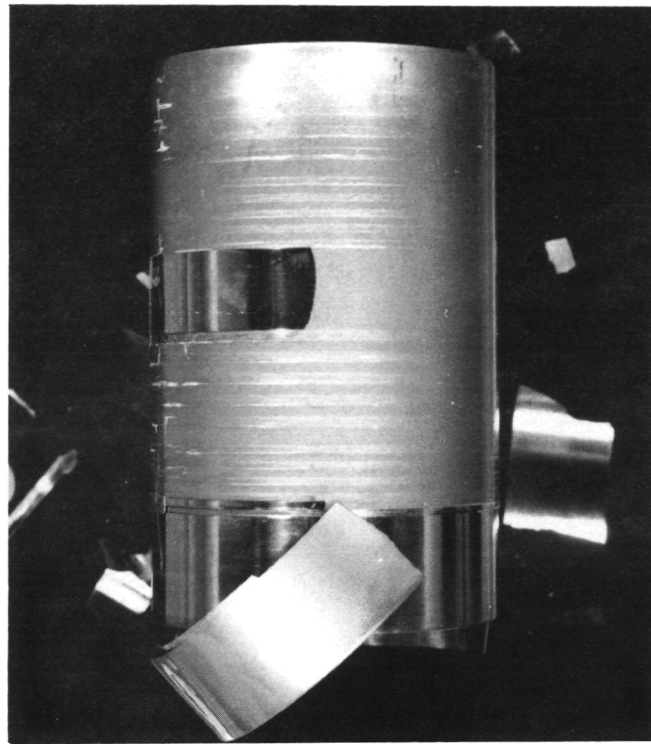
Run 5-83-023 As-Coated

Mag 1X

FD 267758

*Figure III-44. PWA 1447 Sputtered Over PWA 1447 Test Cylinder, Run 5-83-023
(Final Coat)*

In the next experiment a 0.035 inch hole was drilled all the way through a 0.25 inch thick section of a PWA 1447 rig bar. A piece of aluminum wire was thinned down to 0.35 inch using a solution of NaOH then drawn through the hole filling it completely. The two faces of the bar section were then polished to No. 600 SiC paper to obtain smooth, flat surfaces. The specimen was then coated with 0.001 inch of nickel in a RF Diode sputtering system. No surface irregularities were noted after coating. One face of the specimen was ground down past the nickel coating to expose the PWA 1447/aluminum composite surface. The aluminum was leached out through this hole using a 7 molar NaOH solution held at 140 to 160°F. The leaching process required two hours to complete because of the tendency of the reaction to slow drastically as the excavated hole deepened. This probably occurred because the gas generated by the chemical reaction formed a pocket within the hole and restricted the passage of fresh solution to the aluminum surface. It should be noted that the orientation of the specimen to be leached is of great importance in the leaching process. If the cylinder or blade is placed within the NaOH solution in such a manner that gas bubbles formed must be forced down through a channel, the natural buoyancy of the gas could tend to hold the bubbles inside the inverted hole and slow or even stop the chemical reaction. Any complex structure probably would contain several channels having an "inverted" orientation, so some form of rotation of the specimen during the leaching process would be required.



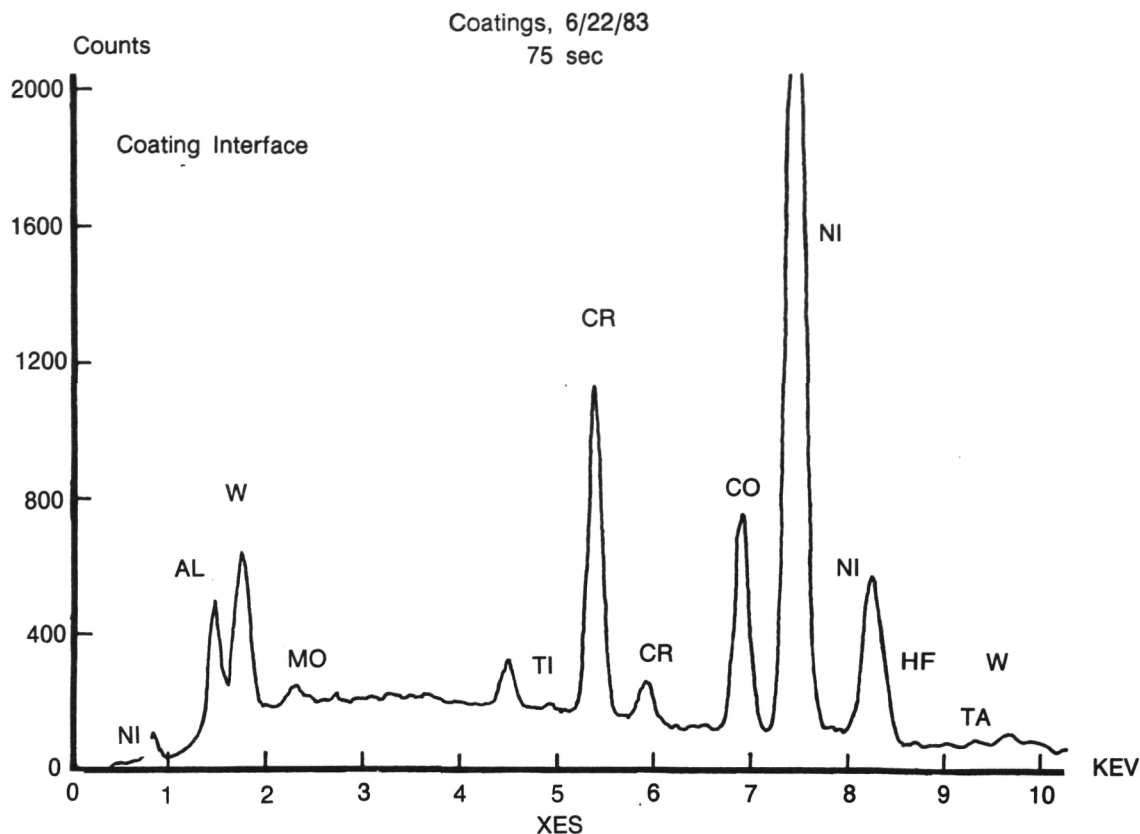
Run 5-83-203 Mag 1X
Shortly After Start of Leaching Cycle

FD 267759

Figure III-45. Appearance of Fluidized Bed Test Cylinder Coated in Run 5-83-023, After NaOH Leach

The steps involved in this experiment as well as the results are illustrated in Figure III-49. This time a bulge did appear in the coating over the hole as predicted. This specimen was next prepared for metallurgical examination of its cross section. Microscopic viewing of the polished cross section, as shown in Figure III-50, revealed that the coating had separated in the area only over the aluminum-filled hole. A gap between the coating and the walls of the hole measured 0.0006 inch wide.

A series of experiments were also run to determine other possible causes for poor coating adherence and to develop a means to overcome this problem. In these experiments, films of PWA 1447 and Ni-200 (commercially pure) were sputtered onto strips of PWA 1447 and Ni-200. Adherence testing of RF diode sputtered Ni-200 on PWA 1447 and Ni-200 strips showed no debonding of the coating up to 10,000 psi, the limit of the tensile tester used. Adherence testing of DC triode sputtered PWA 1447 coating on PWA 1447 and Ni-200 strips also showed no debonding to 10,000 psi. The only coating that showed any sign of failure at these limits was the Ni-200 which was RF diode sputtered onto a vapor blasted PWA 1447 surface. Figure III-51 shows a typical coated strip, in this case PWA 1447 sputtered onto a PWA 1447 substrate which was first vapor blasted, as it emerged from the tensile tester. The bonded pin was still attached indicating no debonding occurred within the limits of the test equipment.

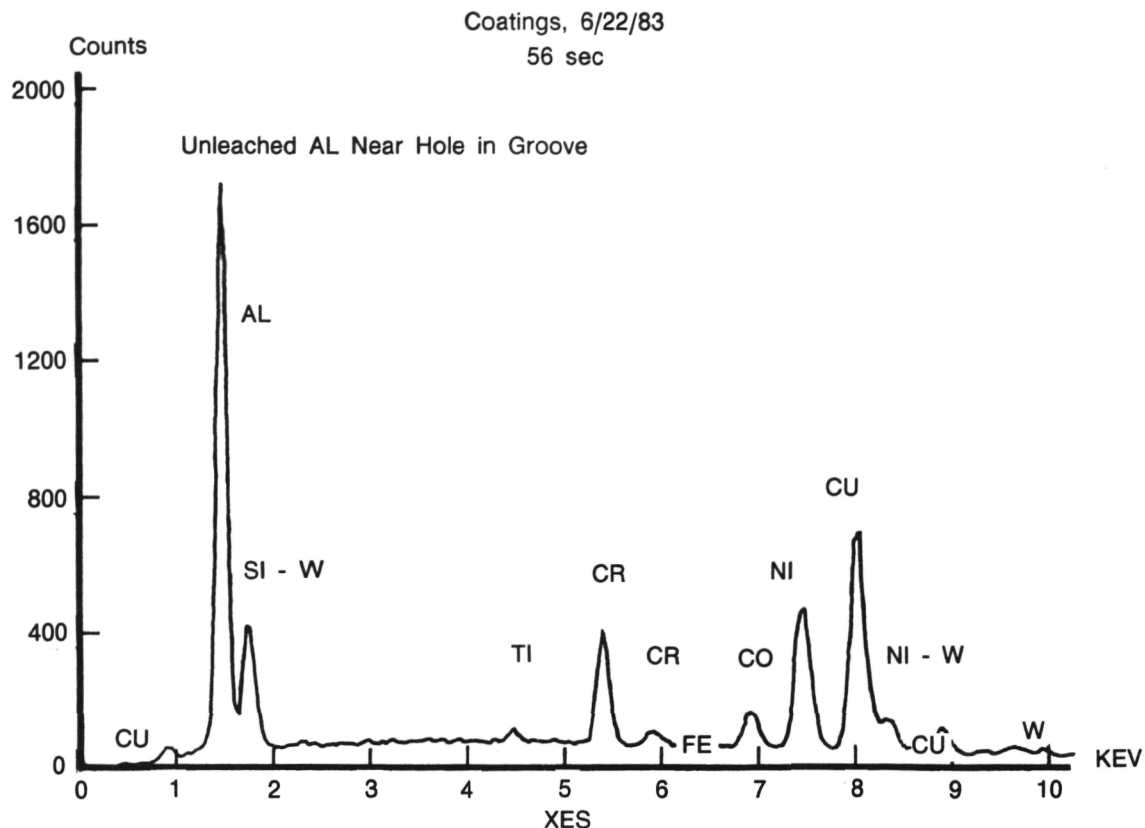


FD 267901

Figure III-46. Results of XES Analysis for Underside of the Debonded Coating

Four strips, each approximately 1.5 inches long by 0.25 inch wide by 0.04 inch thick were bend tested after coating with DC triode sputtered PWA 1447. Two of the strips were made of PWA 1447 material and two of Ni-200. One each of the two materials was prepared by vapor blasting the surface and the other by polishing down to No. 600 grit SiC paper. The strips were bent 90 degrees over a 0.28 inch diameter mandrel. In each case the PWA 1447 coating adhered well to the nickel strip and spalled from the PWA 1447 strip (severely spalled from the polished PWA 1447 strip). Figure III-52 illustrates the appearance of these strips prior to bending. Figure III-53 shows the results of the bend testing.

As a final attempt to resolve the bonding problem between the PWA 1447 substrate and cover layer, a nominal 0.001 inch thick coating of nickel was deposited between the two layers. Specimen appearance and surface topography are shown in Figure III-54. The nodular topography in each case is typical of a cold substrate. The nodular growth is more pronounced over the aluminum wire filler which had a rougher surface than the PWA 1447 land. The nickel closeout layer was essentially nonadherent, as shown in Figure III-55.



FD 267760

Figure III-47. Results of XES Analysis for Unleached Aluminum

Due to the difficulties in depositing a well adherent cover layer on the PWA 1447 fluidized bed test cylinders, it was determined that the technology required to perform this task was not available at this time. An expensive development program would be required to achieve the task. Such a program was out of the scope of the advanced turbine study. A recommendation was made to NASA to cease work on the advanced convectively cooled blade and redirect the program to evaluate the hot core blade.

Appendix A contains a summary of the sputtering work conducted as part of the ATS program. An overview of the state of the art of the sputtering technology is presented, as well as the recommended development program which would be required to resolve the lack of adhesion between the PWA 1447 substrate and the cover layer.

D. TASK 2 — SUBTASK 203, SPECIMEN TEST

This subtask consisted of the fluidized bed testing of the test cylinders simulating the advanced convectively cooled turbine blade.

Table III-7. Comparison of Aluminum Left in Cooling Channel and 4030 Aluminum Wire

<i>Element and Line</i>	<i>Weight %</i>	<i>Atomic %</i>	<i>Precision 2 Sigma</i>	<i>K-Ratio</i>	<i>ITER</i>
AL KA	33.30	53.74	0.91	0.1421	
SI KA	5.16	7.99	0.34	0.0211	
TI KA	0.68	0.62	0.12	0.0062	
CR KA	5.95	4.99	0.41	0.0578	
CO KA	2.60	1.92	0.34	0.0271	
NI KA	12.40	9.20	0.81	0.1277	
CU KA	26.97	18.48	1.42	0.2566	
W KA	12.93	3.06	0.85	0.0661	5
TOTAL	100.00				

NORMALIZATION FACTOR: 0.705

XES Analysis of Material Left in Channel After NaOH Leaching

STANDARDLESS EDS ANALYSIS
(ZAF) CORRECTIONS VIA MAGIC V)

<i>Element and Line</i>	<i>Weight %</i>	<i>Atomic %</i>	<i>Precision 2 Sigma</i>	<i>K-Ratio</i>
AL KA	97.35	97.46	1.35	0.9904
SI KA	2.65	2.54	0.40	0.0096
TOTAL	100.00			

NORMALIZATION FACTOR: 0.981

XES Analysis of 4030 Aluminum Wire Used to Fill Cooling Channels

4041C

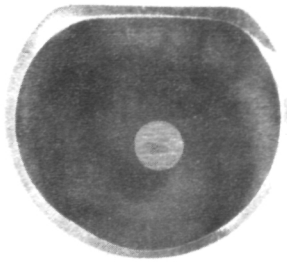
By exposing the cylinders (which were fabricated with several coolant groove-land geometry combinations as shown in Figure III-14) to very rapid temperature changes in the fluidized bed, the high thermal gradients produced by the blade tester rig and the SSME were to be approximated. After this thermal exposure, posttest evaluation of the hardware should have allowed the selection of the optimum coolant groove-land geometry combination.

The rapid temperature changes were to be achieved by rapidly submerging the test specimens in alternate hot and cold silica sand baths. The temperatures in these baths were to have been closely monitored and controlled to ensure the proper ΔT between both baths.

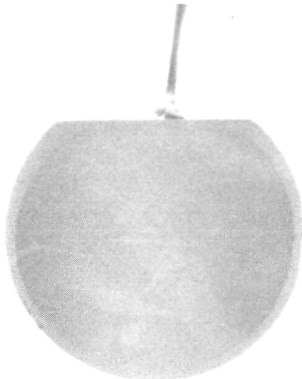
Due to the inability to fabricate the test cylinders, the fluidized bed tests were not performed.

E. TASK 3 — SUBTASK 301, AIRFOIL DESIGN AND ANALYSIS

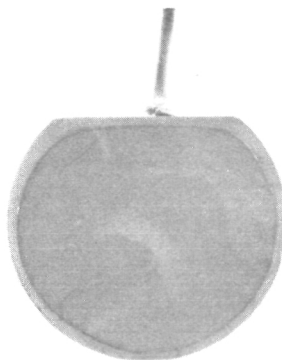
The design of the advanced convectively cooled blade was conducted in parallel to the design and fabrication of the fluidized bed test cylinder to meet the hardware delivery dates required by the program.



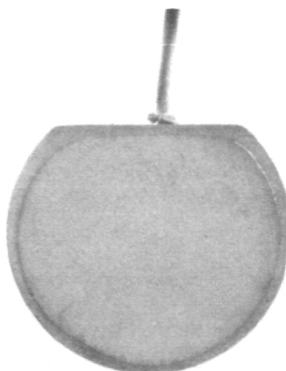
Step 1. A 0.062 inch diameter hole was drilled into a bar section of PWA 1447. The 0.25 inch deep hole was then filled with 4043 aluminum wire. The face was polished smooth and flat.



Step 2. The specimen was coated with 10 mils (0.01 inch) of plated nickel.



Step 3. The specimen was immersed in boiling water for one hour.

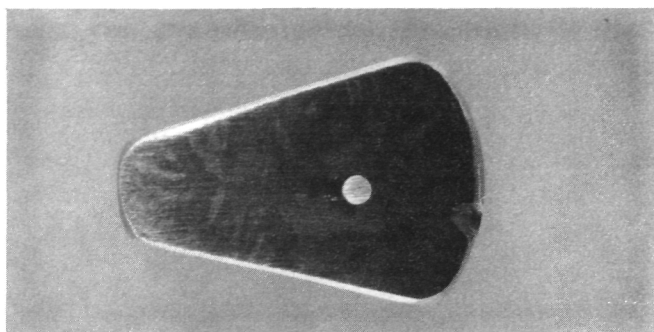


Step 4. Finally, the specimen was heated for 30 minutes in an oven at 200°C.

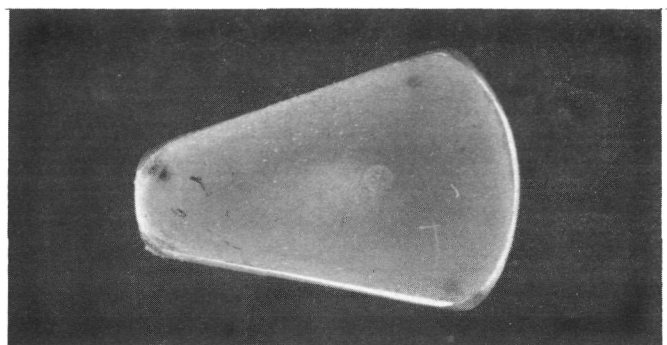
No bulge over the aluminum wire was noted during or after any of the above procedures.

FD 267762

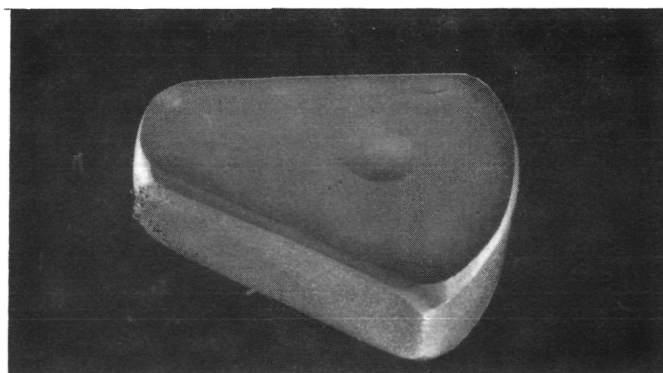
Figure III-48. First Experiment to Investigate Effects of Thermal Expansion Mismatch Between Aluminum and PWA 1447



1. A 0.035 inch hole was drilled completely through a 0.25 in. thick bar section of PWA 1447. A 0.035 inch diameter aluminum wire was drawn through the hole and the composite face was polished flat.



2. The specimen was next coated with 1 mil (0.001 inch) of sputtered nickel in an RF diode discharge.

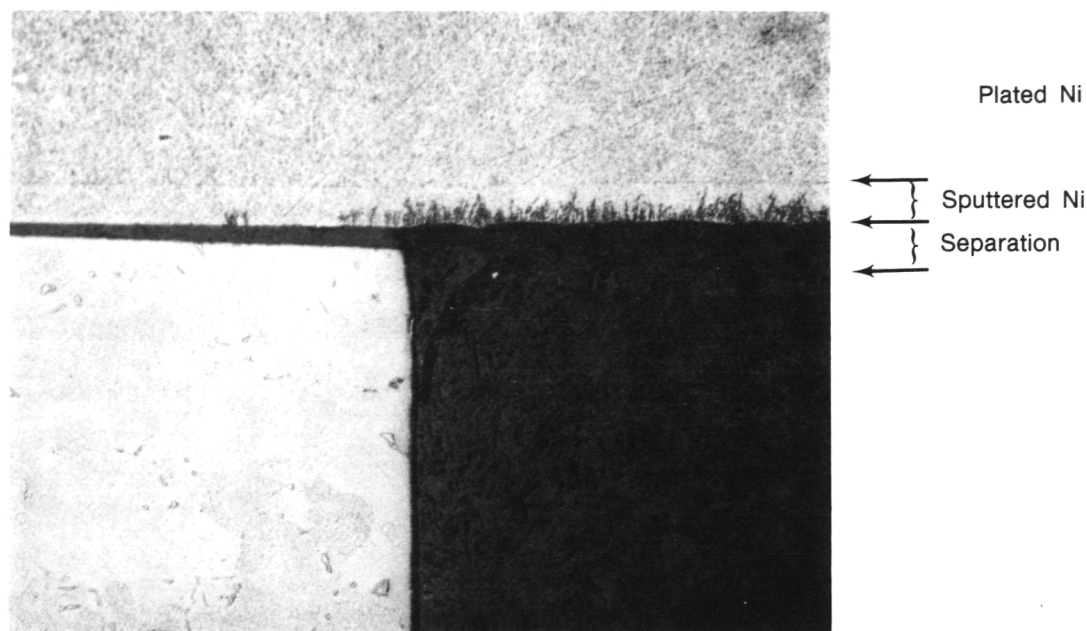


3. After two hours in a NaOH aluminum leaching solution maintained at 140 to 160°F a definite bulge can be seen in the nickel cover over the aluminum wire.

FD 267763

Figure III-49. Effect of Thermal Expansion Mismatch Between Aluminum and PWA 1447

A number of studies were performed in support of this effort. One of the first studies evaluated the effect of coolant film coefficient on maximum metal temperature for typical rig conditions and coolant geometry. The results of this study are shown in Figure III-56. This study showed that increasing the coolant film coefficient above 4000 Btu/hr ft² °F has a small payoff in terms of reduced metal temperature.



Sputtering Run 6-83-083 MN 30806-1 Mag 200X

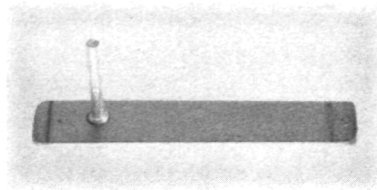
The coating separation at the walls of the hole was measured optically by microscope. A gap of 0.0006 inch was recorded at each side.

FD 267764

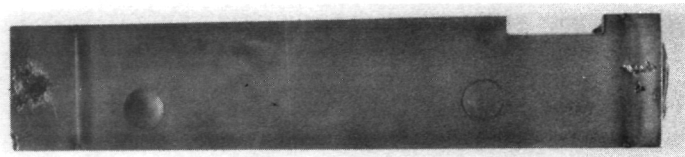
Figure III-50. Cross Section of Bulged Area Over Aluminum Wire Inlaid in PWA 1447 Bar

The pressure distribution and gas bending stresses from the aerodynamic analysis of the SSME blade in the rig are shown in Figure III-57. The low level of gas bending stress confirms that the major component of stress is due to thermals. Our blade design has even lower bending stresses because of the higher moments of inertia associated with a cooled airfoil cross section. The pressure distribution was used for calculating preliminary heat transfer film coefficients for the rig environment.

Figure III-58 shows the preliminary airfoil cross section selected for detailed evaluation. The blade was designed for ease of manufacturing (constant airfoil section without twist or taper, and relatively large leading and trailing edge diameters). These simplifications were made in order to meet cost and deadline commitments. Refinements in the aerodynamics, such as varying the airfoil cross section from root to tip and reducing the trailing edge thickness, are required in a production blade design. This can be achieved in a cost effective manner when production tooling is used.



Adherence Testing of Sputtered PWA 1447 on PWA
1447 Strip Mag 1X



Polished

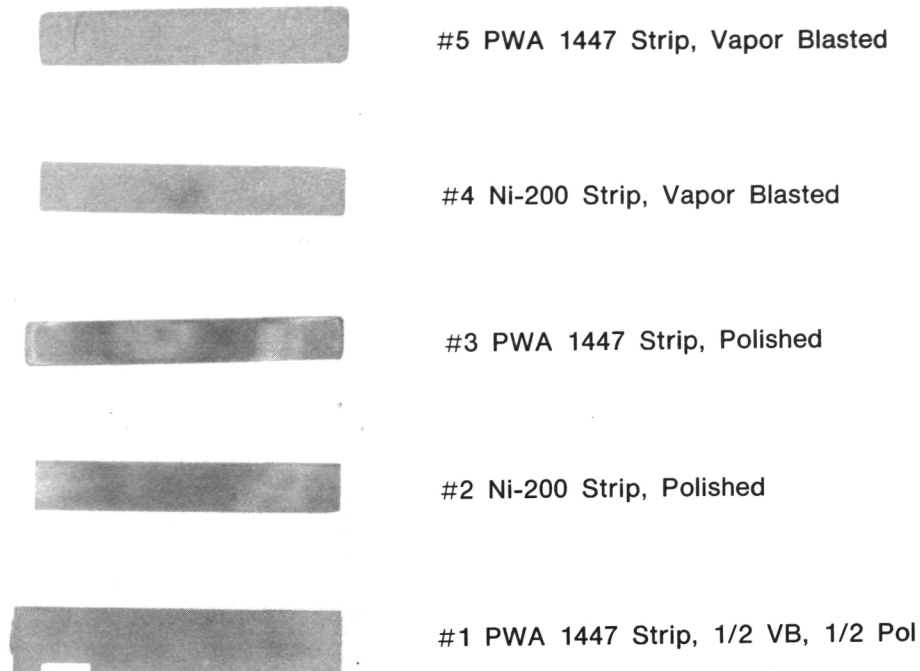
Vapor Blasted

Adherence Test Results, Sputtered PWA 1447 on PWA
1447 Strip With One Side Vapor Blasted and the Other
Side Polished.

FD 267765

Figure III-51. Adherence Testing of Sputtered Coatings on Test Strips

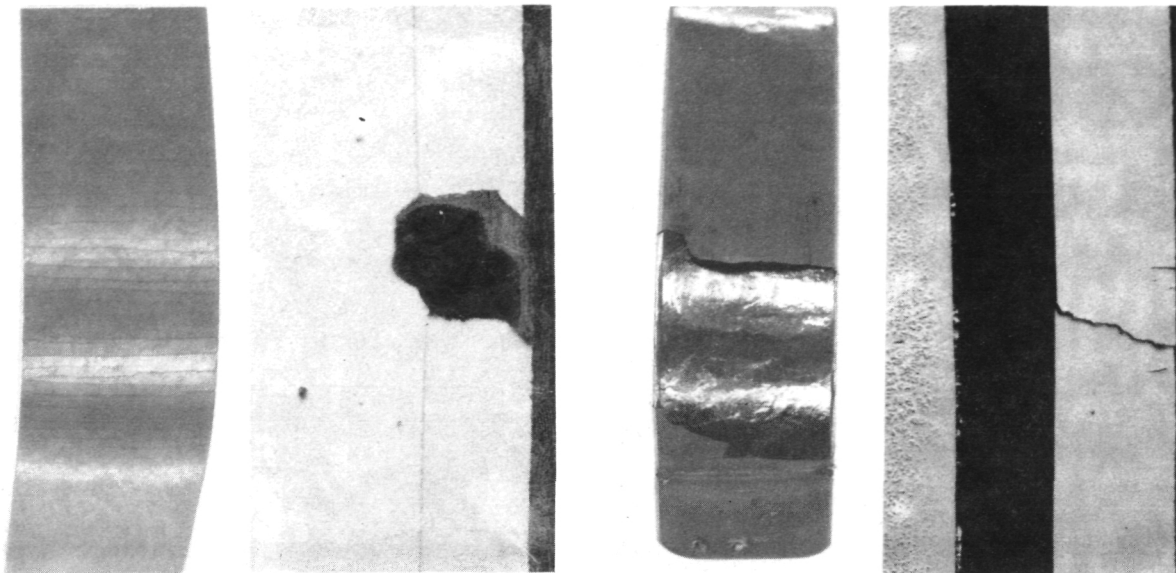
An example of the nodal heat transfer models used in the analysis of the rig heat transfer, for both the methane cooled and hydrogen cooled parts, is shown in Figure III-59. The model depicts one of the coolant passages in the airfoil wall. Since all the passages are the same, only one is modeled. The maximum/average metal temperature for the hydrogen cooled foil is 1359°F/550°F and the maximum thermal strain is 0.40%. The methane cooled foil has a maximum/average metal temperature of 1430°F/966°F and a maximum strain range of 0.225%. These are for a rig hot gas temperature of 1700°F and coolant of 70°F. A quantity of coolant equal to 2% of mainstream flow was used.



FD 267766

Figure III-52. Appearance of Test Strips After Sputtering With 0.01 Inch Coating of PWA 1447

After several iterations the rig blade final outside contour was defined. The final blade contour and the resultant mainstream pressure distribution are shown in Figures III-60 and III-61, respectively. The leading edge and trailing edge diameters are 0.15 and 0.07 inch, respectively. The contour was designed with the intent of providing an easily manufacturable blade with no mainstream separation when running in the rig.



Mag 4X

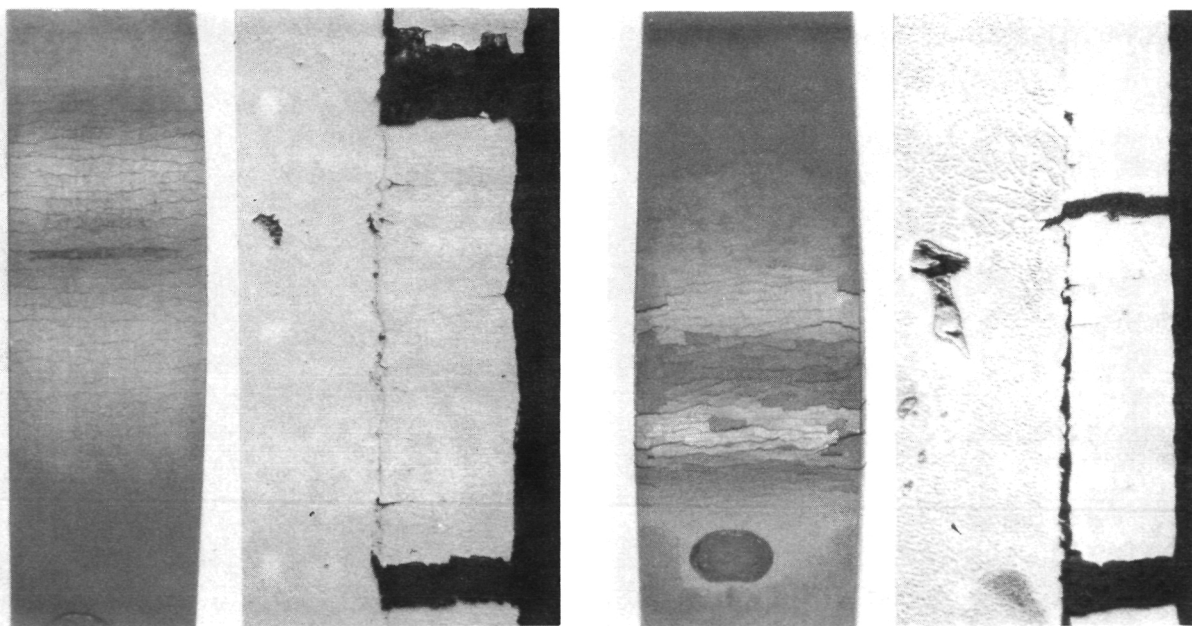
Mag 500X

Mag 4X

Mag 500X

Tab #2 PWA 1447 on Polished Ni-200

Tab #3 PWA 1447 on Polished PWA 1447



Mag 4X

Mag 500X

Mag 4X

Mag 500X

Tab #4 PWA 1447 on Vapor Blasted Ni-200

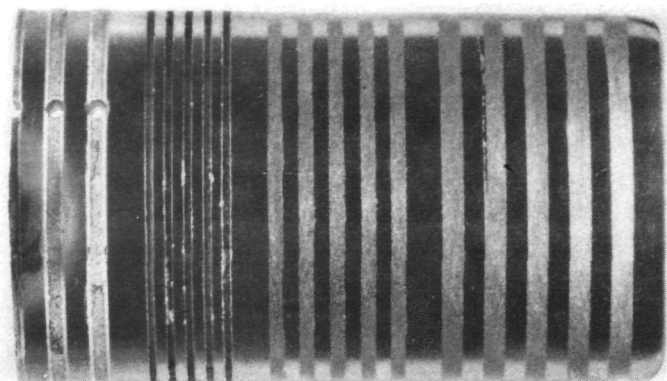
Tab #5 PWA 1447 on Vapor Blasted PWA 1447

FD 267767

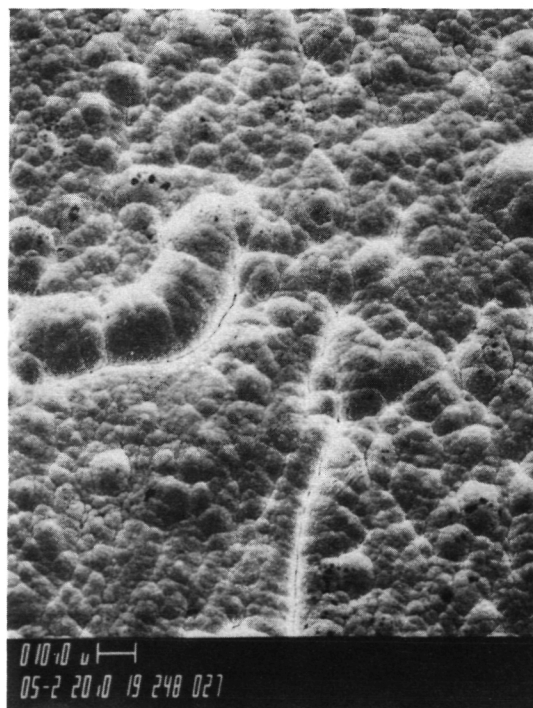
Figure III-53. Results of 90 Degree Bend Testing of Coated Test Strips

The aerodynamic losses associated with trailing edge blockage are an important consideration when evaluating the overall benefit of operating cooled blades at a higher turbine inlet temperature. Since the rig blade contour and coolant passages will be machined from a bar, a relatively large trailing edge was used for ease of manufacture, but production hardware blades will be cast with integral slots. With precision castings smaller trailing edge diameters will be possible, as shown in Figure III-62.

ORIGINAL PAGE IS
OF POOR QUALITY



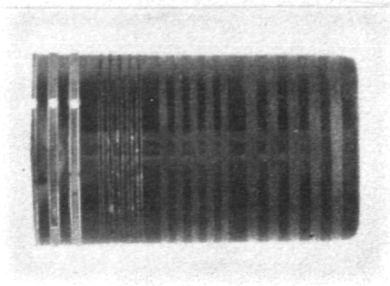
Ni-200 Coating Over Land Surface



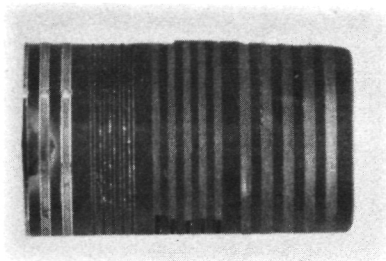
Ni-200 Coating Over Aluminum Surface

FD 267792

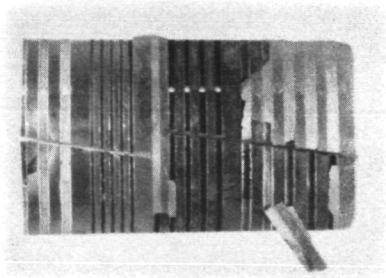
Figure III-54. Specimen from Sputtering Run 6-83-086 SEM Photographs 500× Magnification



As Coated With Ni-200
in Sputter Run 6-83-086
Deep Grooves Had Been
Filled With Aluminum
Wire Prior To Coating



Appearance of Specimen
After Leaching of Aluminum
Filler Material With a
NaOH Solution



Appearance of Specimen
After Attempts To Section
for Metallurgical Review

FD 267793

Figure III-55. Adherence Failure of 0.001 Inch Thick Nickel Closeout Layer

In order to determine the size of the central core that runs up the center of the blade, a study was undertaken to determine the effect of wall thickness on thermal strains. The results of the detailed thermal and stress analysis are shown in Figure III-63. The study showed that the thinner the wall, the lower the thermal strains. The minimum wall thickness was chosen to be 0.055 inch which resulted from the structural requirement to limit the stresses and deflections caused by the coolant-to-mainstream pressure differential.

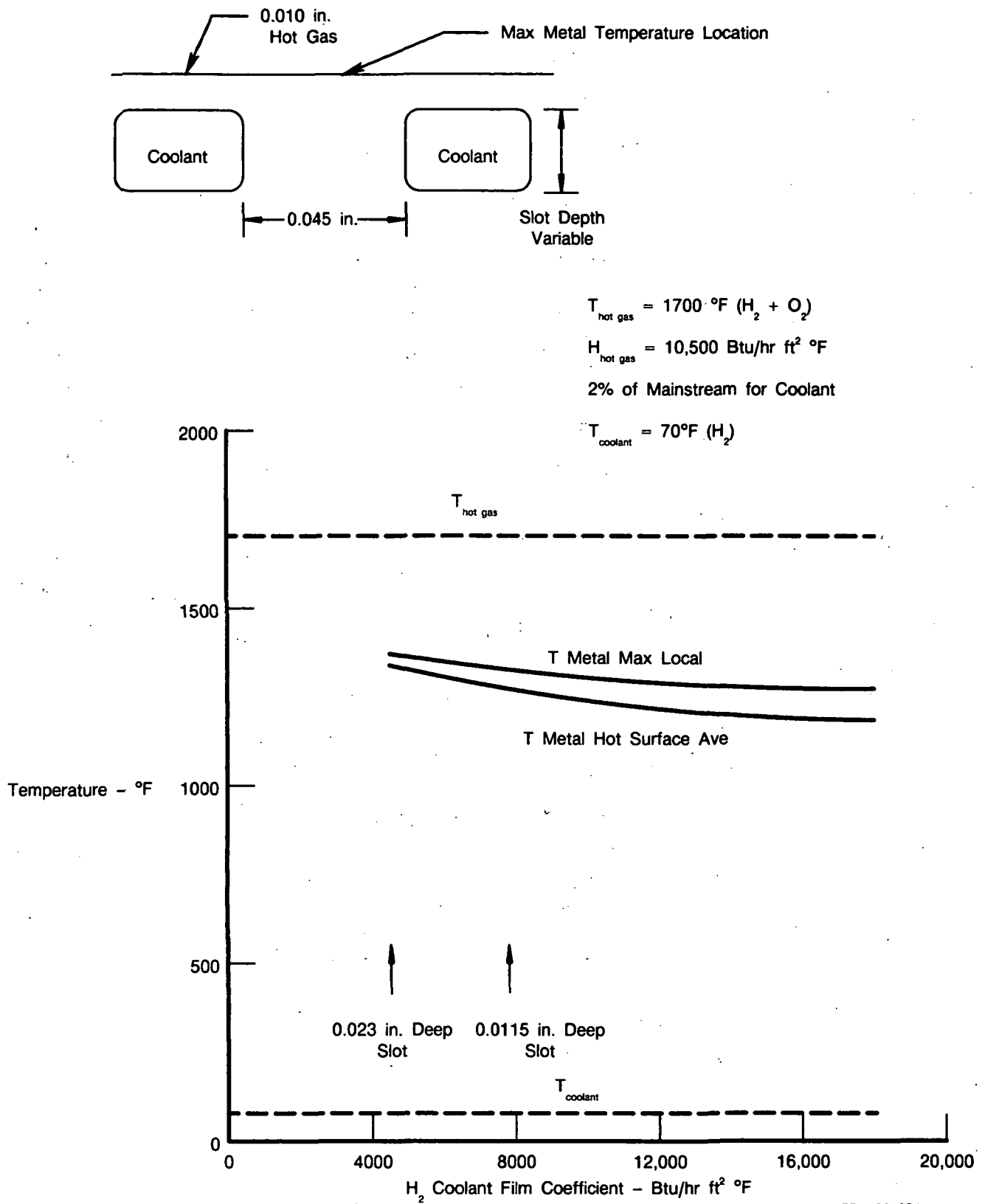
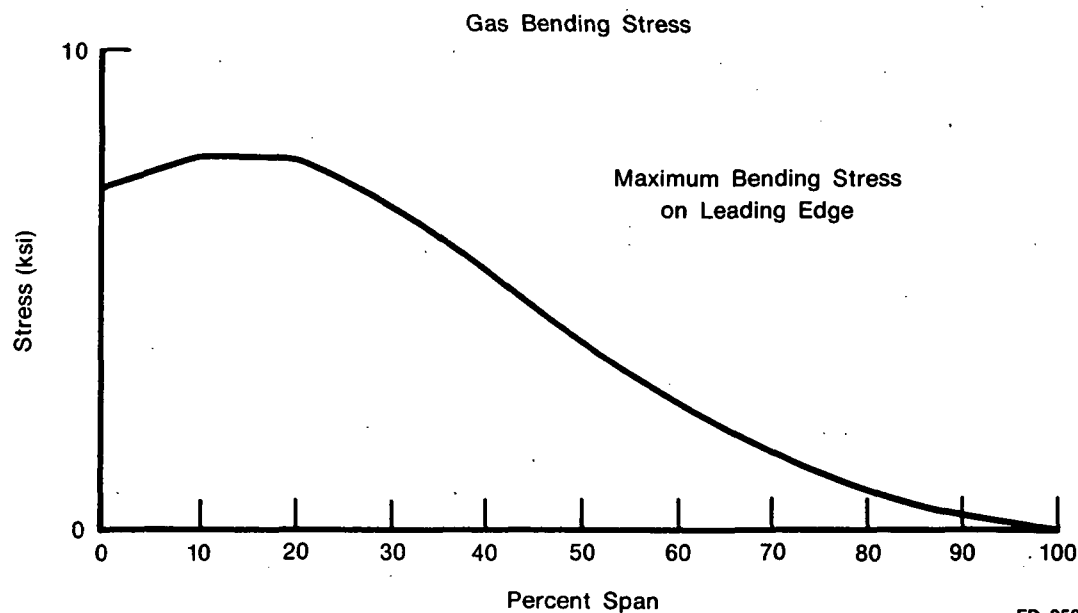
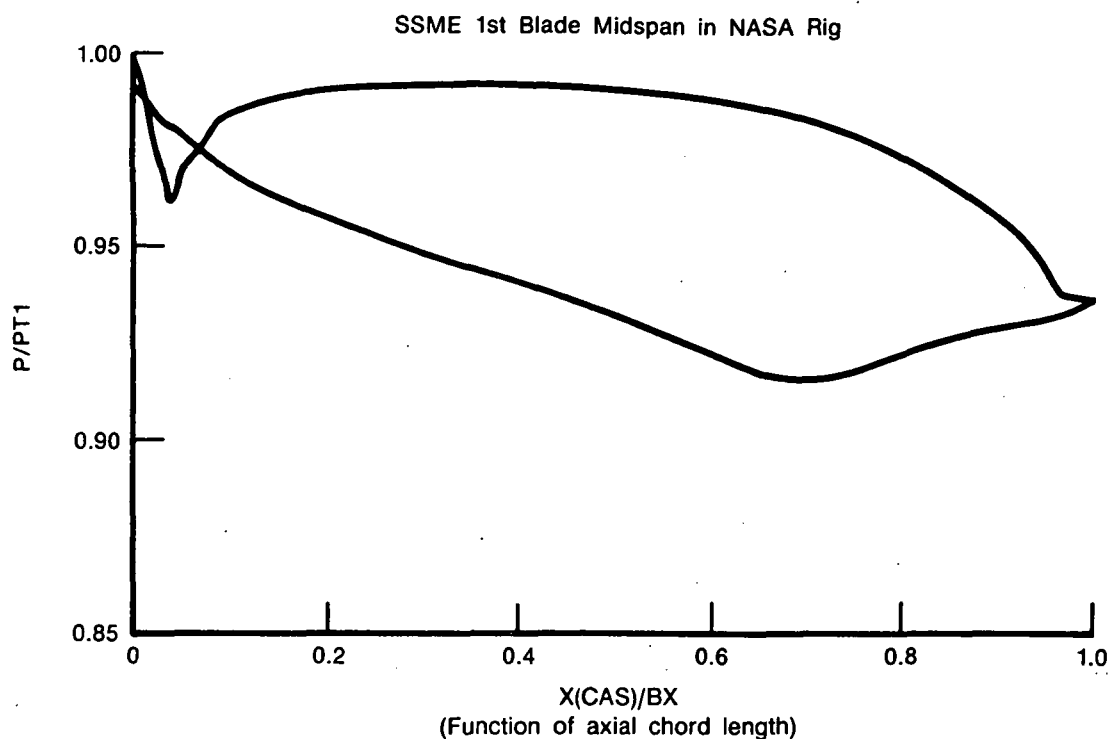


Figure III-56. Effect of Coolant Fluid Coefficient on Blade Metal Temperature for Rig Conditions



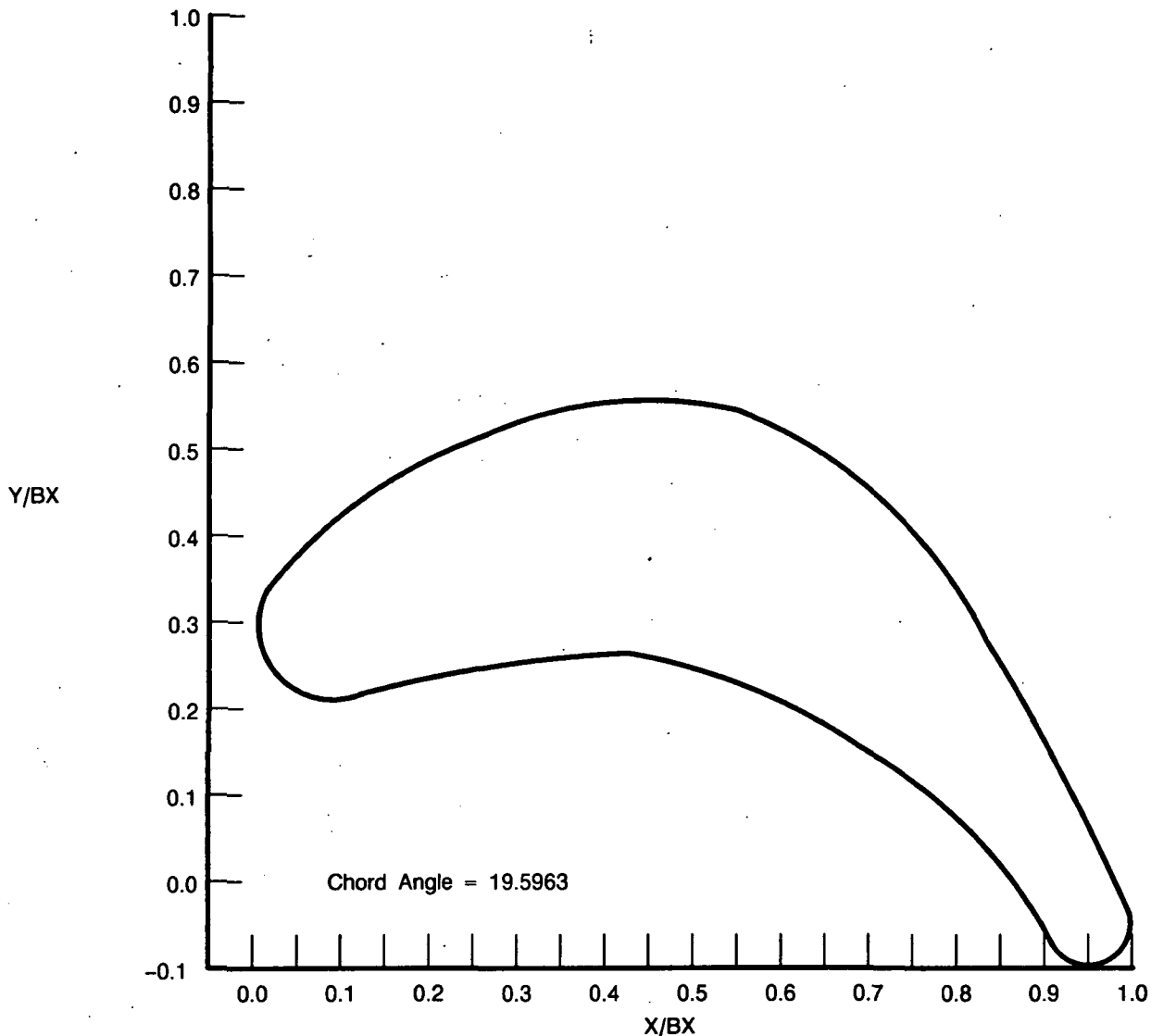
FD 253260

Figure III-57. External Pressure Distribution

1. Preliminary Life Analysis of ATS Cooled Rig Foils

The methane cooled foil and a hydrogen cooled foil were designed and evaluated for testing in the high-pressure NASA cyclic, nonrotating (blade tester) rig. The NASA rig produces a severe cyclic environment as evidenced by the very high acceleration and deceleration rates and hot gas film coefficients of 6,000 to 15,000 Btu/hr ft² °F. Current space shuttle uncooled

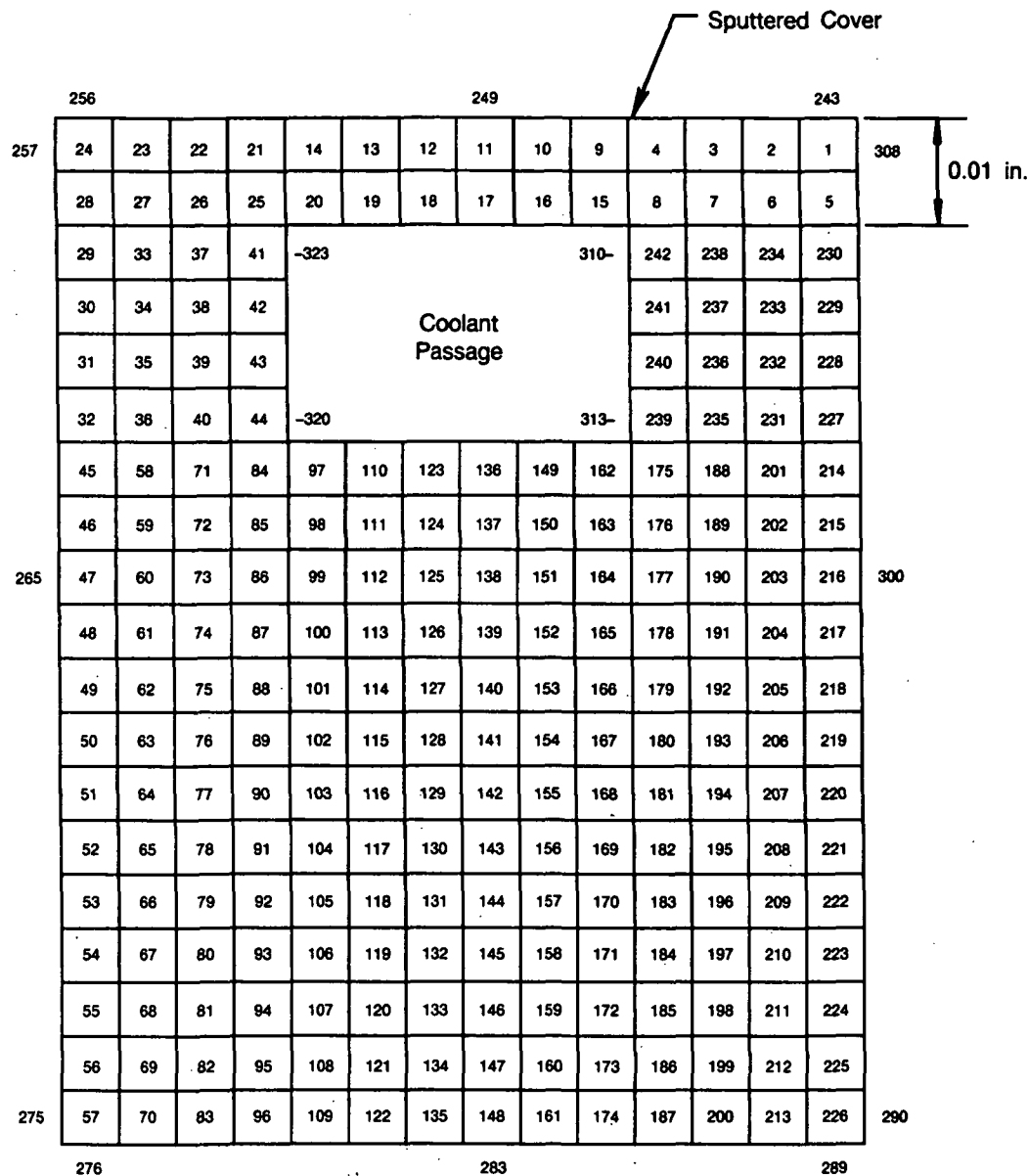
directionally solidified uncoated (DS) Mar-M 246 blades show severe cracking after 5 to 25 cycles in this rig environment.



FDA 301935

Figure III-58. Advanced Turbine Study Preliminary Blade Cross Section

The cooling scheme used (Figure III-64) is a series of chordwise coolant passages which are fed from a radial core through small leading edge holes. The passages discharge at the trailing edge. The coolant passages are 0.0115 inch deep and 0.035 inch wide separated by 0.045 inch lands. The passage lies 0.010 inch from the outside surface, thus minimizing the large metal temperature drop through the wall in this high heat flux application. The foils flow the equivalent of 2% of total mainstream flow.



FDA 301936

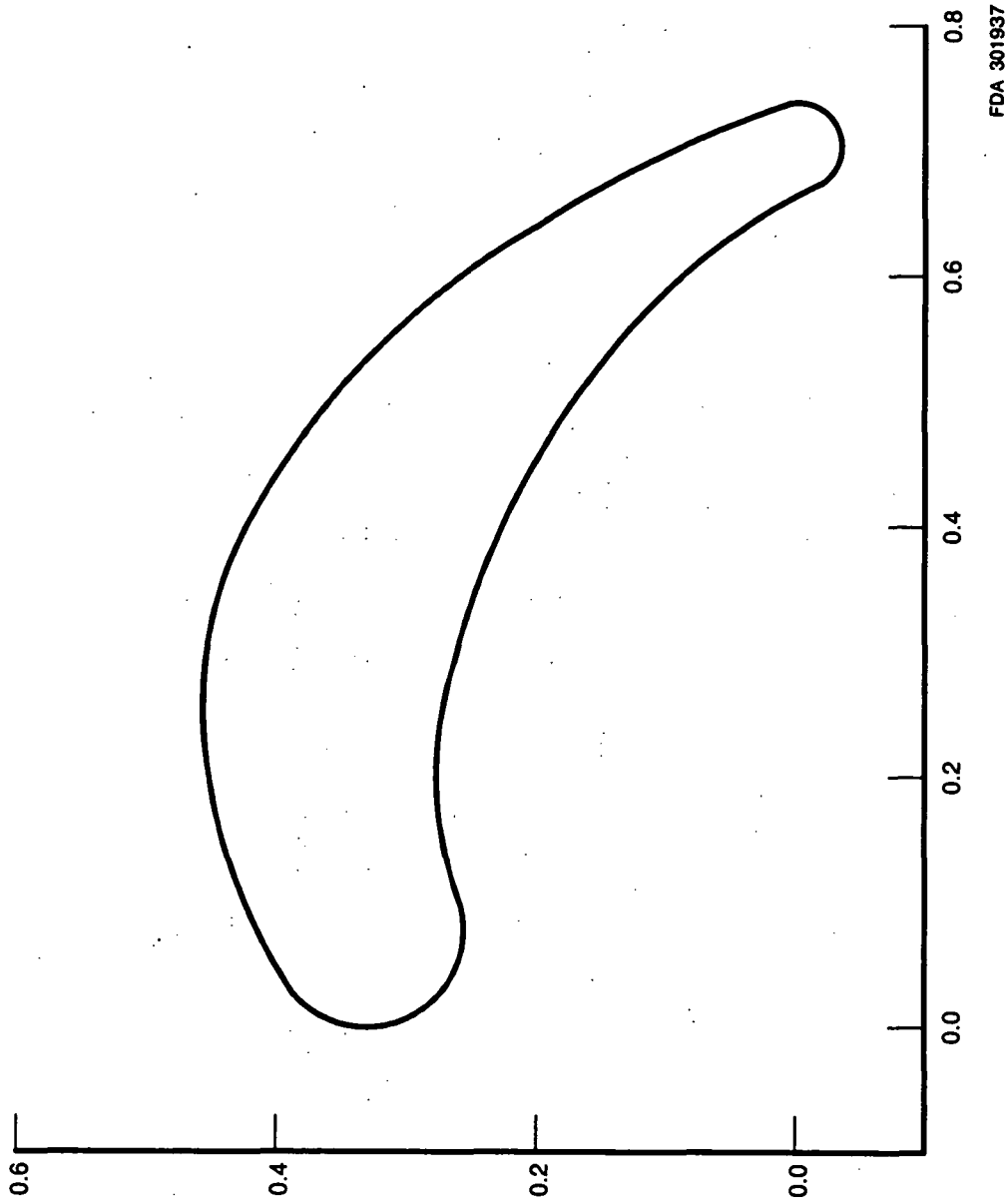
Figure III-59. Nodal Breakup of Wall With Coolant Passage

The cyclic life goal for the blades is 100 cycles. The preliminary life analysis shows the methane cooled foil with a life of 200 cycles and the hydrogen cooled foil with a life of 560 cycles (using average material properties). The coolant is designed for positive outflow in order to provide a graceful wearout mode.

ATS First Blade Mean Section

Airfoil Contour - X vs Y

R1 = 5.095
LED = 0.150
LEER = 1.000
BETA1S = 65.000
DBETA1 = 12.000
R2 = 5.095
TED = 0.070
TEER = 1.000
BETA2S = 25.500
DBETA2 = 2.000
HOL = 0.526
B2GAGE = 24.400
GAMMA = 22.210
BX = 0.738
Z = 63
SCALE = 10.000



FDA 301937

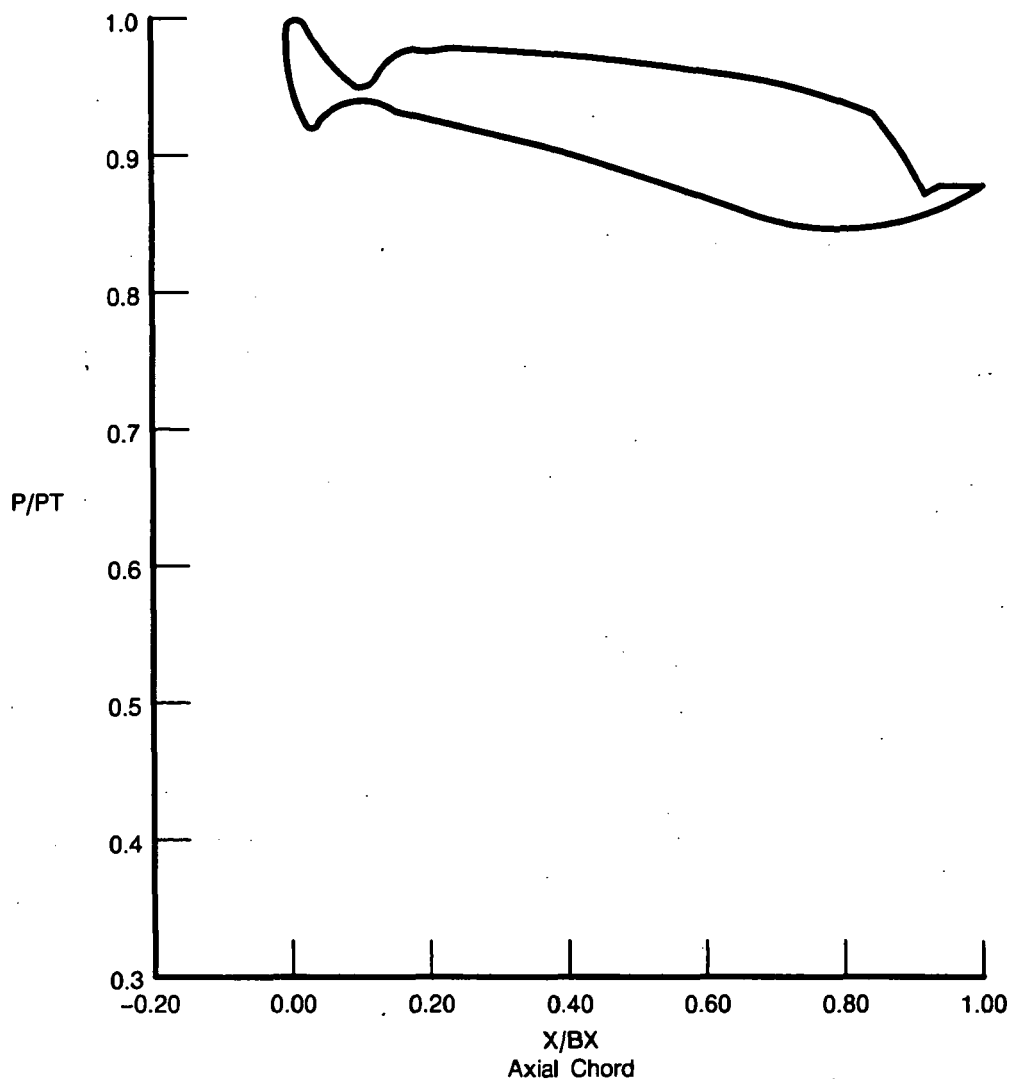
Figure III-60. Advanced Turbine Study Rig Blade Contour

ATS First Blade Mean Section

T882 Pressure Distribution - P/PT vs X/BX

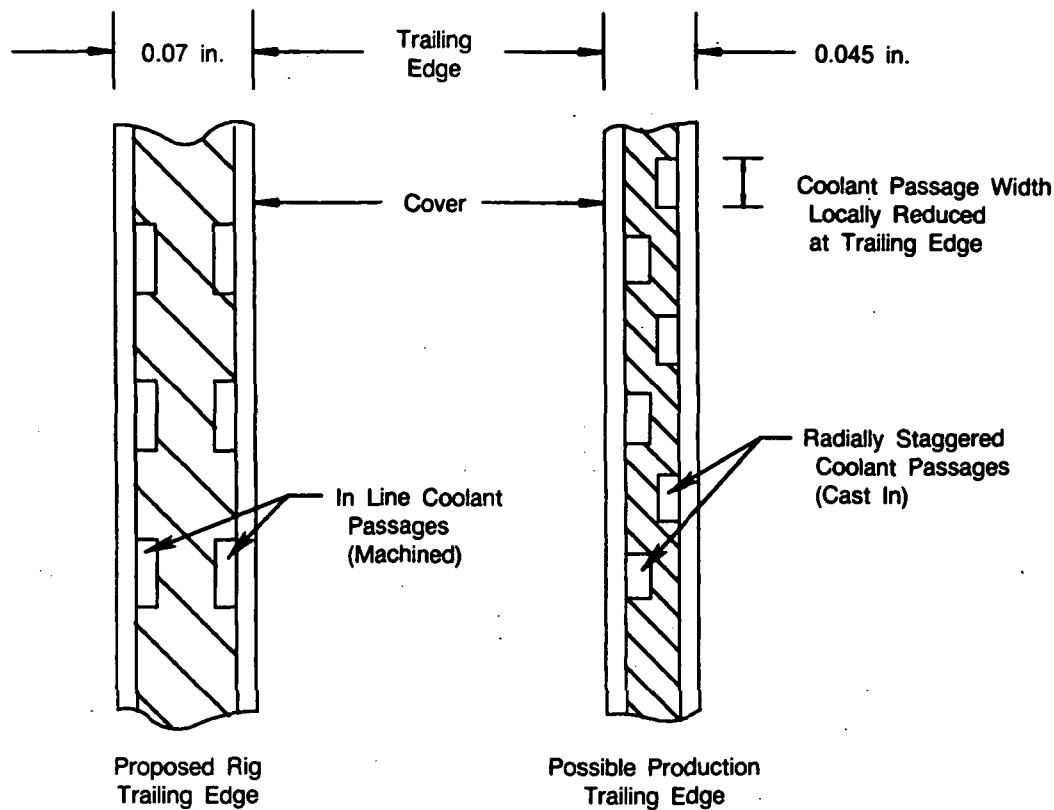
Inlet Mach Number = 0.0 0.178
Inlet Gas Angle = 61.700 61.700
HLE/H1 = 1.000
HTE/HLE = 1.010
H2/HTE = 1.000
H2/H1 = 1.010

Exit Mach No. = 0.396 0.396
Exit Gas Angle = 25.500 25.500
BX = 0.738
Loss (DPT/PT) = 0.020 0.020
Turning = 92.800
Incidence = 3.300

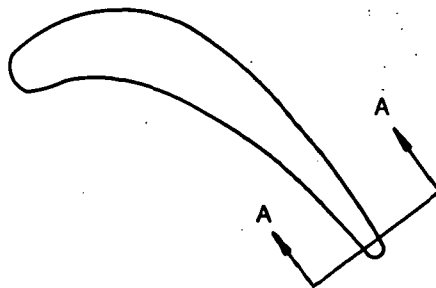


FDA 301938

Figure III-61. Advanced Turbine Study Rig Blade Pressure Distribution



Enlarged Sections A-A Shown Above



FDA 301939

Figure III-62. Method for Reducing Trailing Edge Diameter in Production Hardware

Figures III-65 and III-66 show the transient hot gas temperature and pressure that the NASA rig generates. The steepest parts of the acceleration and deceleration are equal to $9000^{\circ}\text{F}/\text{second}$, which is significantly more severe than a typical jet engine transient. Table III-8 lists the hot gas coolant heat transfer film coefficients and temperatures at various locations around the foil. Note that the film coefficients are significantly higher than those encountered in a jet engine environment. The high film coefficients combined with the rapid transient causes a severe thermal shock for the foils. This translates into high thermal strains in the foil wall. Figures III-67 through III-71 show this strain versus metal temperature for five locations around the hydrogen cooled airfoil. The highest strain range of 0.684% occurs on the suction side at 86%

axial chord just aft of the rear core cavity. This corresponds to a cyclic life of 560 cycles. Figures III-72 through III-76 show the strain versus metal temperature for five locations around the methane cooled foil. The highest strain range of 0.82% occurs on the suction side at 86% axial chord just aft of the rear cavity. This corresponds to a cyclic life of 200 cycles. Figure III-77 summarizes the strain range and cyclic life for the hydrogen cooled and methane cooled foils.

In general, the thermal strains in the hydrogen cooled foil should be higher than the methane cooled foil because of the higher heat flux in the hydrogen cooled foil. But in the thick wall section aft of the rear core cavity, the methane configuration shows higher strains than the hydrogen configuration. Compare Figures III-69 and III-70 (H_2) versus Figures III-74 and III-75 (CH_4). Note that on the methane, Figures III-74 and III-75, that the maximum strains peaks out during the transient while on the hydrogen (Figures III-69 and III-70) the highest strains are very close to the steady-state values. To help understand the difference between the hydrogen and methane strains aft of the second core cavity, two uncooled analyses were conducted for this location: one analysis used H_2 and O_2 combustion products and the other analysis used CH_4 and O_2 combustion productions. Figures III-78 and III-79 show the results of these analyses. Note that the worst strains occur during the transient with no strain at steady state. Comparing Figures III-69, III-74, III-78, and III-79, the cooled methane configuration looks more like the uncooled curves than the hydrogen cooled configuration for the thick walled section aft of the second core cavity. The benefit of methane cooling was a reduction of strain range from 0.859% uncooled to 0.82% cooled, while the benefit of hydrogen cooling was to reduce strain range from 0.973% uncooled to 0.684% cooled. Thus, thicker wall sections should be minimized for methane cooled parts.

The results of this study are based on detailed transient thermal and strain analysis. The nodal configurations simulating different locations on the foil are provided in Figures III-80 through III-83.

The thermal strain ranges of Figures III-67 through III-76 were converted to cyclic life using Figure III-84. The summary is presented in Figure III-77. Metal temperatures at full power are given in Figures III-85 and III-86.

2. Conclusions of Preliminary Life Analysis

- Hydrogen and cooling provides good cyclic life for both thin (0.055 inch) and thick wall (0.11 inch) sections.
- Methane cooling provides good cyclic life for thin wall sections (0.55 inch). But for thick wall sections (0.11 inch), methane cooling shows poor cyclic life improvement.
- Both the methane and hydrogen cooled foils will exceed the 100 cycle life requirement. (Lives were obtained using nominal material properties.)

The analysis of the cooled rig blade identified the thick section aft of the rear cavity as being the life limiting region in the blade. A study was performed to identify the improvement in life that can be obtained by extending the rear core cavity further back. Figure III-87 shows the two cross sections that were analyzed. Section A-A is 0.139 inch thick and is located aft of the rear core, which has a trailing edge diameter of 0.035 inch. Section B-B is 0.11 inch thick and is located aft of the extended core, which has a trailing edge diameter of 0.010 inch. A detailed thermal/strain analysis of the two different configurations showed the following results:

	<u>0.139 Inch Section</u>	<u>0.11 Inch Section</u>
CH ₄ Cooled	0.912%/108 cycles	0.784%/260 cycles
H ₂ Cooled	0.743%/345 cycles	0.656%/730 cycles
		(Strain Range/Cyclic Life)

By extending the rear core further aft, the cyclic life of the part was increased by a factor of more than two.

Two methods of cooling the blade tip cap were considered, as shown in Figure III-88. A film cooled design was investigated. Using 0.5% flow* (25% of the entire blade flow) to cool the tip cap, the film would exit out of 18 0.006-inch diameter holes equally spaced around the tip cap. This design was deemed unacceptable due to the large quantity of flow and the resultant poor film coverage.

A convectively cooled design was also investigated. The same type of grooves used to cool the air flow was used to cool the tip cap, using a cooling flow of only 0.16%. Unlike the film cooled design, the convective design provides positive cooling capability. The film cooled design could be a source of problems, if the hot gas secondary flows wash the film off the surface of the foil. Conversely, this condition does not affect the convectively cooled design.

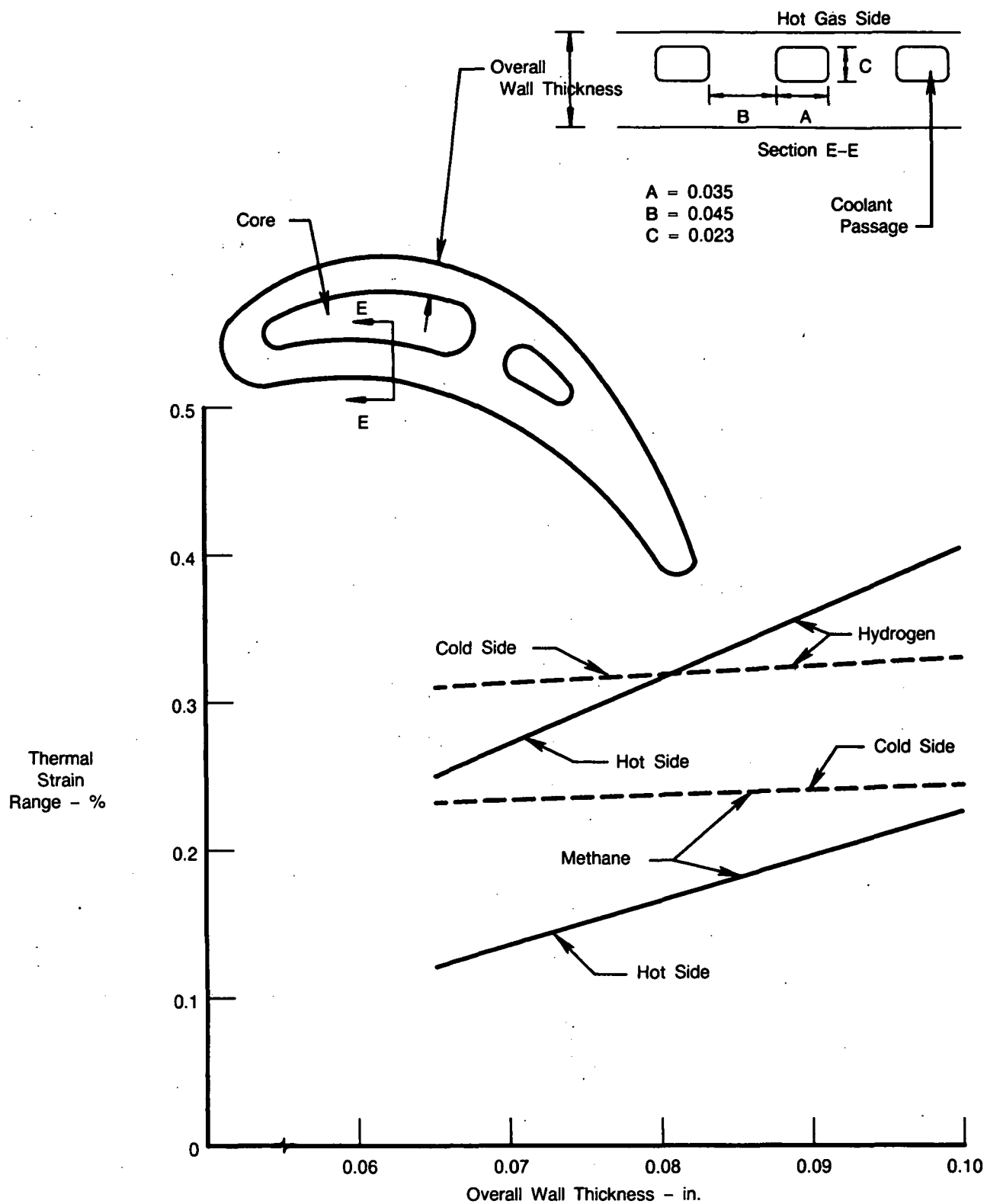
For this reason, and the reduced cooling flow requirement, the convective cooling tip cap design was chosen over the film cooled design. The convective cooling tip cap design will have slightly lower temperatures and strains than the rest of the blade, since the hot gas temperature should be slightly lower along the rig endwalls than in the middle of the rig.

The nodal breakup for the low cycle fatigue life study of the uncooled slave airfoils is shown in Figure III-89. The same hot gas transient used to analyze the cooled foil was used in this analysis. The maximum strain range was found to be 1.58% on the suction side, Node 192. This strain range is far in excess of our LCF data for PWA 1447 material. Using a gross extrapolation of the LCF curve, the cycle life of the slave airfoil was found to be less than 10 cycles.

* Note: Percent flow is defined according to the following equation

$$\text{Coolant Flow} = \frac{(\text{Total Rig Inlet Flow}) \times (\% \text{ Flow})}{3}$$

where flows are in pounds per second and 3 is the number of foils in the rig.



FDA 301940

Figure III-63. Thermal Strain Versus Overall Wall Thickness for Rig Conditions

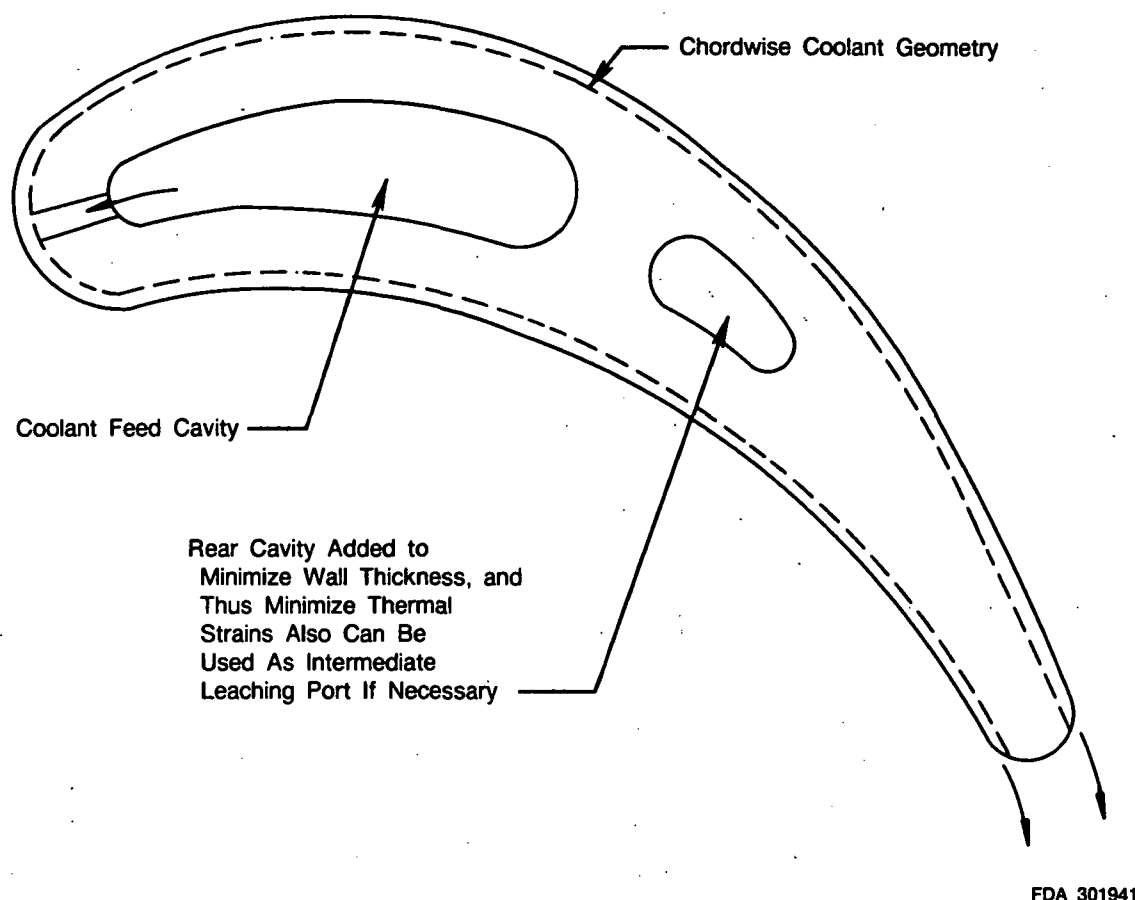


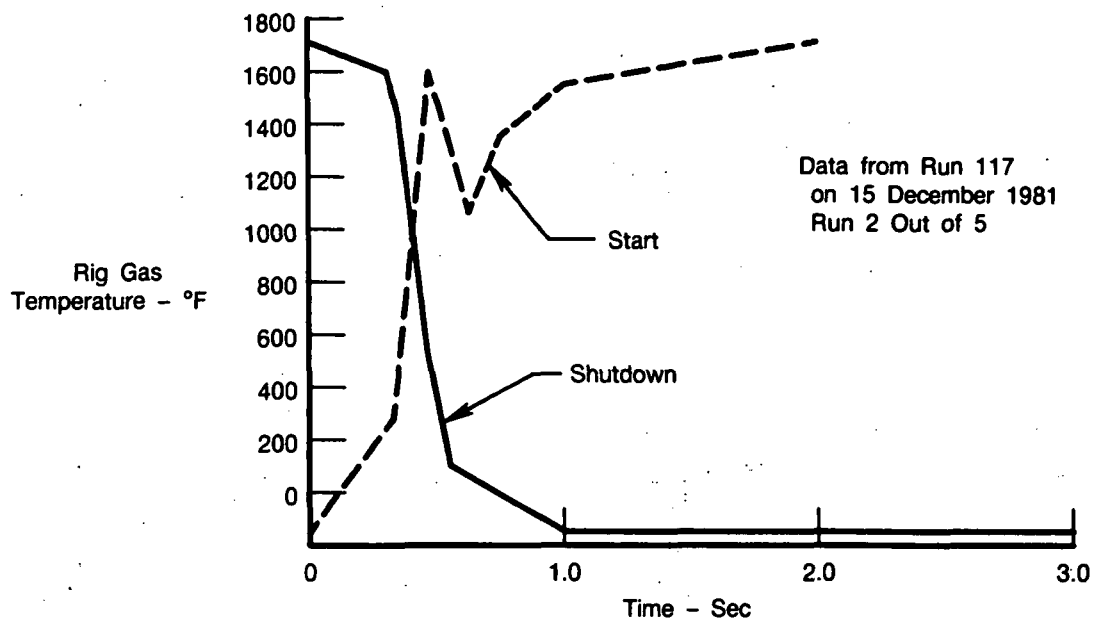
Figure III-64. Rig Blade Coolant Geometry

The information obtained from the previously discussed design studies was used to generate the geometry of the advanced convectively cooled airfoils and their associated hardware. Even though the fluidized bed test had not yet been performed, a decision was made to select the optimum coolant groove-land geometry combination based on the information available. This decision was made with the understanding that modifications to the drawings could be made prior to the hardware fabrication commitment if the fluidized bed test results warranted it. The coolant groove geometry selected for the engineering drawing was 0.035 ± 0.002 inch wide by 0.012 ± 0.002 inch deep. The selected spacing between the slots was 0.035 inch wide nominally.

Table III-9 lists the part numbers and titles of the engineering layout and drawings for the advanced convectively cooled hardware. This table also lists the figure numbers for these drawings, which are contained in Appendix B.

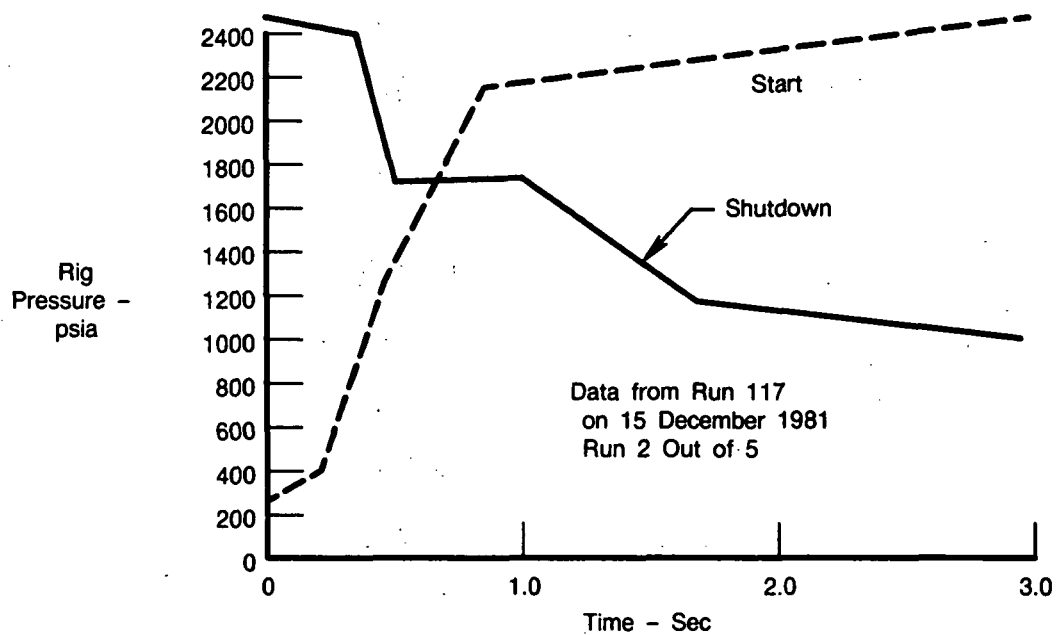
F. TASK 4 — AIRFOIL FABRICATION AND TASK 5 — TEST FOLLOW UP

Due to the inability to successfully fabricate the fluidized bed test cylinders, the airfoil fabrication, test and test follow-up were not performed.



FDA 301942

Figure III-65. Rig Transient Hot Gas Temperatures



FDA 301943

Figure III-66. Rig Transient Hot Gas Pressure

Table III-8. Hydrogen and Methane Configurations At Full Power ($T_{\text{hot gas}} = 1700^{\circ}\text{F}$)
 Heat Transfer Film Coefficients (h) are in $\text{Btu/hr ft}^2 ^{\circ}\text{F}$

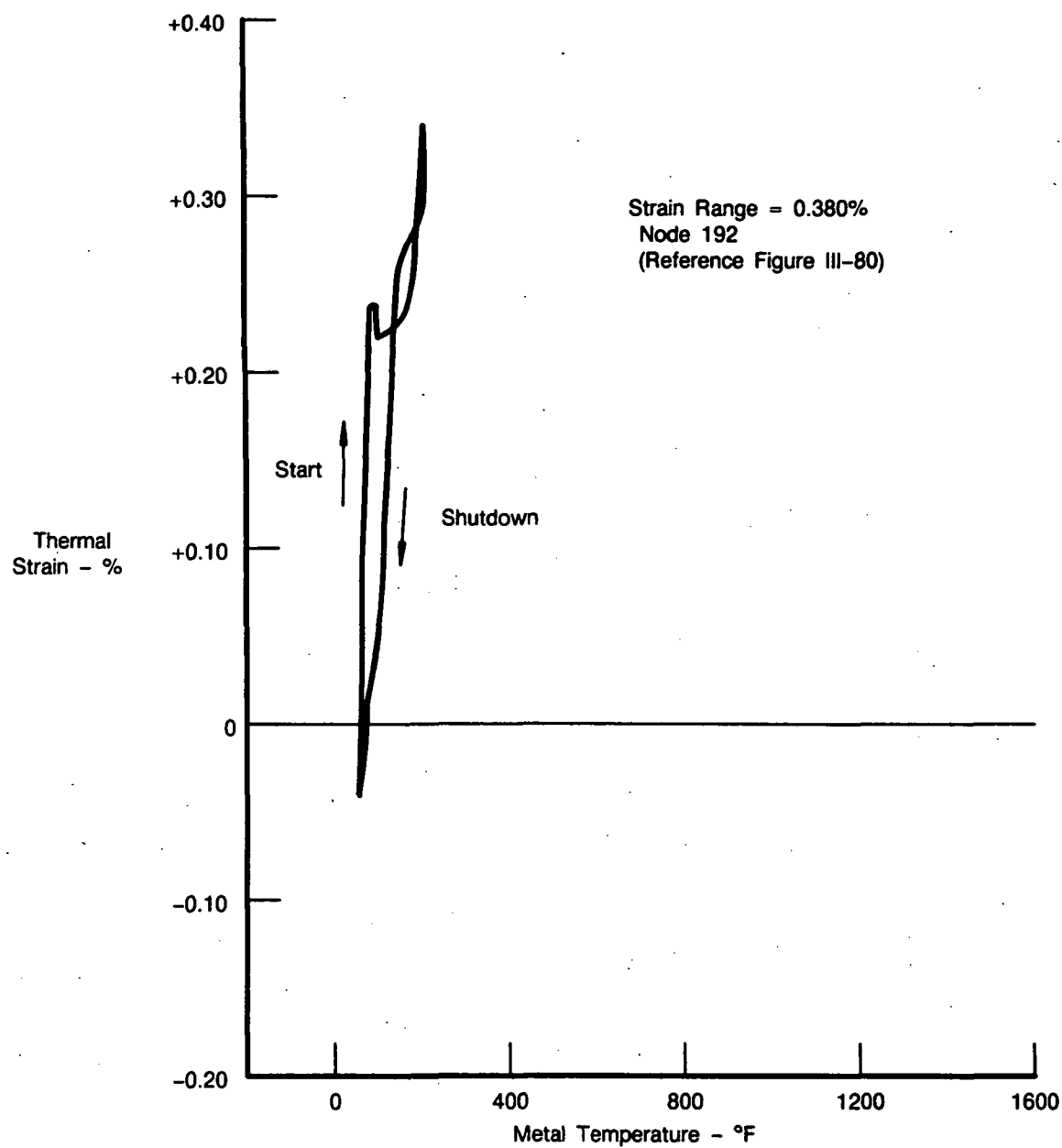
	$h_{\text{hot gas}}$	h_{coolant}	T_{coolant} ($^{\circ}\text{F}$)
<i>Hydrogen Configuration</i>			
SS, 30% Axial Chord	15,500	11,000	150
PS, 30% Axial Chord	10,100	11,000	150
SS, 86% Axial Chord	15,300	11,000	266
PS, 75% Axial Chord	11,400	11,000	266
Trailing Edge	13,600	11,000	337
<i>Methane Configuration*</i>			
SS, 30% Axial Chord	9,800	2,700	210
PS, 30% Axial Chord	6,400	2,700	210
SS, 86% Axial Chord	9,700	2,700	417
PS, 75% Axial Chord	7,200	2,700	417
Trailing Edge	8,600	2,700	542

*For the methane configuration, we plan on simulating the
 $\text{CH}_4 + \text{O}_2$ hot gas with H_2O_2 run at lower temperature to give
 the same heat flux.

4041C

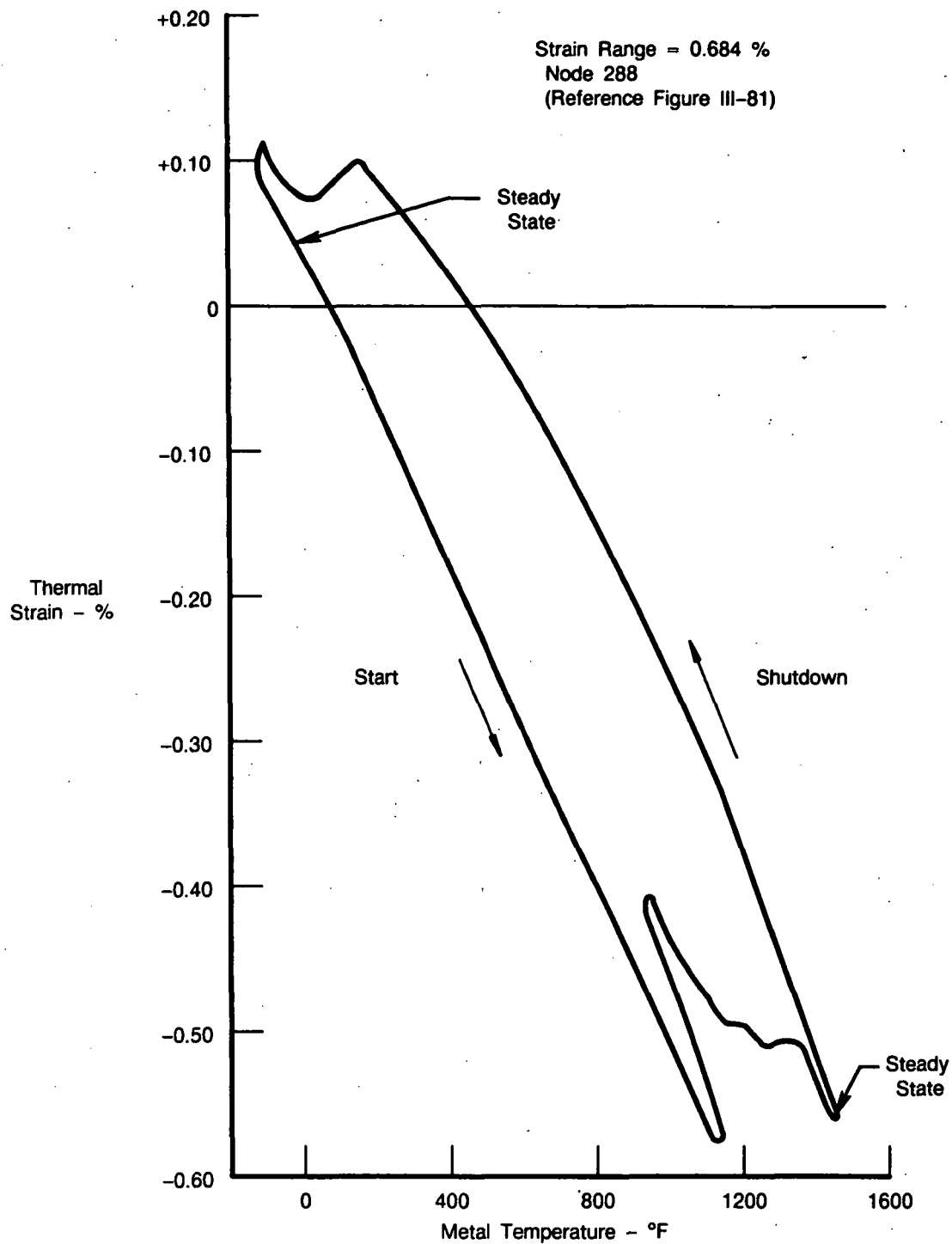


III-73



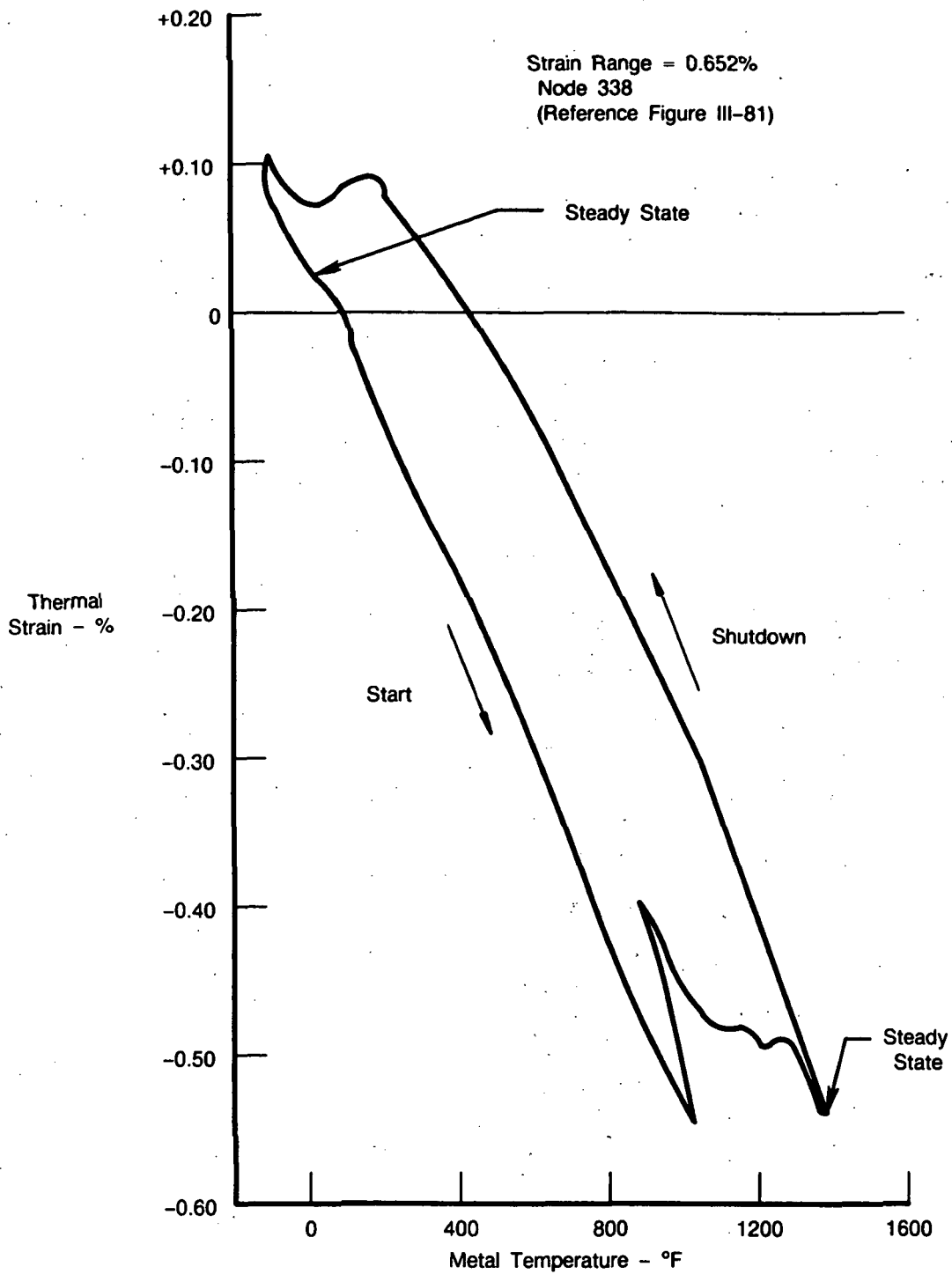
FDA 301945

Figure III-68. H_2 Cooled ATS Blade Thermal Strain Versus Metal Temperature for Worst Node on Pressure Side, 30% Axial Chord



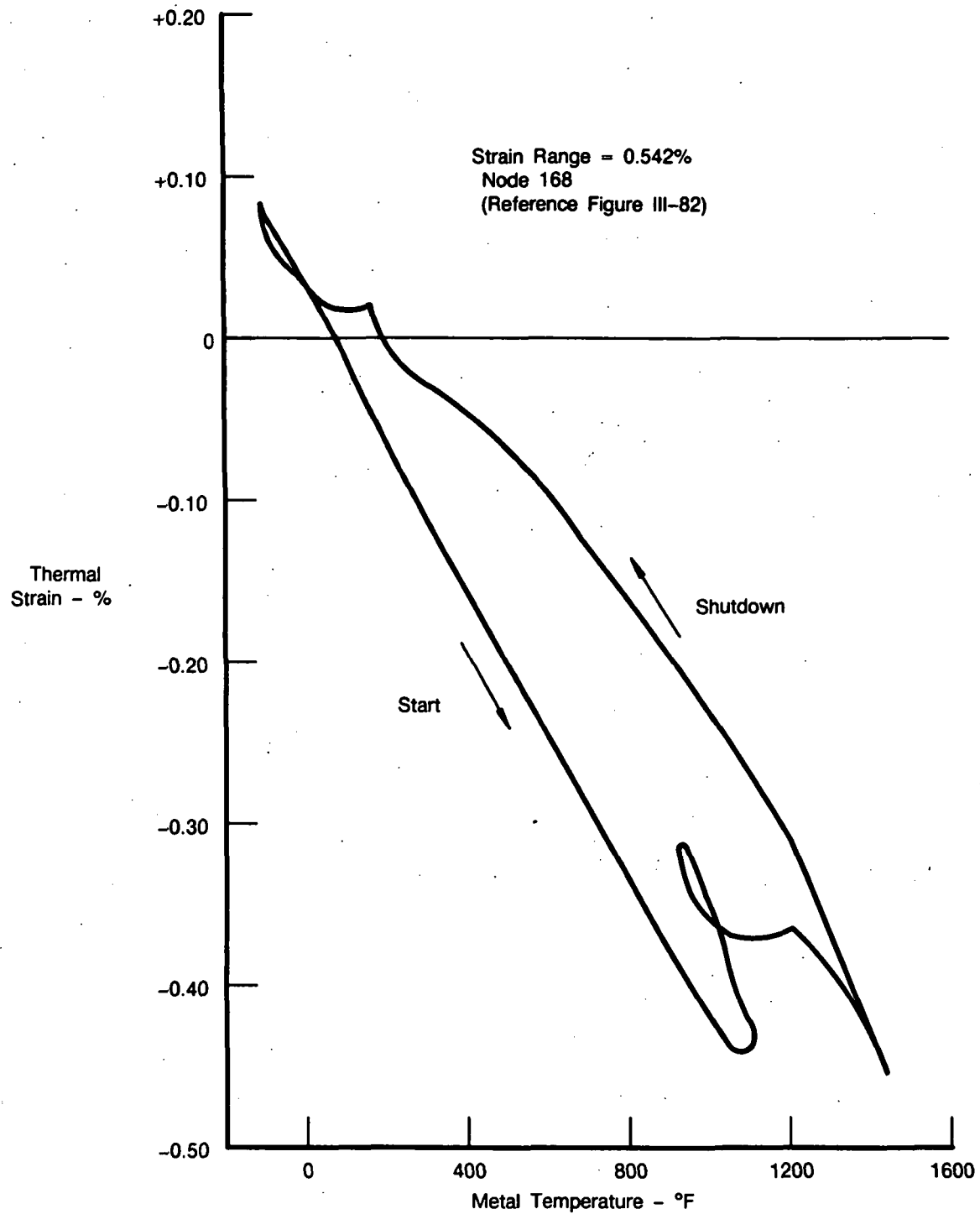
FDA 301946

Figure III-69. H_2 Cooled ATS Blade Thermal Strain Versus Metal Temperature for Worst Node on Suction Side, 86% Axial Chord



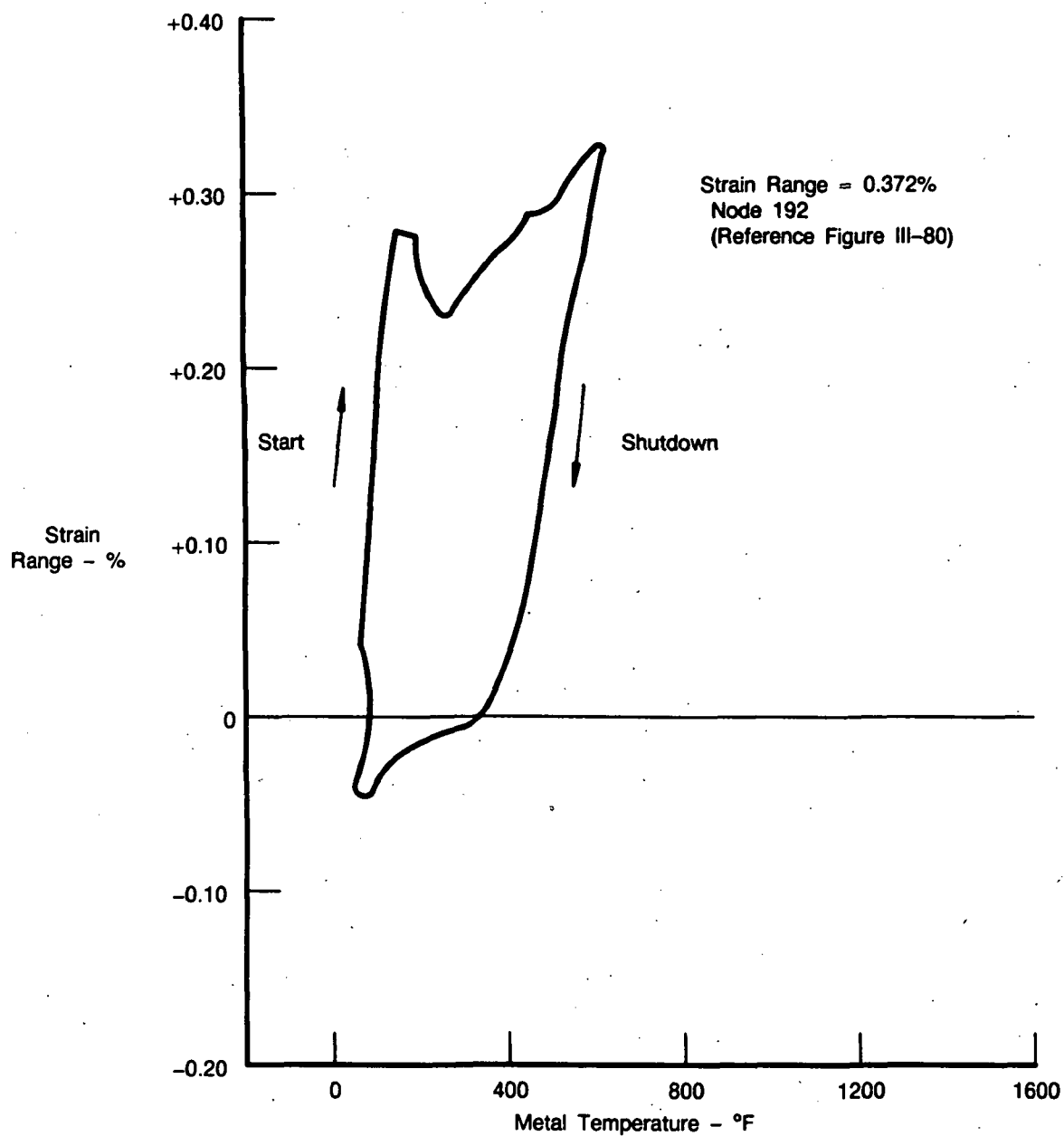
FDA 301947

Figure III-70. H_2 Cooled ATS Blade Thermal Strain Versus Metal Temperature for Worst Node on Pressure Side, 75% Axial Chord



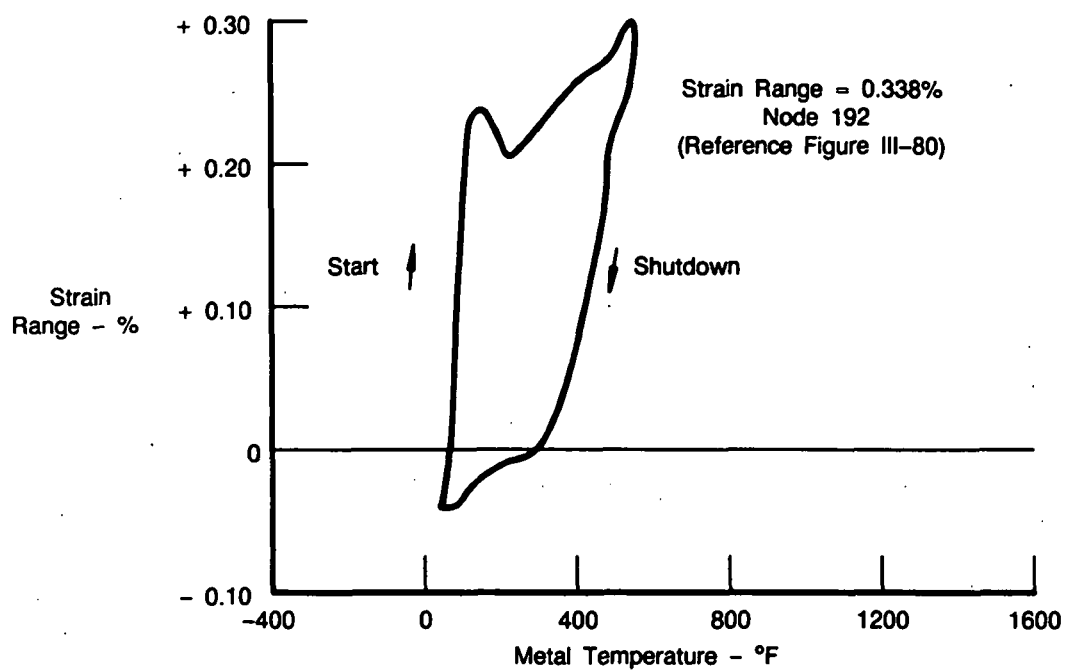
FDA 301948

Figure III-71. H_2 Cooled ATS Blade Thermal Strain Versus Metal Temperature for Worst Node on Trailing Edge



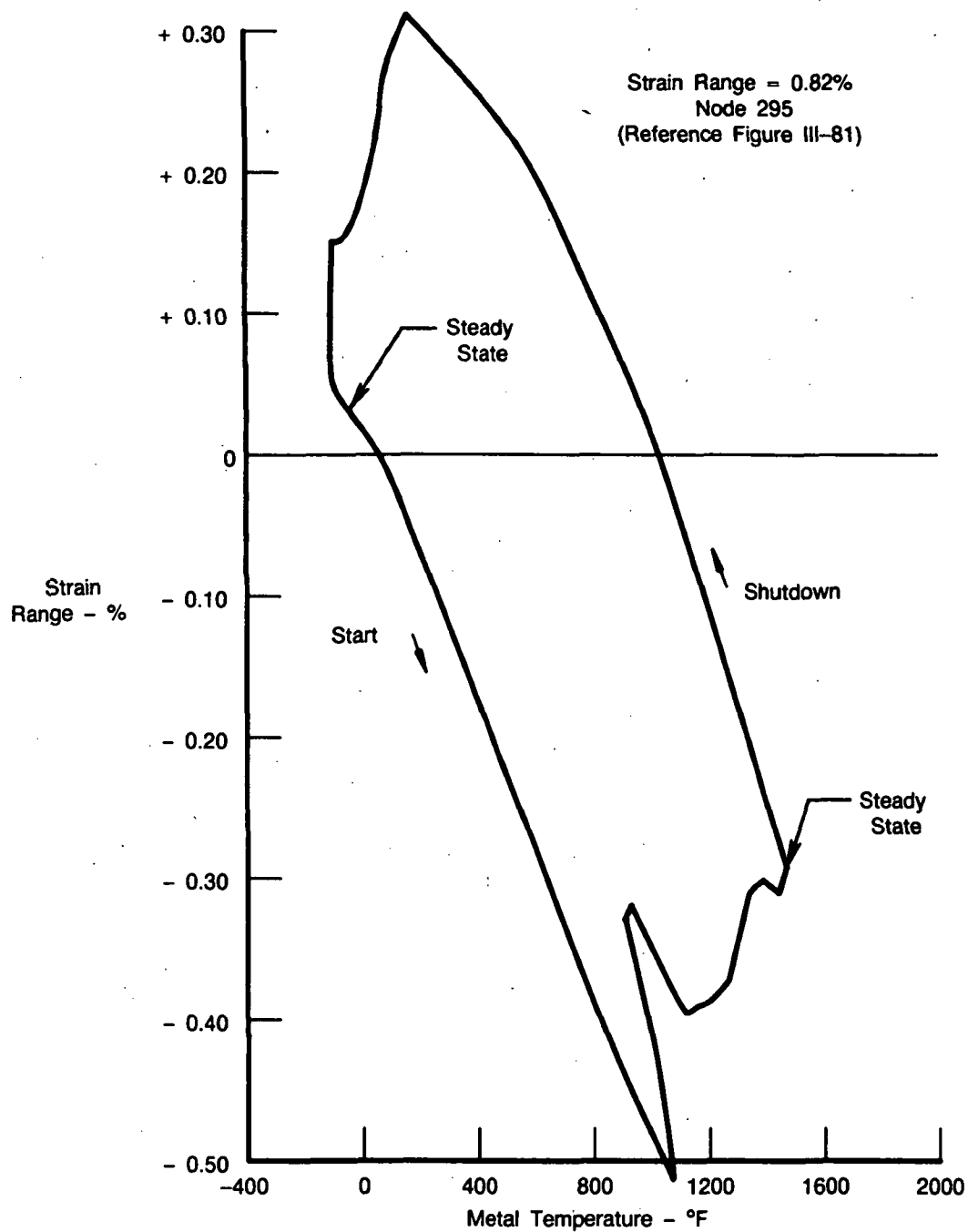
FDA 301949

Figure III-72. CH_4 Cooled ATS Blade Thermal Strain Versus Metal Temperature for Worst Node on Suction Side, 30% Axial Chord



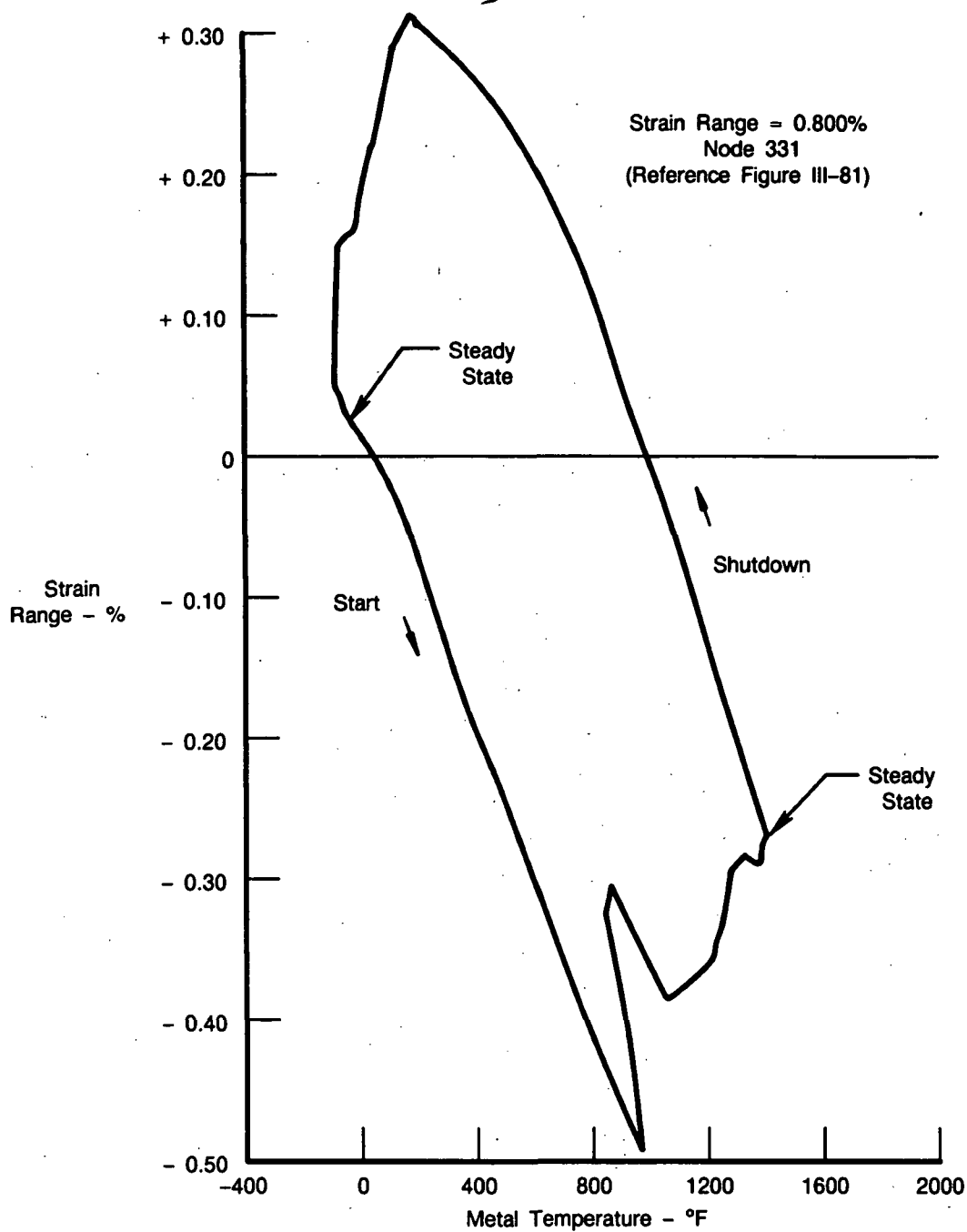
FDA 301950

Figure III-73. CH_4 Cooled ATS Blade Thermal Strain Versus Metal Temperature for Worst Node on Pressure Side, 30% Axial Chord



FDA 302501

Figure III-74. CH_4 Cooled ATS Blade Thermal Strain Versus Metal Temperature for Worst Node on Suction Side, 86% Axial Chord



FDA 302502

Figure III-75. CH_4 Cooled ATS Blade Thermal Strain Versus Metal Temperature for Worst Node on Pressure Side, 75% Axial Chord

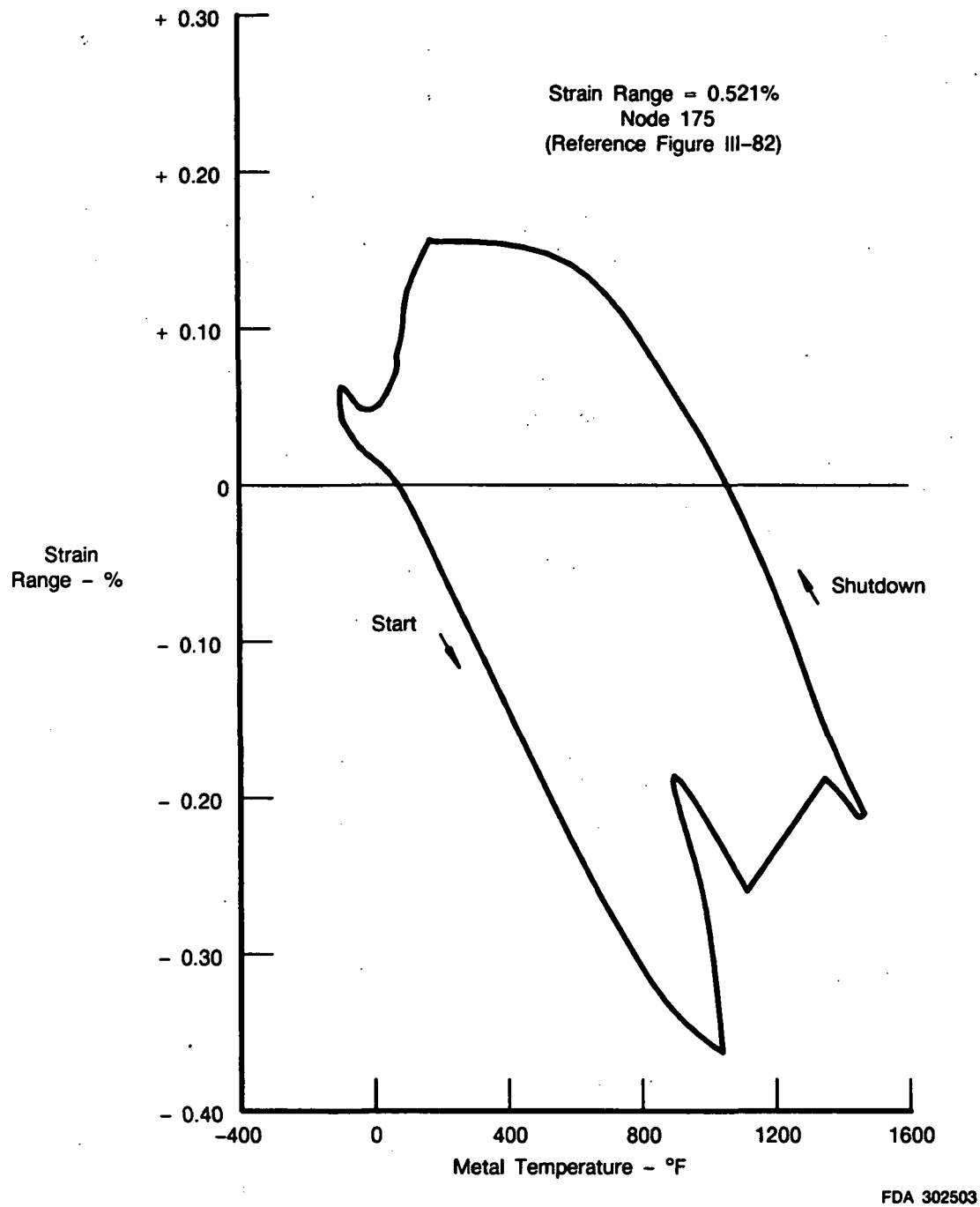
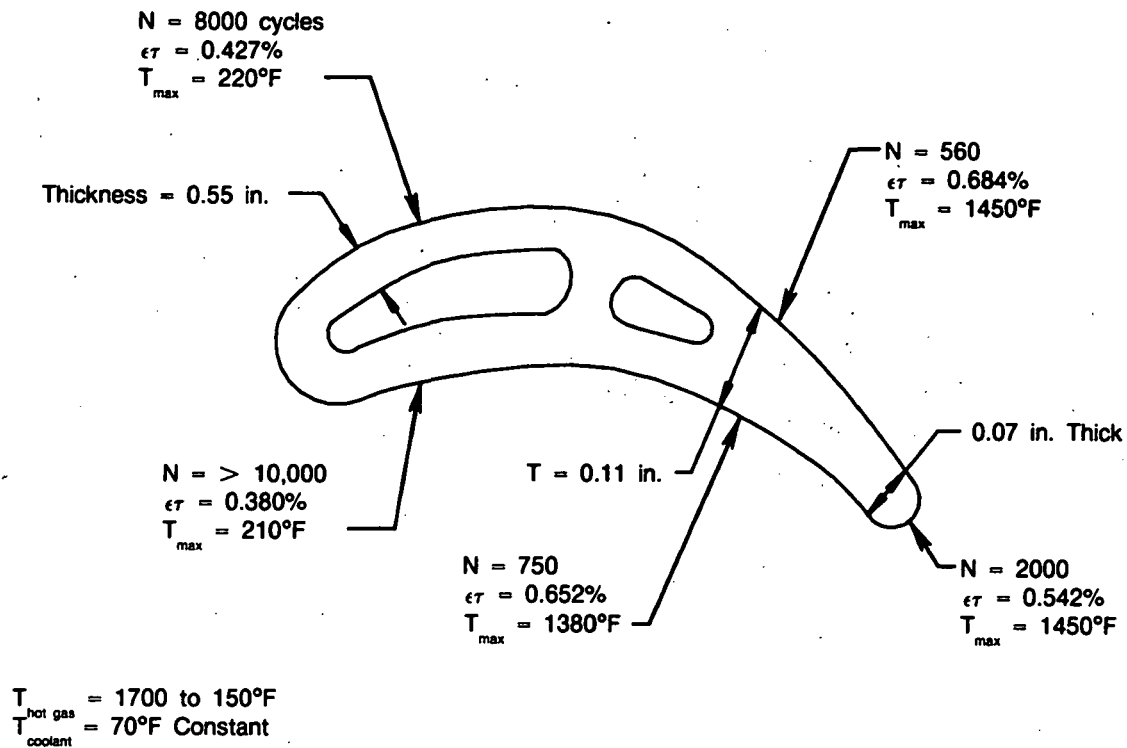
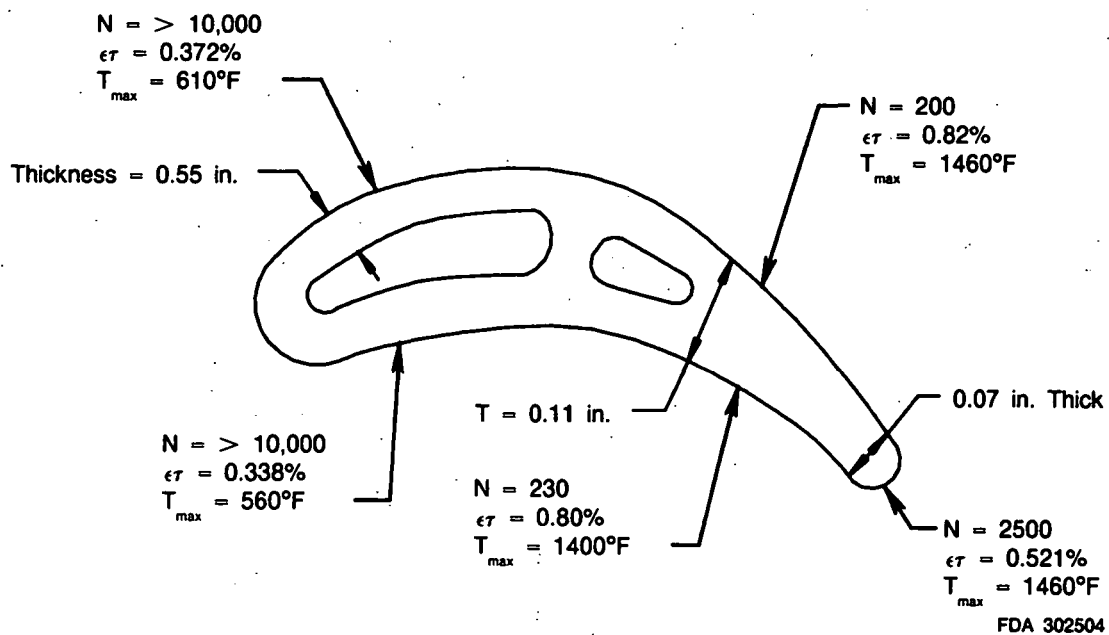


Figure III-76. CH_4 Cooled ATS Blade Thermal Strain Versus Metal Temperature for Worst Node on Trailing Edge

HYDROGEN CONFIGURATION

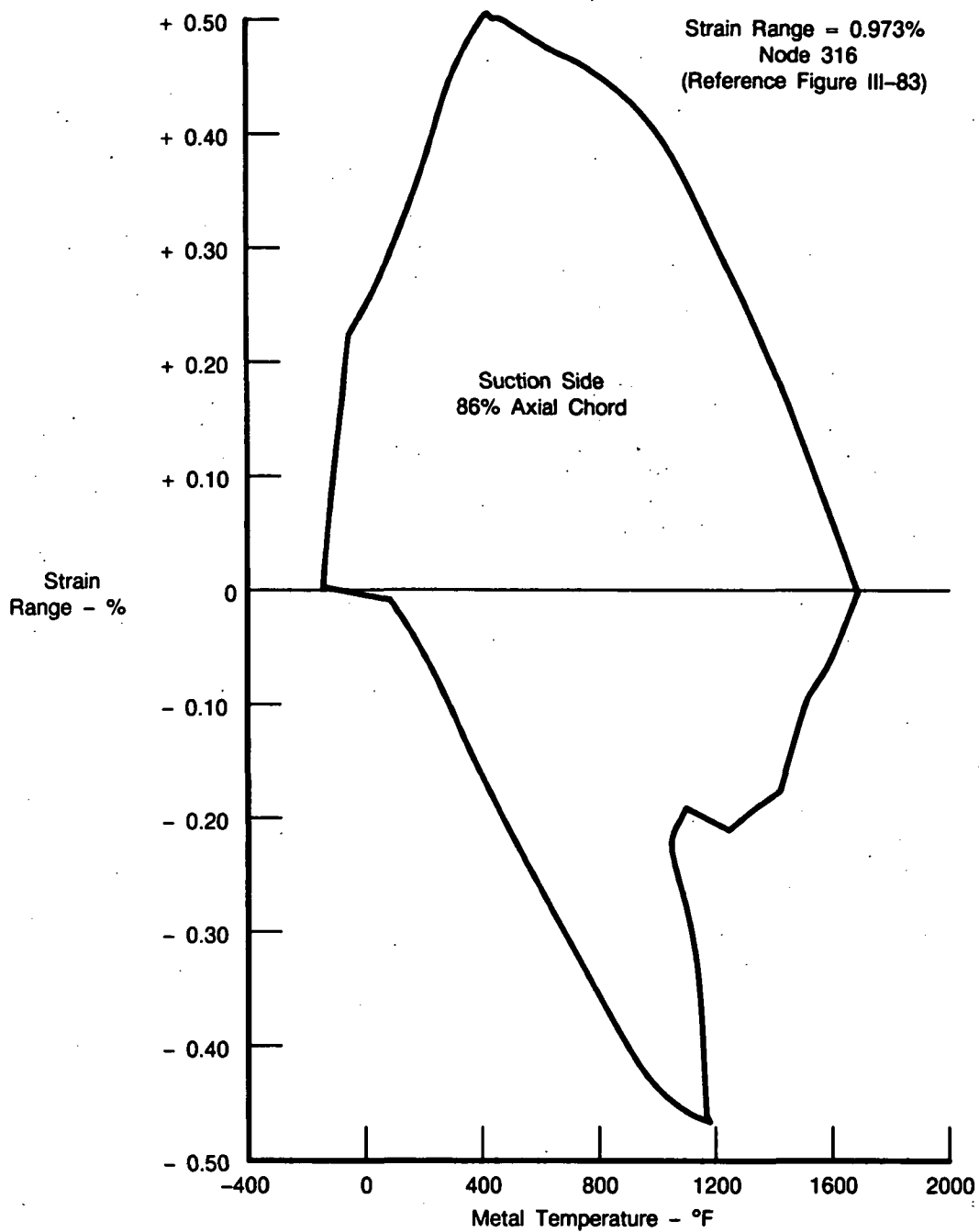


METHANE CONFIGURATION



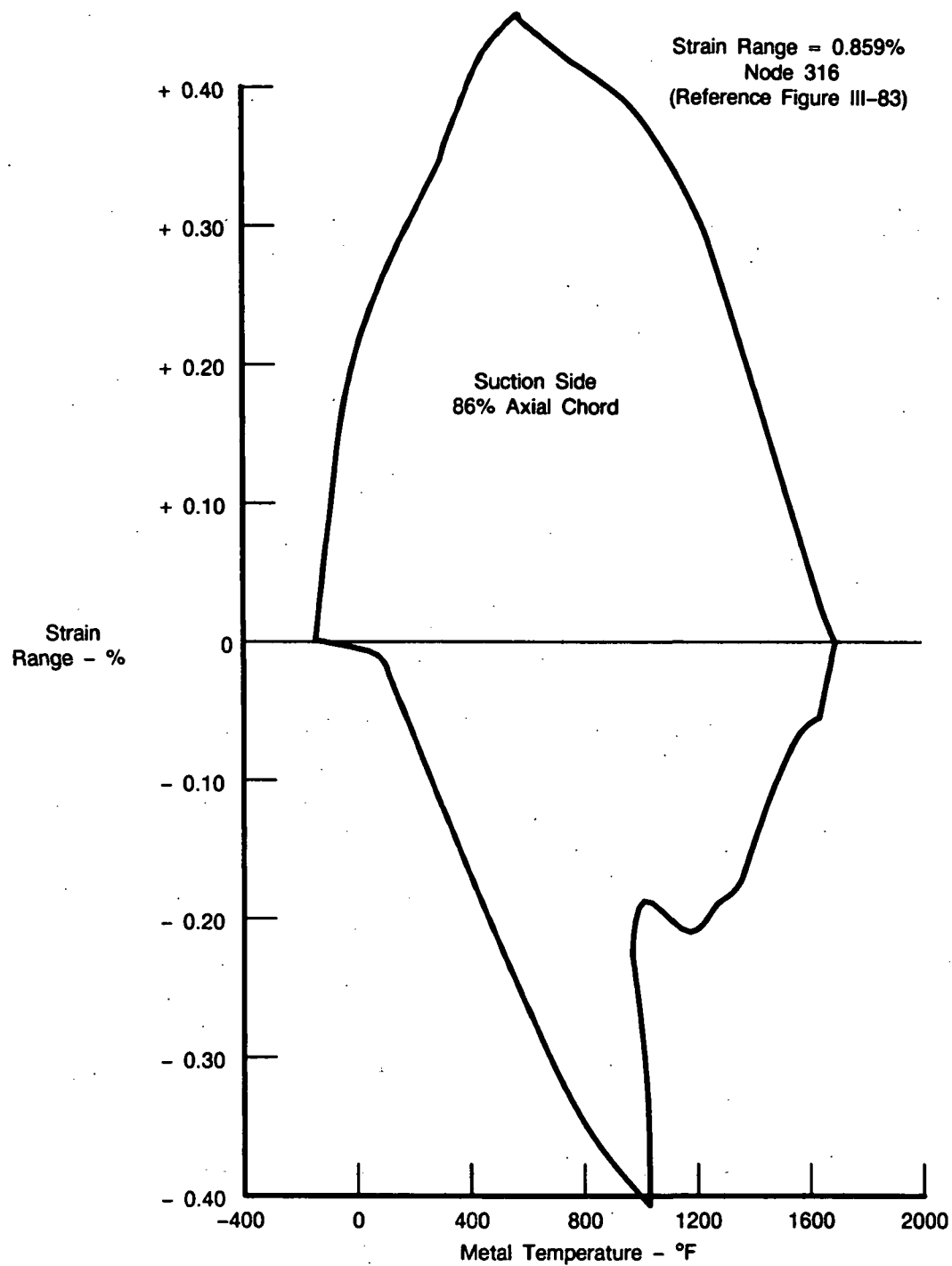
FDA 302504

Figure III-77. Cyclic Life Summary



FDA 302505

Figure III-78. Uncooled ATS Blade Thermal Strain Versus Metal Temperature — $H_2 + O_2$ Combustion Products



FDA 302506

Figure III-79. Uncooled ATS Blade Thermal Strain Versus Metal Temperature — $\text{CH}_4 + \text{O}_2$ Combustion Products

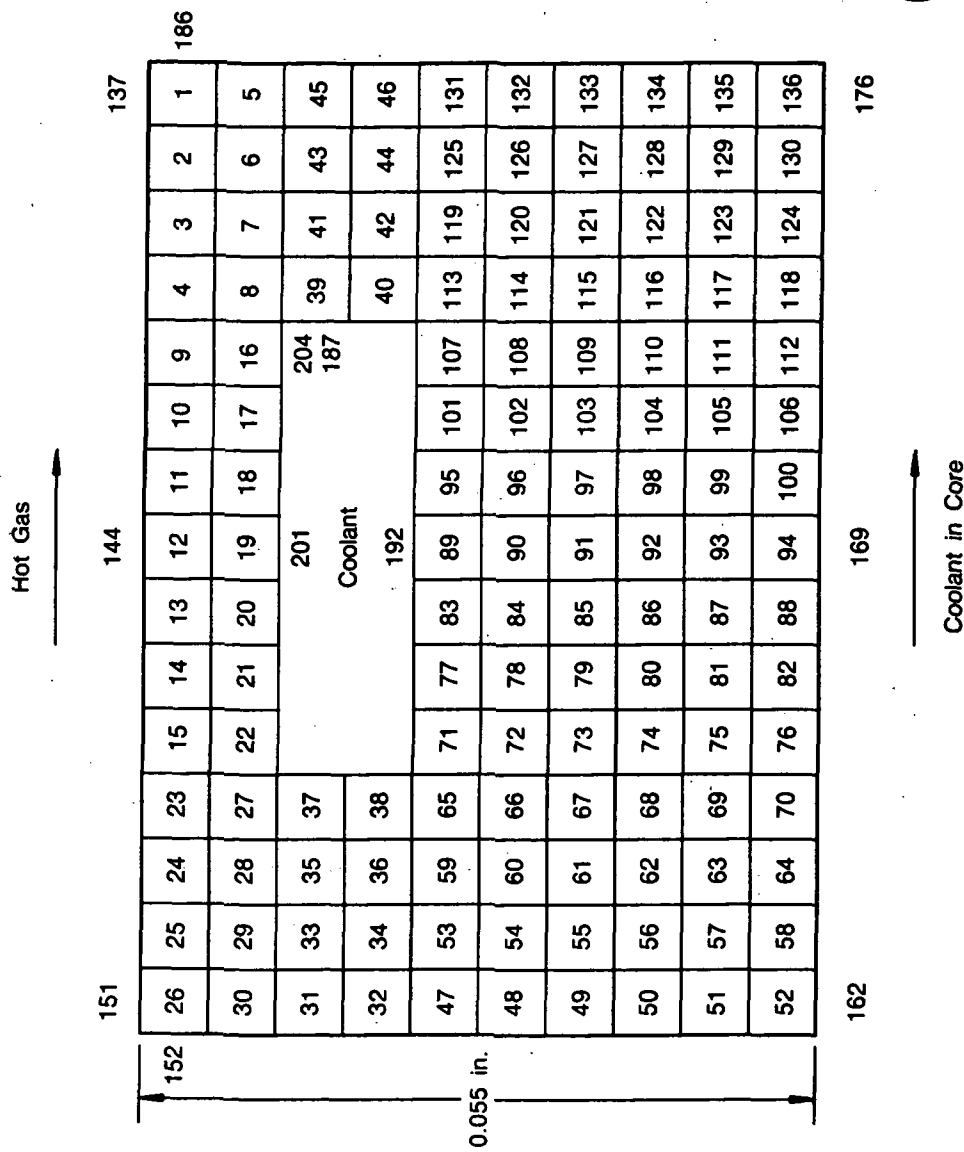


Figure III-80. Nodal Breakup for Suction and Pressure Side, 30% Axial Chord

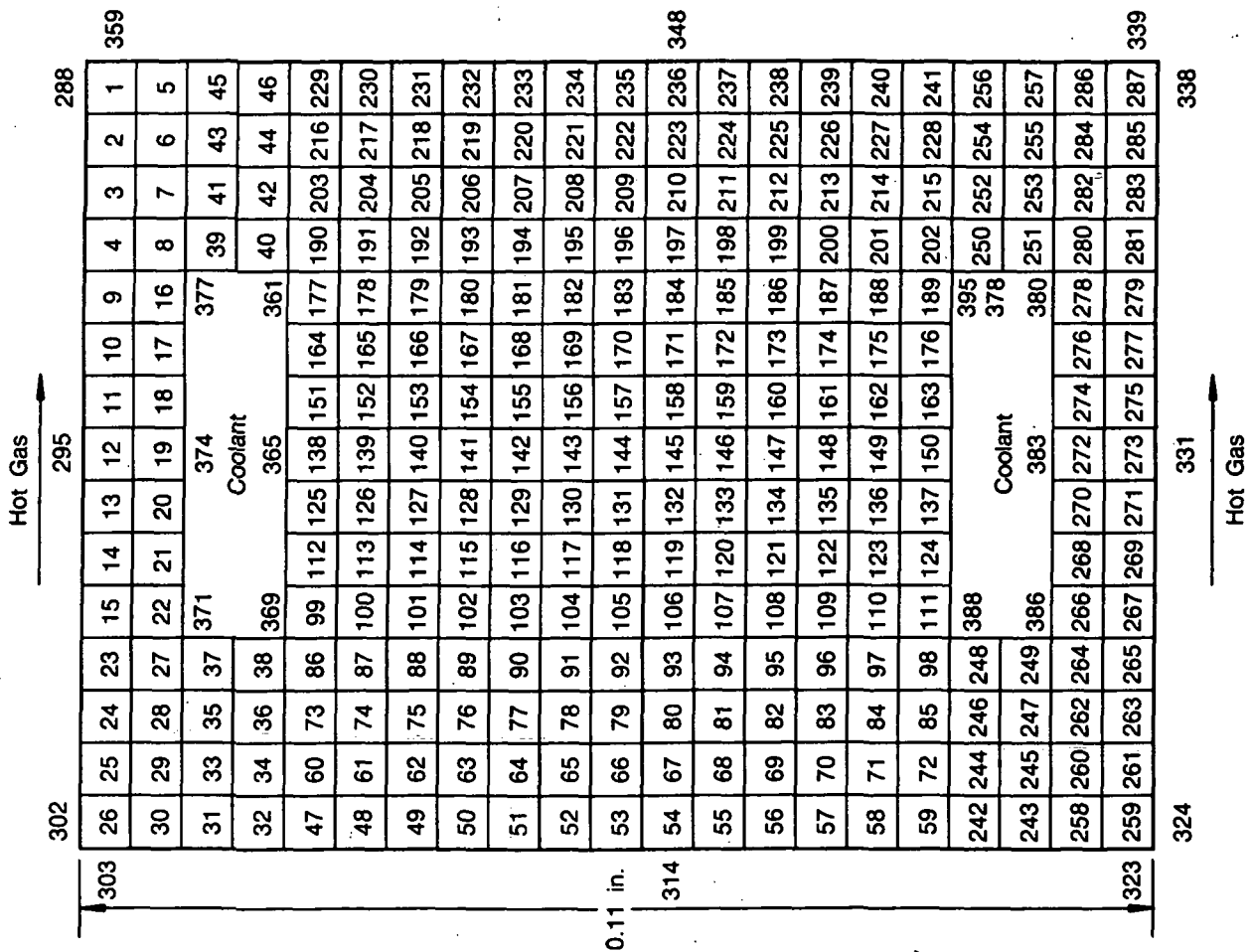
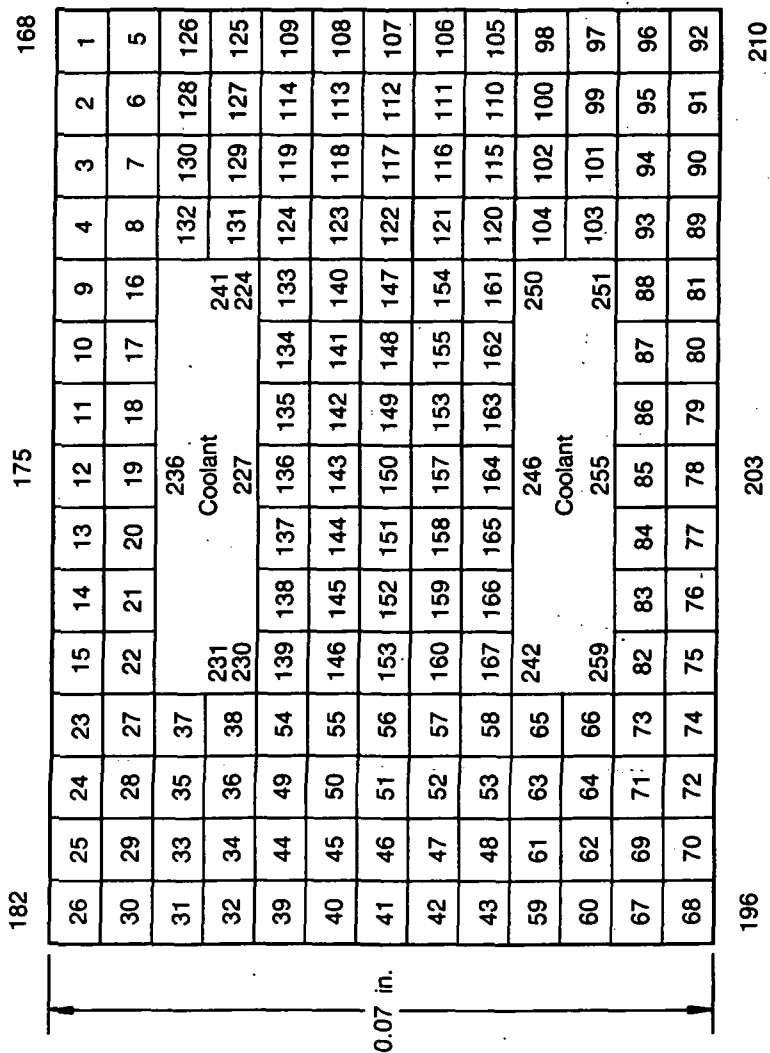


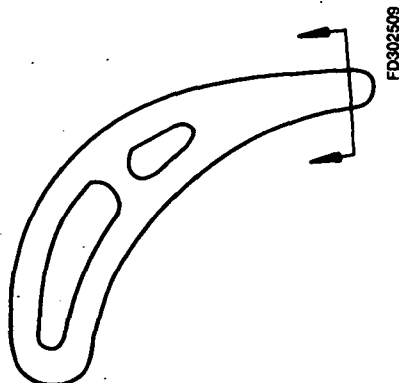
Figure III-81. Nodal Breakup for Region Aft of the Rear Cavity

Hot Gas



Hot Gas

Figure III-82. Nodal Breakup for the Trailing Edge



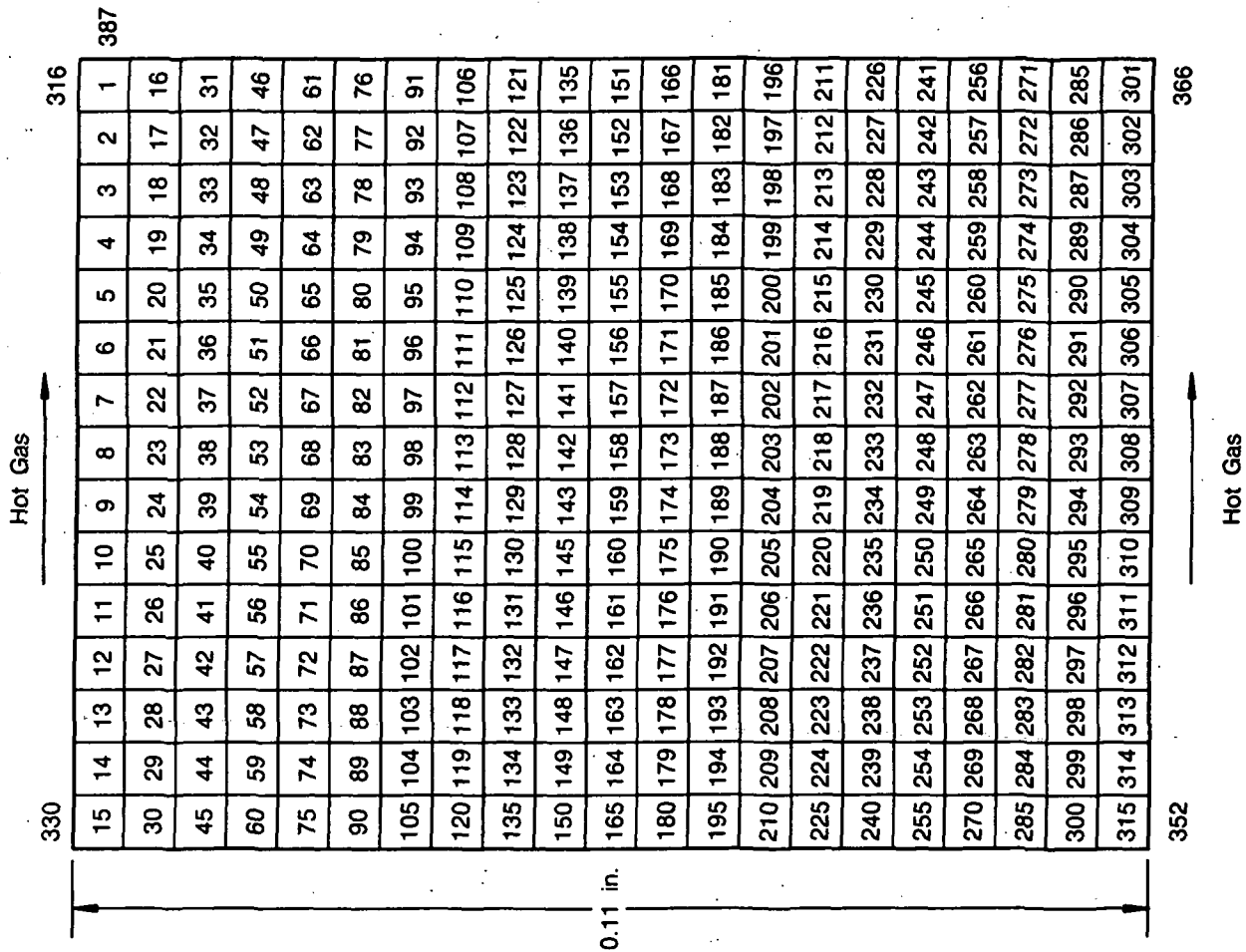


Figure III-83. Nodal Breakup Simulating Uncooled Blade Section

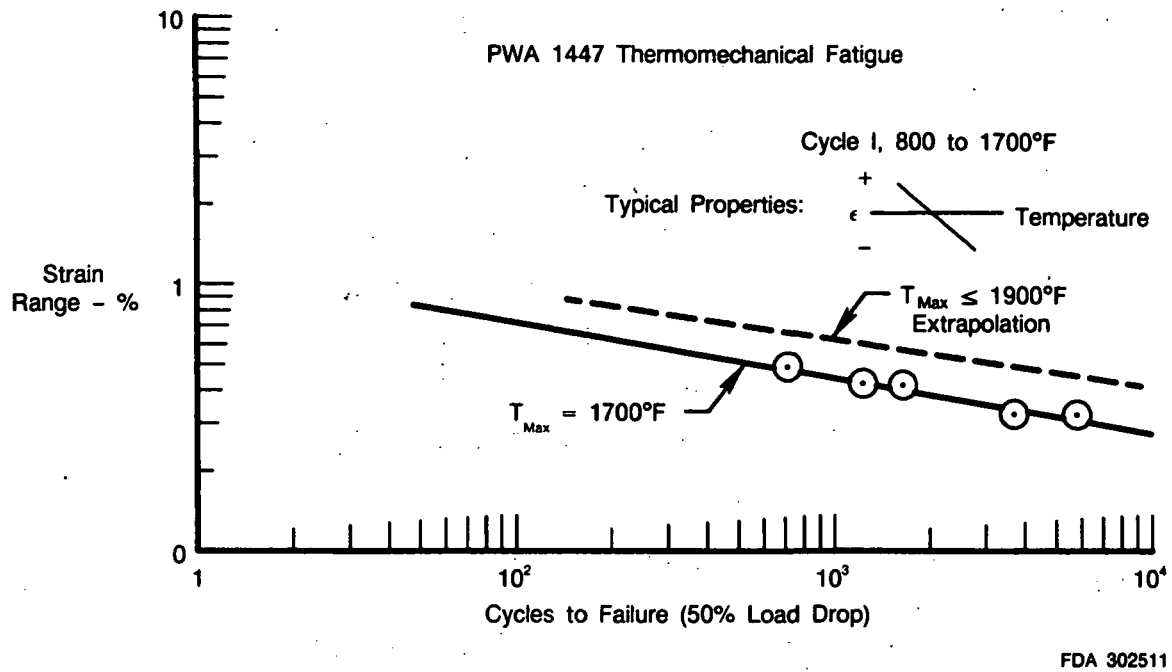


Figure III-84. PWA 1447 Thermomechanical Fatigue

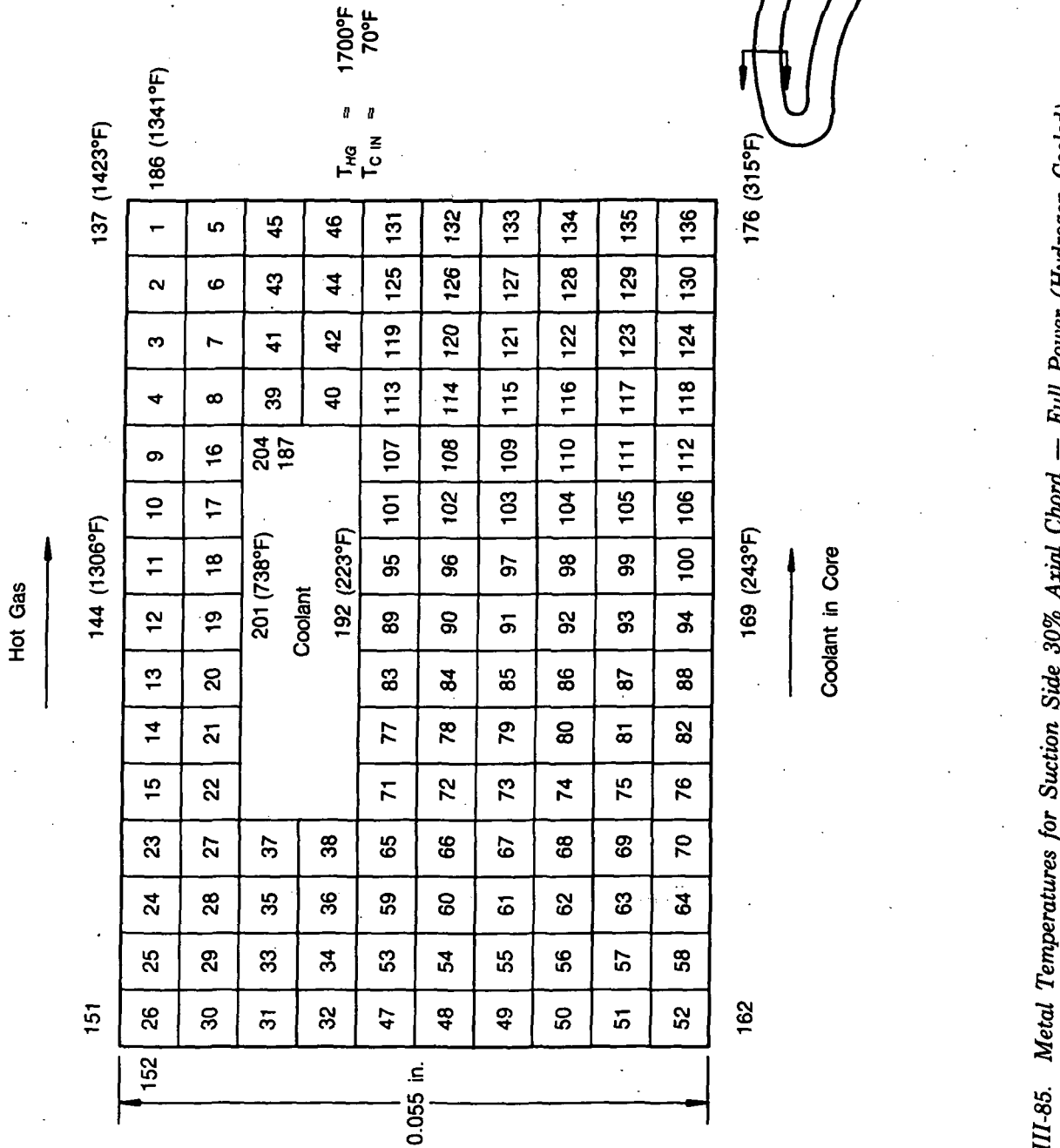


Figure III-85. Metal Temperatures for Suction Side 30% Axial Chord — Full Power (Hydrogen Cooled)

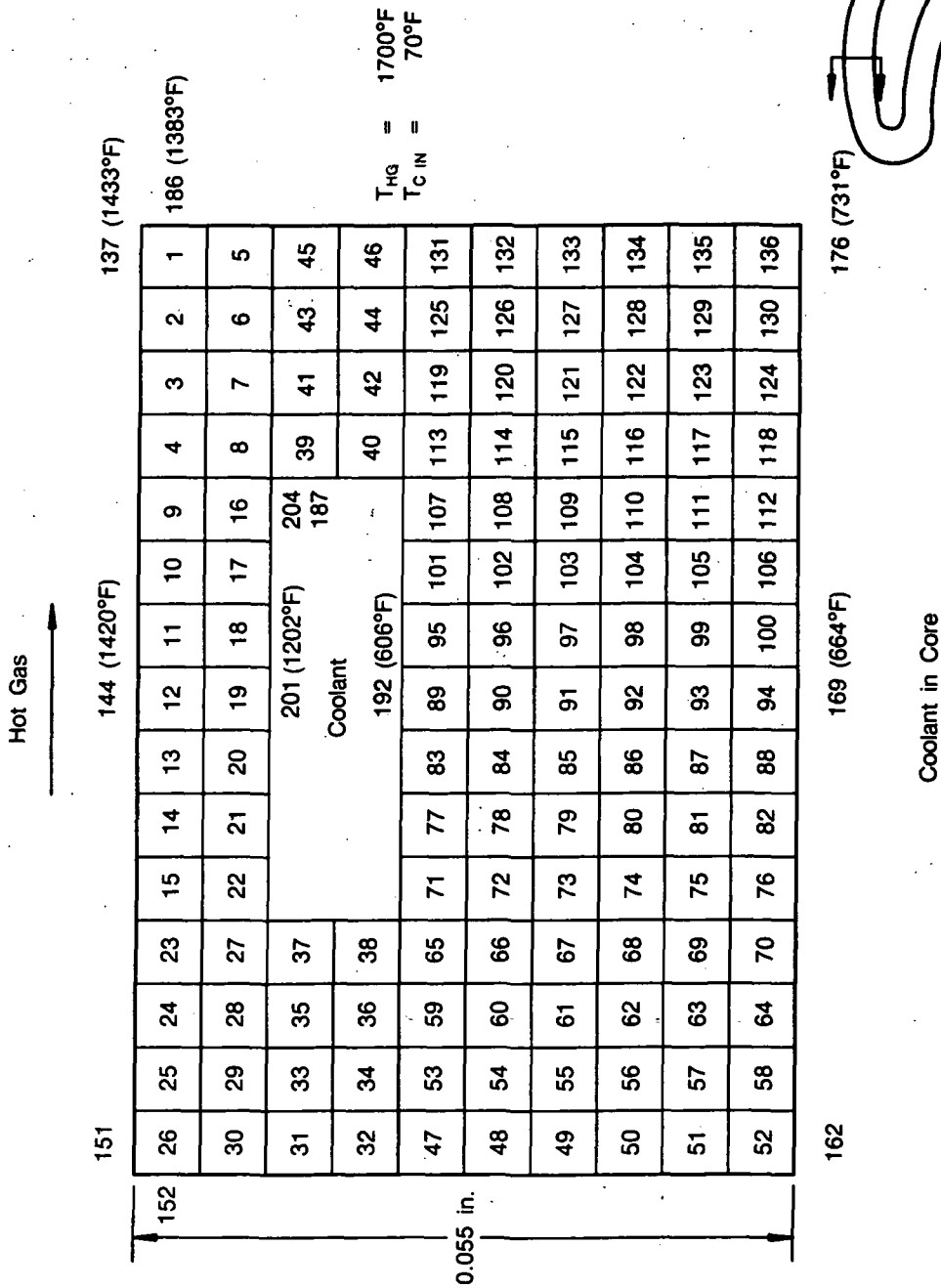
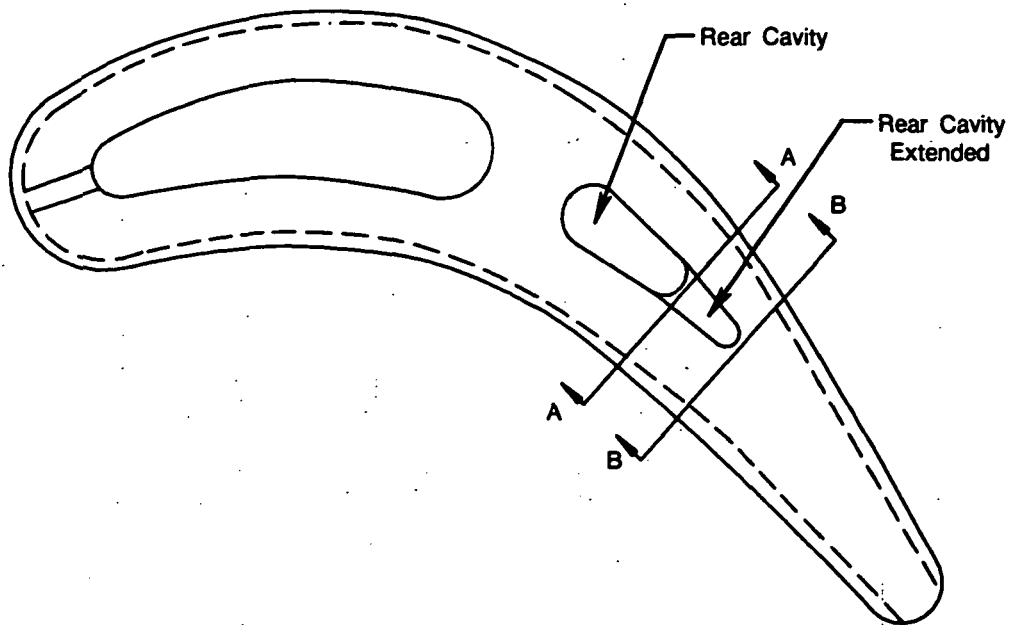
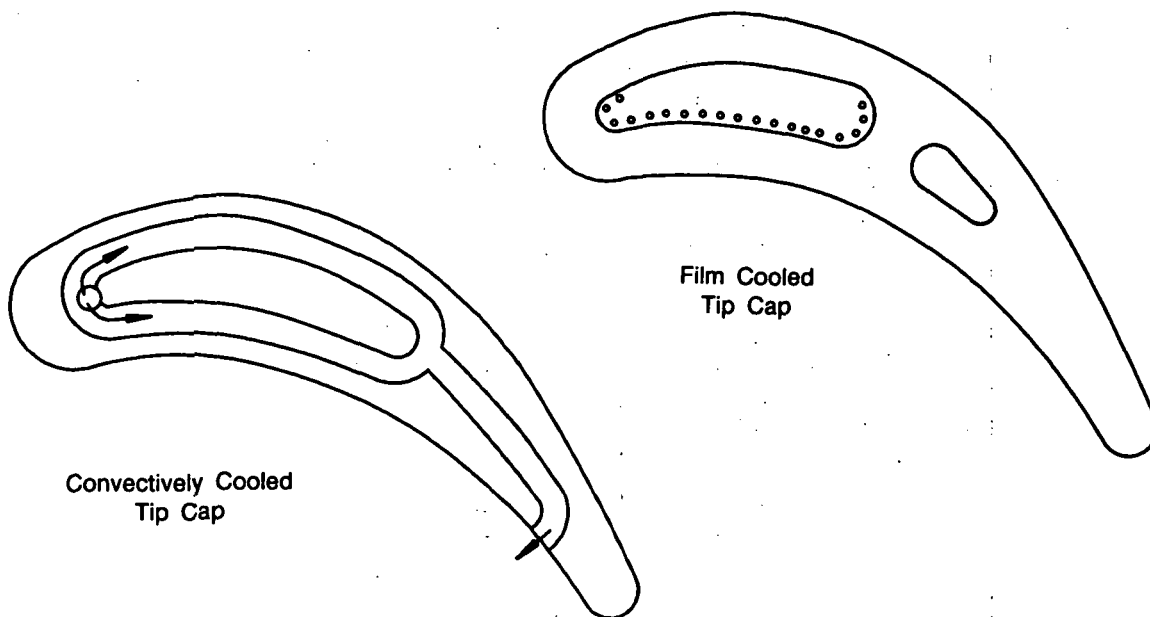


Figure III-86. Metal Temperatures for Suction Side 30% Axial Chord — Full Power (Methane Cooled)



FDA 302514

Figure III-87. Advanced Turbine Study Blade With Extended Rear Cavity



FDA 302515

Figure III-88. Advanced Turbine Study Blade Tip Cap Cooling Methods Investigated

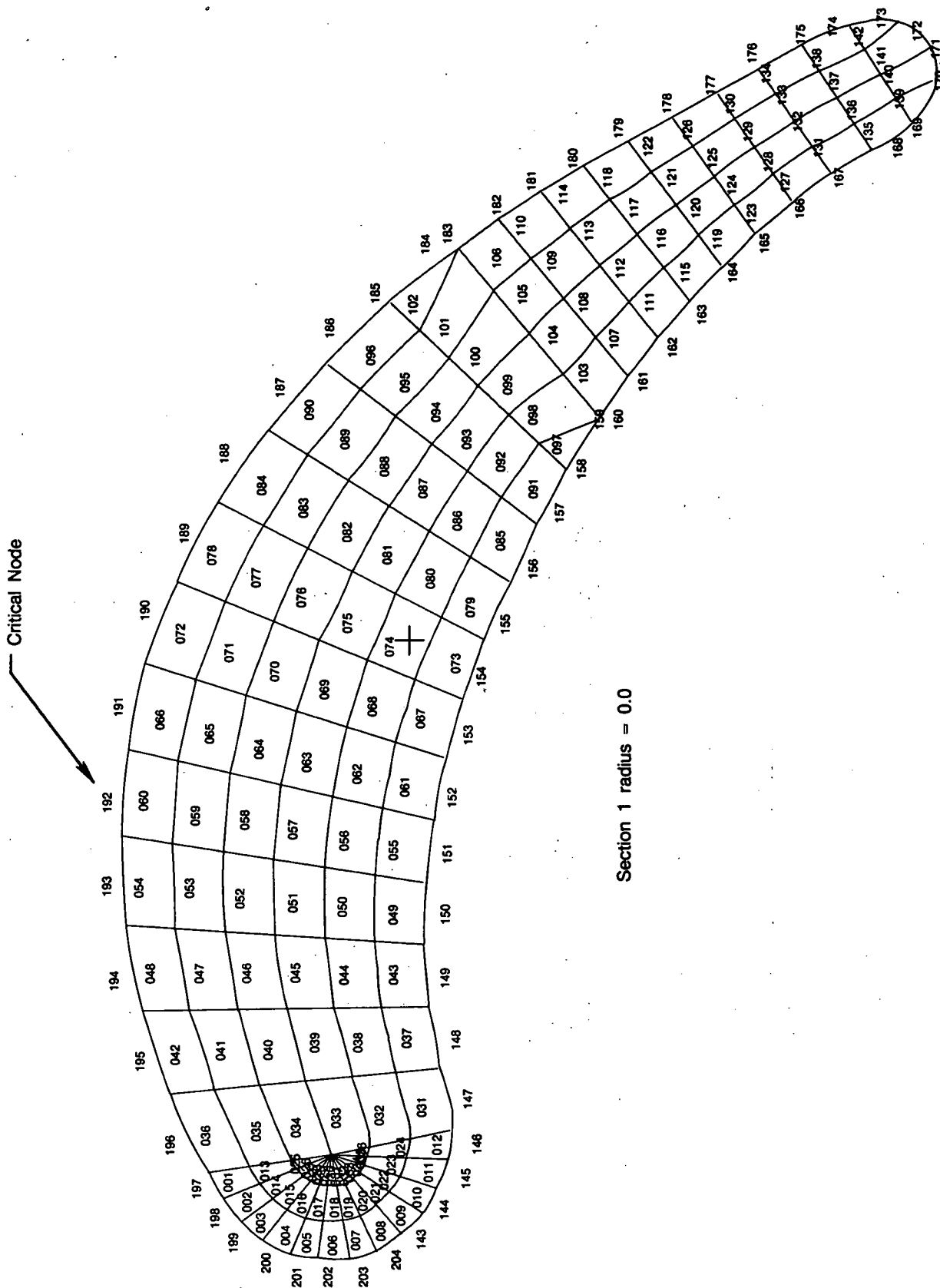


Figure III-89. Nodal Breakup of Uncooled Slave Airfoil

FD 302516

Table III-9. Advanced Convectively Cooled Hardware Drawings

<i>Part/No.</i>	<i>Title</i>	<i>Figure No.</i>
L-238386	L/O Cooled Turbine Blade Test Rig	B-1
T2185434	Cover — Assembly	B-2
T2185435	Blade — Assembly	B-3
T2185436	Blade	B-4
T2185437	Seal	B-5
T2185440	Seal	B-6
T2184088	Gasket 0.185 × 0.375 × 0.062	B-7
T2184089	Screw-Machine, 0.164-32 × 1.500, Fillister	B-8

4041C

SECTION IV

TECHNICAL ACTIVITY — REDIRECTED PROGRAM

The original Advanced Turbine Study (ATS) Program consisted of an advanced convective cooling configuration as a means of improving the turbine horsepower output at elevated temperatures for high-pressure reusable rocket applications. This type of cooling configuration features external cooling grooves on the turbine airfoil surface, which is then coated with a thin cover. The thin cover conducts heat to the coolant and minimizes the high thermal strains encountered in the severe heat flux environment of a rocket turbine.

Fabrication difficulties encountered during the sputtering of the external cover indicated that an extensive development program was required to execute this cooling design. A program of this magnitude was beyond the scope of the original Advanced Turbine Study Program. Studies also showed small or no horsepower payoff, for a hydrogen cycle, at elevated turbine inlet temperatures and constant airfoil life using this type cooling.

Although this type cooling is still considered the best way to efficiently cool rocket turbine airfoils without severely sacrificing horsepower output, study results indicated that a program redirection was required.

Pratt & Whitney recommended that the Advanced Turbine Study Program be redirected to fabricate a hot core type blade which would provide improved turbine blade life over a conventional solid blade. This type hollow blade, with hot gas flowing through it, could be tested in the NASA facility to quantify its life improvement. This improved life could then be traded for increased turbine inlet temperature (TIT) for higher output horsepower at a given life requirement, or the improved life could be traded for reduced replacement cost for a given TIT and mission requirement.

The life improvement and/or the increase in TIT capability for the hot core blade was derived from a reduction in thermal strain. The thermal strain in the blade was reduced by thinning the blade wall thickness, thus reducing the thermal gradient across the blade walls. This was achieved by coring the blades. By flowing mainstream flow through the core cavity a further reduction in thermal gradient can be achieved, thus creating reduction in thermal strain and an increase in life and/or TIT capability.

The hot core blade design fabricated from PWA 1480 single-crystal (SC) material (Reference Figure II-3, Section II) shows a predicted potential of 3.5 times life improvement over a solid blade design. For the sake of simplicity and cost savings, P&W manufactured these blades to the same configuration (no twist and no taper) as the previously designed Advanced Turbine Study blades.

A. TASK 1 — HARDWARE DESIGN

Task 1 consisted of the design of the hot core blade (Reference Figure II-3) and the generation of engineering drawings which were used to fabricate the blades and blade holding fixture.

To relate the life prediction system to actual test results obtained in the Space Shuttle Main Engine (SSME) blade tester rig, an analysis of the root section of the SSME 1st-stage turbine blade was performed. In this analysis, the thick cross section near the blade ID was broken up into nodes as shown in Figure IV-1. A transient analysis was conducted using the blade tester rig transient recorded on 15 December 1981, run 117, the second cycle out of five. Since the SSME blade material, Mar-M 246 directionally solidified (DS), is not built into P&W's

material library, a similar nickel-base alloy, PWA 1422, was used for this analysis. As shown in the table of Figure IV-1, the material properties are quite similar. Results of the analysis yielded a thermal strain range of 1.59% maximum occurring on the convex surface. Using the low cycle fatigue (LCF) data for Mar-M 246 DS as shown in Figure IV-2, the cyclic life of the SSME blade is predicted to be less than 100 cycles. Note that the data in Figure IV-2 is for transversely loaded (LCF) specimens. This is the weak direction for directionally solidified material. Thus, we would expect the airfoil cracking to be in the radial direction. The prediction of less than 100 cycles agrees fairly well with rig test results. It must be remembered that the prediction uses the general isothermal LCF data and not specific thermal mechanical fatigue data which simulates the exact strain-temperature history of the rig part. Therefore, a more accurate prediction can not be made with the available data.

Next, a detailed analysis of the solid slave foil designed for the original programs (but fabricated out of PWA 1480 material) was made at the same rig conditions. The strain range was found to be 1.59%. The nodal breakup of this foil is shown in Figure IV-3. The maximum thickness of this foil closely resembles the shuttle blade root section and consequently has a similar thermal response. The life of the PWA 1480 solid slave will be similar to the shuttle blade based on the limited amount of transverse data, as shown in Figure IV-2. However, the data of Figure IV-4 shows PWA 1480 distinctly better than Mar-M 246 DS and SC with transverse loading at a lower temperature (1400°F). But the higher temperature data (Figure IV-2) will more closely match the rig cycle with maximum temperature of 1700°F.

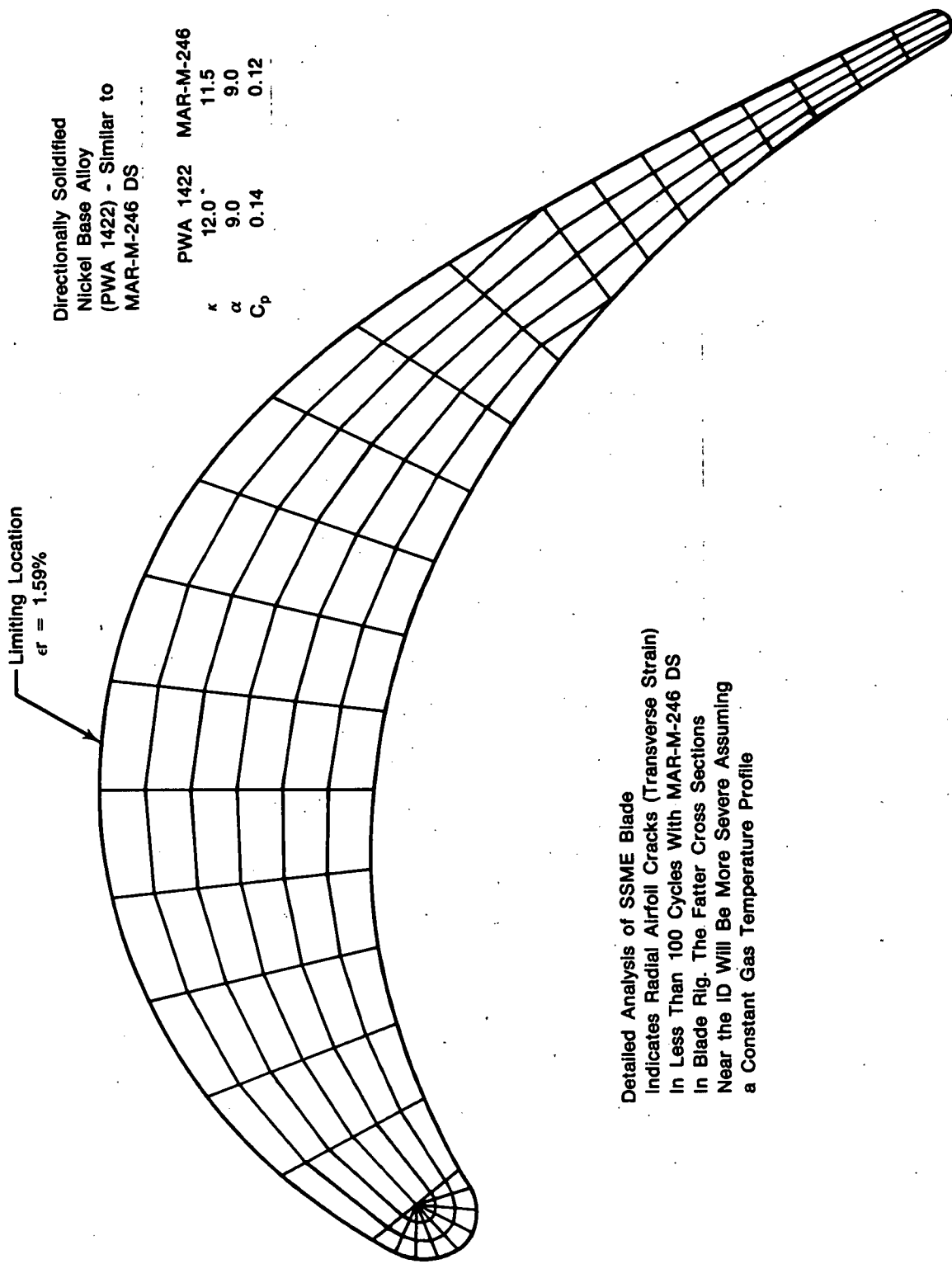
To improve the LCF life of the solid foil, the part was cored and a study was made where various levels of mainstream flow were passed through the foil. The following results were obtained:

No internal flow — 1.23% strain range
 0.52% flow/blade row — 1.18% strain range
 1.17% flow/blade row — 1.17% strain range.

At 0.52% flow, the strain was reduced from 1.23% for the cored, no flow case, to 1.18%. However, the strain barely changed by doubling the flow. Thus, the 0.52% flow case was selected as the best choice for reducing the thermal strains on a solid foil. Referring to Figure IV-2, the cyclic life improvement is shown below.

Solid Foil	1.59% Strain	64 Cycles
Cored Foil With 0.52% Hot Flow	1.18% Strain	225 Cycles
Life Improvement	$\frac{225}{64} = 3.5$ times	

Based on the previously discussed studies, three different blade configurations were designed: a solid blade, a cored hollow blade, and a cored hollow blade with an orifice in its pressure side (hollow blade with a hole). The orifice was sized to allow 0.52% of mainstream flow (per blade row) to pass through the blade core.



FD 267785

Figure IV-1. Space Shuttle Main Engine 1st-Stage Blade, Section B-B

NAS8-33561 Data

LCF in H₂ Atmosphere at 5000 psig

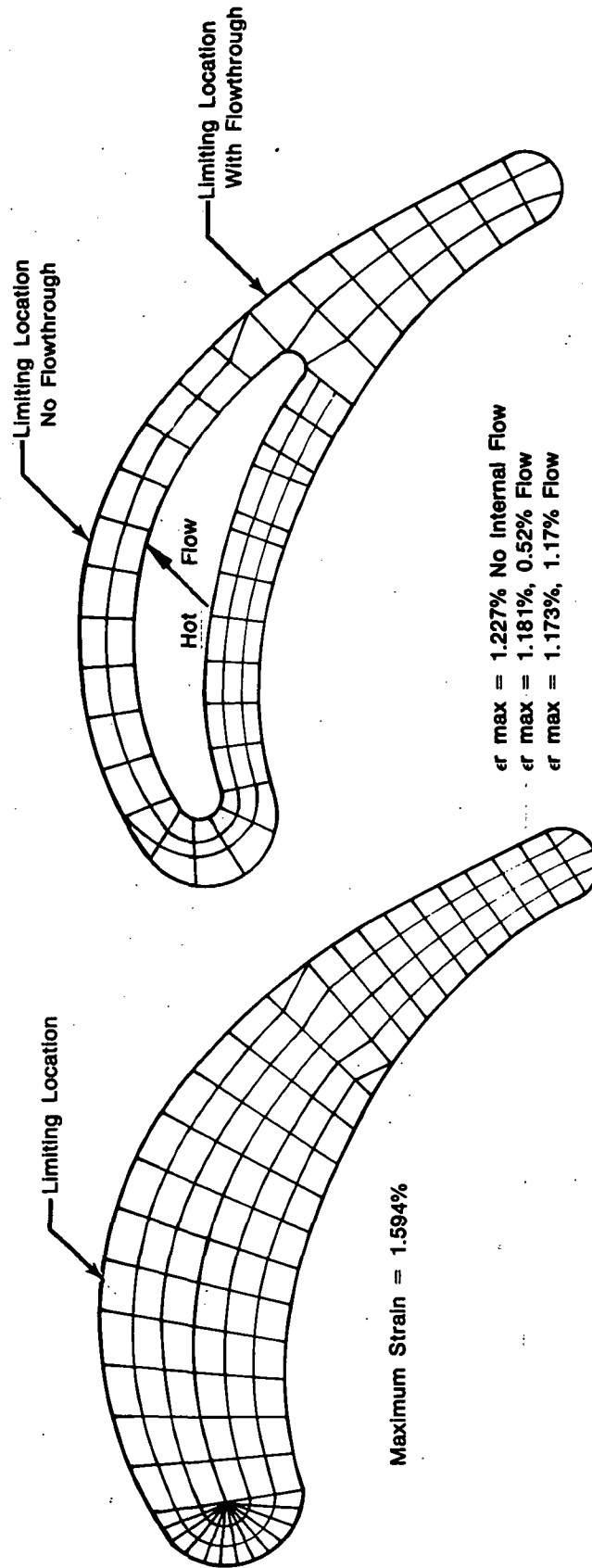
Transverse PWA 1480, 1600°F

$w = H_2 + 50\% H_2O$ Vapor



Figure IV-2. Strain Range Versus Cycle Life

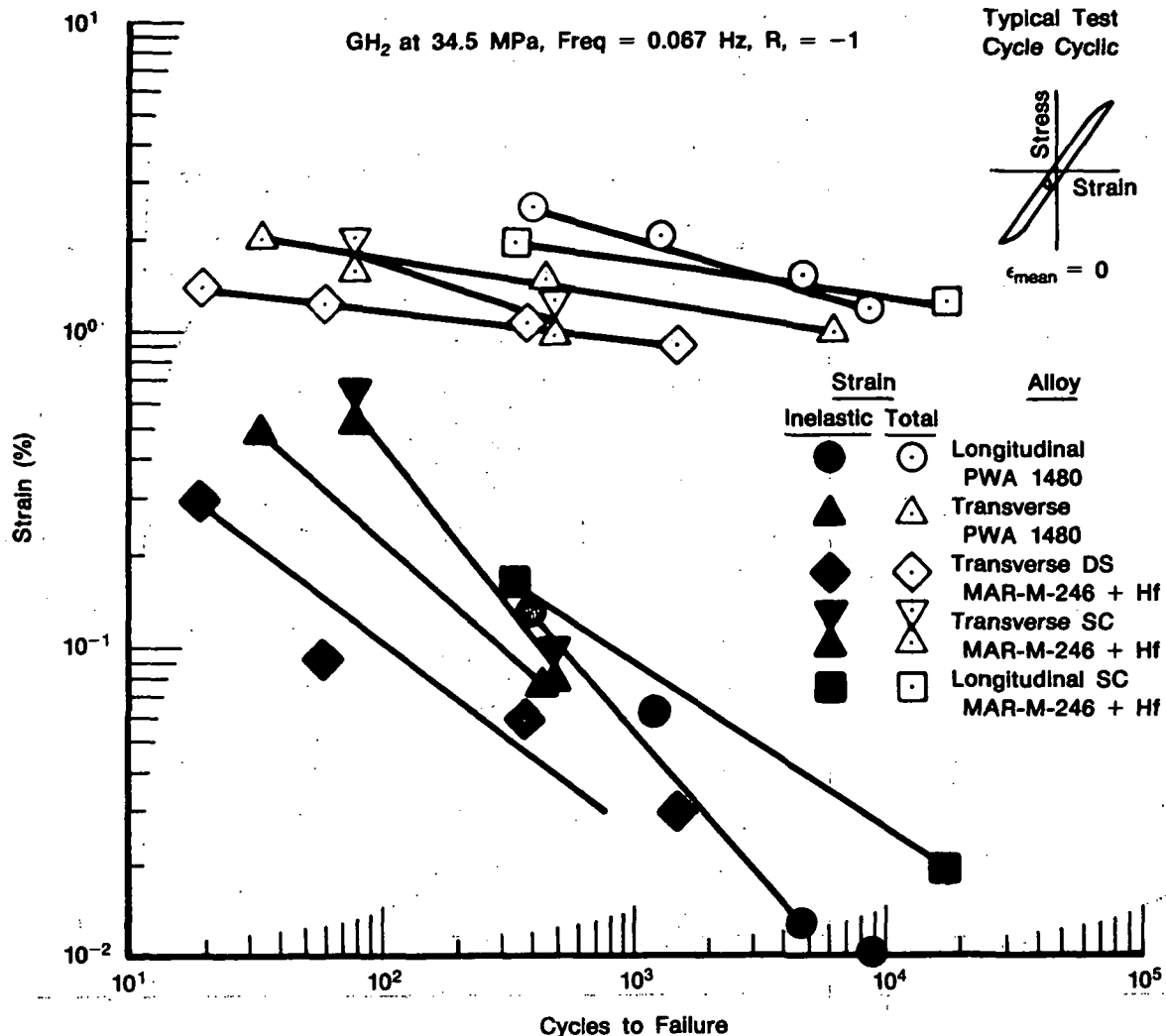
PWA 1480 Material, Rig P/P Distribution
Single-Crystal Nickel Alloy



FD 267797

Figure IV-3. Advanced Turbine Study Uncooled Foil Low Cycle Fatigue Life Improvement

THIS IS FROM FINAL REPORT NAS8-33561



FD 218696

Figure IV-4. Comparison of PWA 1480 (Longitudinal and Transverse) Transverse Single Crystal and Directionally Solidified, Mar-M 246 + Hf and Longitudinal Single Crystal, Mar-M 246 + Hf in GH₂ at 34.5 MPa, Frequency = 0.067 Hz, R = -1, Temperature = 760°C (1400°F)

The P&W layout drawing for the ATS is shown in Appendix B, Figure B-1 (Drawing No. L-238386). This layout was originally used in the design of the advanced, convectively cooled turbine blade, and was updated to reflect the hot core blade design. These changes are designated as change "A" in the Alteration column of the drawing, and mainly consist of the addition of items 12 through 17, with related views and information. These items reflect the hot core blade design with and without the pressure side orifice, the solid blade, and the updated blade holding fixture.

Engineering drawings for the hot core blade hardware were generated and released to production. Table IV-1 is a list of these engineering drawing numbers (part numbers), descriptions, and corresponding figure numbers in Appendix B.

Table IV-1. Hot Core Blade Hardware Drawings

<i>P&W Part Number</i>	<i>Description</i>	<i>Figure No.</i>
T2185593	Cover — Assembly of	Figure B-9
T2185592	Blade (Hollow)	Figure B-10
T2185594	Blade (Solid)	Figure B-11
T2185437	Seal	Figure B-5
T2184088	Gasket	Figure B-7
T2184089	Screw — Machine	Figure B-8

3959C

Figure B-9 shows the cover assembly (P/N T2185593) of the blade holding fixture. A dash ("—") drawing system is used to identify the different detail parts in each assembly. The parts list is shown in the lower righthand corner of the drawing, above the title block. The dash one part number (T2185593-01) identifies the cover assembly, the dash two part number (T2185593-02) identifies the cover detail, and the dash three part number (T2185593-03) identifies the plug that is brazed to the cover detail to form the cover assembly. The cover assembly is designed in two parts to facilitate its fabrication using the wire electrical discharge machining (EDM) method.

Figure B-10 illustrates the hollow blade assembly (P/N T2185592). The dash one part number (T2185592-01) designates the hollow blade with an orifice in the pressure side, and the dash two part number (T2185592-02) shows the hollow blade without the pressure side orifice. Figure B-11 shows the solid blade assembly.

Figure B-5 depicts the seal (P/N T2185437) used to connect the cavity in the instrumented blade to the blade holding fixture. The layout drawing for the Advanced Turbine Study (Figure B-1) shows the assembly of the blades to the cover.

Figure B-8 illustrates the machine screws (P/N 2184089) used to secure the turbine blades to the cover fixture. Figure B-7 shows the gasket (P/N 2184088) originally used under the head of the screws (shown in Figure B-8).

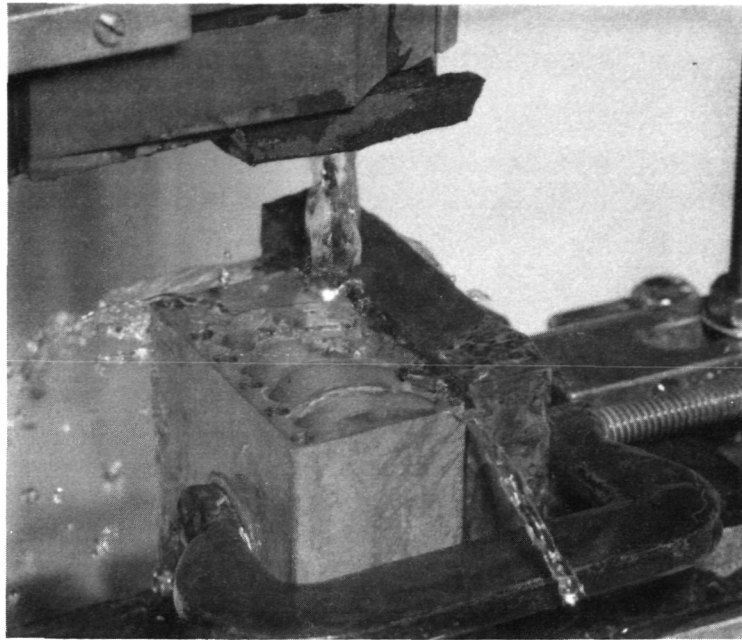
B. TASK 2 — HARDWARE FABRICATION

Task 2 consists of the procurement of raw materials and the fabrication and instrumentation of the hot core blade hardware.

Production hot core airfoils would be fabricated by casting. Because of the costs associated with the tooling required for airfoil casts, it was decided to fabricate the hot cored blades by electrical discharge machining (EDM) them from blocks of PWA 1480 single-crystal material. This was followed by electrical chemical machining (ECM) to remove the EDM recast layer. Figure IV-5 shows the hot core blade blanks being wire EDM'd out a PWA 1480 single-crystal material block.

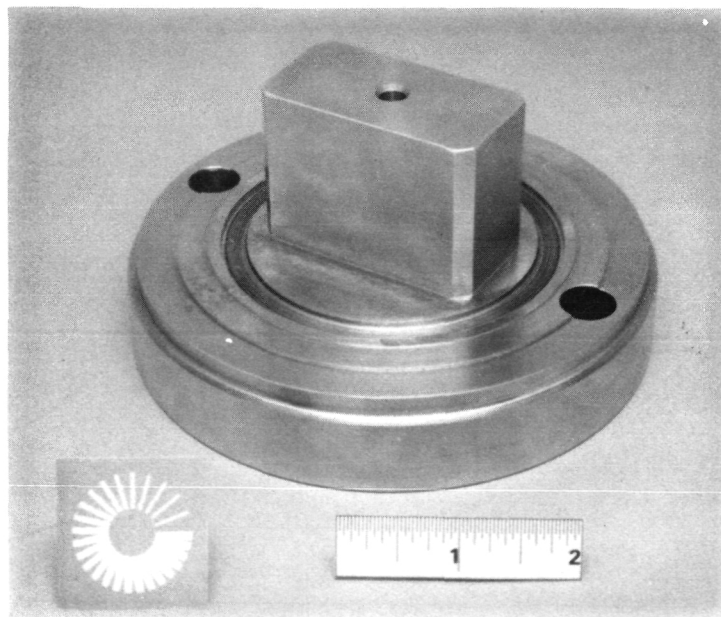
The blade holding fixture was fabricated from a cylindrical section of A1S1 347 SST material. The fixture was turned, milled, and drilled. The blade holding pockets were then wire EDM'd. Subsequent to the wire EDM of the pockets, previously wired EDM plugs were brazed in place to form the outer (bottom) face of the blade holding fixture. Figure IV-6 depicts the blade holding fixture at an intermediate step during the manufacturing.

ORIGINAL PAGE IS
OF POOR QUALITY



FE 357810-4

Figure IV-5. Wire EDM of ATS Hot Core Blade from PWA 1480 Single-Crystal Material Block



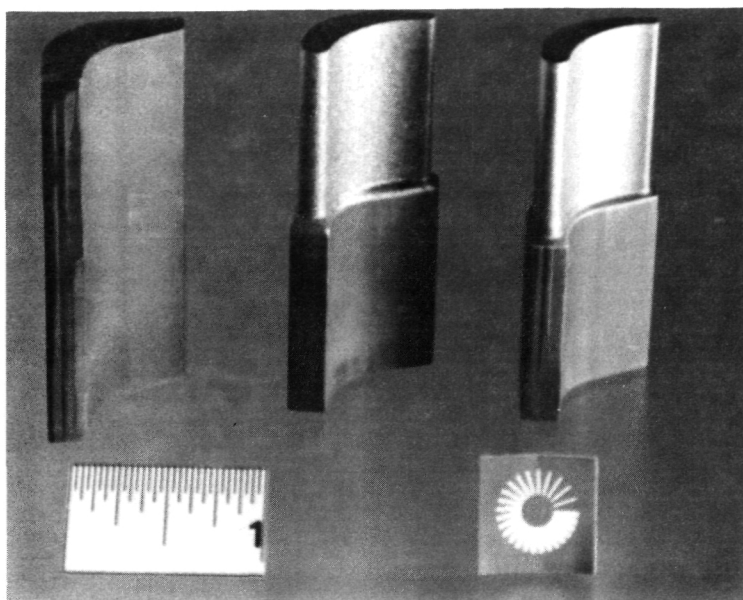
KFAE 347763

Figure IV-6. Cover Assembly of Blade Holding Fixture

To determine the proper operating parameters for the EDM equipment, several solid blades were machined out of IN100 material. Some of these blades are shown in Figure IV-7. The blade on the left is a wire EDM blank, machined to the blade root dimensions, i.e., EDM'd out of a block of raw material. The airfoil shape is then produced by two passes using the plunger EDM

ORIGINAL PAGE IS
OF POOR QUALITY

method: one pass for a rough cut, with approximately 0.006 inch of overstock (blade shown in center), and a final finishing pass (blade shown on right). The striations shown on the platform leading edge of the blade will not exist in a deliverable part. A deliverable part will also have a more gradual blending of the airfoil portion into the blade root than the blades shown in Figure IV-7.



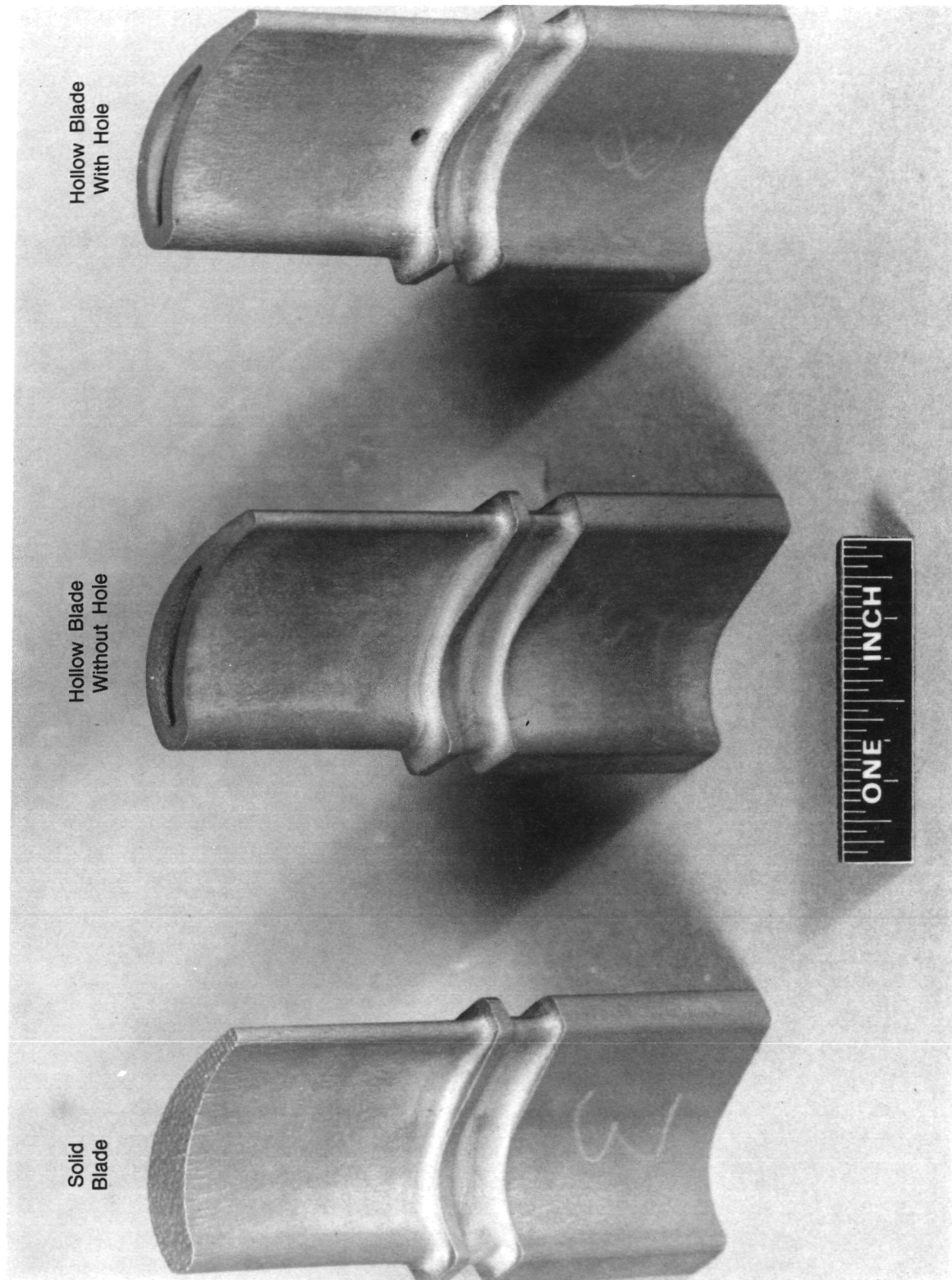
FE 357596

Figure IV-7. *Electrical Discharge Machined Blades (IN100 Material)*

Figure IV-8 illustrates the three different blade configurations: solid blade (P/N T2185594), hollow blade without a hole (P/N T2185592-02), and hollow blade with a hole (P/N T2185582-01). The hollow blade without a hole has 0.055 inch wall thickness. A similar part (P/N CKD 2078, Figure B-12 in Appendix B) with a 0.035 inch wall thickness was fabricated and delivered to NASA for testing. The third blade configuration has a 0.050 inch diameter hole in the blade pressure side near the root, and has the same wall thickness as the blade without the hole. Removing blade cores reduces the thermal gradient within the blades, therefore reducing the thermal strain. By locating a hole on the pressure side of the blade, the temperature gradient is further reduced by allowing hot mainstream gasses to flow through the blade core. The resulting strain reduction allows the turbine blade life to be extended, or it can be traded for an increase in TIT. A similar effect is achieved by reducing the blade's wall thickness.

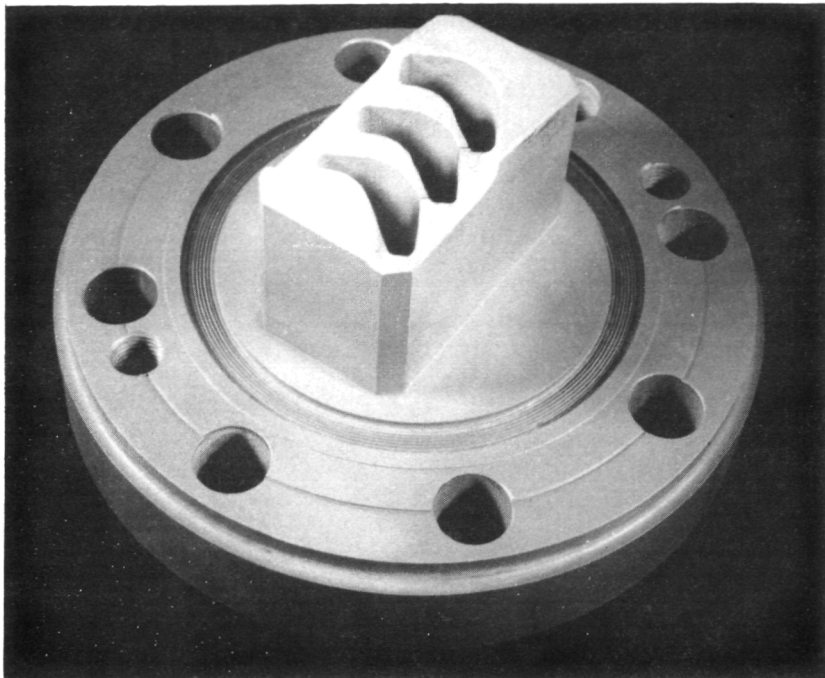
The completed blade holder, shown in Figure IV-9, was designed to fit the existing NASA blade tester rig and to support the ATS blade without using expensive fir tree or dovetail attachments. Slots were cut into the holder wall, near the trailing edge that separates the center pocket from the two outer pockets. These slots, which run the full depth of the pockets, provide thermal relief of the part during exposure to severe thermal cycles.

ORIGINAL PAGE IS
OF POOR QUALITY



FD 295949

Figure IV-8. PWA 1480 Single-Crystal Blade Configurations



FE 358184

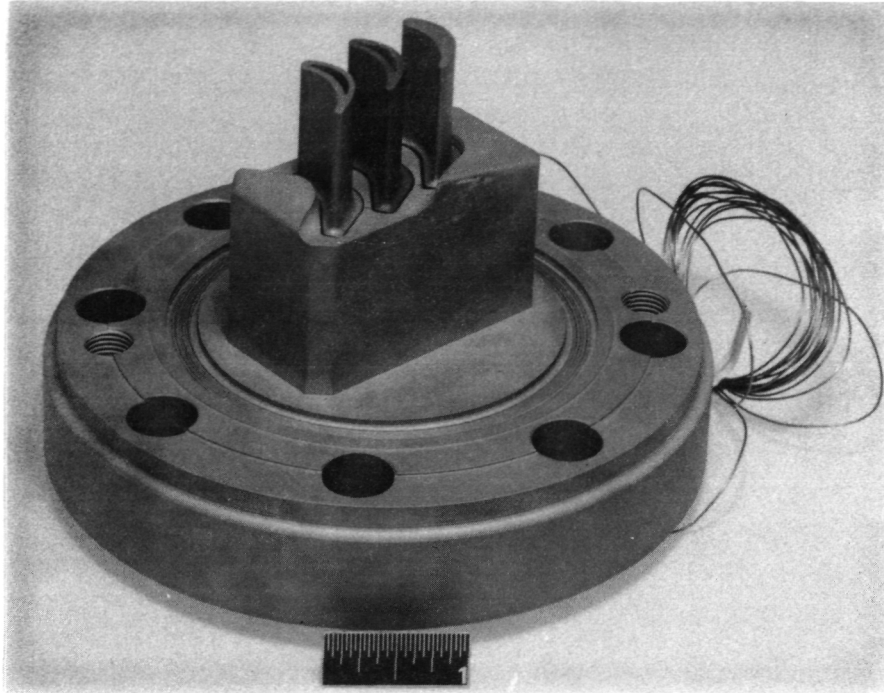
Figure IV-9. Advanced Turbine Study Blade Holder

The ATS blades installed in the blade holder assembly are shown in Figure IV-10. Two hollow blades (0.055 inch wall thickness) — one with a hole (center) and one without a hole (left) — and one solid blade (right) were installed in the holder. The center blade was instrumented with a thermocouple as evidenced by the thermocouple lead shown in the figure.

Six of the 13 blades fabricated and delivered to NASA were instrumented with chromel/alumel thermocouples. The thermocouples were placed on the pressure side of the core cavity wall, approximately $\frac{1}{3}$ of the blade span away from the tip of the blades. Table IV-2 provides the serial numbers of all blades delivered to NASA, the type of blades, and if they were instrumented.

Prior to delivery to NASA, the blades underwent grain etch and Laue X-ray to verify grain quality and grain primary orientation. Appendix C contains the Materials Laboratory report covering this evaluation.

Upon the completion of the laboratory evaluation, the blades, blade holding fixture, and associated hardware were delivered to NASA for testing in the SSME blade tester rig. Table IV-3 lists the hardware delivered to NASA.



FE 231340

Figure IV-10. Blade Holder With Advanced Turbine Study Blades Installed

Table IV-2. ATS Blades Serial Numbers

Serial No.	Part No.	Type
1	T2185592-02	Hollow Without Hole*
2	T2185594	Solid
3	T2185594	Solid
4	T2185592-02	Hollow Without Hole*
5	T2185592-02	Hollow Without Hole
6	T2185592-01	Hollow With Hole*
7	T2185592-01	Hollow With Hole*
8	T2185592-01	Hollow With Hole
9	T2185594	Solid
10	CKD 2078	Hollow Without Hole, Thin Wall
11	CKD 2078	Hollow Without Hole, Thin Wall*
12	T2185594	Solid
13	CKD 2078	Hollow Without Hole, Thin Wall*

*Instrumented

3959C

Table IV-3. ATS Hardware Delivered to NASA

<i>Part No.</i>	<i>Part Name</i>	<i>Quantity</i>
T2185593	Cover, Assy of	1
T2185592-01	Blade (Hollow With Hole)	3
T2185592-02	Blade (Hollow Without Hole)	3
T2185594	Blade (Solid)	4
T2185437	Seal	10
T2184089	Screw Machine	30+6=36*
T2184088	Gasket	30
CKD 2087	Gasket, Washer	30*
CKD 2078	Blade (Hollow Without Hole, Thin)	3

* See Task 3, Turbine Blade Testing and Data Analysis,
for section on leak repair of blade holding fixture.

3959C

C. TASK 3 — TURBINE BLADE TESTING AND DATA ANALYSIS

Task 3 consists of conducting the turbine blade tests at NASA and the evaluation of the test results. The hot core blade concept test program that was submitted to NASA is repeated below.

Hot Core Blade Test Program

The test rig thermal cycle should provide a nominal chamber temperature of 1700°F and a nominal chamber pressure of 2500 psi at the maximum operating condition. At the minimum operating condition, the nominal chamber temperature should be -350°F and the nominal chamber pressure should be 160 psi. An excursion from the minimum operating condition to the maximum operating condition and back to minimum operation condition constitutes a cycle. The fuel should be H₂, and O₂ is used as the oxidizer. Each thermal cycle should take approximately 16 seconds, or 80 seconds for a five cycle test. The above conditions were obtained from a memorandum to distribution, dated 15 April 1982, from Mr. Dumbacher (subject: Summary of SSME Turbine Blade Coating Test Program) and should reflect current rig operating capability and practice. This memorandum was provided to P&W by Mr. Rex Bailey.

Two hollow blades (one with a pressure side orifice and one without) and a solid blade will be installed in the holding fixture provided by P&W. The blade in the center position will be instrumented with a thermocouple, which must be attached to suitable recording equipment. All standard test rig measurements (e.g., test rig chamber pressure, chamber temperature, propellant flow rates, etc.) should also be recorded. The blades should be cycled through the following sequence:

1. 5 cycles, inspect visually, record any distress
2. 5 cycles, inspect visually, record any distress
3. 5 cycles, inspect visually, record any distress
4. 10 cycles, fluorescent penetrant inspection, record any distress, photograph

5. 25 cycles, inspect visually, record any distress
6. 25 cycles, fluorescent penetrant inspection, record any distress
7. After 75 cycles, continue testing until all articles have failed or a maximum of 225 cycles.

The above testing sequence is subject to change, depending upon intermediate test results and inspection findings.

If during inspection period, a test blade exhibits sufficient distress such that it is determined that the blade will not survive the test until the next inspection interval, that blade should be removed and replaced with one of the additional solid blades provided by P&W.

In order for NASA to provide the necessary recording equipment, a description of the instrumentation for the hot core blade is provided. The two hollow hot core blades will each be instrumented with two chromel/alumel thermocouples. Each of the thermocouple leads will be terminated with standard female Marling connectors.

During ATS hardware fit and leak checks on NASA's blade tester rig, combustion products were found leaking through the blade holder assembly. The hardware leaked at the boltheads that secure the blades to the blade holder, at the orifice where the thermocouple lead exits the blade holding fixture, and at a braze joint within the body of the blade holder. The braze joint was required to fill the cavities caused during the manufacturing process when the airfoil pockets were wire EDM'd into the blade holding fixture. Plugs (the same material as the blade holder) were wire EDM'd and brazed in place to fill the outer section of the airfoil pockets. The hardware was returned to P&W to correct the leak condition.

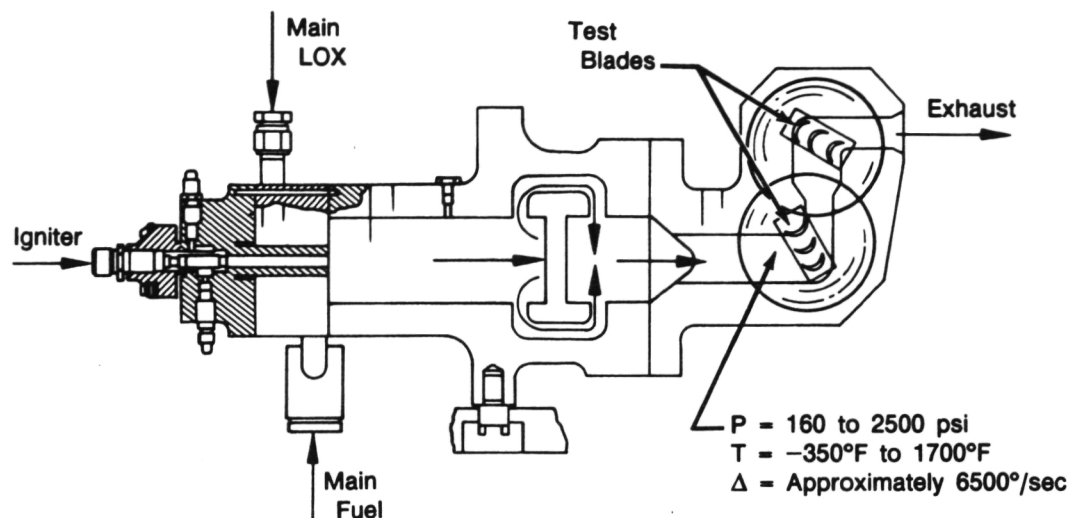
The reoperation consisted of fusion welding the plugs to the body of blade holding fixture on the outer surface of the blade holder. This surface was built up an additional 0.085 inch min. Subsequently the six boltholes were redrilled and respot faced, as shown in Appendix B, Figure B-13. New washers (Appendix B, Figure B-14) were machined out of soft nickel material to act as gaskets between the boltheads and the recently machined spot faces. The thermocouple lead leak was eliminated by fabricating an adapter (Appendix B, Figure B-15). The adapter was aligned with the instrumentation hole and welded onto the outer face of the blade holding fixture. The thermocouple lead could then be routed through the small diameter hole in the adapter and brazed to its long, narrow neck with low temperature braze (for easy removal of the instrumentation lead). Upon completion of the reoperation, the hardware was leak checked and returned to MSFC for test.

1. Thermal Cycle Test Results

The Marshall Space Flight Center (MSFC) thermal cycle testing under the Advanced Turbine Study has enabled P&W to validate its turbine airfoil LCF design system and to demonstrate a SSME airfoil concept that will exceed the 120* cycle LCF life requirement. Metallurgical superiority of the P&W single-crystal alloy (PWA 1480) is due, primarily, to the absence of grain boundaries where thermal fatigue cracks initiate. The absence of carbides in the PWA 1480 matrix also enhances the LCF improvement. Testing has shown, however, that the most important influence on turbine airfoil LCF life (or strain range) is configuration.

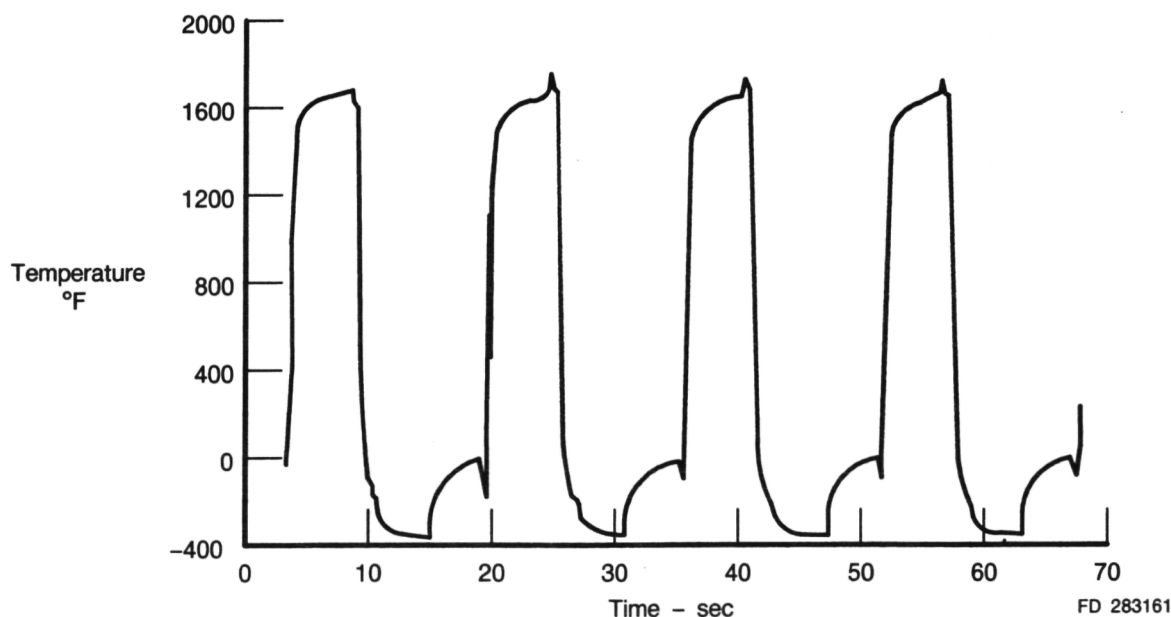
*P&W life goal is 2X NASA's 60 cycle life goal.

On 11 September 1984, testing began at MSFC using P&W airfoil specimens in the NASA thermal cycle test rig (Figure IV-11) mounted on test stand No. 116. At the time of this writing, two tests evaluating six P&W airfoil specimens have been conducted. One specimen simulating the P&W improved SSME high-pressure fuel turbopump (HPFTP) blade design demonstrated a LCF life in excess of the 60 cycle goal, in the simulated SSME environment, as shown in Figure IV-12.



FD 283160

Figure IV-11. Marshall Space Flight Center Thermal Cycling Rig



FD 283161

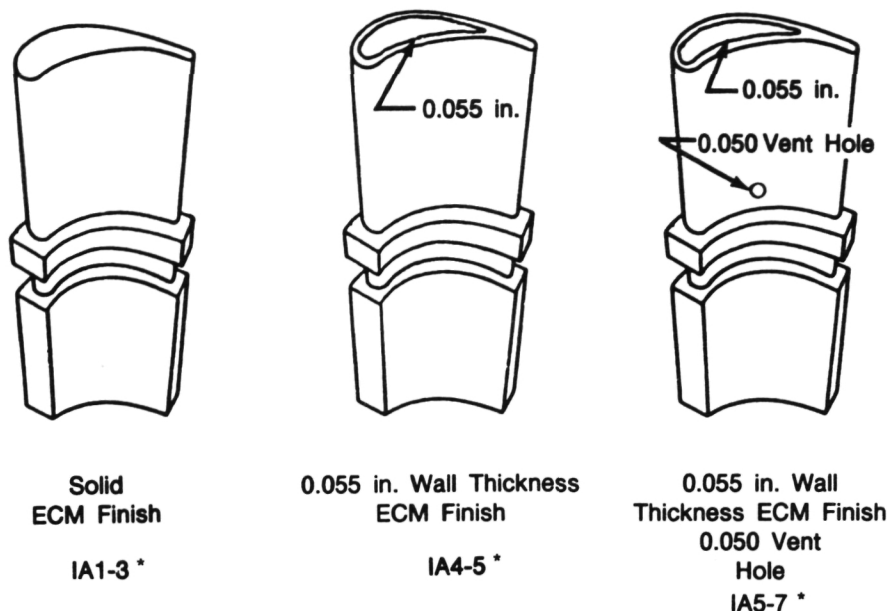
Figure IV-12. Thermal Cycling Test Environment

The initial test objective was to establish a baseline using three specimens described in Table IV-4. All three test specimens, as shown in Figure IV-13, were machined using electrical discharge machining (EDM) followed by electrochemical machining (ECM) to remove the recast layer. The calculated strain range of the ECM finish condition specimens from the initial test are shown in Table IV-4.

Table IV-4. Test No. 1 Specimen Configuration and Strain Range

Specimen No.	Wall Thickness (in.)	Strain Range (%)
1	0.190 (solid)	1.59
2	0.055 (hollow)	1.23
3	0.055 (hollow vented)	1.18

3959C



*Dash Number Corresponds to Blade Serial Numbers in Table IV-2

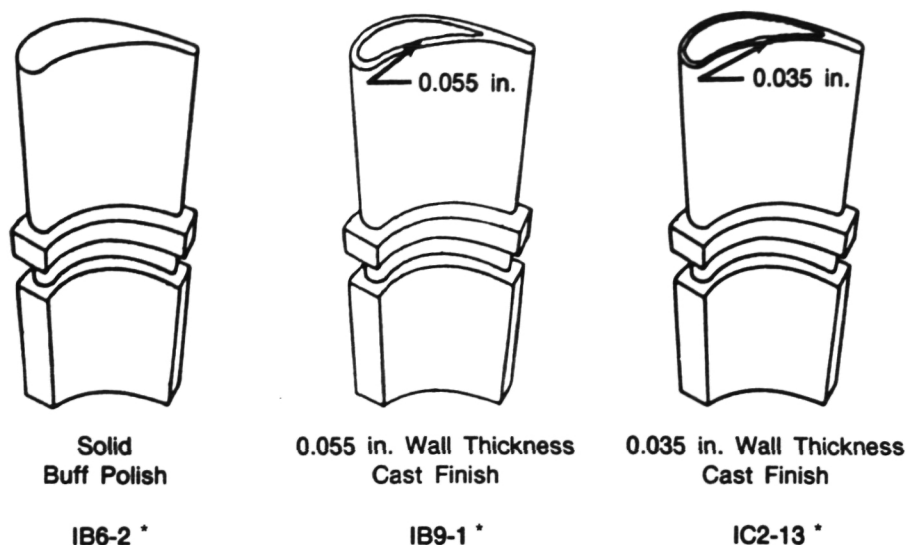
FD 290874

Figure IV-13. Test 1 PWA 1480 Single-Crystal Material

Specimen No. 1 simulated the current SSME HPFTP 1st-stage turbine blade airfoil shape and strain range, but substituted PWA 1480 single-crystal for Mar-M 246 DS alloy. Specimens No. 2 and 3 are cored configurations with reduced wall thickness to 0.055 inch, with the No. 3 blade also demonstrating the advantage of hot gas circulating into the core through a 0.050-inch diameter hole on the pressure wall near the platform fillet radius.

Test No. 1 progressed with inspections at cycle intervals of 5, 10, 23, 33, 43, 53, 63, and 71 cycles. Microscopic examination (25X), supplemented by black-light photography of the fluorescent penetrant inspection (FPI) results, was used to evaluate the blades condition. Initial cracks and crack propagation were carefully mapped.

The second test was conducted on three different specimens, as shown in Figure IV-14. Airfoil specimens 4 and 5 were similar in configuration to the No. 1 and 2 from the initial test, but with improved external finishes. Specimen No. 6 contained an enlarged core which thinned the wall thickness to 0.035 inch, closely simulating the P&W HPFTP blade designs. Calculated strain ranges are presented in Table IV-5.



*Dash Number Corresponds to Blade Serial Numbers in Table IV-2

FD 290875

Figure IV-14. Test 2 PWA 1480 Single-Crystal Material

Table IV-5. Test No. 2

Specimen No.	Wall Thickness (in.)	Strain Range (%)
4	0.190 (solid improved finish)	1.59
5	0.055 (hollow improved finish)	1.23
6	0.035 (hollow improved finish)	0.94

3959C

Specimen No. 4 was identical to No. 1 except the airfoil surface was polished to eliminate the surface pitting associated with the ECM process. Specimen No. 5 was similar to No. 2 except its airfoil surfaces were polished and then vapor blasted to remove polishing lines and to simulate a cast airfoil finish. Specimen No. 6 is the first test airfoil simulating the lower strain range of the P&W SSME HPFTP designs. Similar to specimen No. 5, it too has a surface finish simulating a cast airfoil.

Test No. 2 progressed through 73 cycles with inspection intervals at 3, 10, 11, 15, 23, 26, 30, 32, 37, 47, 54, 62, and 73 cycles. Tests 1 and 2 inspection intervals and initial crack determination are depicted in Figure IV-15. Photographic documentation of the several test configurations is shown in Figure IV-16. Detailed inspection of the parts was aimed toward initial crack detection and subsequent propagation. Figures IV-17 and IV-18 depict crack initiation and progression throughout the two tests. General conclusions from this testing are:

- The preferred P&W thin-wall airfoil design with P&W 1480 single-crystal material has the potential to meet LCF life goals and double the current SSME HPFTP blade life
- Initial cracking generally occurred on the pressure side, in the platform fillet radius
- Cored parts are significantly more crack resistant than solid parts
- Thin wall and ventilated parts are the superior configurations for this rocket engine environment.

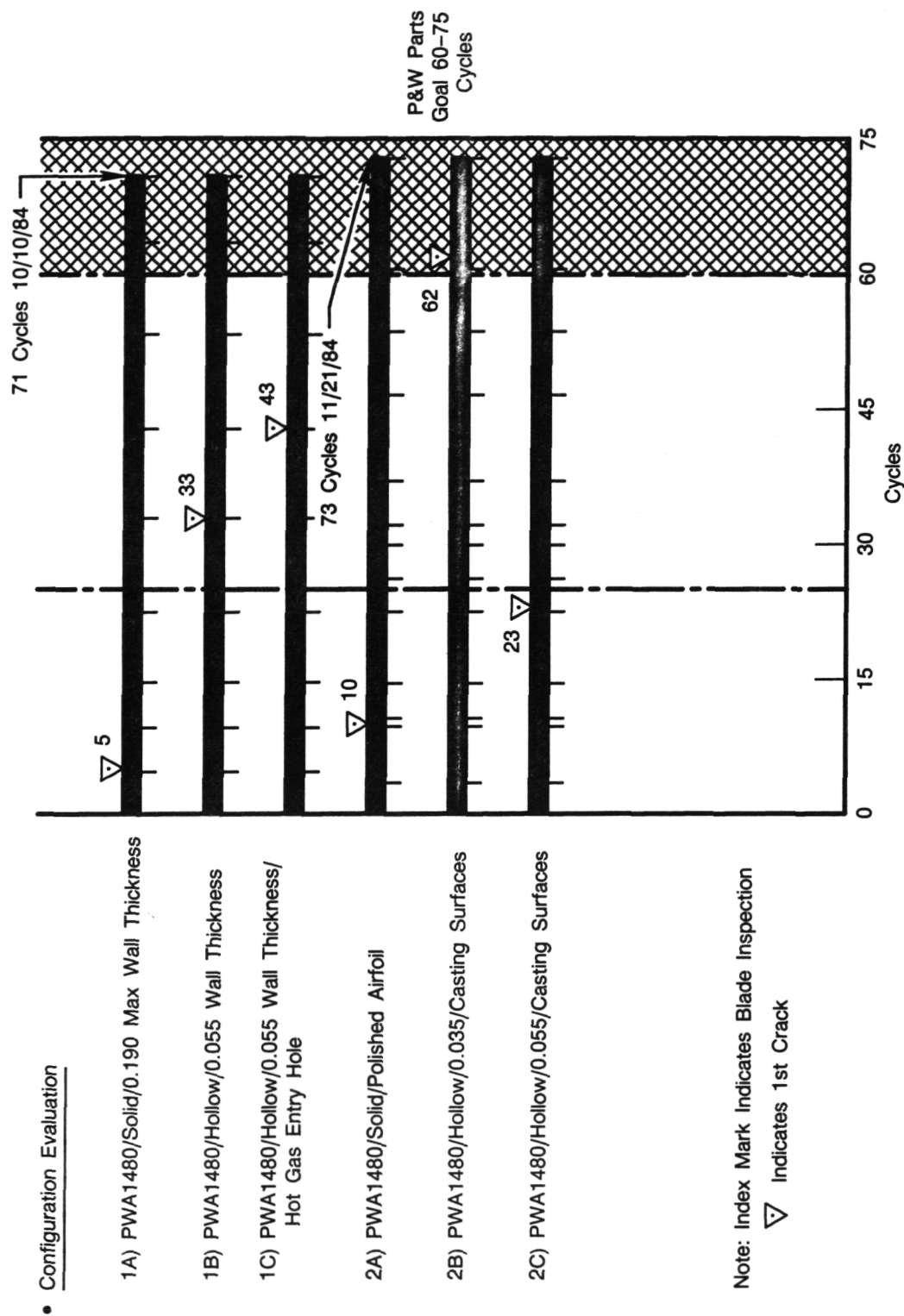


Figure IV-15. Inspection Intervals and Crack Initiation

ORIGINAL PAGE IS
OF POOR QUALITY

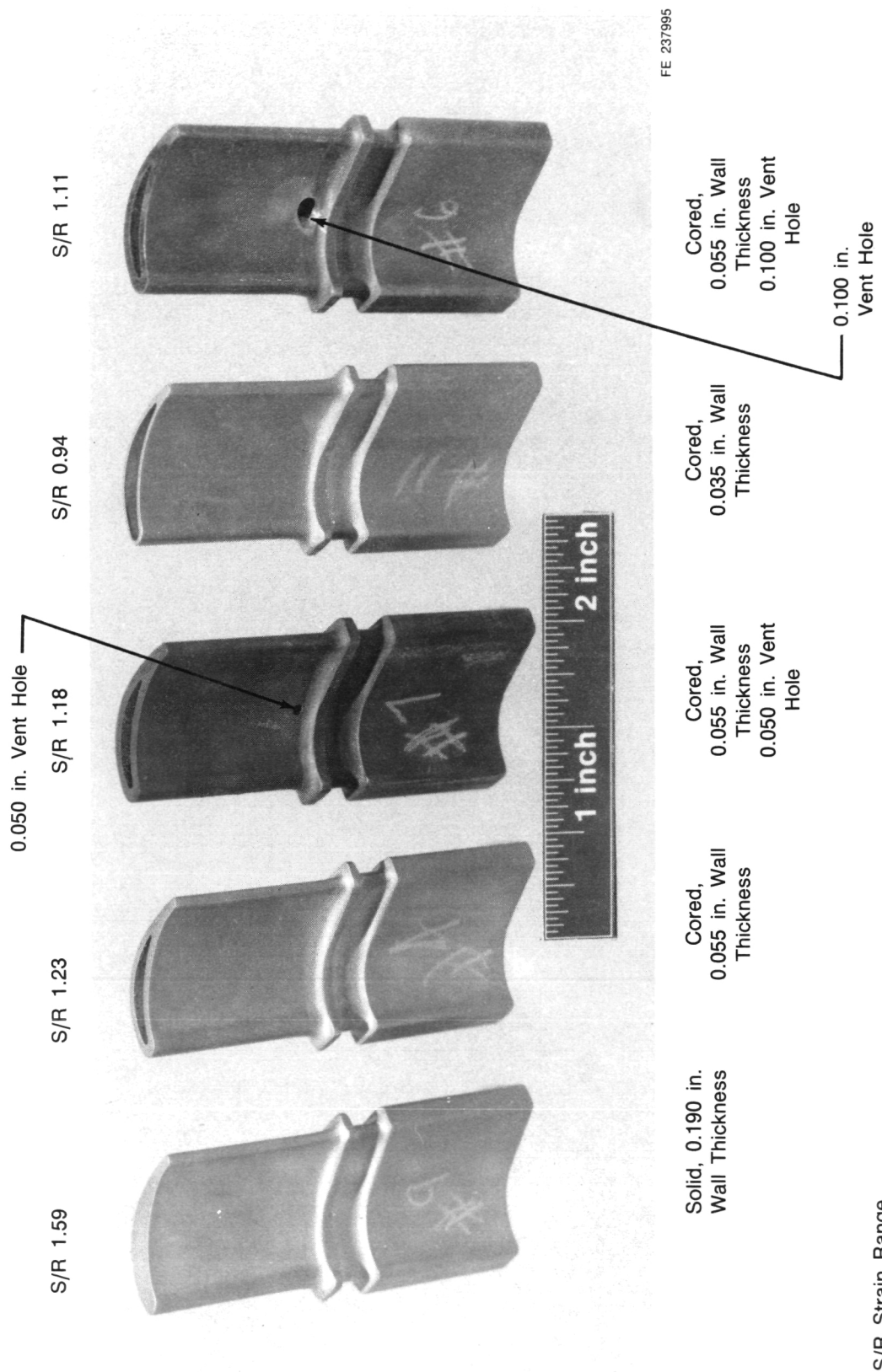


Figure IV-16. Initial Thermal Cycle Test Specimens Machined from Cast PWA 1480 Single-Crystal Test Bars

FD 290877

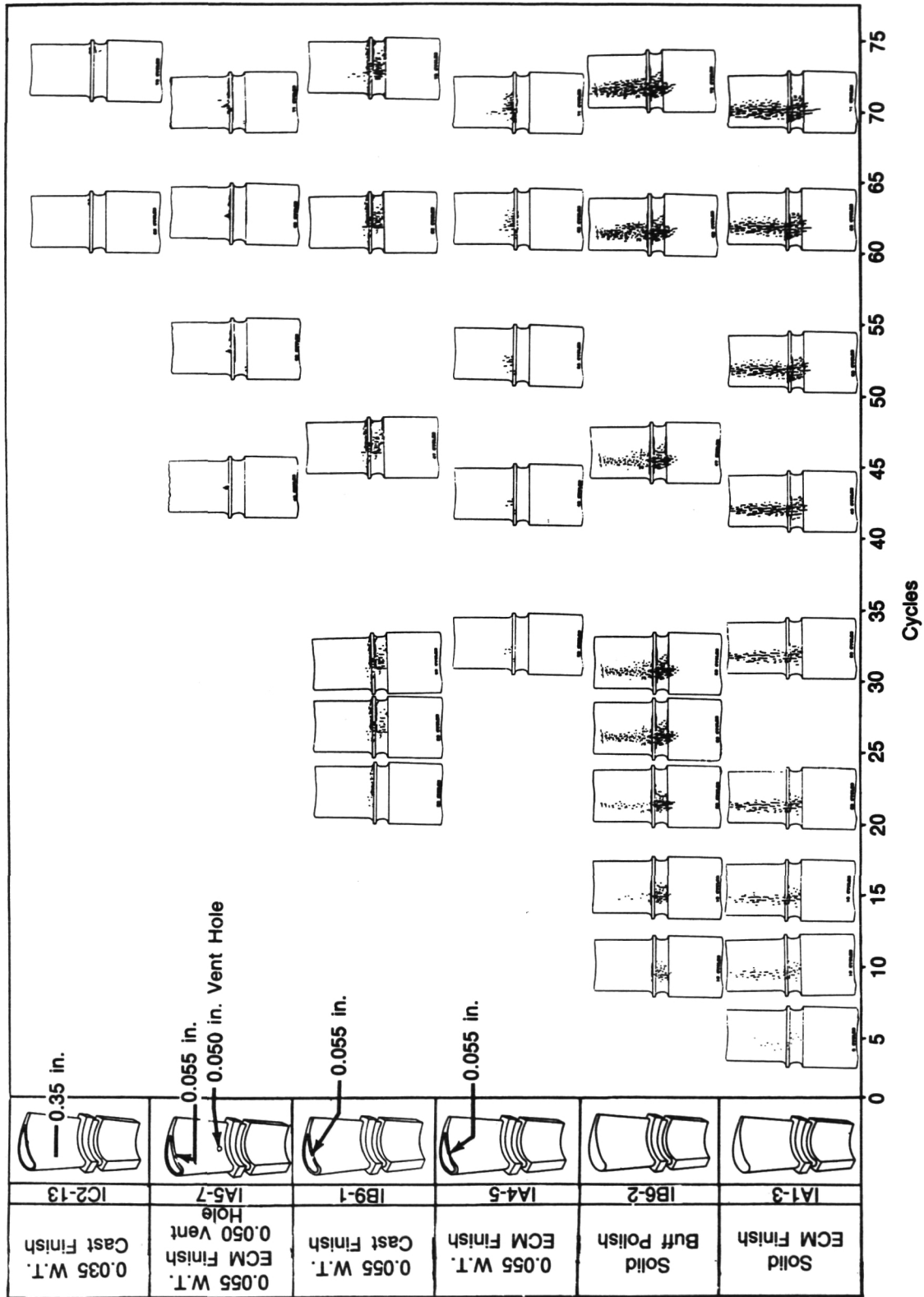


Figure IV-17. Thermal Cycle Test Results, Pressure Side

FD 290878

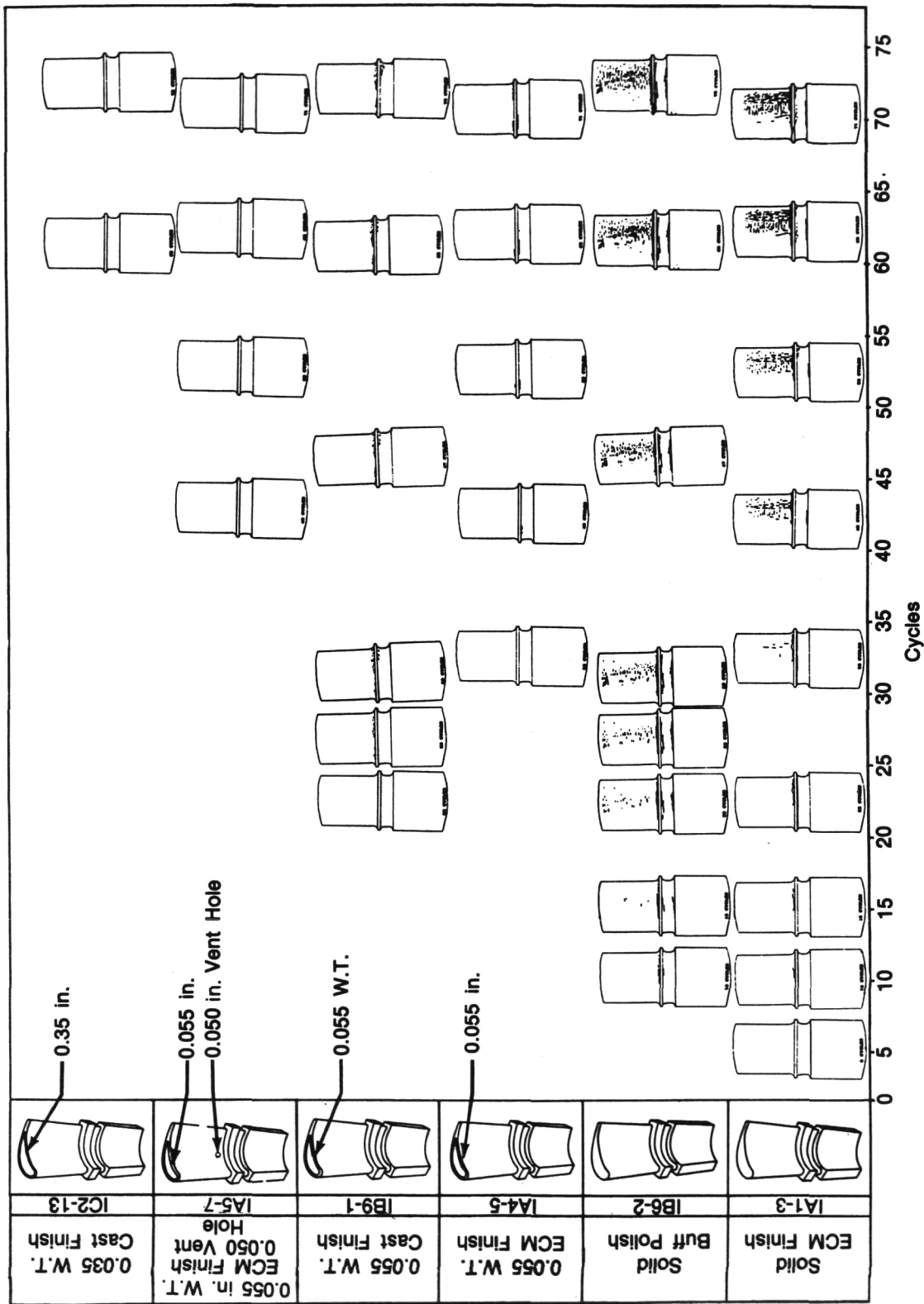


Figure IV-18. Thermal Cycle Test Results, Suction Side

2. Metallurgical Analysis

Completion of two series of tests on specimens made from PWA 1480 (nickel-base single-crystal alloy) has supported the potential selection of this alloy for use in SSME turbine airfoil applications. Distress evident on these specimens corresponds to locations of calculated maximum strain due to thermal stresses. Alloy PWA 1480 has been extensively characterized in thermal mechanical fatigue (TMF) under simulated turbojet engine conditions. The life of the engine parts closely matched the life estimated from extrapolation of this data.

The test airfoils had surface connected cracks which have features similar to laboratory TMF samples. Maximum depth of cracking was seen at the fillet radius, of approximately 0.030 inch, becoming more shallow when approaching the blade tip. Specimen 1A1-3, solid airfoil specimen simulating the current SSME design, was cut up and extensively evaluated in the P&W Metallurgical Laboratory. Figure IV-19 shows the condition of the part after 71 cycles of testing, the location of the blade's section, and defines the LCF crack patterns. Photomicrographs shown in Figures IV-20 through IV-25 document the extent of crack propagation into the structure of the airfoil.

Surface finish affects crack initiation. The three test airfoils from Test No. 1 exhibited surface pitting from the machining and grain etching operations. This surface is shown in Figure IV-26. The location of the pitting corresponds to the dendrite cores of the single-crystal. Post-test evaluation showed cracks connecting these pits.

In the second test sequence an attempt was made to improve the surface finish of the parts by hand polishing. The solid part (No. 4) was polished to a brushed appearance. This finish did not significantly improve the crack initiation life of the part, but did change the direction of cracking. The cracks followed the polishing grooves across the span of the airfoil, indicating the sensitivity of crack alignment to surface finish. Specimens No. 7 and 8 were polished and vapor blasted to a matte casting surface finish. Tests with these specimens simulating a cast finish showed that crack initiation was not associated with surface anomalies.

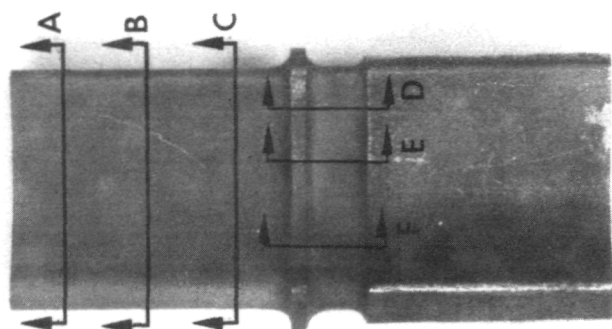
The correlation of hydrogen embrittlement on the life of these parts is incomplete. Analysis methods used to date have not given any positive indications of embrittlement. Material testing has indicated that most materials, PWA 1480 included, are least affected by hydrogen embrittlement at either cryogenic or high temperatures, and that maximum embrittlement occurs at room temperature (RT). By extrapolating this characteristic to the test condition a minimal effect of hydrogen will be expected since rapid heating and quench rates make the hydrogen exposure at RT a small portion of the total cycle duration.

3. Resumption of Testing

When testing resumes, specimens listed in Table IV-6 and identified as Serial Nos. 4, 6, 9, 11, 12, R1, R2, R3, and R4, will be available for evaluation. Serial Nos. 4 and 9 will define the degree of LCF improvement with increased substrate densification via HIP processing. Serial No. 6 will assess the benefit of increased hot gas circulation in the core cavity. The 0.100-inch diameter hot gas entry hole is aligned with the direction of hot gas flow to increase internal circulation in the platform region where initial cracking has been observed due to the high thermal strain associated with the heavier thickness in this area. Serial No. 11 is a duplicate of the successful blade specimen (Serial No. 13). This particular specimen (Serial No. 11), while manufactured identical to Serial No. 13, has a grain anomaly that could have a degrading effect on LCF life. The defect is a "high angle grain boundary" that is documented in the photos shown in Figure C-8, Appendix C. This part warrants test to evaluate the influence of grain anomalies on LCF life. Serial Nos. R1 through R4 are duplicates of the different blade designs, but fabricated out of NASA-supplied Mar-M 246 alloy for material comparison with the PWA 1480 SC material.

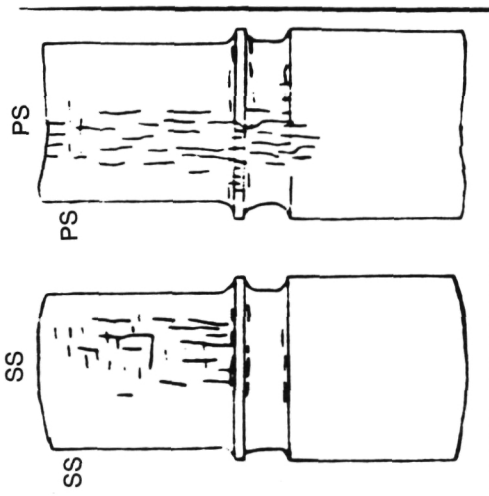
ORIGINAL PAGE IS
OF POOR QUALITY

FD 301909

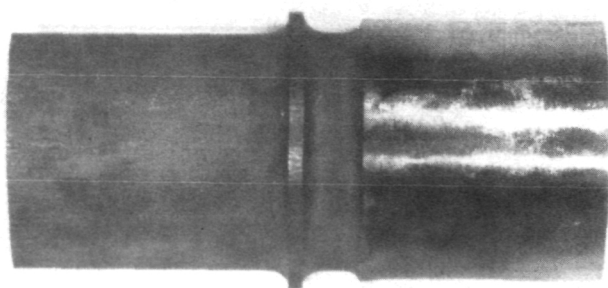


Mag: 1-1/2X

Sectioning of Blade No. 3



Solid Airfoil
0.190 Max W.T.
71 Cycles



Mag: 1-1/2X

Figure IV-19. Low Cycle Fatigue Crack Patterns After 71 Cycles of Testing

FD 301910

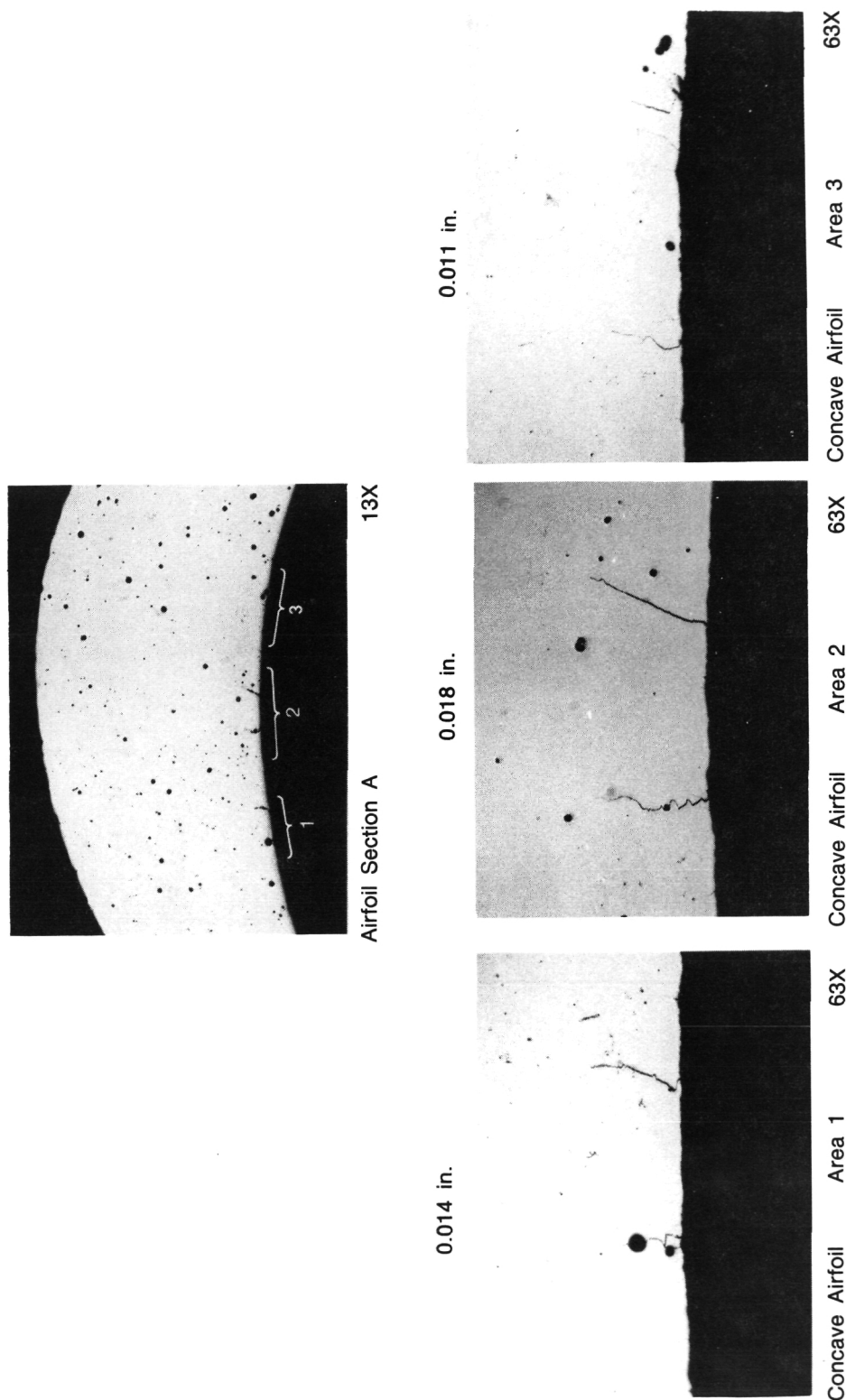
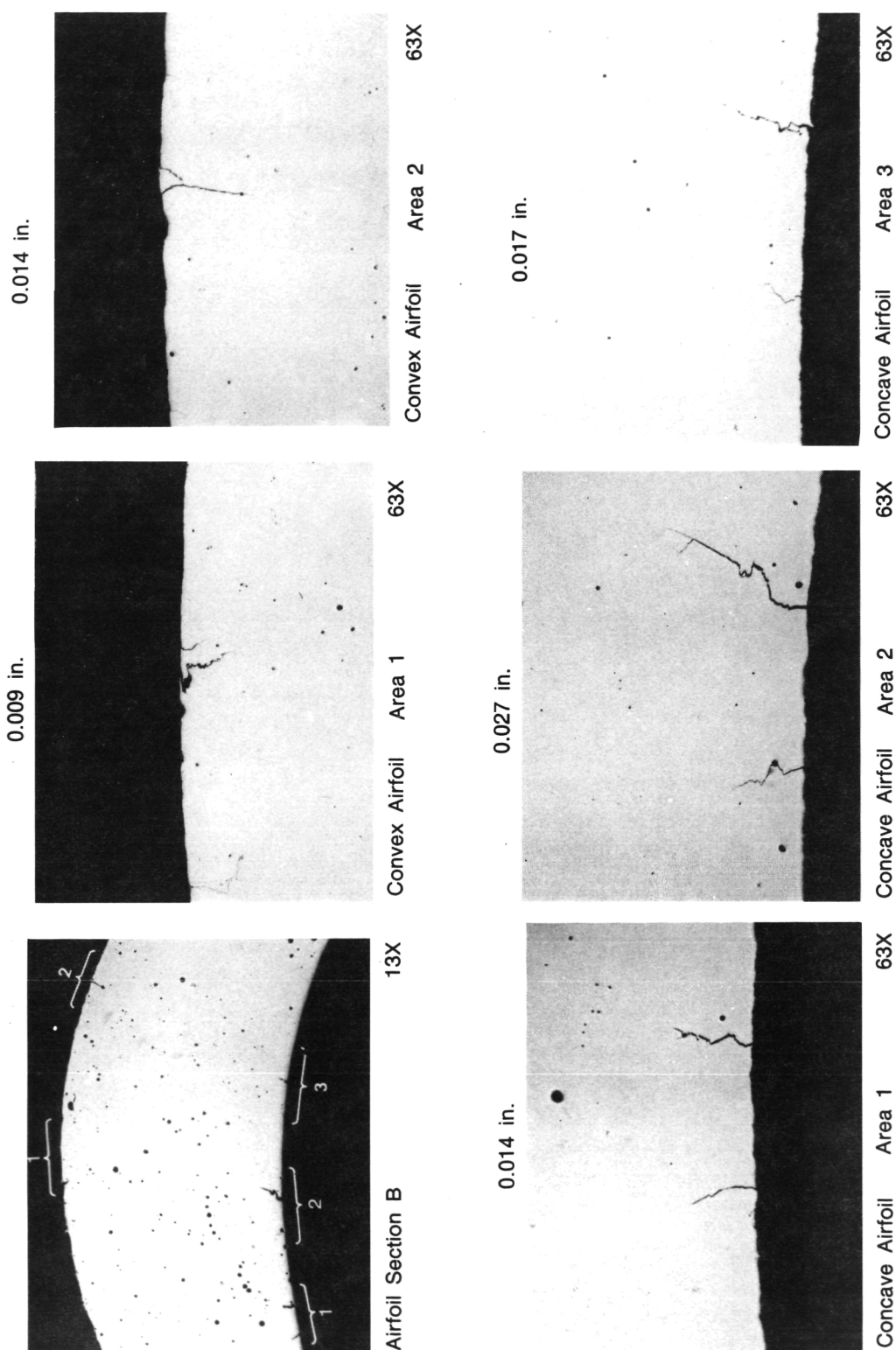


Figure IV-20. Airfoil Section A Crack Propagation

ORIGINAL PAGE IS
OF POOR QUALITY



FD 301911

Figure IV-21. Airfoil Section B Crack Propagation

FD 301912

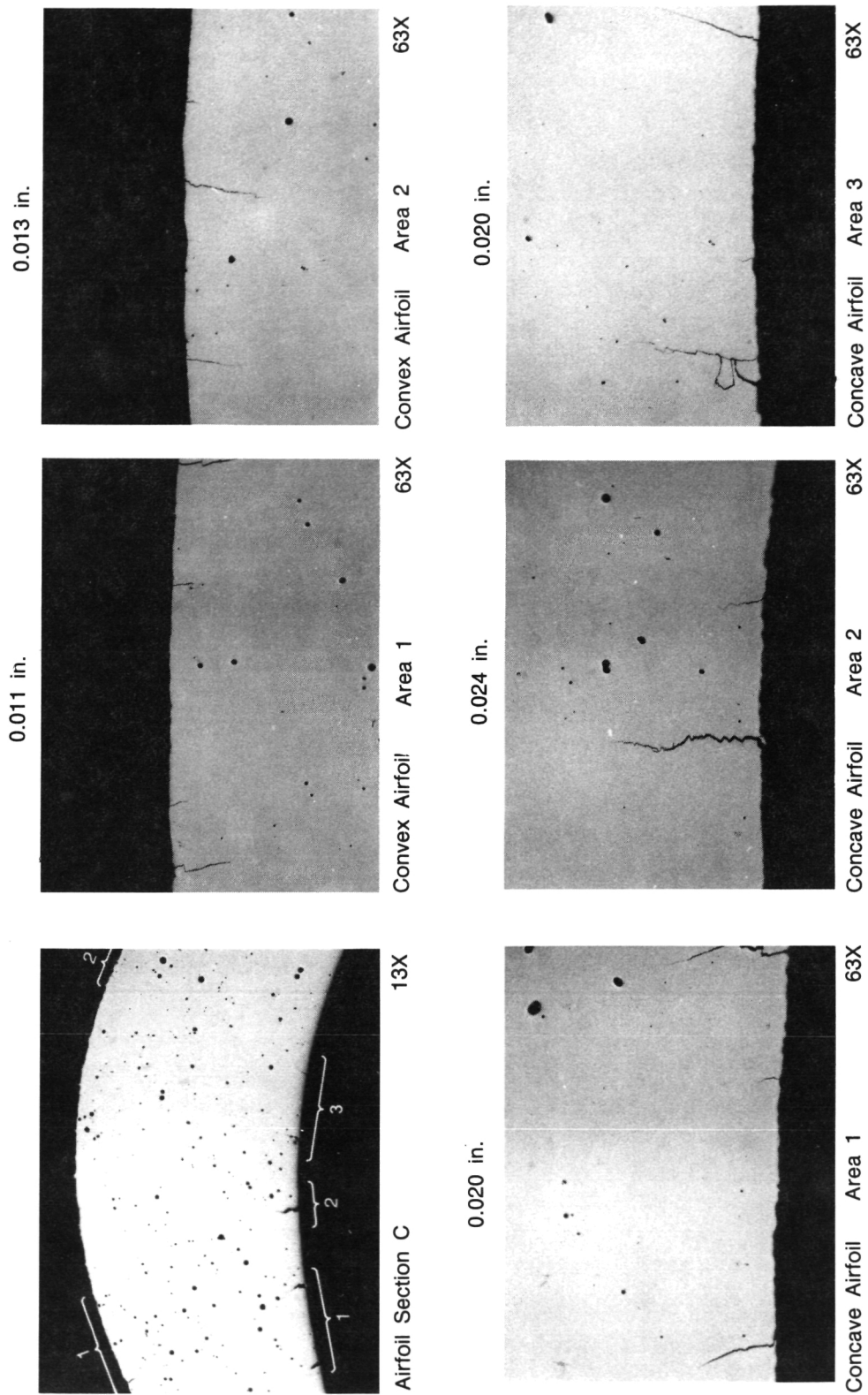
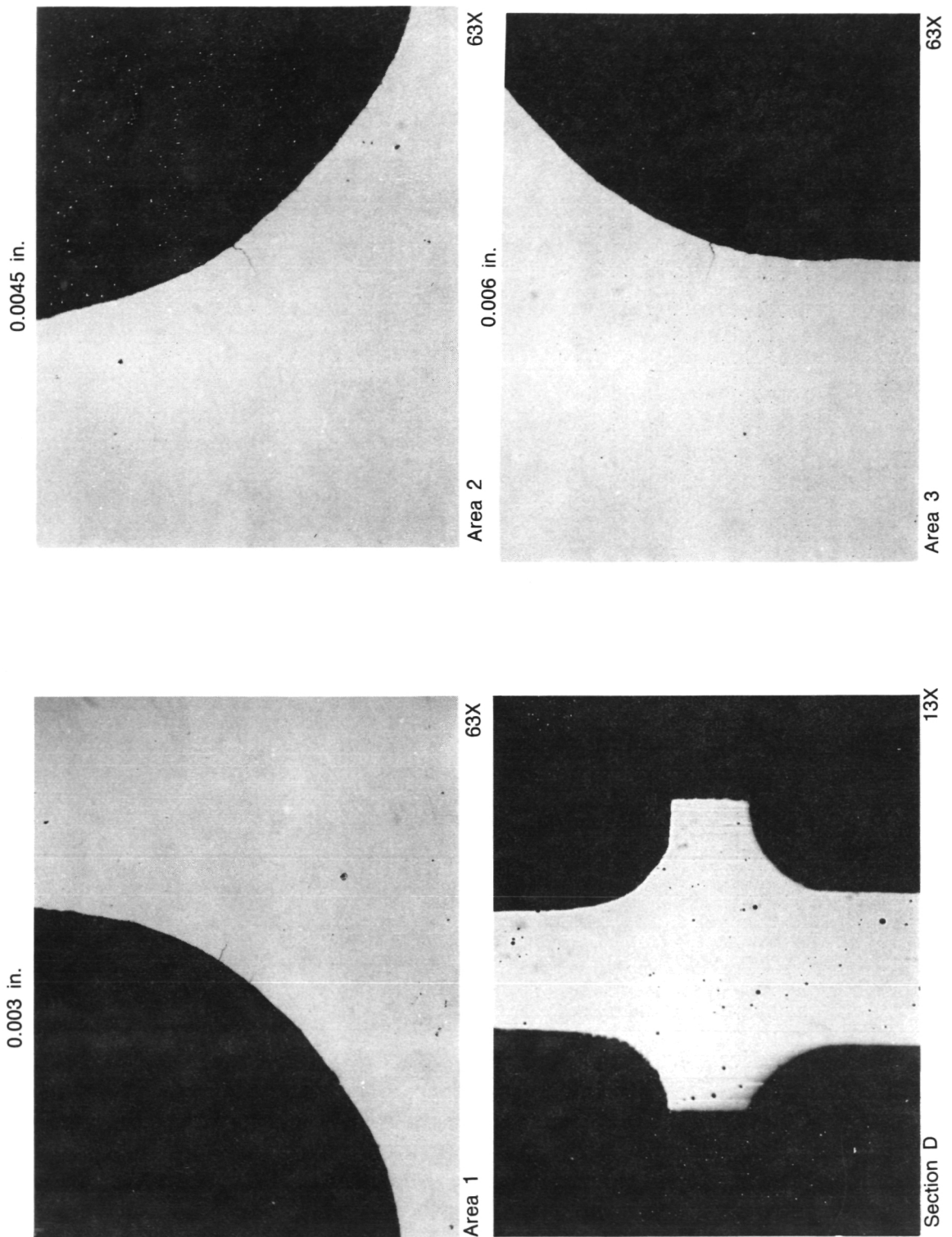


Figure IV-22. Airfoil Section C Crack Propagation



FD 301913

Figure IV-23. Airfoil Section D Crack Propagation

ORIGINAL PAGE IS
OF POOR QUALITY

FD 301914

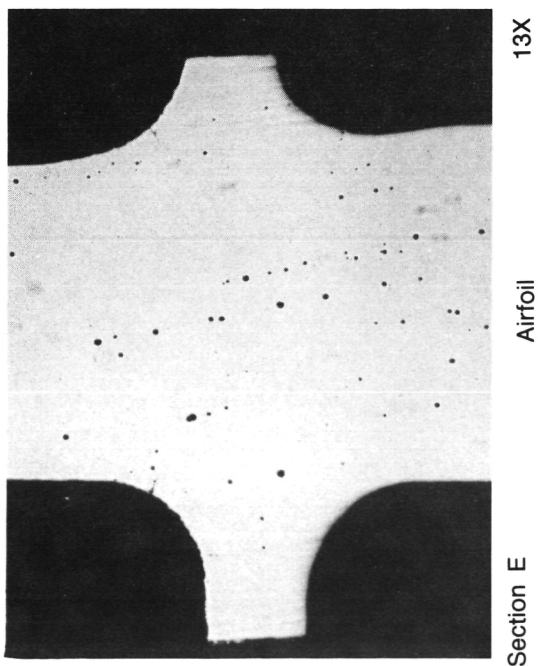
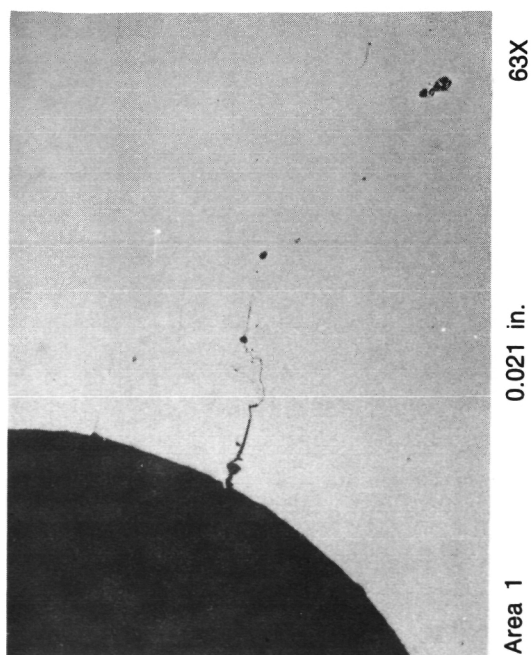
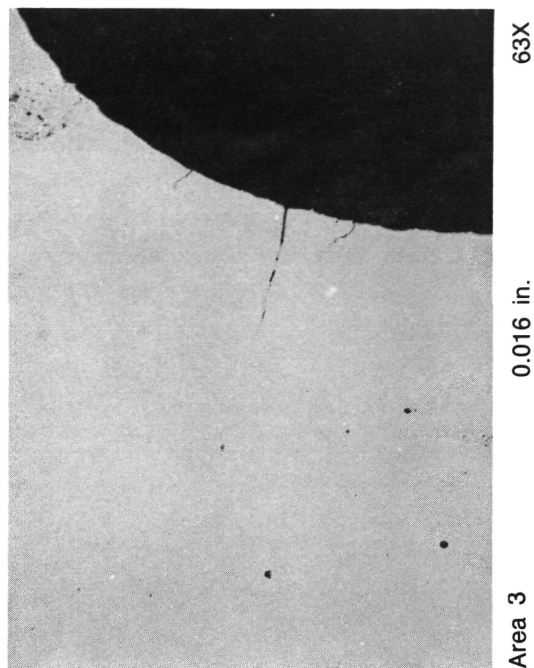
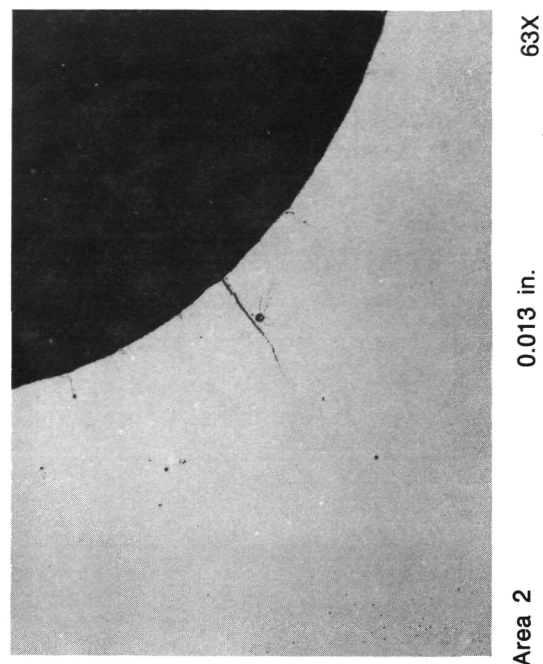
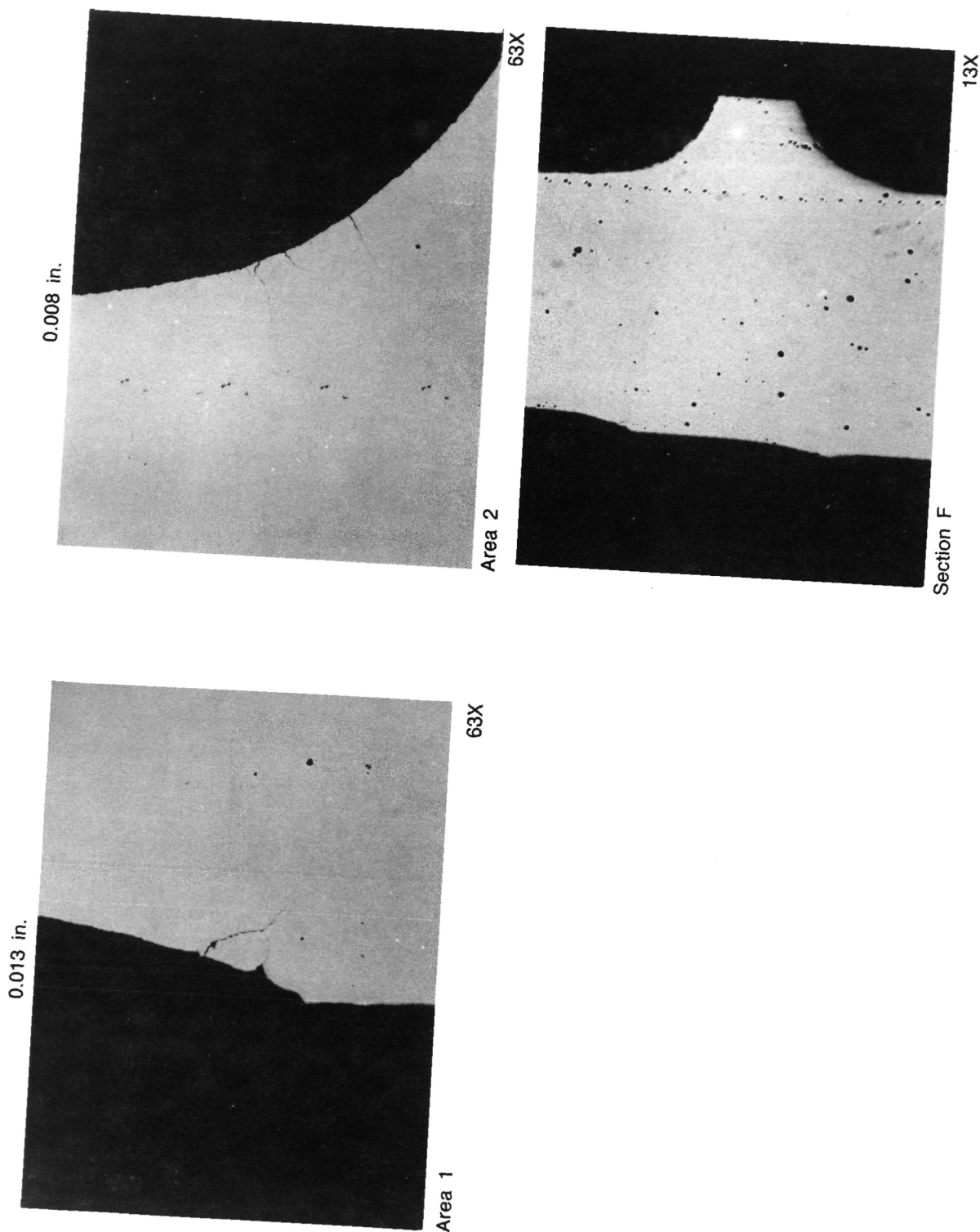


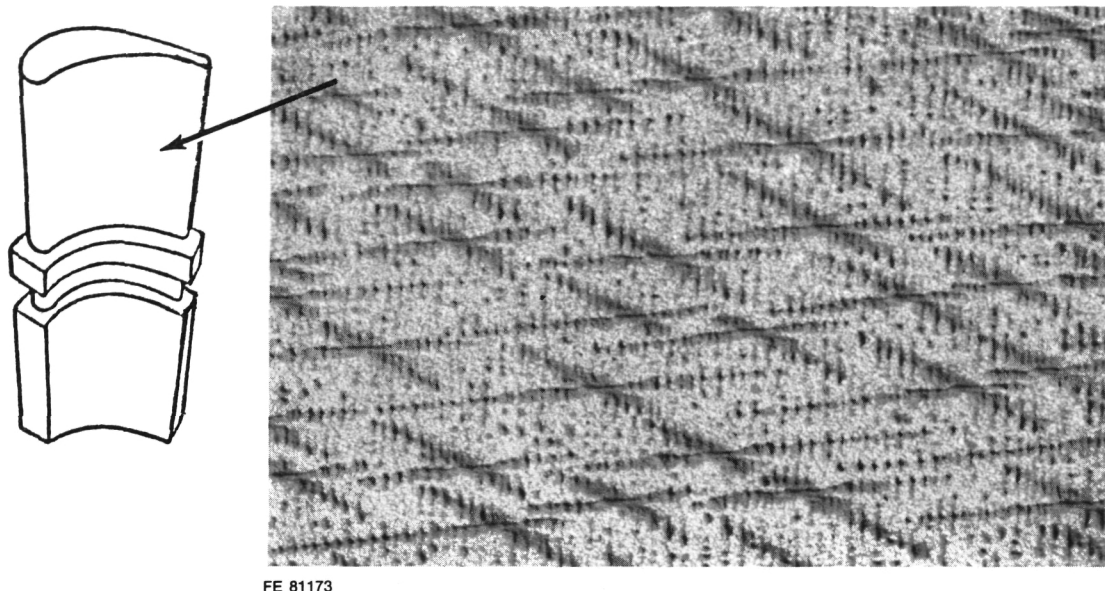
Figure IV-24. Airfoil Section E Crack Propagation



FD 301915

Figure IV-25. Airfoil Section F Crack Propagation

ORIGINAL PAGE IS
OF POOR QUALITY



FD 290879

Figure IV-26. Surface Pitting on Initial Low Cycle Fatigue Rig Test Specimens

At NASA's request four additional blades were delivered to MSFC under Contract Modification 12. The material used was Mar-M 246, which was supplied by NASA. The hollow blade configuration had no vent holes and is described below.

<u>S/N</u>	<u>Description</u>	<u>Reference P/N</u>
R1	Hollow (0.035 in. wall)	CKD 2078
R2	Hollow (0.055 in. wall)	T2185592-2
R3	Solid	T2185594
R4	Solid	T2185594

These specimens are also identified in Table IV-6 as Serial Nos. R1 through R4. These test specimens will provide an excellent correlation between the Rocketdyne SSME alloy and P&W's single-crystal alloy (PWA 1480).

Table IV-6. Thermal Cycling Test Candidate Airfoil Test Specimens

Serial No.	Material	Solid/Hollow	Wall Thickness (in.)	Vent Hole	Finish	Test No.	Initial LCF		Remarks
							Crack	Cycles	
3	PWA 1480	Solid	0.190	No	ECM	1	1	5	Test 1, first cracks at 5 cycles
5	PWA 1480	Hollow	0.055	No	ECM	1	1	33	Test 1, first cracks at 33 cycles
7	PWA 1480	Hollow	0.055	0.050	ECM	1	1	43	Test 1, first cracks at 43 cycles
2	PWA 1480	Solid	0.190	No	ECM	2	2	10	Test 2, first cracks at 10 cycles
1	PWA 1480	Hollow	0.055	No	Casting	2	2	23	Test 2, first cracks at 23 cycles
13	PWA 1480	Hollow	0.035	No	Casting	2	2	62	Test 2, first cracks at 62 cycles, continue past 73 cycles
9	PWA 1480	Solid	0.190	No	Casting				HIP
4	PWA 1480	Hollow	0.055	No	Casting				HIP
6	PWA 1480	Hollow	0.055	0.100	Casting				Increased circulation (vane design)
10	PWA 1480	Hollow	0.035	No	Casting				High angle grain boundary
*R3	Mar-M 246	Solid	0.190	No	Casting				Baseline with Rocketdyne alloy
*R4	Mar-M 246	Solid	0.190	No	Casting				Baseline with Rocketdyne alloy
*R2	Mar-M 246	Hollow	0.055	No	Casting				Baseline with Rocketdyne alloy
*R1	Mar-M 246	Hollow	0.035	No	Casting				Baseline with Rocketdyne alloy

*Test specimens machined from Rocketdyne alloy (raw material supplied by MSFC).

3859C

SECTION V

CONCLUSIONS AND COMMENTS

The difficulties encountered during the fabrication of the closeout layer for the advanced convectively cooled scheme precluded the evaluation of the original approach for cooling turbine blades in the high-temperature environment encountered in today's high-pressure reusable liquid rocket engines. These difficulties consisted of the absence of adhesion between the sputtered closeout layer and the parent material of the substrate blade. The lack of adhesion was attributed to the formation of surface oxides or impurities on the surface of the blade.

If these problems could be overcome and an alternative method for applying the closeout layer (the key to the advanced convectively cooled design) could be developed, the advanced convectively cooled blade concept would then become a strong potential candidate for increasing the life and performance of turbine blades in high-pressure liquid rocket applications, especially for hydrocarbon fueled rocket engines. Due to complexities encountered during the fabrication process, the advanced convectively cooled blade must be regarded as an area of technology in need of further basic research.

On the other hand, the use of PWA 1480 advanced single-crystal materials and the hot core blade design can bring near-term payoffs in liquid rocket turbine blade life and performance. The benefits of the implementation of these technologies have been clearly demonstrated by the results of the testing performed with the hardware fabricated in the Advanced Turbine Study Program.

Optimization of the hot core blade design should be pursued. Hot core blade implementation into an aerodynamically optimized design (twisted and tapered blade) and the evaluation of its benefits in a real application appear to be the logical steps to follow.

APPENDIX A SUMMARY OF SPUTTER DEPOSITION WORK

A. INTRODUCTION

Sputter deposition is one of the physical vapor deposition techniques in which a coating is built up on a substrate - essentially atom by atom. In a physical sputter deposition system, ions are accelerated to a target with sufficient energy to knockout or "sputter" atoms from the target surface. These sputtered atoms travel with considerable velocity until intercepted by the substrate to build up a coating. The process can be accomplished by a beam of ions (or neutral atoms) or by accelerating ions from the plasma of a gas discharge which is established near the target.

Sputter deposition technology has reached a level of maturity that is beyond the laboratory curiosity stage. Numerous substrate-coating combinations have been demonstrated — particularly elemental or simple compound thin films for electronic and optical applications. Fewer combinations of thick alloy deposits on engineering material substrates have been investigated. In either case, work on new combinations proceeds from experience and not by precise modeling or knowledge of the deposition process. Definitive experiments would require a detailed characterization of substrate, coating, and electrical discharge which includes:

- Adhesion
- Coating structure, defects, and crystallography (including orientation)
- Composition of substrate surface and coating including trace elements
- Coating stress, thickness, and hardness
- Substrate roughness
- Substrate temperature
- Mechanically worked subsurface layer (Beilby or selvedge layers)
- Mechanical properties of the coating
- Coefficient of thermal expansion for the coating
- Chemical solubility of coating and substrate
- Process parameters — plasma characteristics and particle species, energy and density impacting the substrate.

Obtaining these details involves designing intricate experiments and characterizing the results with sophisticated techniques. However, this is seldom done due to the considerable expense involved.

Experience which served as the background for this deposition program included:

- NASA LeRC contracts NASA CR 134824, NASA CR 135153, and NASA CR 159637, "Development of Sputtered Techniques for Thrust Chambers." In this program, thick copper, titanium, and nickel-base alloys were

deposited and characterized. Bulk coating properties were obtained. Copper alloys were welded. Two thrust chamber throats were fabricated as illustrated in Figure A-1 by sputter deposition of thick Cu-0.15 Zr over sputter deposited aluminum filler.

- NiCoCrAlY coatings are routinely sputter deposited on turbine airfoils to a 0.005 inch thickness in a system designed specifically for this purpose. Deposits up to 0.100 inch thick have been deposited in the same equipment. Forty-eight F100 1st-stage turbine blades can be coated in a six hour cycle in this system.
- NiCoCrAlY alloys have been deposited at rates in excess of 0.007 inch per hour in the hollow target system used in this program.

The next three sections in this summary of sputter deposition will cover the following:

- Selected details on the sputter deposition process
- Deposition work done to date and conclusions reached
- Additional work required to complete the program.

It will be found that many of the technical elements required for this program have been worked out and that the sputter deposition process is sufficiently versatile to accomplish the task. No technical impossibilities are known at this time.

B. SPUTTER DEPOSITION — ELEMENTS OF THE PROCESS

Earlier in this report, a sputtering system equipment and some of the deposition process were described briefly. In this section, the sputter deposition process will be described in more detail to provide the background for understanding program deposition work to date. The discussion will be directed particularly to the substrate and those factors that affect adhesion of a coating to it.

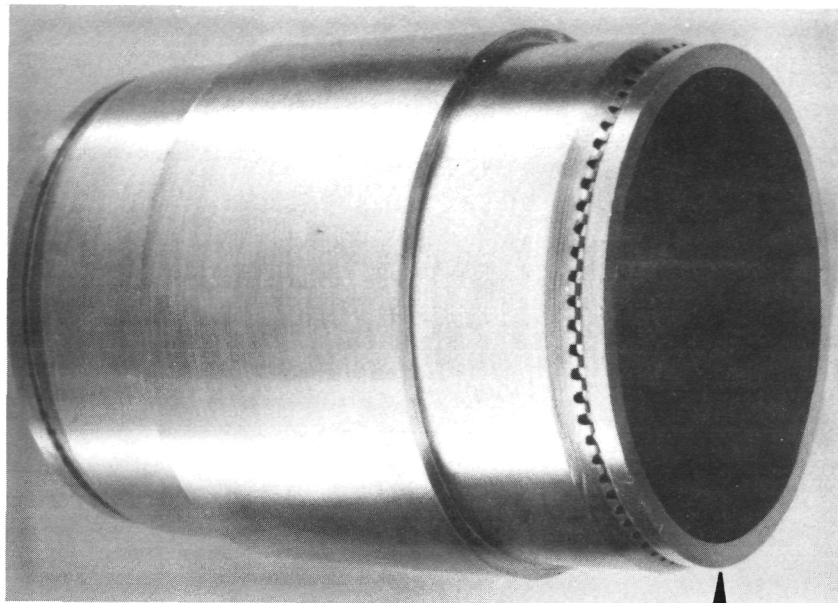
The starting point for substrate phenomena will be the coating growth process. Electron microscope work on defined single-crystal surfaces has shown that the process proceeds by:

- Atom impact
- Atom lateral movement
- Nucleation
- Island growth
- Coalescence of islands
- Thickness buildup.

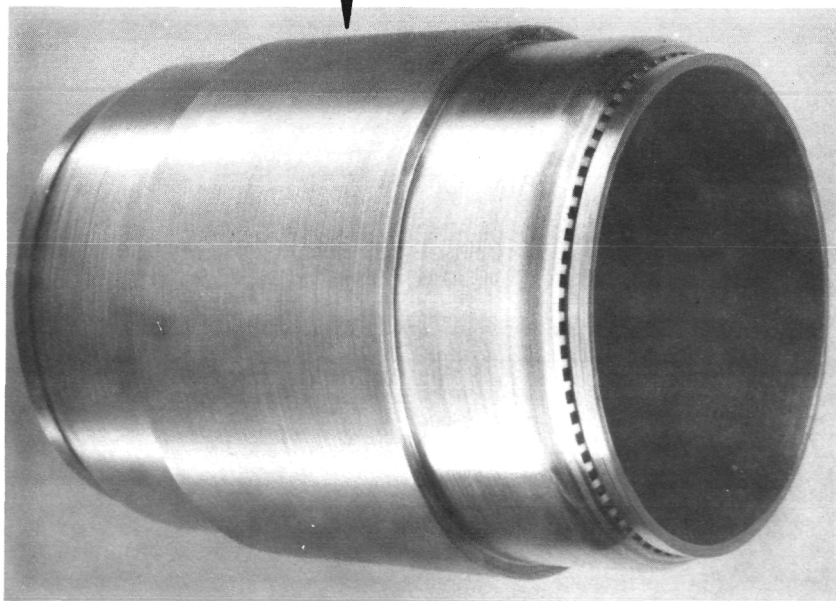
While these steps cannot be demonstrated precisely on the surface of an engineering material, they should apply to a sufficient extent to guide modeling of important process parameters.

ORIGINAL PAGE IS
OF POOR QUALITY

FD 267788



GF Substrate II-5P



GF Substrate I-36

Sputtered
AMZIRC

Figure A-1. GF Substrates After Machining and Leaching Aluminum Filler

Work with thick deposits has demonstrated that coating structure and growth habit, indicative of modification of the basic growth process, are influenced by substrate surface features. These are:

- Surface macro defects such as scratches, pits and protrusions (cleaning particle grit, diffusional artifacts, dust, etc.)
- Substrate temperature
- Angle between the surface plane and the adatom flux
- Surface composition and crystal structure.

Adverse effects on coatings, such as leaders (through defects) and poor adhesion, are minimized or eliminated by careful substrate preparation and manipulation of process parameters, which was discussed in this report.

The basic growth process can also be modified by interaction of energetic particles with the substrate and/or the growing deposit (a continuously changing substrate). Energetic particles originating at the sputtering system target include:

- Electrons
- Neutral atoms of target material (the adatoms)
- Reflected neutral sputtering gas atoms
- Photons
- Negative ions.

Particles originating from the gas discharge (plasma) include:

- Ions of sputtering gas
- Electrons
- Neutral atoms
- Photons
- Chemical complexes (molecules).

In a gas discharge sputter deposition system, these particles cannot be controlled independently of each other.

However, these particles can be controlled to a sufficient extent to affect modification of coating adherence and growth habit. For example:

Increasing Target Voltage

- Increases the average adatom energy
 - Increases adhesion (ion mixing, implantation, etc.)
 - Heats target which may cause elemental diffusion, phase changes, and outgassing of the target and radiation heating of the substrate.
 - Sputtering gas burial (pumping)

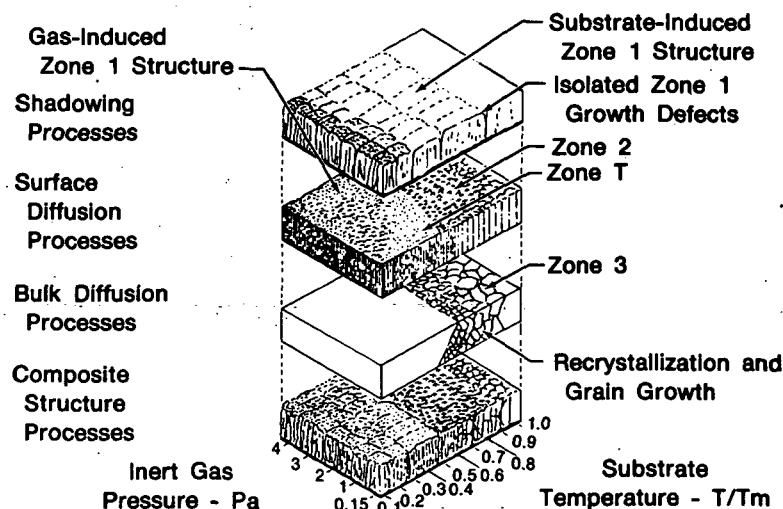
- Increases secondary electron energy
 - Heats the substrate
 - Probably affects nucleation rate
- May increase deposition rate if in range where yield is still increasing

Increasing Negative Substrate Bias Voltage

- Reduces coating thickness buildup rate by re-sputtering
- Heats the substrate
- Modifies coating structure by forward sputtering to fill grooves and eliminate shadowing
- Cleans or contaminates, depletes alloys of select elements, forms artifacts, and enhances diffusion depending on substrate temperature, species present, and duration of bombardment

*Increasing the Discharge Pressure**

- Decreases average adatom energy by increasing collisions with neutral gas atoms
- Modifies electric field details at substrate and target through sheath spacing changes
- Probably affects the nucleation process.



FD 124536

Figure A-2. Coating Structure as a Function

* A phenological description of growth habit as a function of discharge pressure and substrate temperature has been given by Thornton as illustrated in Figure A-2.

One of the prime requisites in any coating work is the adhesion of the coating to the substrate. Adhesion can be classified as two types — mechanical and chemical. Mechanical adhesions is an interlocking of the coating with substrate hills and valleys. Chemical adhesion takes numerous forms with actual interdiffusion of the substrate and coating being an important mechanism in metallic systems. If mechanical adhesion is disregarded, adhesion will depend on the chemical composition of the substrate, and in particular, on "contaminants" on the surface. Oily layers of any thickness preclude adherence. Extremely thin layers of oxides and other stable compounds and elemental material such as carbon and boron can act as barriers to interdiffusion. (Stable compounds are not always detrimental and are sometimes deposited deliberately to aid adherence in many hard coating systems).

Oily films are usually completely eliminated by cleaning the substrate before installation in the sputtering system. A typical process is scrubbing with deionized water and alcohol rinses. Improperly designed vacuum pumping systems may replace the layer in the system. Elimination of diffusion barriers is more difficult since the barrier can be formed during the early stages of the deposition cycle including the so called "sputter cleaning" cycle. Initial substrate heatup can cause diffusion of elements from the substrate to or over the surface. Establishing the plasma in an unbaked deposition system can "scrub" water vapor and other contaminants from all surfaces. Water vapor can be disassociated into oxygen and hydrogen which are both persistent in the system. Application of low negative voltages to the substrate can actually form oxide layers instead of cleaning it. These same layers may be formed on the target and then sputtered off. Other sources of contamination are virtual leaks (from unvented blind-tapped holes), the sputtering gas and the target material.

Substrate cleaning in the deposition system can be accomplished by one or all of the following techniques:

- Heating the substrate
- Ion bombardment with sputtering gas (usually argon or krypton)
- Hydrogen gas mixture to reduce oxides (forming gas)
- Oxygen mixture to gasify carbon to CO and CO₂ which can be pumped out of the system
- Intermittent pump down to ultra high vacuum during one of the above cleaning processes.

The cleaned surface will not be atomically clean. However, it will be sufficiently clean for an adherent coating to form.

The proof of surface cleaning can be obtained from testing for adhesion. Typical adhesion tests include:

- Epoxy stud pull test (good to 10,000 psi on thin films)
- Scratching
- Diamond indent
- Energy pulse (peening, ultrasonic, laser, etc.)
- Shearing
- Bending.

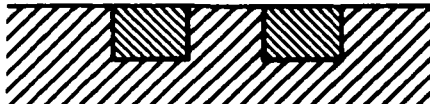
Of course not all of these tests can be applied to every material and quantifying the adhesion can be difficult. In this program, adhesion must be sufficient to withstand any stress

developed during handling, leaching, and if required, peening of the 0.010 inch thick closeout layer.

If adhesion is not obtained, substrate surfaces must be looked at in detail with surface sensitive instruments (auger electron spectroscopy, etc.). Correlations are then made with process parameters.

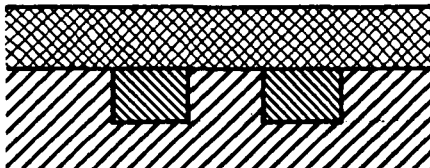
C. SUMMARY OF DEPOSITION WORK TO DATE

The program was started with the straightforward approach shown schematically in Figure A-3. Several differently sized grooves are machined in cylindrical specimens. The grooves are filled and excess filler removed to present a smooth substrate surface to the adatom flux. After cleaning, the cylinders are installed in the coater, and the PWA 1447 closeout layer is deposited. The filler material is removed to leave passages in the structure. Optional steps such as peening of the closeout layer and heat-treating may be required.

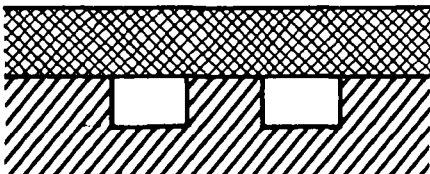


- Fill Grooves With Removable Filler

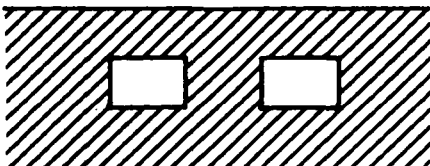
- Sputtered Aluminum
- SiO₂ Slurry
- Aluminum Wire



- Sputter PWA 1447 Cover



- Remove Filler Material



- Heat-Treat To Homogenize If Necessary

FD 267789

Figure A-3. Direct Approach to Fabricating Convectively Cooled Structures

Each step of the general approach was subject to side experiments before a cylindrical specimen was attempted. The following results were obtained from these experiments:

1. Filler Materials

- Interdiffusion of sputtered aluminum and the PWA 1447 substrate was excessive at substrate temperatures greater than 900°F. At substrate temperatures below 700°F the aluminum appeared to be highly stressed and easily debonded from the substrate. A 6061 aluminum target was used and the substrates were cooled to various degrees by their proximity to a water-cooled mandrel.
- Although filling of larger grooves with aluminum wire was satisfactory the wire could not be contained in the shallowest (0.012 inch deep) grooves due to a lack of a vertical side wall. The radius from the groove corners and the rounding of the land edges effectively eliminated a vertical wall on these grooves.
- The colloidal silica lacked both adhesion to the groove walls and cohesion to itself. This sand-like material was pulled out by the closeout layer. This type of filler may still have merit with a different formulation.

2. Sputtered PWA 1447 Closeout Layer

- Deposition under normal conditions in the hollow target systems caused excessive interdiffusion of the aluminum filler and closeout layer. Temperature was approximately 1200°F at the substrate.

3. Aluminum Leaching

- Aluminum was leached satisfactorily from a simulated filled groove. This groove was formed by electroplating nickel over a 4043 wire which was positioned on a Ni-200 base material. A sodium hydroxide solution at 150°F with periodic ultrasonic agitation removed all of the aluminum from a 1.0 inch length of a 0.035 by 0.012 inch (cross section) groove in 120 minutes.

4. Closeout Layer Characteristics

- Electron microprobe testing revealed that the closeout layer material was the same composition (within experimental error) as the target material.
- Hardness of the as-deposited material was 429 HV which compared nicely with the 395 HV for the cast PWA 1447 substrate bar.

One cylindrical specimen was filled by a combination of aluminum wire inlay and sputter deposition. This cylinder was placed over the water-cooled mandrel and rotated during the PWA

1447 closeout layer deposition. The cylinder had an excellent appearance after deposition but suffered extensive debonding of the closeout layer during the leaching cycle. Delamination occurred even at the end portion of the cylinder which was 0.5 inch away from the nearest grooves. Although the delamination left several large pieces of the debonded closeout layer material intact, the zone one type structure (essentially through defect network) was evident (Figure A-3). Even though this type of structure might possibly have been peened (with filler still in the grooves) to "cure" the defects, cooling actual turbine blades with this type of coating structure would not be practical.

At this point, another approach was planned as shown in Figure A-4. The heart of the alternative approach was to have a cylindrical substrate that could be closed out without temperature limitations imposed by the aluminum filler. The higher temperature during deposition would benefit both adhesion and structure of the closeout layer. Nickel was chosen for the intermediate 0.001 inch thick (nominal) layer for two reasons. First, this 0.001 inch layer must be adherent and defect free. With the end product in mind, a "cold" sputtering process (Figure A-5) was chosen to deposit this layer. Use of an elemental material would be more amendable than an alloy to the deposition techniques used to obtain the required properties. Secondly, a nickel target for this system was available. It was recognized that this nickel layer would require a structure homogenizing heat treatment schedule.

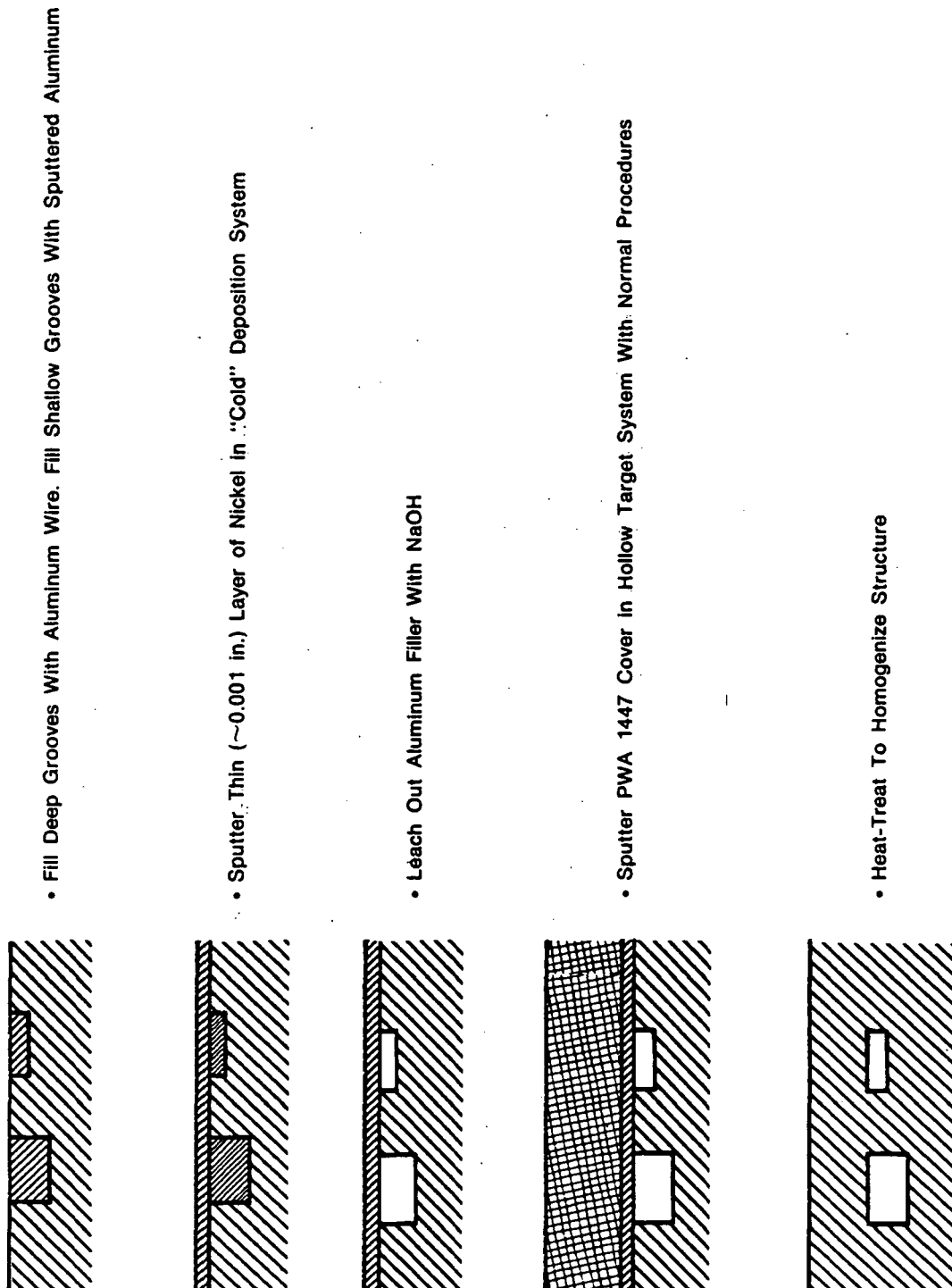
The results to date of the alternative approach are summarized below:

- Thin nickel films deposited in the RF diode system on Ni-200 and PWA 1447 substrates are adherent to the 10,000 psi limit of the epoxy-bonded tensile stud test. Thin films are required for this test which precluded testing the 0.001 inch thick closeout layers by this technique.
- Full thickness Ni closeout layers over aluminum wire-filled PWA 1447 substrates were not adherent. Like the cylindrical specimen described in Section B, appearance after deposition was excellent, but debonding occurred during leaching.
- For a side experiment in the hollow target coater, PWA 1447 was deposited (0.001 inch) onto PWA 1447 and Ni-200 substrates. The substrates were attached to the water-cooled mandrel to simulate conditions used for the filled cylinder substrates. Bend tests showed that the deposit was adherent to the Ni-200, but not to the PWA 1447.

These adherence results point to surface contamination as being the key problem rather than a difference in coefficient of thermal expansion between the aluminum filler and the PWA 1447 substrate. Calculations have shown that the difference is not sufficient to strain the closeout layers under the deposition and leaching conditions used.

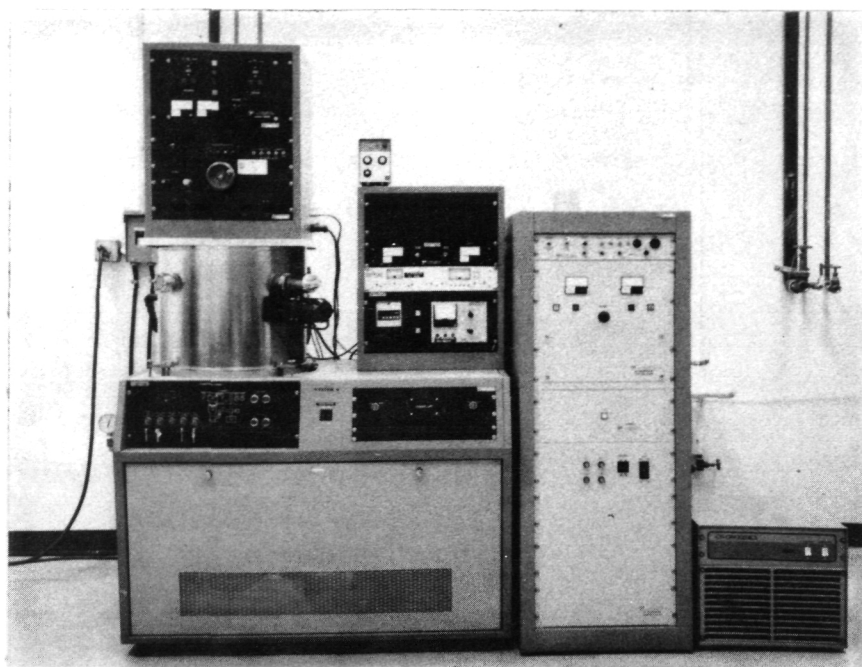
D. PROGRAM REQUIRED TO COMPLETE SPUTTERING WORK

Evidence to date requires that details of the PWA 1447 surface be examined to determine the cause of the lack of adhesion. A program to achieve this is outlined below where the species remaining on the surface versus the processing parameters will be examined. Also their effect on adhesion (and possibly on structure) will be determined. A parallel program should be run to determine the heat treatment schedule required to homogenize the closeout layer(s) and to obtain bulk (or better than) PWA 1447 mechanical properties. Additional materials would be required. The program would be expensive and lengthy due to nonavailability of surface characterizing equipment at P&W.

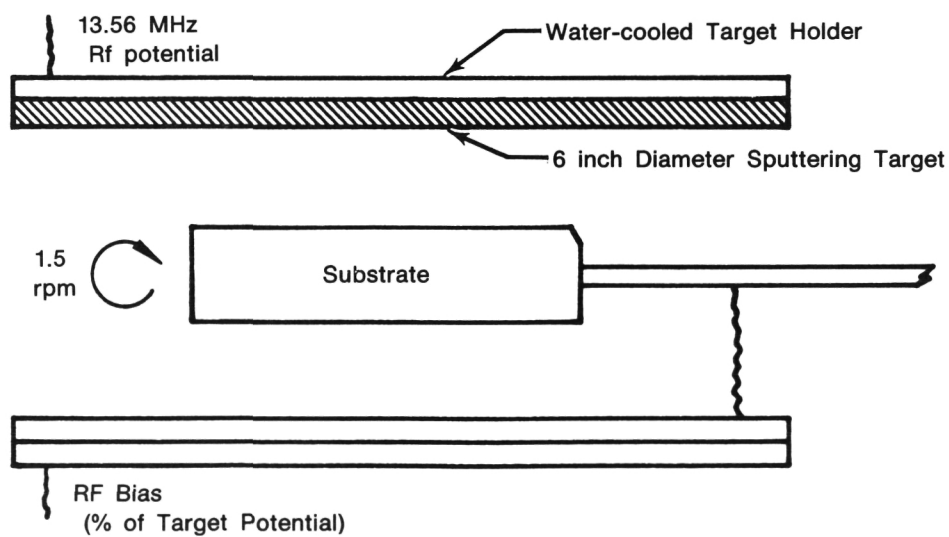


FD 267780

Figure A-4. Plan for Alternative Approach to Fabricating Connectively Cooled Structure



a. System Equipment — Planar Target RF Diode Sputtering System



b. Schematic of Deposition Chamber (Not to Scale)

FD 267791

Figure A-5. Radio Frequency (RF) Diode Sputtering System

1. The experimental program for depositing the 0.001 inch layer is as follows:

- a. Prepare flat and cylindrical substrates, with and without grooves (cast, machine, and degrease).
- b. Characterize substrate surface finish and composition.
- c. Fill grooved substrates with pure aluminum and Al alloy fillers. Refinish and degrease.
- d. Characterize filled substrate surface finish and composition.
- e. Clean substrates in the vacuum system — a parameter study — using both filled and unfilled substrates (not simultaneously).
- f. Characterize clean substrate surface compositions and structures.
- g. Deposit closeout layer over substrate cleaned with selected parameters — use filled and unfilled substrates.
- h. Characterize the deposits for adhesion, structure, topography, and stress.
- i. Characterize any debonded material to establish cause of adhesive failure.
- j. Determine effects (if any), of the gas discharge plasma and deposition parameters and adjust for adhesion as required.
- k. Process filled and unfilled cylindrical specimens with best parameters (clean, closeout, and leach).
- l. Overcoat 0.001 inch thick closeout layers with a nominal 0.015 inch of PWA 1447 and machine to 0.010 inch thickness (peen if necessary). Leach the grooved cylinders, heat-treat (from parallel program), and fluidize bed test.

2. The parallel program to establish homogenizing heat treatment schedule is as follows:

- a. Deposit 0.001 inch of Ni on PWA 1447 specimens and overlay with PWA 1447. Machine specimen to have an even 0.010 inch thick (total) closeout layer. Characterize as-deposited structures. Peen if necessary.
- b. Diffuse with selected heat schedules. Characterize the heat-treated structures for structure, composition, and diffusional type defects. Note: If excessive void formation at the interfaces persists, iterate this program using specimens without the 0.001 inch Ni layer. Assuming Ni caused the diffusional defects, change the program at step 1.g to include a 0.001 inch PWA 1447 layer.

- c. With best parameters, sputter deposit, heat-treat and fabricate mechanical test specimens to compare best sputtered material mechanical properties with case material properties.
 - d. Iterate as necessary (change hollow target composition, etc.) to optimize properties of the sputtered material.
- 3. The alternate approaches to this program are as follows:
 - a. With the closing out of airfoils in mind, investigate electroformed Ni for the 0.001 inch thick closeout layer. If this were successful, the filler machining step would be eliminated in the process. The Camin Lab process may lend itself to fabricating this layer.
 - b. Alternate sputtering processes, such as planar magnetron and post-magnetron sputtering, could be investigated.
 - c. These processes are intermediate in temperature and may be used to deposit thick PWA 1447 layers over the aluminum filler without excessive substrate heating and interdiffusion of filler with the substrate and closeout layer. By this same reasoning, sputter deposition, if required, of the aluminum filler could be accomplished on an uncooled substrate.
- 4. Nondestructive quality control techniques for a manufacturing process should be investigated early in any program.
- 5. The materials required are as follows:
 - a. PWA 1447 flat casting for cut up into test specimens substrates including mechanical test specimen substrates
 - b. PWA 1447 cast cylinders — plain and for grooving
 - c. PWA 1447 cast disk for 6 inch diameter target fabrication
 - d. Modified PWA 1447 cast hollow target.

**APPENDIX B
ADVANCED TURBINE STUDY
ENGINEERING DRAWINGS**

FOLDOUT FRAME

FOLDOUT FRAME

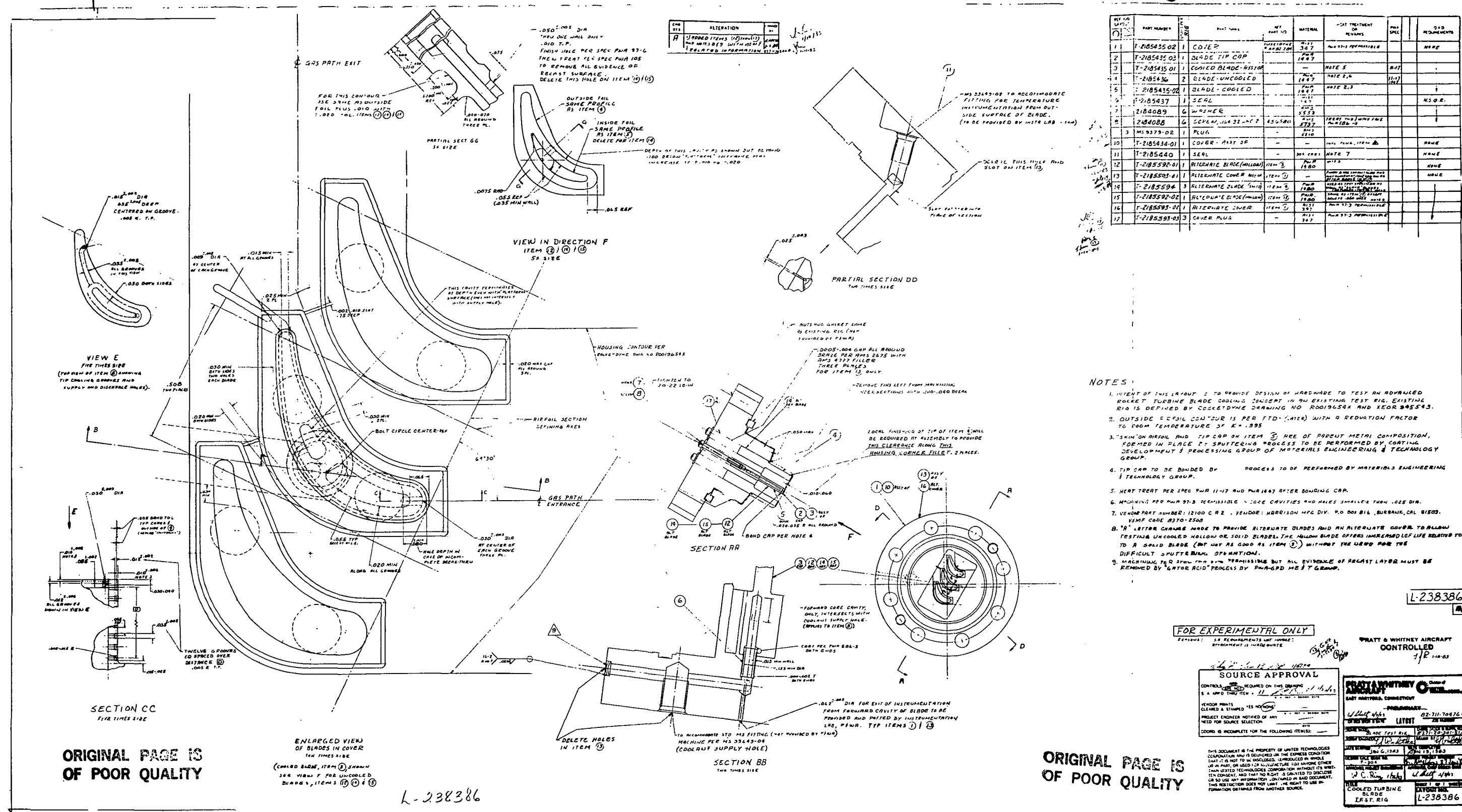


Figure B-1. Layout Drawing for the Advanced Turbine Study (Reduction of Original, Not to Scale)

FOLDOUT FRAME

2 FOLDOUT FRAME

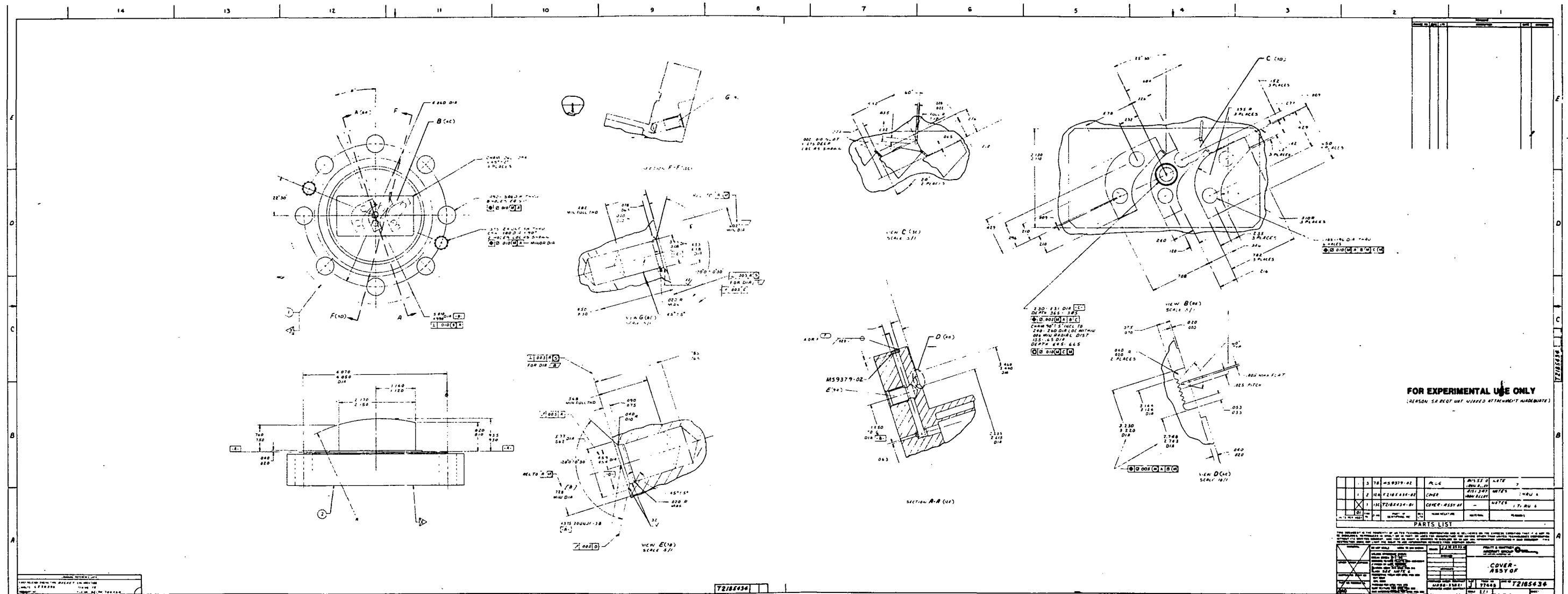


Figure B-2. Detail Parts Drawing — Cover (Reduction of Original, Not to Scale)

ORIGINAL PAGE IS
OF POOR QUALITY

ORIGINAL PAGE IS
OF POOR QUALITY

ORIGINAL PAGE IS
OF POOR QUALITY

ORIGINAL PAGE IS
OF POOR QUALITY

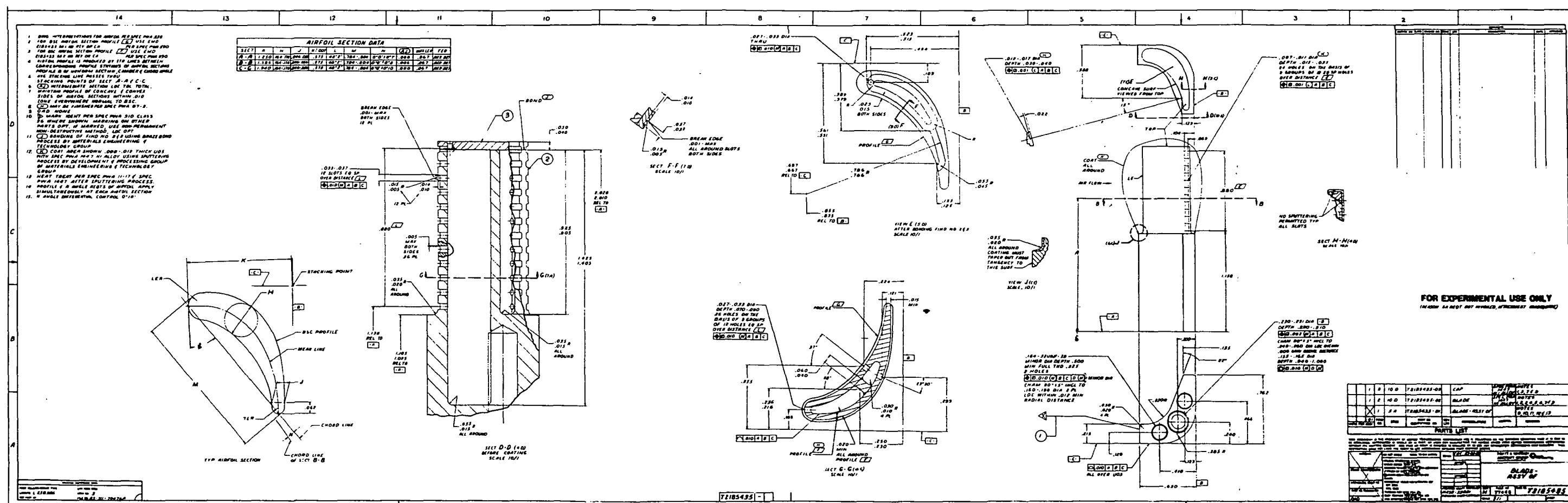


Figure B-3. Detail Parts Drawing — Blade (Reduction of Original, Not to Scale)

FOLDOUT FRAME

2 FOLDOUT FRAME



B-5

1. (B) TREAT PER SPEC PWA 586-3.
OTHER AREAS OPT & MAY BE INCOMPLETE.

SEAL-

T2185437

Figure B-5. Detail Parts Drawing — Seal (Reduction of Original, Not to Scale)

VENDOR: HARRISON MFG DIV.
BURBANK, CAL.
ITEM IDENT NO: 12100 CR 2.

THIS DOCUMENT IS THE PROPERTY OF UNITED TECHNOLOGIES CORPORATION AND IS DELIVERED ON THE EXPRESS CONDITION THAT IT IS NOT TO BE DISCLOSED, REPRODUCED IN WHOLE OR IN PART, OR USED FOR MANUFACTURE FOR ANYONE OTHER THAN UNITED TECHNOLOGIES CORPORATION WITHOUT ITS WRITTEN CONSENT; AND THAT NO RIGHT IS GRANTED TO DISCLOSE OR SO USE ANY INFORMATION CONTAINED IN SAID DOCUMENT. THIS RESTRICTION DOES NOT LIMIT THE RIGHT TO USE INFORMATION OBTAINED FROM ANOTHER SOURCE.

72185440		REVISONS		DATE		APPROVED	
CHANGE NO.	LTR	DESCRIPTION					

VENDOR: HARRISON MFG DIV.

BURBANK, CAL.

ITEM IDENT NO: 12100 CR 2.

SEAL-

THIS DOCUMENT IS THE PROPERTY OF UNITED TECHNOLOGIES CORPORATION AND IS DELIVERED ON THE EXPRESS CONDITION THAT IT IS NOT TO BE DISCLOSED, REPRODUCED IN WHOLE OR IN PART, OR USED FOR MANUFACTURE FOR ANYONE OTHER THAN UNITED TECHNOLOGIES CORPORATION WITHOUT ITS WRITTEN CONSENT; AND THAT NO RIGHT IS GRANTED TO DISCLOSE OR SO USE ANY INFORMATION CONTAINED IN SAID DOCUMENT THIS RESTRICTION DOES NOT LIMIT THE RIGHT TO USE INFORMATION OBTAINED FROM ANOTHER SOURCE.

PRATT & WHITNEY
AIRCRAFT GROUP
UNITED TECHNOLOGIES
EAST HARTFORD, CONNECTICUT, USA

DRAWN	J.C. LEWIS	83-03-29	CHECKED	83-03-29	APPROVED	83-03-29	83-03-29
DO NOT SCALE		WORK TO DIM SHOWN		UNLESS OTHERWISE SHOWN:			
				BREAK EDGES .003 - .015			
				CORNERS TO HAVE FILLETS .005 - .020 R			
				FINISH BY MTL REMOVAL			
				MARK IDENT PER SPEC PWA 310			
				CLASS			
				PROTECTIVE TREAT PER SPEC PWA 830			
				EXT CODE			
				INTL CODE			
				THREADS PER SPEC PWA 355			
				SURF TEXTURE PER SPEC PWA 362			
				DWG INTERPRETATIONS PER SPEC PWA 360			
MATERIAL							
OTHER SPECIFICATIONS							
CASTING NO. STRIP NO							
PART NO. FORGING NO							
QAD NONE							

PREPARED UNDER CONTRACT
N458-33821

FURNISHED UNDER CONTRACT

SIZE
A

FSCM NO.
77445

DWG NO.
T2185440

SCALE
NONE

SHEET

.. 3. 1. 2. 3. 4. 5. 6. 7. 8. 9. 10. 11. 12. 13. 14. 15. 16. 17. 18. 19. 20. 21. 22. 23. 24. 25. 26. 27. 28. 29. 30. 31. 32. 33. 34. 35. 36. 37. 38. 39. 40. 41. 42. 43. 44. 45. 46. 47. 48. 49. 50. 51. 52. 53. 54. 55. 56. 57. 58. 59. 60. 61. 62. 63. 64. 65. 66. 67. 68. 69. 70. 71. 72. 73. 74. 75. 76. 77. 78. 79. 80. 81. 82. 83. 84. 85. 86. 87. 88. 89. 90. 91. 92. 93. 94. 95. 96. 97. 98. 99. 100. 101. 102. 103. 104. 105. 106. 107. 108. 109. 110. 111. 112. 113. 114. 115. 116. 117. 118. 119. 120. 121. 122. 123. 124. 125. 126. 127. 128. 129. 130. 131. 132. 133. 134. 135. 136. 137. 138. 139. 140. 141. 142. 143. 144. 145. 146. 147. 148. 149. 150. 151. 152. 153. 154. 155. 156. 157. 158. 159. 160. 161. 162. 163. 164. 165. 166. 167. 168. 169. 170. 171. 172. 173. 174. 175. 176. 177. 178. 179. 180. 181. 182. 183. 184. 185. 186. 187. 188. 189. 190. 191. 192. 193. 194. 195. 196. 197. 198. 199. 200. 201. 202. 203. 204. 205. 206. 207. 208. 209. 210. 211. 212. 213. 214. 215. 216. 217. 218. 219. 220. 221. 222. 223. 224. 225. 226. 227. 228. 229. 230. 231. 232. 233. 234. 235. 236. 237. 238. 239. 240. 241. 242. 243. 244. 245. 246. 247. 248. 249. 250. 251. 252. 253. 254. 255. 256. 257. 258. 259. 260. 261. 262. 263. 264. 265. 266. 267. 268. 269. 270. 271. 272. 273. 274. 275. 276. 277. 278. 279. 280. 281. 282. 283. 284. 285. 286. 287. 288. 289. 290. 291. 292. 293. 294. 295. 296. 297. 298. 299. 300. 301. 302. 303. 304. 305. 306. 307. 308. 309. 310. 311. 312. 313. 314. 315. 316. 317. 318. 319. 320. 321. 322. 323. 324. 325. 326. 327. 328. 329. 330. 331. 332. 333. 334. 335. 336. 337. 338. 339. 340. 341. 342. 343. 344. 345. 346. 347. 348. 349. 350. 351. 352. 353. 354. 355. 356. 357. 358. 359. 360. 361. 362. 363. 364. 365. 366. 367. 368. 369. 370. 371. 372. 373. 374. 375. 376. 377. 378. 379. 380. 381. 382. 383. 384. 385. 386. 387. 388. 389. 390. 391. 392. 393. 394. 395. 396. 397. 398. 399. 400. 401. 402. 403. 404. 405. 406. 407. 408. 409. 410. 411. 412. 413. 414. 415. 416. 417. 418. 419. 420. 421. 422. 423. 424. 425. 426. 427. 428. 429. 430. 431. 432. 433. 434. 435. 436. 437. 438. 439. 440. 441. 442. 443. 444. 445. 446. 447. 448. 449. 450. 451. 452. 453. 454. 455. 456. 457. 458. 459. 460. 461. 462. 463. 464. 465. 466. 467. 468. 469. 470. 471. 472. 473. 474. 475. 476. 477. 478. 479. 480. 481. 482. 483. 484. 485. 486. 487. 488. 489. 490. 491. 492. 493. 494. 495. 496. 497. 498. 499. 500. 501. 502. 503. 504. 505. 506. 507. 508. 509. 510. 511. 512. 513. 514. 515. 516. 517. 518. 519. 520. 521. 522. 523. 524. 525. 526. 527. 528. 529. 530. 531. 532. 533. 534. 535. 536. 537. 538. 539. 540. 541. 542. 543. 544. 545. 546. 547. 548. 549. 550. 551. 552. 553. 554. 555. 556. 557. 558. 559. 560. 561. 562. 563. 564. 565. 566. 567. 568. 569. 570. 571. 572. 573. 574. 575. 576. 577. 578. 579. 580. 581. 582. 583. 584. 585. 586. 587. 588. 589. 590. 591. 592. 593. 594. 595. 596. 597. 598. 599. 600. 601. 602. 603. 604. 605. 606. 607. 608. 609. 610. 611. 612. 613. 614. 615. 616. 617. 618. 619. 620. 621. 622. 623. 624. 625. 626. 627. 628. 629. 630. 631. 632. 633. 634. 635. 636. 637. 638. 639. 640. 641. 642. 643. 644. 645. 646. 647. 648. 649. 650. 651. 652. 653. 654. 655. 656. 657. 658. 659. 660. 661. 662. 663. 664. 665. 666. 667. 668. 669. 670. 671. 672. 673. 674. 675. 676. 677. 678. 679. 680. 681. 682. 683. 684. 685. 686. 687. 688. 689. 690. 691. 692. 693. 694. 695. 696. 697. 698. 699. 700. 701. 702. 703. 704. 705. 706. 707. 708. 709. 710. 711. 712. 713. 714. 715. 716. 717. 718. 719. 720. 721. 722. 723. 724. 725. 726. 727. 728. 729. 730. 731. 732. 733. 734. 735. 736. 737. 738. 739. 740. 741. 742. 743. 744. 745. 746. 747. 748. 749. 750. 751. 752. 753. 754. 755. 756. 757. 758. 759. 760. 761. 762. 763. 764. 765. 766. 767. 768. 769. 770. 771. 772. 773. 774. 775. 776. 777. 778. 779. 780. 781. 782. 783. 784. 785. 786. 787. 788. 789. 790. 791. 792. 793. 794. 795. 796. 797. 798. 799. 800. 801. 802. 803. 804. 805. 806. 807. 808. 809. 810. 811. 812. 813. 814. 815. 816. 817. 818. 819. 820. 821. 822. 823. 824. 825. 826. 827. 828. 829. 830. 831. 832. 833. 834. 835. 836. 837. 838. 839. 84

1238386 (11)

Figure B-6. Detail Parts Drawing — Seal

1. B PERFECT FORM AT MMC NOT REQD

2184088 -

REVISIONS	DATE	APPROVED

CHARGE NO.	LTR	DESCRIPTION

THIS DOCUMENT IS THE PROPERTY OF UNITED TECHNOLOGIES CORPORATION AND IS DELIVERED ON THE EXPRESS CONDITION THAT IT IS NOT TO BE REPRODUCED, COPIED, OR TRANSMITTED IN ANY FORM OR BY ANY MEANS, ELECTRONIC OR MECHANICAL, INCLUDING PHOTOCOPYING, RECORDING, OR BY ANY INFORMATION STORAGE AND RETRIEVAL SYSTEM, WITHOUT ITS WRITTEN CONSENT; AND THAT NO RIGHT IS GRANTED TO DISCLOSE OR SO USE ANY INFORMATION CONTAINED IN SAID DOCUMENT. THIS RESTRICTION DOES NOT LIMIT THE RIGHT TO USE INFORMATION OBTAINED FROM ANOTHER SOURCE.

MATERIAL
AMS 5553
NI

OTHER SPECIFICATIONS

DO NOT SCALE

WORK TO DIM SHOWN

UNLESS OTHERWISE SHOWN:
BREAK EDGES .003-.005
CORRUS TO NAME PLATE
FINISH TO NAME PLATE
DIM MARK IDENT PER SPEC PMA 310
CLASS / C
PROTECTIVE TREAT PER SPEC PMA 830
EXT CODE
WTL CODE
THICKNESS PER SPEC PMA 345
SURF TEXTURE PER SPEC PMA 342
DWG INTERPRETATIONS PER SPEC PMA 350

CASTING NO. STRIP NO.

PART NO. FORGING NO.

QAD 2184088

DRAWING REFERENCE DATA

FIRST RELEASE-ENGINE TYPE

LAYOUTS L-238306

REF PART NO.

DRWING REFERENCE DATA

END AREA CODE 00 00 000 G02

ITEM NO. 7

FILE NO. B2-711-70476 A

UNITED TECHNOLOGIES CORPORATION

GASKET-

.185 x .375 x .062

SIZE **71443** **DWG NO** **2184088**

SCALE **5/1** **SHEET**

T2184088

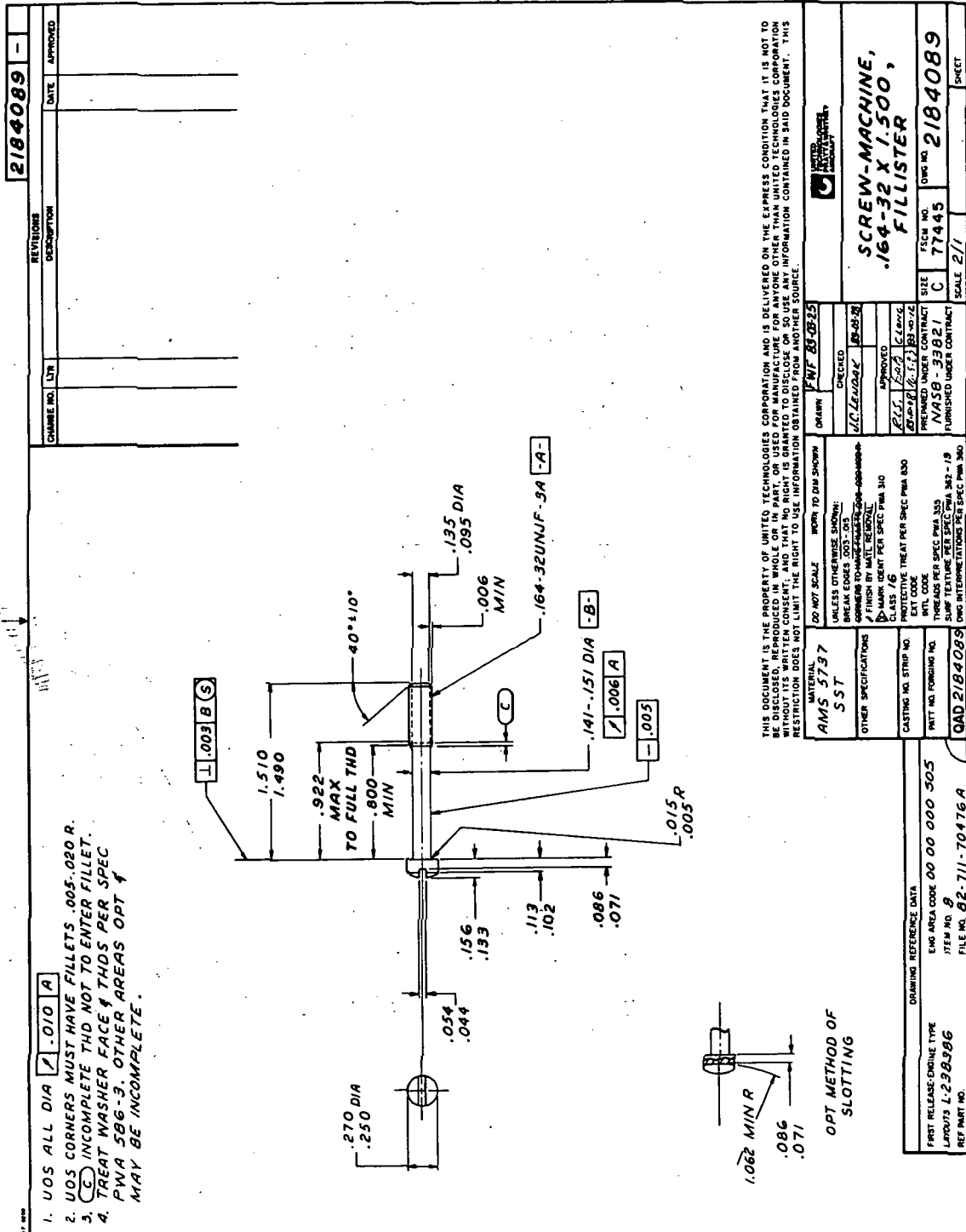


Figure B-8. Detail Parts Drawing — Machine Screw (Reduction of Original, Not to Scale)



2 FOLDOUT FRAME

ORIGINAL PAGE IS
OF POOR QUALITY

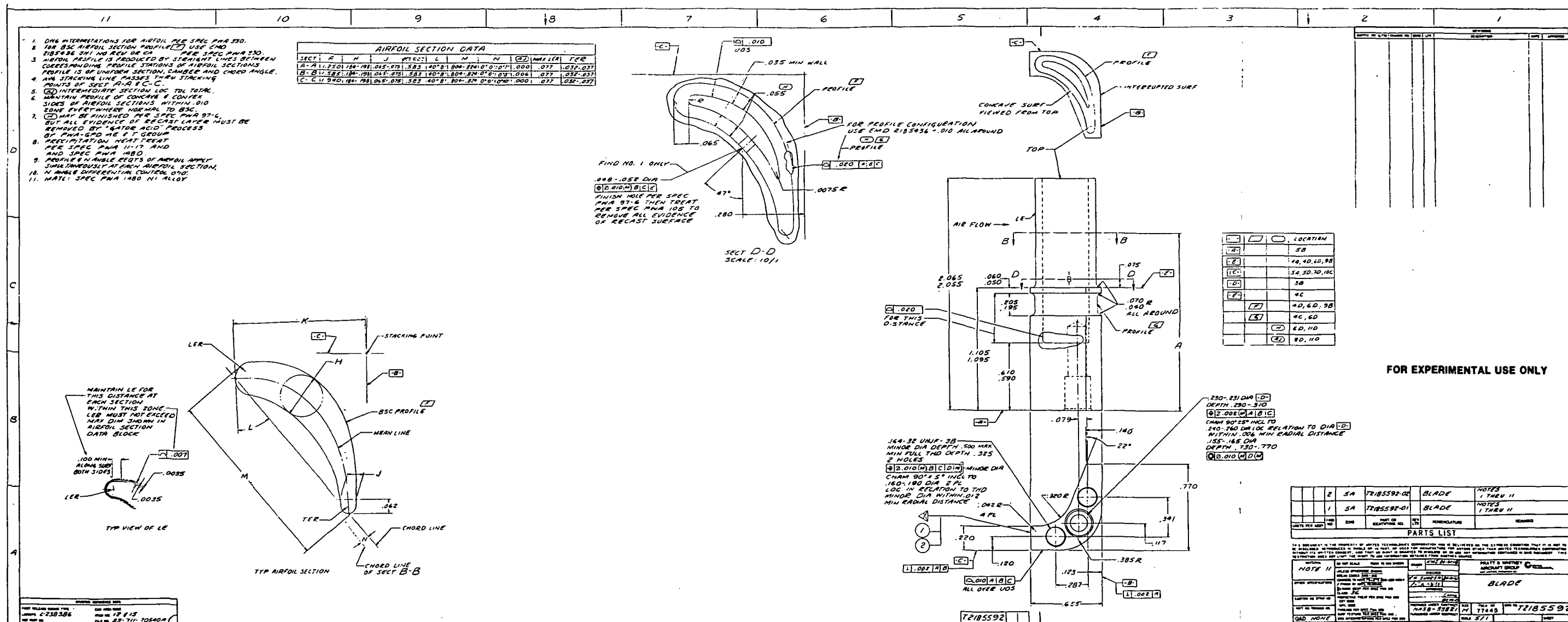
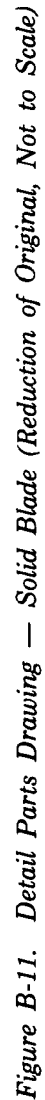


Figure B-10. Detail Parts Drawing — Hollow Blade (Reduction of Original, Not to Scale)

FOLDOUT FRAME

2 FOLDOUT FRAME



K&S 10 8188 10-78 MCE4386

174 19000 105 1 0 0 0

102 077

WORK TO DIMENSIONS GIVEN—
DO NOT SCALE

UNLESS OTHERWISE SPECIFIED

—BREAK SHARP EDGES .003-.018
—CORNERS TO HAVE FILLETS
— .003-.020 RAD

8702 077

SAME AS P/N T-2185592-02 EXCEPT WALL THICKNESS BETWEEN
THE EXTERIOR SURFACE OF THE AIRFOIL AND THE CORE CAVITY SHOULD BE
.035 ± .005 INCH.

APE: W.C. RING X-5366

NOTICE TO ALL PERSONS RECEIVING THIS DRAWING

THIS DRAWING IS ONLY CONDITIONALLY ISSUED, AND NEITHER RECEIPT NOR POSSESSION THEREOF CONFERS OR TRANSFERS ANY RIGHT IN, OR LICENSE TO USE, THE SUBJECT MATTER OF THE DRAWING OR ANY DESIGN, OR TECHNICAL INFORMATION SHOWN THEREON, NOR ANY RIGHT TO REPRODUCE THIS DRAWING OR ANY PART THEREOF, EXCEPT FOR MANUFACTURE BY VENDORS FOR UNITED TECHNOLOGIES CORPORATION AND FOR MANUFACTURE UNDER THE CORPORATION'S WRITTEN LICENSE NO RIGHT TO REPRODUCE THIS DRAWING IS GRANTED UNLESS BY WRITTEN AGREEMENT WITH OR WRITTEN PERMISSION FROM THE CORPORATION, NOTWITHSTANDING THE FOREGOING, NOTHING CONTAINED IN THIS NOTICE SHALL PREVENT THIS DRAWING FROM BEING REPRODUCED OR USED TO THE EXTENT CONTEMPLATED BY ANY APPLICABLE CONTRACT OR USED TO THE EXTENT CONTEMPLATED ORATION AND THE GOVERNMENT OF THE UNITED STATES.

THERE IS NO SUBSTITUTE FOR QUALITY


NAME J. H. CASTRO	APPROVED X-3126	TITLE ATS BLADE - .035" WALL THICKNESS
DATE 6-11-84	PRATT & WHITNEY AIRCRAFT GROUP Government Products Division 	MATERIAL PWA 1480
		SPEC. 1
		SKETCH NO. CKD 2078
		CLASS A
		SHEET NO. 1
		NO. OF SHEETS 1

Figure B-12. ATS Blade — 0.035 Inch Wall Thickness

CKD2078


CLD 2089



NOTICE TO ALL PERSONS RECEIVING THIS DRAWING

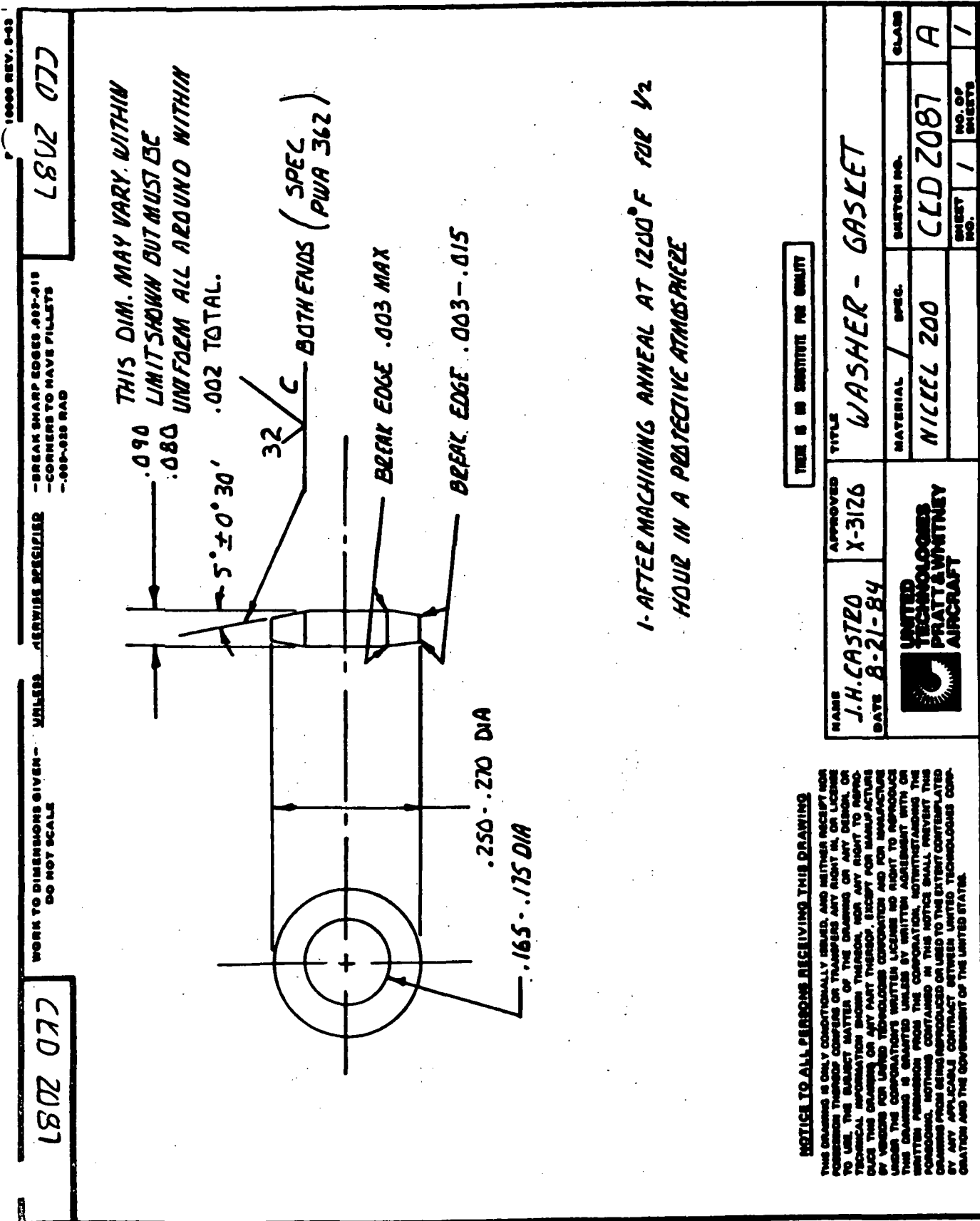
THIS DRAWING IS ONLY CONDITIONALLY ISSUED, AND NEITHER RECEIPT NOR POSSESSION THEREOF CONFERS ON TRANSFEREE ANY RIGHT IN, OR LICENSE TO USE, THE SUBJECT MATTER OF THE DRAWING OR ANY DESIGN, OR TECHNICAL INFORMATION SHOWN THEREON, NOR ANY RIGHT TO REPRODUCE THIS DRAWING OR ANY PART THEREOF. RECEIPT FOR MANUFACTURE BY VENDORS FOR UNITED TECHNOLOGIES CORPORATION AND FOR MANUFACTURE UNDER THE CORPORATION'S WRITTEN LICENSE NO RIGHT TO REPRODUCE THIS DRAWING IS GRANTED UNLESS BY WRITTEN AGREEMENT WITH OR WRITTEN PERMISSION FROM THE CORPORATION, NOTWITHSTANDING THE FOREGOING. NOTHING CONTAINED IN THIS NOTICE SHALL PREVENT THIS DRAWING FROM BEING REPRODUCED OR USED TO THE EXTENT CONTEMPLATED BY ANY APPLICABLE CONTRACT BETWEEN UNITED TECHNOLOGIES CORPORATION AND THE GOVERNMENT OF THE UNITED STATES.

THE 100 BEST IDEAS FOR QUALITY

NAME J. H. CASTRO	APPROVED X-3126	TITLE HARDWARE REOPERATION			
DATE 8-21-84	 UNITED TECHNOLOGIES PRATT & WHITNEY AIRCRAFT	MATERIAL	SPEC.	SECTION NO.	CLASS
		—		CCD 2089	A
		—		SHEET NO. 1	TOTAL NO. OF SHEETS 1

USC 2240711
N31173

Figure B-13. Hardware Reoperation



NOTICE TO ALL PERSONS RECEIVING THIS DRAWING

THIS DRAWING IS ONLY CONDITIONALLY ISSUED AND NEITHER REPLY NOR
FORWARD THEREOF CONFER OR TRANSFER ANY RIGHT IN OR LICENSE
TO USE THE SUBJECT MATTER OF THE DRAWING OR ANY DESIGN OR
TECHNICAL INFORMATION SHOWN THEREON, NOR ANY RIGHT TO REPRO-
DUCE THIS DRAWING OR ANY PART THEREOF, EXCEPT FOR MANUFACTURE
BY VENDORS FOR UNITED TECHNOLOGIES CORPORATION AND FOR MANUFACTURE
UNDER THE CORPORATION'S WRITTEN LICENSE AND NOT TO REPRODUCE
THIS DRAWING IS GRANTED UNLESS BY WRITTEN AGREEMENT WITH OR
FORWARD THEREOF FROM THE CORPORATION, EXCEPT THAT THE
FORWARD THEREOF CONTAINED IN THIS NOTICE SHALL PREVENT THE
DRAWING FROM BEING REPRODUCED OR USED TO THE EXTENT CONTAINED
BY ANY APPLICABLE CONTRACT BETWEEN UNITED TECHNOLOGIES COR-
PORATION AND THE GOVERNMENT OF THE UNITED STATES.

Figure B-14. Washer — Gasket

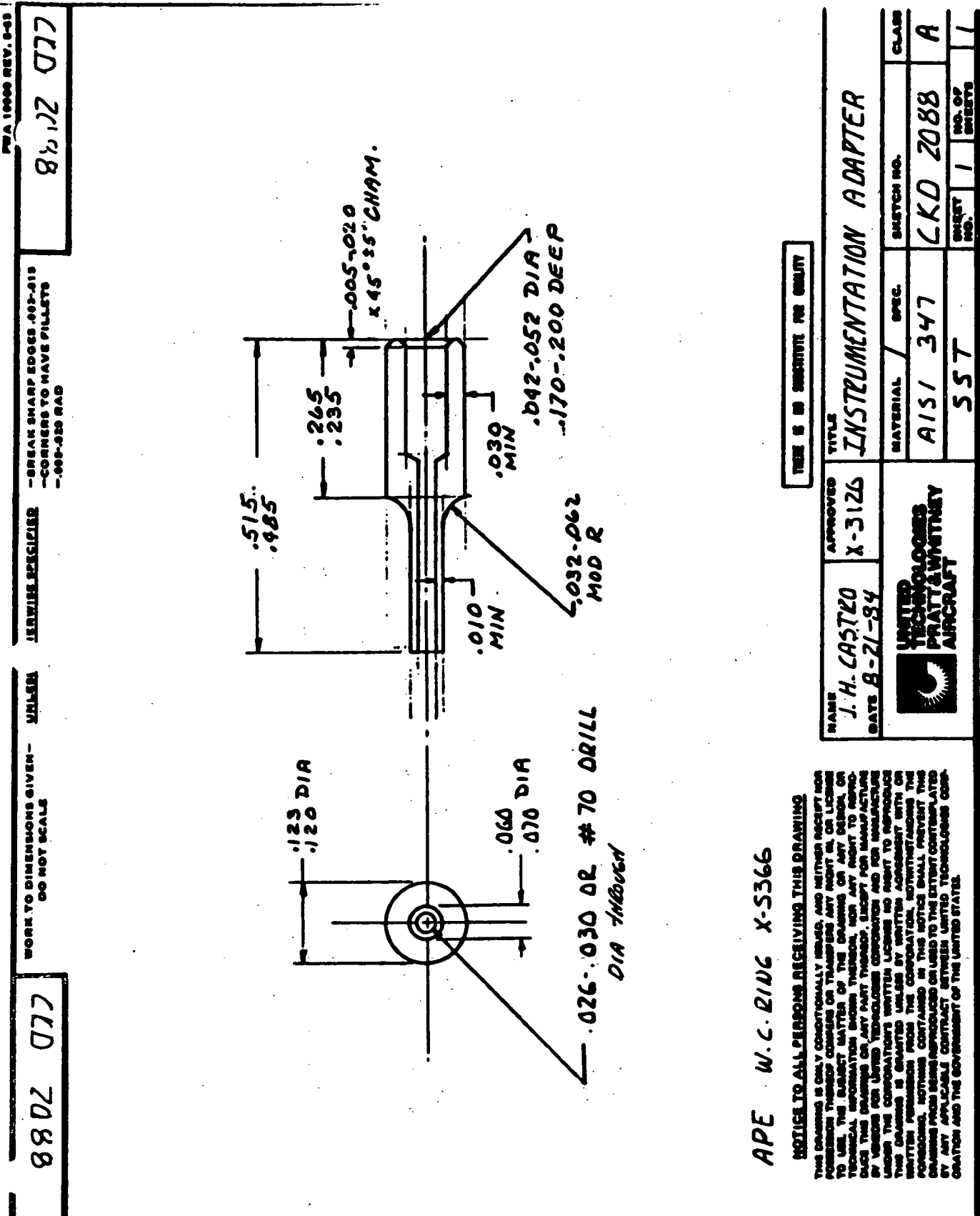


Figure B-15. Instrumentation Adapter

APPENDIX C
VERIFICATION OF ATS BLADE GRAIN QUALITY AND ORIENTATION BY GRAIN ETCH
AND LAUE X-RAY METHODS

**PRATT & WHITNEY AIRCRAFT GROUP**

GOVERNMENT PRODUCTS DIVISION

MATERIALS ENGINEERING & TECHNOLOGY**PRATT & WHITNEY CONTROLLED**MEET NO. 26133PROGRAM IR&DCHARGE NO. E271-30-200-72DATE 8-27-84CASTING JOB A190MEMORANDUM REPORTREQUESTED BY J. H. Castro (3126) Department RL10 EngineeringSend To: H. M. Gibson, D. E. Paulus, J. L. Price, T. A. Rackley III, C. C. Rhemer,W. C. Ring, C. B. Stevens, D. C. Stewart, D. B. TiptonWork Requested Perform grain etch and Laue X-ray to verify grain quality and
primary orientation.PERTINENT DATA

Part Name: SSME Turbine Blade
Serial Number: 1 - 13
Material Spec.: PWA 1480
Mfg. Source: PWA Manchester Foundry
Machining: GPD

RESULTS

Primary orientation recorded on all thirteen blades was within the commonly accepted limit of 15°. Three blades (S/N 8, 9, 11) contained low angle boundaries which would be acceptable while blade S/N 10 contained several high angle boundaries and was considered unacceptable.

Reported by C. M. Biondo

Approvals _____

Ext. 5273

Tables: 2

Figures: 9



L/N 26133

REPORT

As part of an advanced turbine study, NASA Contract NAS 833821, PWA 1480 blades machined to the Rocketdyne configuration will be tested in a rig at Huntsville, AL along with Rocketdyne blades cast in MAR-M-246. The initial effort consisted of evaluating eight cast PWA 1480 blocks supplied by Manchester Foundry (see Report, ME&T 25608). From the investigation two blocks were selected and thirteen blades (of varying designs) were subsequently EDM'd from the blocks at Government Products Division as shown in Figure 1.

All blades were grain etched and Laue X-ray was used to verify primary orientation and measure mismatch on any grain boundaries. Primary orientation was determined by taking Laue X-ray shots on the tip of the blade as outlined in Figure 2. There is no current standard which specifies quality requirements for this blade configuration, but in all cases the primary orientation recorded (Table I) was within the commonly accepted limit of 15°.

Typical grain etched condition of all thirteen blades is shown in Figures 3 - 9. Four blades (S/N 8, 9, 10, 11) were observed to contain grain boundaries which were then Laue X-rayed to determine mismatch between the specific grain and the parent crystal. Three blades (S/N 8, 9, 11) contained low angle boundaries which would be acceptable to existing specification limits (CVS-6) while blade S/N 10 contained several high angle boundaries and was considered unacceptable.

X-RAY DIFFRACTION RESULTS:

<u>BLADE</u>	<u>ORIENTATION</u>	<u>(α)</u> <u>DEGREES OFF AXIS</u>
1	[100]	10
2	[100]	10
3	[100]	9
4	[100]	9
5	[100]	10
6	[100]	9
7	[100]	9
8	[100]	9
9	[100]	11
10	[100]	7
11	[100]	7
12	[100]	8
13	[100]	9

TABLE I

X-ray diffraction data showing measurement of primary (100) orientation for each test blade.

L/N 26133

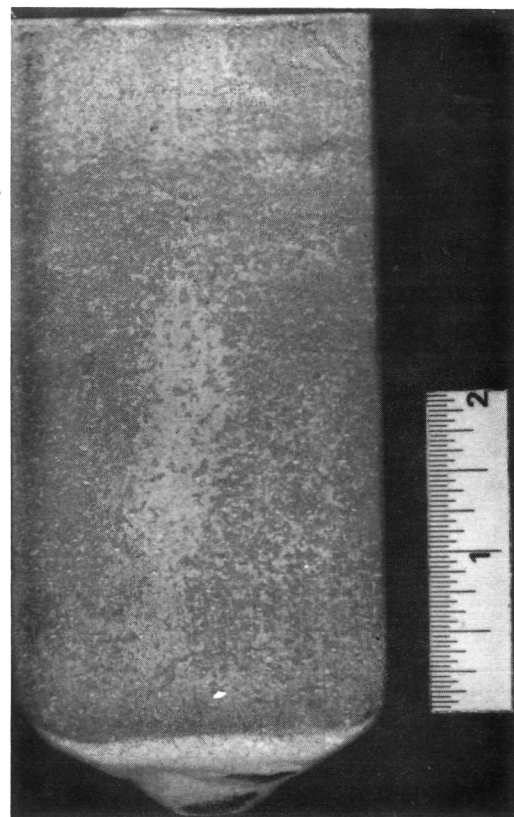
X-RAY DIFFRACTION RESULTS:

BLADES	TILT MISMATCH (T)	ROTATION MISMATCH (R)	TOTAL MISMATCH
8-A, 8-B	1	0	1
8-A, 9-B	1	1	1
10-A, 10-C	12	8	14
10-B, 10-C	2	3	4
10-D, 10-E	8	12	15
10-F, 10-G	5	5	7
10-G, 10-H	2	1	2
11-A, 11-B	1	1	1

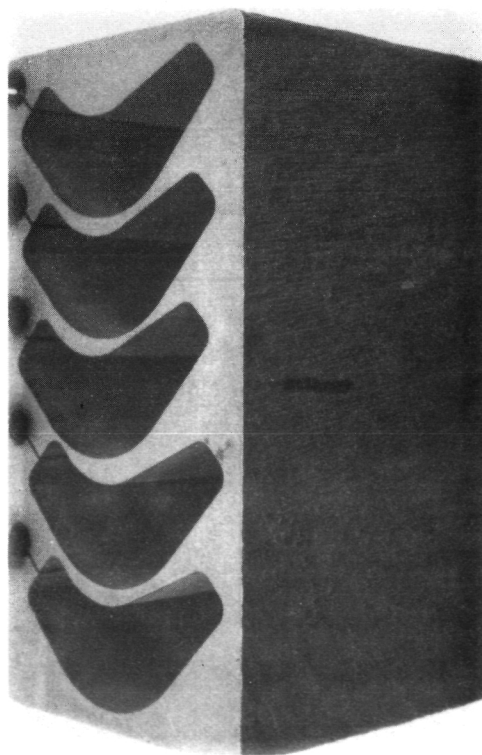
TABLE II

X-ray diffraction data giving measurement of grain mismatch on blades which contained defects. Figures 5, 6, 7 outline the location of Laue shots and labeling of specific grains to determine mismatch.

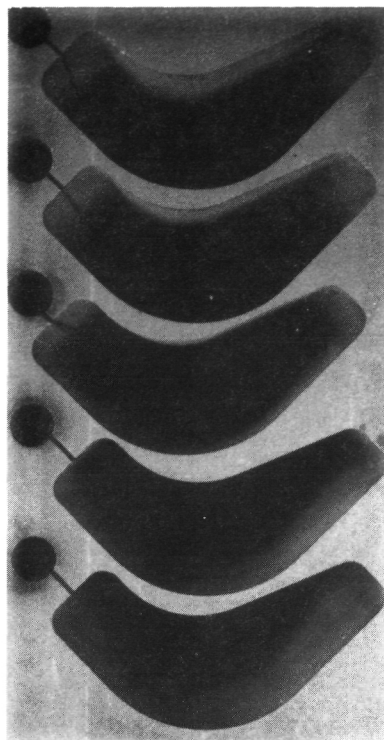
L/N 26133



FAL 76710
Mag 3/4X



Mag 2X



Mag 2X

ORIGINAL PAGE IS
OF POOR QUALITY

FD 295950

Figure C-1. As-Received View (Top) of Typical Cast PWA 1480 Blade Block Supplied by Manchester Foundry. Experimental Blades Were EDM'd Out of Selective Blade Blocks (Bottom) at P&W

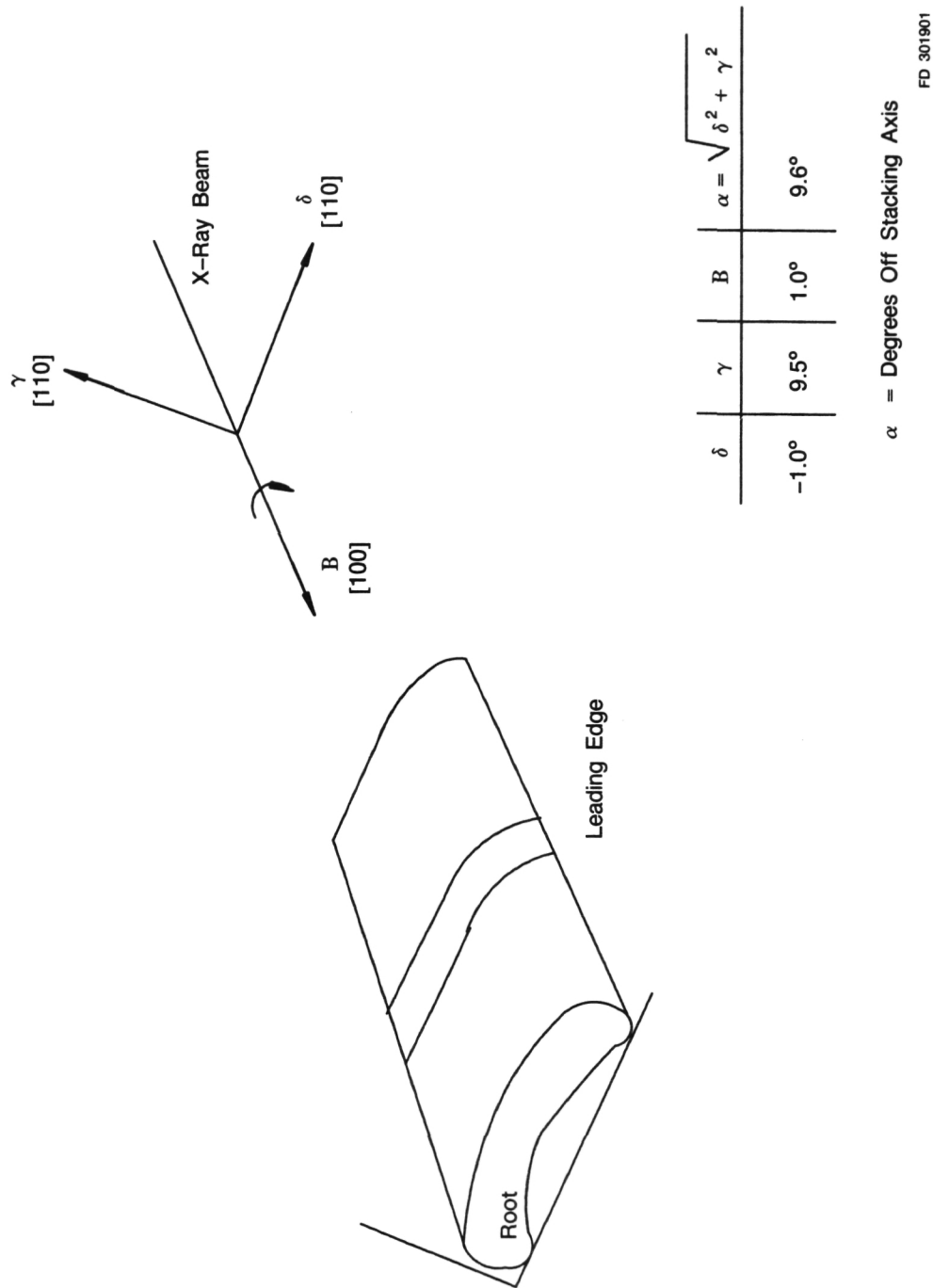
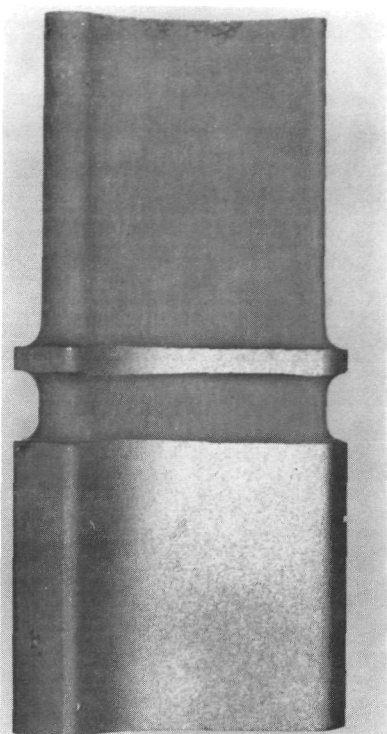


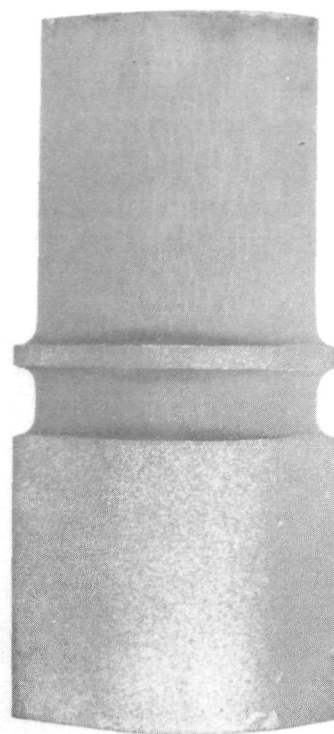
Figure C-2. Diagram of Laue X-ray Shot to Determine Primary Orientation of Blade and Typical Example of Calculation

ORIGINAL PAGE IS
OF POOR QUALITY

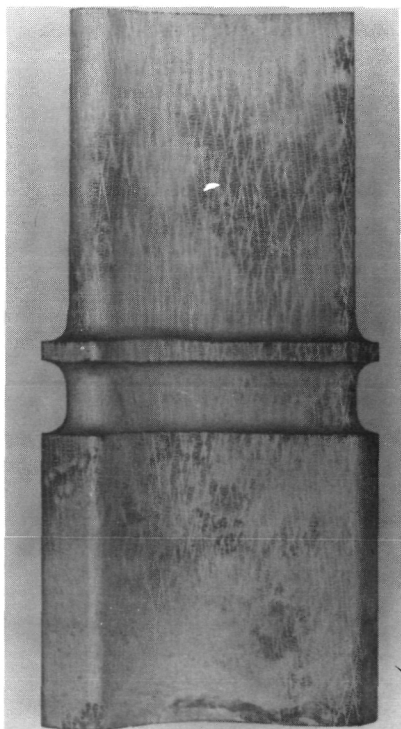
Pratt & Whitney
FR-19009-1



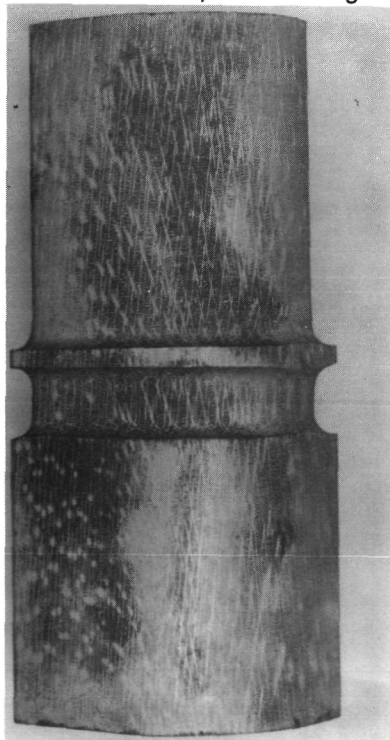
FAL 79653 S/N 1 Mag 2X



FAL 79654 S/N 1 Mag 2X



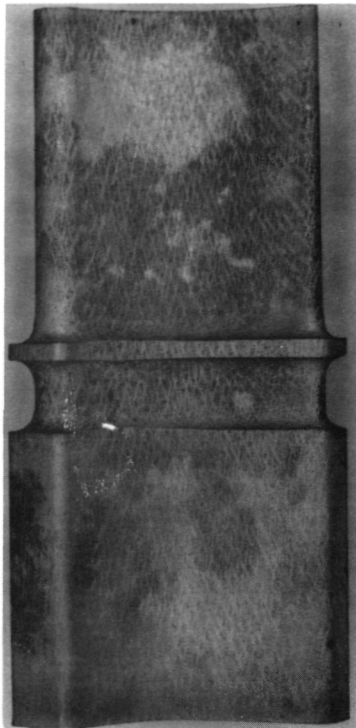
FAL 79655 S/N 2 Mag 2X



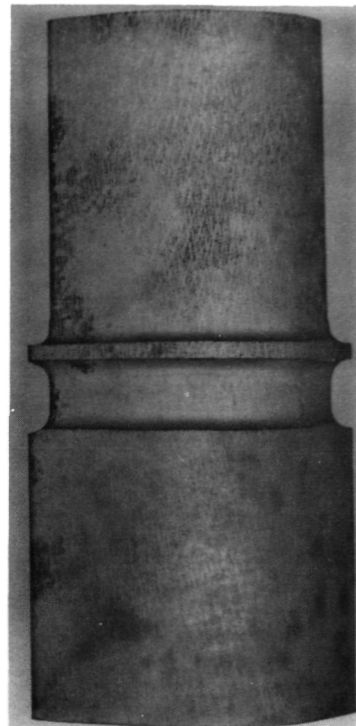
FAL 79656 S/N 2 Mag 2X

FD 301902

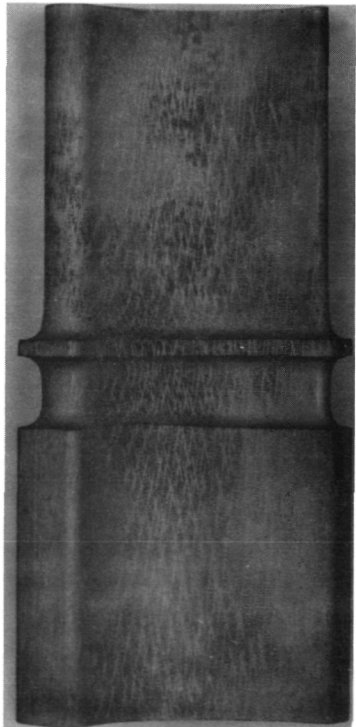
Figure C-3. Grain Etched Condition of Experimental Blades



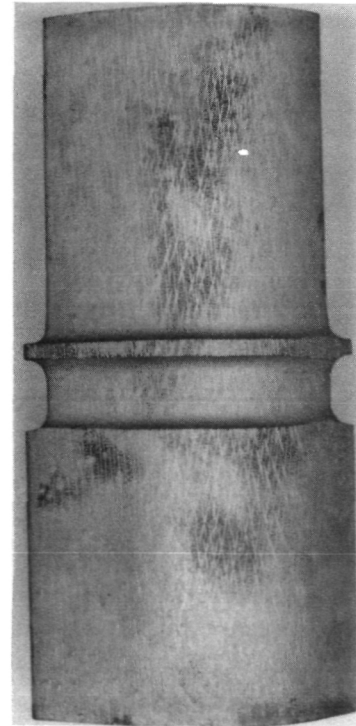
FAL 79657 S/N 3 Mag 2X



FAL 79658 S/N 3 Mag 2X



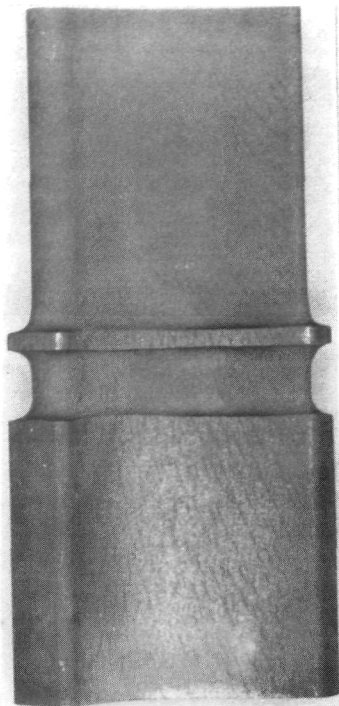
FAL 79659 S/N 4 Mag 2X



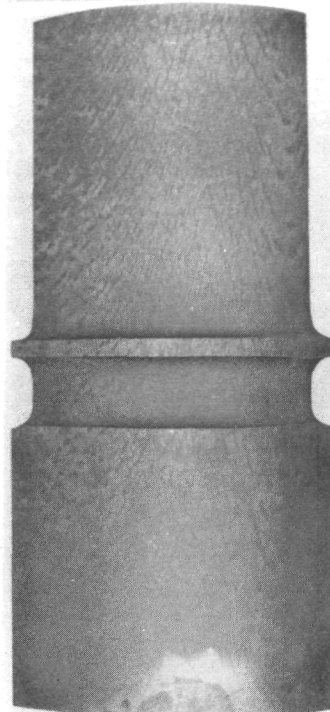
FAL 79660 S/N 4 Mag 2X

FD 301903

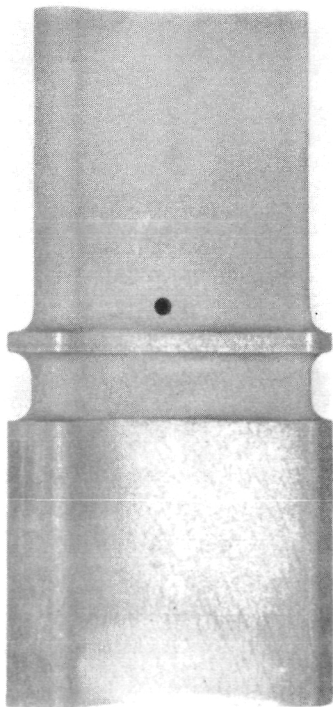
Figure C-4. Grain Etched Condition of Experimental Blades



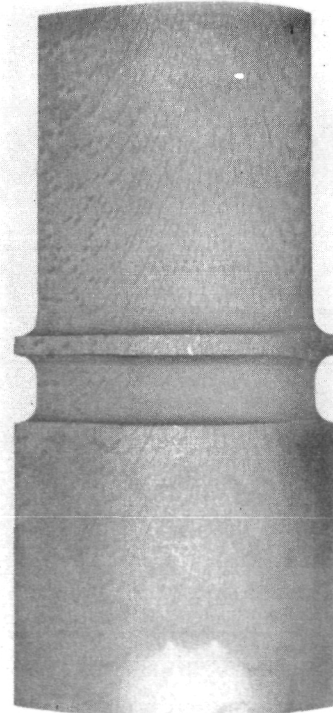
FAL 79689 S/N 5 Mag 2X



FAL 79690 S/N 5 Mag 2X



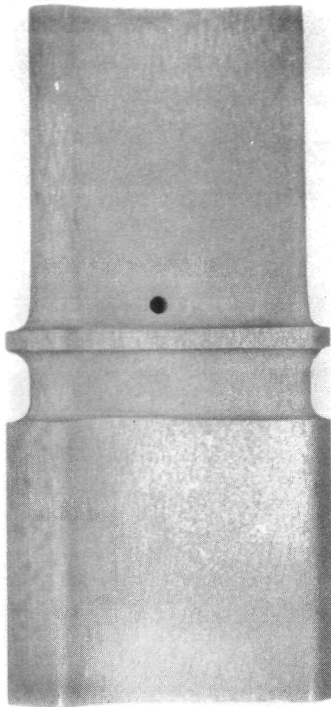
FAL 79691 S/N 6 Mag 2X



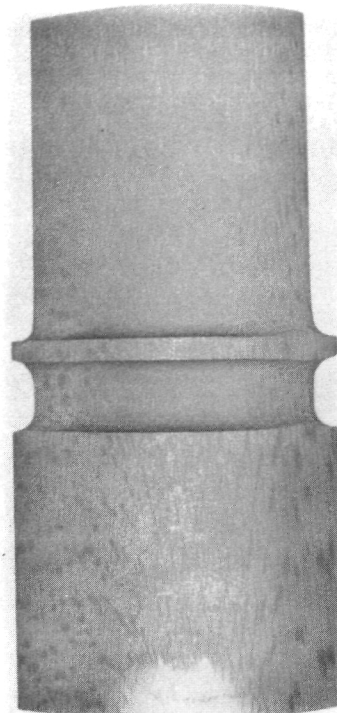
FAL 79692 S/N 6 Mag 2X

FD 301904

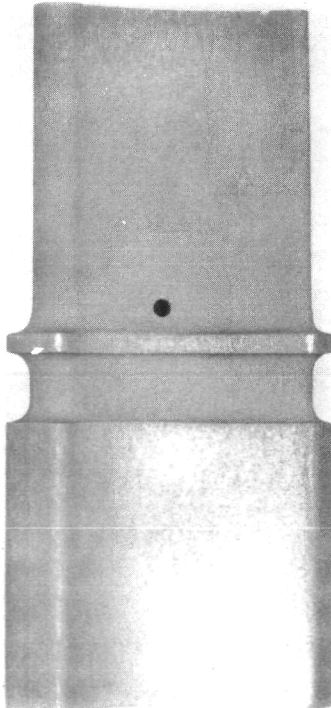
Figure C-5. Grain Etched Condition of Experimental Blades



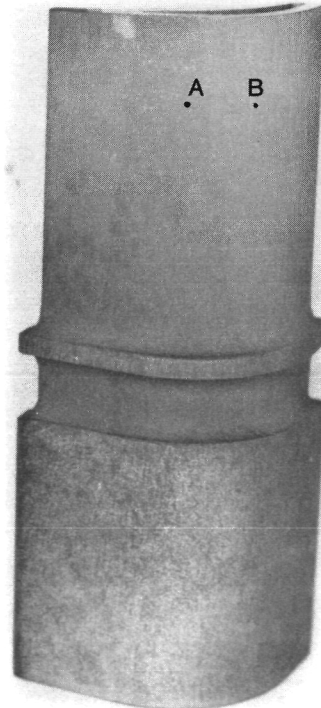
FAL 79693 S/N 7 Mag 2X



FAL 79694 S/N 7 Mag 2X



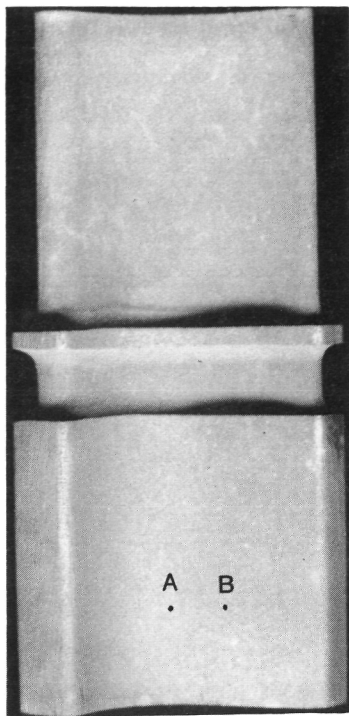
FAL 79695 S/N 8 Mag 2X



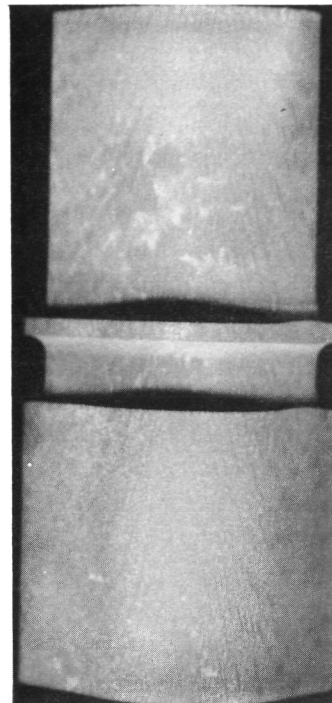
FAL 79697 S/N 8 Mag 2X

FD 301905

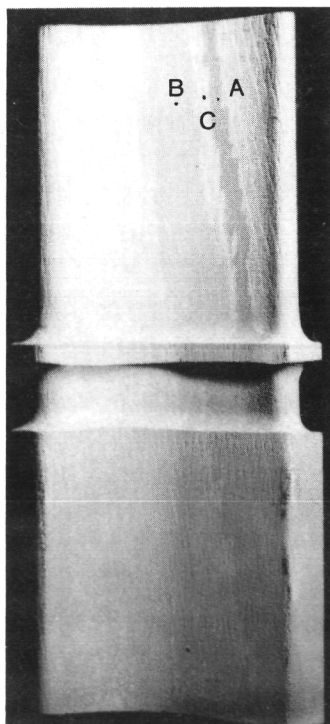
Figure C-6. Grain Etched Condition of Experimental Blades



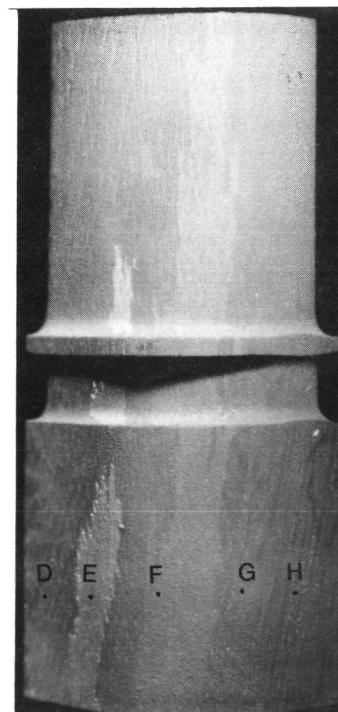
FAL 80661 S/N 9 Mag 2X



FAL 80662 S/N 9 Mag 2X



FAL 80663 S/N 10 Mag 2X

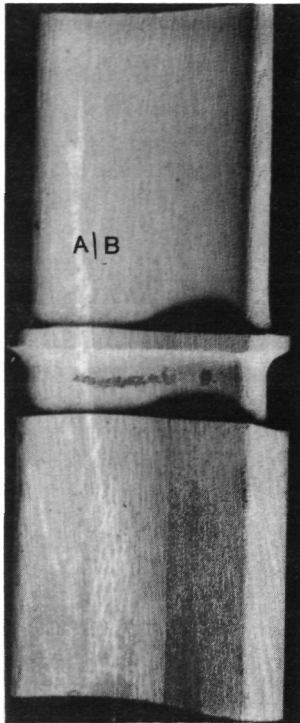


FAL 80664 S/N 10 Mag 2X

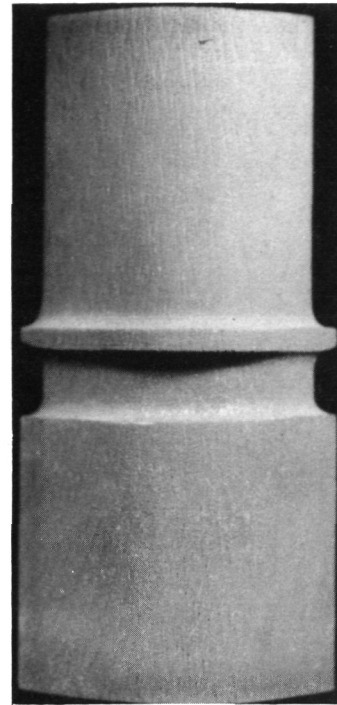
FD 301906

Figure C-7. Grain Etched Condition of Experimental Blades

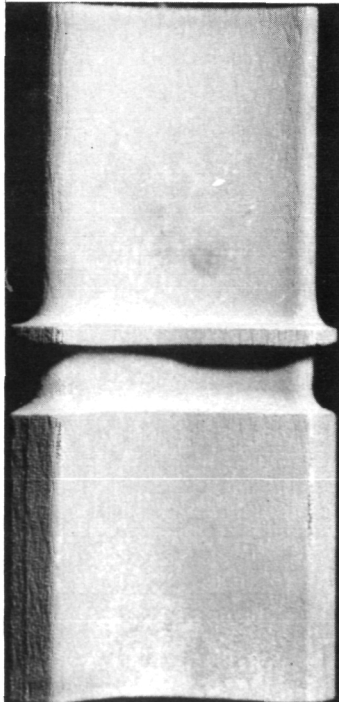
ORIGINAL PAGE IS
OF POOR QUALITY



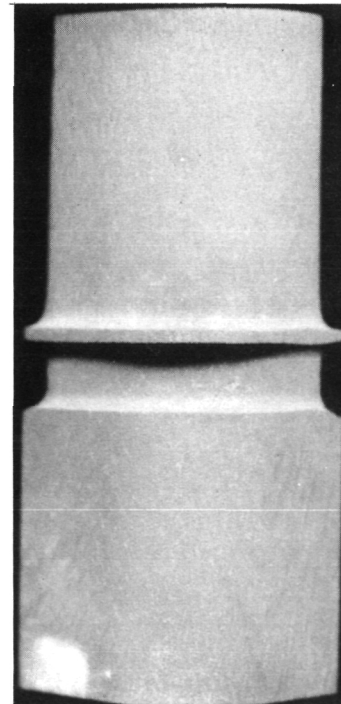
FAL 80665 S/N 11 Mag 2X



FAL 80666 S/N 11 Mag 2X



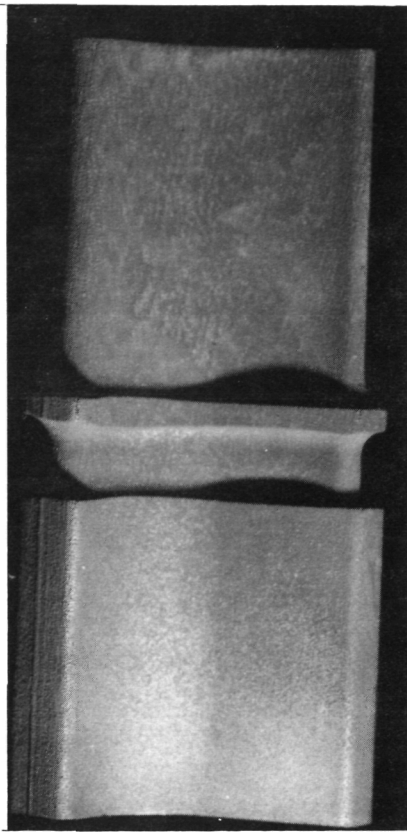
FAL 80667 S/N 12 Mag 2X



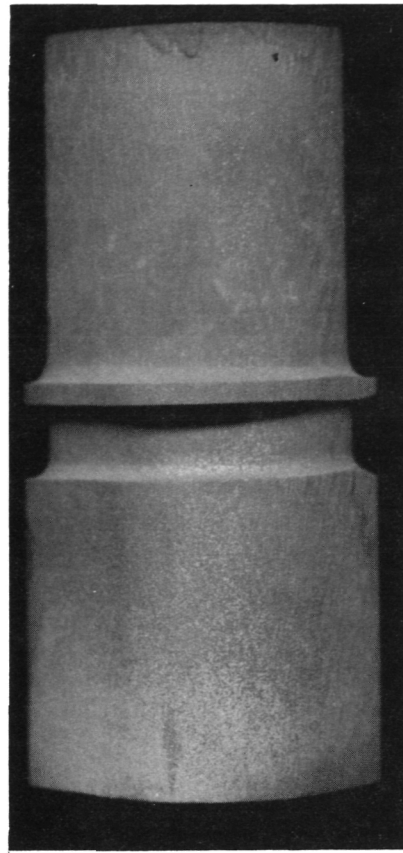
FAL 80668 S/N 12 Mag 2X

FD 301907

Figure C-8. Grain Etched Condition of Experimental Blades



FAL 80669 S/N 13 Mag 2X



FAL 80670 S/N 13 Mag 2X

FD 301908

Figure C-9. Grain Etched Condition of Experimental Blades